DEVELOPING METHODS TO PREVENT OR TREAT MICROBIAL COLONISATION OF TITANIUM DENTAL IMPLANT SURFACES

by

KRUNAL NARENDRAKUMAR

A Thesis submitted to the University of Birmingham for the degree of

DOCTOR OF PHILOSOPHY

Biomaterials Unit

School of Dentistry

The University of Birmingham

October 2014

Dedicated to my mum, Racca Bai Naendralal and brother, Dipen Narendrakumar

ABSTRACT

Titanium (Ti) dental implants are increasingly used because they provide a successful treatment modality for the replacement of missing teeth. However, "success" has traditionally been defined as the retention of the Ti dental implant and does not take account of the presence or absence of destructive peri-implant inflammatory diseases such as peri-implant mucositis and peri-implantitis. Peri-implant diseases are caused by the pathogenic bacterial biofilms colonising the dental Ti surface and disease progression can eventually lead to dysfunctional and unaesthetic outcomes.

The overall thesis goal was to develop methods to prevent bacterial adhesion to Ti implant surfaces or treat already existing biofilms. Experiments were first conducted to investigate the relationship between bacterial adhesion of *S sanguinis, E coli, S mutans* and *F nucleatum* and topological features of common Ti Grades used for the manufacture of dental implants. The Ti surface topologies were thoroughly characterised with SEM, non-contact laser profilometry and contact angle analyses. Reproducible model systems were identified to be used in further studies to disrupt biofilm formation. Early bacterial adhesion was also investigated on engineered Ti surfaces created with the Scanning laser melting (SLM) or on Ti nanotubule surfaces. Bacterial adhesion was found to decrease on the SLM prepared surfaces and on certain nanotubule surfaces suggesting potentially promising routes to reducing early bacterial surface colonisation.

Subsequently photoactivation of Ti surfaces was investigated on thermally or anodically oxidised Ti. The experiments demonstrated the potential to pre-treat TiO_2 surfaces to reduce the bacterial viability of early colonising *S sanguinis, E coli, S mutans* and *F nucleatum*. The outcomes could potentially be employed both as a prophylactic or potentially an in situ treatment regime for peri-implant disease. Finally chemo-disinfection was investigated on *S sanguinis* and *S mutans* biofilms with a novel Eucalyptus Oil (EO) based mouth wash formulation. EO was demonstrated to increase the permeation of Chlorhexadine Gluconate and subsequently significantly reduce the viability of *S sanguinis* and *S mutans* biofilms. The findings of these studies show some promise to be used to inform the management of peri-implant disease.

ACKNOWLEDGEMENTS

TABLE OF CONTENTS

List of Figures

List of Tables

Abbreviations

LIST OF FIGURES

100 hr thermal treated and 150 hr thermal treated Grade V Ti-6Al-4V alloy samples were irradiated at an irradiance of 922 mW/ cm^2(25% intensity) for 60 s.

LIST OF TABLES

LIST OF ABBREVIATIONS

°	Degrees
°C	Degrees Celcuis
µg	Microgram
µL	Microlitre
µM	Micro Molar
µm	Micrometer
3D	Three-Dimensional
ANOVA	Analysis of Variance
ASTM	American Society for Testing and Materials
BA	Blood Agar
BHI	Brain Heart Infusion
$CaCl_2$	Calcium Chloride
CD	Centres for Disease Control and Prevention
CFU	Colony Forming Units
CH	Chlorhexidine Digluconate
cm	Centimetre
cm²	Centimetre Squared
CO	Compact Oxide
Cp	Commercially Pure
CpTi	Commercially Pure Titanium
DI	Deionised Water
E coli	*Escherichia coli*
EDX	Energy-dispersive X-ray spectroscopy
EO	Eucalyptus Oil
eV	Electron Volt
F nucleatum	*Fusobacterium Nucleatum*
G	Gram
H	Hour
H_2NaO_4P	Sodium Dihydrogen Orthophosphate
H_2O	Water
H_2O_2	Hydrogen Peroxide
HMDS	Hexmethyldisilazane
HPLC	High Performance Liquid Chromatography water
II	Two
IPA	Isopropyl Alcohol
IV	Four
K_2HPO_4	Potassium Hydrogen Phosphate
KCl	Potassium Chloride
KeV	Kilo Electron Volt
KV	Kilovolts
L	Litre
M	Molar
mA	Milliamp

MB	Methylene Blue
MBC	Minimum Bactericidal Concentration
MIC	Minimum Inhibitory Concentration
min	Minute
mL	Millilitre
mm^2	Millimetre Squared
MRSA	Methiciliin-Resistant *Staphylococcus aureus*
ms	Millisecond
mW	Milliwatt
Mw	Molecular Weight
N	Sample Number
NaCl	Sodium Chloride
NAD	Nicotinamide Adenine Dinucleotide
ND:YAG	Neodymium-doped Yttrium Aluminium Garnet
Nm	Nanometer
No.	Number
NP	Nanopore
NT	Nanotubule
PBS	Phosphate Buffered Saline
pH	Potential of Hydrogen
ppm	Parts Per Million
Ra	The arithmetic mean deviation of the roughness profile from the mean line.
Rc	Mean height of the roughness profile elements
Rku	Kurtosis of roughness profile is a measure of the sharpness of the profile peaks
RLU	Relative Light Units
ROS	Reactive Oxygen Species
Rp	The maximum distance between the peak and the mean line in the sampling length
Rpm	Revolutions per Minute
Rq	Root mean square of deviation (peaks and valleys) from the mean line
Rsk	Skewness (Rsk) is a measure of the average of the first derivative of the surface (the departure of the surface from symmetry)
Rt	The maximum distance between valley and peak in the sampling length
Rv	The maximum distance between the valley and the mean line in the sampling length
Rz	The average vertical distance, in microns, between valleys and peaks across a sample surface
S mutans	*Streptococcus mutans*
S sanguinis	*Streptococcus sanguinis*
s	Second
SD	Standard Deviation
SEM	Scanning Electron Microscopy
SiC	Silicon Carbide

SLM	Scanning Laser Melting
Ti	Titanium
TiO_2	Titanium Dioxide
Ti-6Al-4V	Grade 5 Titanium Alloy (Titanium, Aluminium, Vanadium)
TMTC	Too Many To Count
TSB	Tryptone Soya Broth
UV	Ultraviolet
V	Five
V	Volts
v/v	Volume per Volume
W	Watt
w/v	Weight per Volume
XPS	X-ray Photoelectron Spectroscopy
XRD	X-ray Diffraction

CHAPTER 1: INTRODUCTION

1.1 History of dental implants.

The concept of dental implants has been considered for over 5000 years with archaeological evidence revealing that ancient Egyptians attempted to implant precious stones and metals into the jaw bones of corpses where teeth had been lost; this was seen as a preparation for the afterlife (Cranin, 1970; Mckinney, 1991). The earliest case of a functional dental implant from ancient times has been dated to the first or second century AD when a Gallo-Roman man was found with a wrought iron device embedded in his right second upper premolar region (Crubezy et al., 1998). It was however not until the 19th century that endosseous (placing of implants within bone) dental implants were considered seriously when Maggilio, a dentist at the University of Nancy, France, reported using bespoke gold implants placed directly into a tooth socket (Ring, 1995a; Ring 1995b). By the mid-20th century subperiosteal (on top of bone), endosteal (within the bone) and transosteal (through the bone) implants had been developed, fabricated from a variety of materials; however they were unpredictable in terms of their retention and soft tissue reactions (Caswell and Clark, 1991: Thomas, 1999). In addition during these early years infection was a constant problem (McKinney, 1991) and it was not until the serendipitous discovery of osseointegration and the use of titanium (Ti) that dental implants as a successful treatment modality to replace missing teeth became a reality.

1.1.1 Osseointegration.

Osseointegration was discovered in a study unrelated to dental research which was carried out in 1952 by Professor Per-Ingvar Brånemark, a Swedish orthopaedic surgeon. The study

involved placing Ti chambers into the fibula of rabbits to enable intravital imaging of blood flow. At the end of the study the investigators discovered that the chambers could not be removed and were assumed to have integrated into the bone (Brånemark, 1959). This phenomenon was thought to have potential application in dentistry and as a result experimental studies were conducted in the jaw bones of dogs (Weiss et al., 1981). Osseointegration is defined as a "direct structural and functional connection between ordered, living bone and the surface of a load carrying implant" (Brånemark, 1983).

The first clinical use of a Ti "root-implant" in humans was reported in 1965 (Adell et al., 1981). Subsequently clinical trials lasting 15 years (1965-1980) were carried out in edentulous humans, in which "2768 Ti fixtures were installed in 410 edentulous jaws of 371 consecutive patients" of which 81% of fixtures in upper jaws remained stable and 91% of the fixtures were found to be stable in the lower jaws over the follow-up period (Adell et al., 1981). The trials established that the process of osseointegration was maintained in the long-term and that endosseous Ti root implants were a viable treatment modality.

The predictability of Ti fixtures being retained has led to the development of a large number of root form endosseous dental implant systems which consist of the root form fixture, the abutment and the permanent crown (figure 1.1).

Figure 1.1. Mechanical components of a titanium dental implant consisting of a) crown, b) abutment c) fixture, Image obtained from: http://www.implantium.co.uk.

a) Crown (typically manufactured from ceramic or metal-ceramic)

b) Abutment (typically manufactured from Ti, CoCr, ceramic or cast precious metal alloy)

c) Fixture (typically manufactured from commercially pure or alloyed Ti)
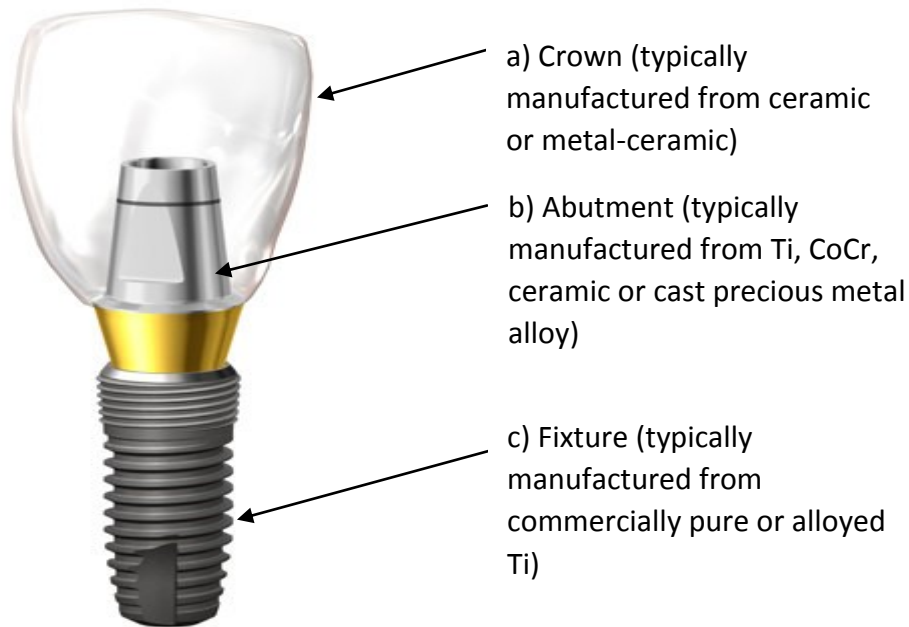
Osseointegration plays the vital role in the success of dental implant procedures (Brånemark, 1959). Once an implant is placed a wound healing cascade occurs (figure 1.2). The healing stages often overlap in vivo with chemotactic, endocrine, paracrine, autocrine regulatory processes playing a vital role in de novo bone formation (Schwartz and Boyan, 1994).

Figure 1.2. The process of wound healing following implantation. The first process occurs immediately after implant placement, the surface is conditioned by the adsorption of serum proteins, metal ions, sugars, lipids and cytokines produced by immune cells. In the first 3 days after implantation, undifferentiated mesenchymal cells are attracted to the surface of the implant with the presence of chemotactic factors. Once attracted to the surface of the biomaterial, the mesenchymal cells attach and proliferate with the aid of endocrine/paracrine factors. At this point the mesenchymal cells synthesize their own extracellular matrix which includes growth factors and cytokines that subsequently modify the surface of the implant. From days 3-6 of the healing stage, with the help of endocrine/paracrine/autocrine signalling factors, mesenchymal cells undergo osteoblastic differentiation and produce the bone matrix known as osteoid. (Schwartz et al., 1991). After 6-14 days, the cells begin to calcify the matrix and finally after 21 days, osteoclasts are recruited to remodel the newly woven bone. Illustration obtained from Schwartz and Boyan (1994).
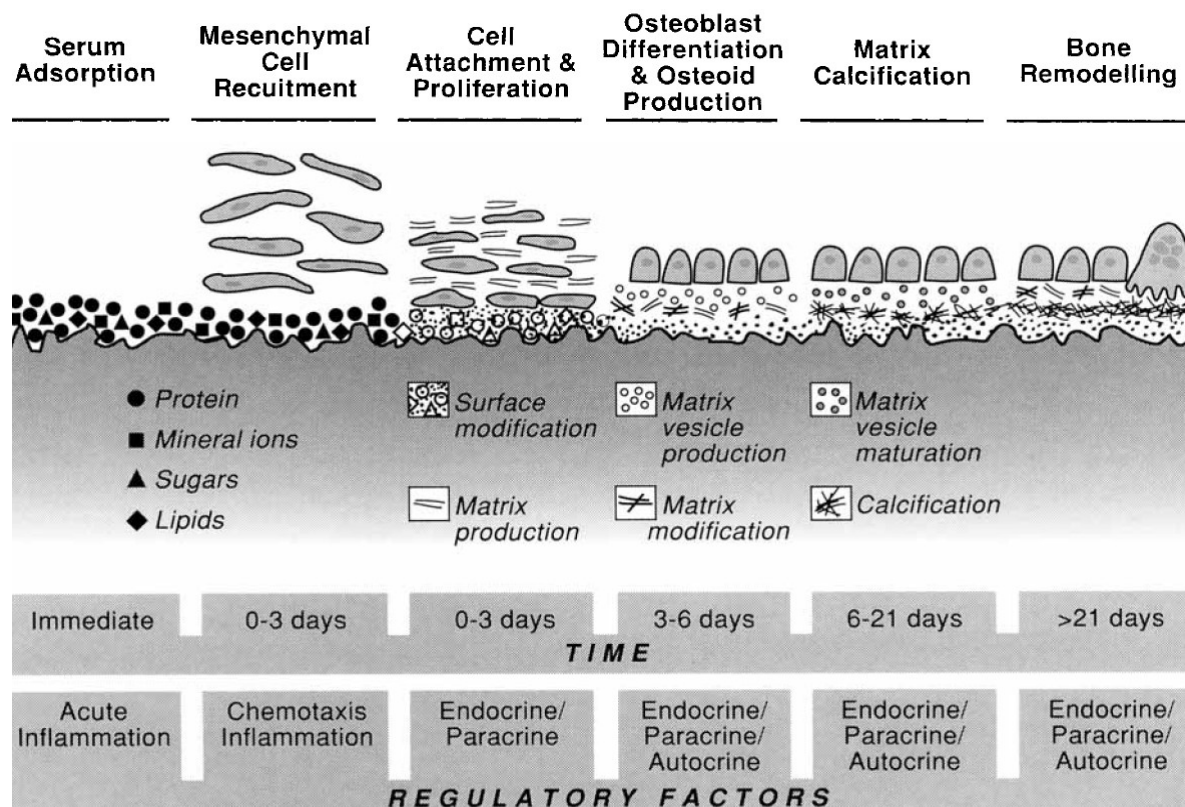
1.2 Ti as a biomaterial for dental implants.

Ti and its alloys are favoured for the fabrication of dental and orthopaedic implants because of the metals' ability to osseointegrate with the host bone (Pye et al., 2009). In addition, Ti

possesses many physico-mechanical properties which make it desirable as a biomedical implant material including high fatigue strength, good formability and machinability, and corrosion resistance in-vivo conferred by a passive resilient layer of TiO_2 on its surface (Liu et al., 2004 & Kim TN et al., 2007). It is with this passive TiO_2 surface that the favourable biological interactions of osseointegration and immunopassivity occur (Schwartz and Boyan, 1994). A variety of Ti biomaterials have been used to manufacture dental implants including commercially pure titanium (CpTi), also known as unalloyed titanium; in ASTM grades I, II, III and IV and the Ti-6Al-4V alloy (ASTM Grade V). The most common grade of CpTi for dental implants currently is ASTM grade IV which contains approximately 0.5 % Fe as an impurity (Straumann, 2010). In orthopaedics Ti grades with higher yield strengths are more commonly used to manufacture medical devices and include Ti-6AL-4V and Ti-6Al-4V-ELI (extra low interstitial) (McCracken, 1999). Ti-6Al-4V ELI has been developed for use in biomedical implants by lowering the amount of oxygen and iron impurities which improves its ductility and toughness against fracture (McCracken, 1999). A small number of commercially available dental implant systems use Ti-6Al-4V as opposed to CpTi. The Composition of Grade II, IV and V Ti determined by atomic emission plasma spectrometry is reported in table 1.1.

Table 1.1: The composition of Grade II, IV and V Ti (wt %) determined by ASTM standards.

Element	Grade II	Grade IV	Grade V
Vanadium	-	-	4
Aluminium	-	-	6
Nitrogen	0.03	0.05	-
Carbon	0.08	0.08	-
Hydrogen	0.015	0.015	-
Iron	0.30	0.50	0.25
Oxygen	0.25	0.40	0.2
Titanium	99.33	98.96	90

1.3 The formation of biofilms in the oral cavity.

Bacterial aggregates on teeth were first reported by Antonie Van Leewenhoek in 1684 who described observing "animals" as being present on the surface of his own teeth (Leeuwenhoek, 1684; cited by Donlan and Costerton, 2002). Since then the importance of oral microbes in dental diseases has been recognised widely and it has been identified that in the oral environment microbes exist in complex biofilms. The term "biofilm" was first introduced by Costerton in 1978 when he demonstrated that the composition of bacterial aggregates is sensitive to the nutritional needs of the environment and the metabolic needs of the micobiotica (Costerton, 1978, cited by Newman and Wilson, 1999). The definition has since had to be updated after researchers observed further characteristics of bacterial biofilms. An improved definition of a bacterial biofilm was introduced as "a microbially derived sessile community characterised by cells that are irreversibly attached to a substratum or interface or to each other, are embedded in a matrix of extracellular polymeric substances that they have produced, and exhibit an altered phenotype with respect to growth rate and gene transcription" (Donlan and Costerton, 2002). The implication is that the behaviour of microbes in a biofilm differs from those found in isolation and studies of isolated microbes may hold less clinical relevance.

In the oral environment, the naturally occurring biofilm is known as dental plaque (Marsh, 2004). The formation of dental plaque can be divided into the supragingival, in which the formation of biofilm occurs above the gingival (gum) margin, and subgingival, where biofilms form within the subgingival pocket (Kolenbrander et al., 2010). Biofilm formation at these sites begins when bacterial cells adhere to either hard surfaces such as teeth or a material

that has been coated with salivary pellicles; adhere to desquamating epithelial tissue or adhere to other bacteria (Fröjd et al., 2011 and Kolenbrander et al., 2010).

The salivary pellicle or the acquired pellicle is initially adsorbed on any oral surface which is free of bacteria. The pellicle is a proteinaceous layer composed of adsorbed proteins, enzymes, glycoproteins and other macromolecules (Bennick et al., 1983 and Kolenbrander et al., 2010). The formation of the acquired pellicle occurs almost instantaneously on a clean surface in the oral cavity. Initially pellicle precursor proteins with high affinity to hydroxyapatite such as statherin and proline rich proteins adsorb to the surface because of surface charge (Kolenbrander et al., 2010). Ionic interactions, van der Waals forces and hydrophobic interactions mediate the subsequent development of the pellicle layer (Oss, 1986, Teughels, 2006, Hannig and Hannig, 2009). During the early stages of the acquired pellicle formation, the adsorbing proteins undergo an unfolding and flattening process. This adds to increase the surface area of the protein and hence the surface is rapidly covered. The next stage is characterised by a continuous adsorption of biomolecules from the oral fluids onto the protein covered surface (Hannig and Hannig, 2009).

The salivary pellicle plays an important role in the formation of a biofilm and mediates initial microbial colonisation. The initial or pioneer species that colonize a surface in the oral cavity are the *Streptococci* and *Actinomyces* species. Early colonising Streptococcus species include *oralis, mitis, sanguinis, gordonii and Actinomyces* species include *oris and naeslundii* (Kolenbrander et al., 2010). It is thought that the initial colonisers bind onto the tooth surface attaching to receptors adsorbed to the salivary pellicle, such as statherin, bacterial cell fragments, sialylated mucins, salivary agglutinin, alpha amylase and proline-rich proteins

(Kolenbrander et al., 2002). As pioneer species colonise the surface (teeth or biomaterial) further microbes become capable of attachment through adhesion-receptor interactions to immobilized bacteria, a process known as co-adhesion (Bos et al., 1996). Many bacteria form partnerships with others, the bacteria *Fusobacterium nucleatum* forms the most partnerships because of its ability to co-aggregate with other bacteria that are involved in the initial, early and late colonisation stages of the complex biofilm formed on the surface of the implant (Kolenbrander et al., 1993). The complexity and heterogeneity of the oral biofilm formation is illustrated in figure 1.3.

Figure 1.3. The formation of a complex bacterial plaque that forms on the tooth surface after the formation of an acquired pellicle. The formation of this plaque is similar to the biofilm that is formed on the surface of dental implant systems. The acquired pellicle enables the adhesion of proteins and adhesions which results in the recruitment of early colonisers and subsequent late colonisers. The bacterial species previously known as *S sanguinis* has many receptors that are present on the surface of the bacteria and acts as a major initial contact to which the early bacterial colonisers are able to bind. The early colonisers are linked to the late colonisers by forming adhesion and receptor links with *F nucleatum*. The key aspect of the diagram illustrates that there is an important link between the initial colonisation and subsequent adhesion of late colonisers for the formation of a bacterial biofilm community. The figure was obtained from Kolenbrander (1993).

1. *Streptococcus oralis, Streptococcus mitis*
2. *Streptococcus oralis, Streptococcus sanguinis*
3. *Streptococcus gordonii*
4. *Capnocytophaga sputigena*
5. *Capnocytophaga ocharcea*
6. *Propionibacterium acnes*
7. *Capnocytophaga gingivalis*
8. *Actinomyces israelii*
9. *Haemophilus parainfluenzae*
10. *Veillnella atypica*
11. *Actinomyces naeslundii*
12. *Prevotella denticola*
13. *Fusobacterium nucleatum*
14. *Aggregatibacter actinomycetemcomitans*
15. *Prevotella intermedia*
16. *Treponema denticola*
17. *Porphyromonas gingivalis*
18. *Selenomonas flueggei*
19. *Eubacterium* spp.

1.4 Success of dental implants.

Dental implants are an effective treatment modality to replace missing teeth or to secure prosthesis and are a largely predictable treatment with a high success rate. Success rates reported vary according to the individual study but typical values are: complete fixed prostheses 87-99 % success over 15-20 years; overdentures 86-97 % success over 10-15 years; fixed partial dentures have a 86-100 % success rate over 10-15 years; and single tooth replacement has a 87-97 % success rate over 10 years (Wennerberg and Albrekttson, 2011). "Success" has however been traditionally defined as the retention of the dental implant in the mouth and does not account for the presence or absence of peri-implant inflammatory diseases which may lead to progressive bone loss and deterioration of the gingival soft tissue architecture.

1.5 Mechanism and prevalence of peri-implant disease.

Peri-implant diseases are inflammatory conditions that affect the soft and hard tissues that are present around dental implants. Peri-implant diseases can be classed as peri-implant mucositis, which is defined as "inflammation of the soft tissues surrounding the teeth without the loss of bone" or peri-implantitis which is defined as the "destructive inflammatory process that affects the soft and hard tissues around osseo-integrated implants, leading to the formation of a peri-implant pocket and loss of supporting bone" (Albrektsson et al., 2004). Peri-implant mucositis is a reversible process however it can progress to peri-implantitis and can result in the failure of a dental implant (Mombelli et al., 2000 & Lindhe et al., 2008). Currently the process leading to disease progression from mucositis to peri-implantitis is poorly understood.

At the 6th European workshop on periodontology in 2008 it was reported that peri-implant mucositis occurs in approximately 80 % of patients with dental implants and there was some degree of peri-implantitis in between 28 and 56 % of patients (Lindhe et al., 2008). The report stated that peri-implant disease is likely to become particularly significant in the elderly population where a loss of manual dexterity and a decreased salivary flow predispose to poor hygiene around dental implant fixtures (Lindhe et al., 2008).

In 5-8% of cases where dental implants have been lost due to loosening failure were associated with sepsis (Pye et al., 2002). Dental implants are embedded in bone but penetrate the overlying soft tissues creating a discontinuity which allows potentially pathogenic bacteria to adhere and proliferate on the surfaces of the implant. As a consequence direct bacterial action or due to the host response, inflammatory changes can occur which cause a loss of osseointegration (Rimondini, 2003). The microbiota associated with peri-implantitis is complex with bacterial species such as P*orphyromonas gingivalis, Tannerella forsynthia, Aggregatibacter actinomyecetemcomitans, Prevotella intermedia* and *Fusobacterium* species being commonly present (Koyanagi et al., 2010). Pye et al., (2002) described the microbiotic flora present around failing implants being similar to that found in periodontitis. However, with progressive bone loss there is a transition of the microbial flora from "a predominately Gram positive non-motile, aerobic and facultative anaerobic composition towards a flora with a greater proportion of Gram-negative motile, anaerobic bacteria" (Williams, 1990; Albrektsson & Isidor, 1994; Kotsovilis et al., 2008).

1.6 Risk factors that may lead to the establishment and progression of peri-implant mucositis and peri-implantitis.

A number of risk factors have been identified that may lead to the establishment and progression of peri-implant mucositis and peri-implantitis.

1.6.1 Poor oral hygiene.

Lindquist et al. (1997) observed a clear relationship between peri-implant bone loss around osseointegrated mandibular implants and poor oral hygiene of patients over a 10 year observation period. In common with periodontal diseases it is clear that the reduction of microbes on the implant surface through oral hygiene measures is associated with healthier gingival tissues and a reduced risk of progressive bone loss around the implant.

1.6.2 A history of periodontitis.

An increasing number of patients who have lost teeth due to periodontitis receive dental implant reconstructions. Several studies have identified that patients with a previous history of periodontitis are more susceptible to peri-implant disease (Heitz-Mayfield, 2008, and Meffert, 1996). The correlation of peri-implant disease with a history of periodontitis implicates similar risks and a similar pathogenesis. Periodontitis is understood to be mediated by the nature of the individual host immune response to the presence of groups of potentially pathogenic bacteria (Heitz-Mayfield, 2000).

1.6.3 Smoking.

Smoking is a significant risk factor for periodontitis and hence a large number of studies have been conducted to investigate an association with peri-implantitis. It is known that cigarette

smoke has over 4000 known constituents including carbon monoxide, hydrogen cyanide, reactive oxygen radicals and the psychoactive molecule nicotine (Benowitz, 1996). Pabst et al. (1995) demonstrated with *in vitro* studies a direct inhibition of neutrophil and monocyte-macrophage defensive functions by high concentrations of nicotine. Further studies have identified a significant increase in the risk for peri-implant disease in patients that smoke when compared with non-smokers (Ataoglu et al., 2002; Gruica et al., 2004; Mcdermott et al., 2003) with clinical parameters of disease including bleeding on probing (BOP), pocket depth (PD), peri-implant mucosal inflammation and bone loss (Haas et al., 1996). It is understood that smoking results in a decreased blood flow around the inserted implant which impacts on initial wound healing and makes the area more susceptible to chronic inflammation and bone loss (Roos-Janasåker et al., 2006).

1.6.4 Alcohol consumption.

Alcohol has been suggested to have a synergistic relationship with smoking as a risk factor for peri-implant disease. Galindo-Moreno et al. (2005) studied the effect of alcohol in conjunction with smoking habits on peri-implant bone loss in 185 patients after three years. The investigators identified that in addition to the effects of smoking on increased peri-implant marginal bone loss, the patients who consumed >10 g of alcohol per day and smoked had increased bone loss when compared to the tobacco use alone.

1.6.5 Diabetes.

Diabetes has been strongly associated as a risk factor for periodontal disease and diabetic patients may exhibit delayed wound healing and an increased susceptibility to infections (Fiorellini and Nevins, 2000). In a cross-sectional study of 212 non-smoking Brazilian patients

with functioning implants present between 6 months and 5 years Ferreira et al., (2006) demonstrated that the prevalence of peri-implant disease was 64.6 % in diabetic patients when compared with 8.9 % in the healthy population. The study demonstrated that alongside periodontitis there is a significantly greater risk of peri-implantitis in diabetic patients.

1.6.6 Genetic factors.

Extensive research has been conducted to identify 'genetic' risk factors for peri-implant disease. In particular there has been focus on the expression of interleukin (IL)-1α, (IL)-1 β and the specific inhibitor IL-1 receptor antagonist (IL)-ra which is essential in the regulation of the inflammatory response. Wilson and Nunn, 1999 found that there was no association between bone loss and implant failure and the IL-1 genotype. In a contradicting study Felotzis et al., (2003) found that there were significant differences between marginal bone losses in patients that were heavy smokers compared to non-smokers with a IL-1 positive genotype. In patients that did not have the (IL)-1 positive genotype, no significant difference was observed. It is thought that the effect of smoking could have synergistic effects with the IL-1 genotype for increasing bone loss. The studies carried out by Jansson et al., (2005) and Laine et al., (2005) also found that there was an association between smoking and the loss of the IL-genotype however it is clear that further studies with larger patient numbers are needed to confirm this.

1.7 The similarities and differences between periodontitis and peri-implantitis.

It is evident that periodontal disease and peri-implant disease have similar risk factors and disease characteristics. Heitz-Mayfield and Lang (2000) reported that the majority of studies

have demonstrated that the subgingival microbiotica which is present around teeth and implants that are diseased are similar although some subtle differences did exist. One such difference is the presence of increased levels of *S aureus* in the deep peri-implant pockets and a tendency towards suppuration rather than bleeding-on-probing alone (Heitz-Mayfield and Lang., 2000).

Histopathological analysis of peri-implantitis tissues have described the inflammatory lesion to contain high concentrations of B cells and plasma cells which is similar to what is observed in periodontitis. However, one major difference of peri-implantitis when compared with periodontitis is that the periodontitis lesion is walled off in a tissue fibre compartment and as a result the inflammatory cell infiltrates do not penetrate the alveolar bone (Listgarten, 1996). It has also been observed that peri-implantitis lesions are expected to progress more rapidly and consequently require immediate intervention (Heitz-Mayfield and Lang, 2000).

1.7.1 Anatomy of teeth and implants.

When considering similarities and differences between periodontitis and peri-implantitis it is important to recognise the anatomical differences that exists in the peri-implant tissues between teeth and implants. The major difference is the presence of a periodontal ligament (PDL) surrounding teeth which connects to the cementum surfaces of the tooth root linking it to the surrounding bone (PDL fibres) and soft tissues (gingival fibres). The PDL is highly vascularised, contains proprioceptive nerve fibres and is a source of pluripotent cells. Peri-implant and periodontal inflammation are therefore likely to have some significant differences particularly with respect to healing and repair Listgarten (1996).

1.8 The influence of implant surface topography and bacterial adhesion.

A key difference between implant surfaces and the surfaces of dental hard tissues is the surface topology. Dental implants have been specifically designed to either have roughened fixture surfaces to encourage cellular (osteoblast) interactions and smooth abutment surfaces to facilitate cleaning measures. Microbial attachment is significantly influenced by topology which increases the surface area available for attachment, the surface energy and the propensity for cell attachment and cell trafficking (Yuehuei et al., 1998). Teughels et al. (2006) reported that on rough surfaces bacteria are better protected against displacing shear forces and as a result biofilms are able to mature. A systemic review of 24 papers studying the correlation between oral plaque formation and biomaterial surfaces found a clear relationship between increasing roughness and plaque formation (Teughels et al., 2006). Furthermore the undisturbed plaques on the rough surfaces were able to harbour more complex biofilms consisting of rods, motile organisms and spirochetes (Heitz-Mayfield and Lang 2000).

1.9 Management and treatment of peri-implantitis – current state-of-the-art.

The current 'gold-standard' regimen for the management of peri-implant disease is the Cumulative Interceptive Supportive Therapy (CIST) protocol devised and evaluated at the School of Dentistry, University of Berne in Switzerland (Mombelli and Lang, 1998). The CIST protocol aims to detect peri-implant disease as early as possible and intercept with evidence based appropriate therapy. To determine the severity of peri-implant disease the CIST system requires the patient to be recalled regularly and key parameters in the area around the implant measured. Parameters include the presence of plaque around the implant;

presence of bleeding on probing; increased probing depths and the presence of peri-implant pockets and the loss of bone, as determined by radiographs (Mombelli et al., 2000).

The CIST protocol aims to manage the implant and associated tissues depending on the severity of the peri-implant disease. When the recalled patient is examined the measured parameters indicate a progressive sequential treatment sequence:

1) If there is plaque present around the implant and there is an increased bleeding around the implant area mechanical debridement of the implant is performed with debridement instruments that are made of softer material than titanium. The oral hygiene technique should be checked and instruction given as appropriate.

2) If there is the presence of pus or the detection of peri-implant pockets with a depth of 4-5 mm with bone loss, treatment 1) should be combined with a local antiseptic such as a mouthwash containing 0.2 % chlorhexidine gluconate. There is currently a lack of evidence based work with CHG and peri-implantitis.

3) If peri-implant pocketing is in excess of 5 mm when determined with the aid of a WHO periodontal probe, a radiograph is taken and if there is a clear evidence of bone loss a microbiological sample should is taken to determine the presence of anaerobic bacteria. Treatments 1) and 2) are combined with systemic antimicrobial therapy consisting of 1000 mg Ornidazole for 10 days. 4) If there is a considerable increase in bone loss, surgical techniques may be utilised to correct the tissue morphology or apply bone regeneration techniques only after treatment regimens 1), 2) and 3) have been carried out. The CIST protocol aims to intercept the peri-implant tissue destruction at an early time point to prevent further tissue destruction and explantation of the implant.

The treatment regime and outcome for patients with peri-implantitis is dependent on the severity of the peri-implant infection. There is currently a lack of a standardised classification system to differentiate the severity of the peri-implant infection. Fronum and Rosen (2012) have proposed a standardised classification system to define the infection into early, moderate and advanced categories. The extent of the infection is determined with a combination of detection of bleeding on probing and/or suppuration, the probing depths and use of radiographs to determine bone loss around the affected implant.

1.10 Antimicrobial agents.

A key component of the CIST protocol is the use (and sustained patient use) of an antimicrobial mouthwash to supplement oral hygiene measures. It is important to define the terminology that is used when describing the ability of an antimicrobial solution to either kill "bactericidal" or inhibit bacterial growth "bacteriostatic". The definitions appear to be clear in terms of the antimicrobial ability, however in reality the definitions are not straight forward. The term "bactericidal" is the ability of an agent to kill >99.9% of the bacterial inoculum within the 18-24 hr period and "bacteriostatic" is the ability of an agent to kill 90-99% of the inoculum after the 18-24 hr test period (Pankey and Sabath, 2013).

1.10.1 Chlorhexidine gluconate.

Chlorhexidine gluconate (CHG) was initially introduced in the United Kingdom in 1954 as an antiseptic wound and general skin cleanser; pre-surgical disinfectant and a surgical scrub (Veksler et al., 1991; Sans M, 1989). The antiseptic is recognised as a safe and effective broad spectrum antimicrobial agent (Strydonck, 2012; Jeansonne and White, 1994). The chlorhexidine base is insoluble in water but the digluconate form is water soluble (Boyce and

Pitter, 2002). In the field of dentistry CHG is the most potent antimicrobial agent (Veksler et al., 1991). It is used in mouth rinses to reduce plaque and control inflammation of the gingivae and in the control and disinfection of dental implant surfaces coated with pathogenic microorganisms (Becker, 1990; Jenkins, 1983). It is thought that the potency of the antimicrobial agent is due to its substantivity (the retention of the antimicrobial agent's active form and its subsequent slow release). The mechanism of the antimicrobial activity of CHG is due to the cationic antimicrobial molecule of CHG binding to the negatively-charged microbial cell wall which disrupts the cell membrane destabilises the osmotic balance (Silla, 2008). The bacterial cell membrane disruption caused by CHG consequently prevents bacterial adhesion (Kuyyakanond and Quesnel, 1992). The antimicrobial agent acts bacteriostatically at low concentrations and bactericidally at higher concentrations by causing a precipitation or coagulation of the cytoplasmic components and leads to cell death (Silla, 2008). There is interest in using antimicrobials in the pre-treatment of implant surfaces to prevent infections during surgery (Mombelli and Lang, 2000). In addition to the desirable antimicrobial properties of CHG, the molecule carries a positive charge which enables electrostatic attraction as many of the oral surfaces carry a negative charge enabling adsorption onto implant surfaces such as titanium (Barbour, 2007; Kuyyakanond and Quesnel, 1992).

1.11 Development of novel approaches to prevent or manage dental peri-implant disease.

There is currently a wide body of research devoted to the prevention and/or more effective management of peri-implant disease. Research efforts can be divided into preventative measures through implant surface modification or the development of chemo-mechanical approaches to disinfect the implant surface in-situ.

1.11.1 Ion implantation.

Ion implantation involves the introduction of potentially bioactive elements into the surface of the implant. The antibacterial effect of ion implantation of calcium, nitrogen and fluorine into a CpTi surface on the oral bacteria *Porphyrmonas gingivalis* and *Agregatibacter actinomycetemcomitans* has been studied (Yoshinari et al., 2001). It was demonstrated that fluoride ions significantly inhibited the growth of *P. gingivalis* and *A. actinomycetemcomitans* whilst the other modified surfaces had minimal effect (Yoshinari et al., 2001).

1.11.2 Deposition of silver nano particles.

Silver has been used in the treatment of burns and chronic wounds for centuries, with silver nitrate being reported as used in the treatment of ulcers in the 18th century. However during the 1940s, antibiotics emerged as the standard treatment of bacterial infections and as a result the use of silver in wound treatment has decreased (Klasen, 2000; Richard et al., 2000; Hugo and Russel, 1982; Chopra, 2007). The emergence of resistance to antibiotics has led to researchers to once again try to find novel methods to kill bacteria. One approach has involved coating the surface with an antimicrobial substance to guard against prosthesis-related infection. It is thought that silver exhibits a broad spectrum antimicrobial effect,

preventing bacterial replication by binding to both microbial DNA, preventing bacterial replication and to the metabolic enzymes of the bacterial transport chain which leads to their inactivation (Rai, 2008). Liao et al. *(*2010a) described a novel silver nanoparticle-modified titanium (Ti-nAg) surface that was created by depositing silver nanoparticles onto silanized titanium coupons. Analysis of the surface of the modified titanium surface by energy dispersive x-ray spectroscopy determined that it had sparse depositions of silver with a diameter of approximately 100 nm and a surface composition of 4.26% Ag. It was found that 94% of *Staphylococcus aureus* and 95% of *Escherichia coli* were killed through this approach. A key problem with bactericidal surface modifications is potential cytotoxicity to the host tissues (Liao, 2010b). It has been demonstrated that the dosing of silver nanoparticle modified titanium surfaces can be tailored to maintain anti-microbial activity without inducing cytotoxicity and this technology has now been exploited in the orthopaedic sector (Liao, 2010b).

1.11.3 Using surface topology to inhibit bacterial attachment and growth.

The reduction of microbial adhesion to an implant without the use of drugs could be an attractive method for reducing infection and overcome the use of potentially cytotoxic surface modifications (Campoccia et al., 2006). The formation of the surface biofilm prevents the body's host defence mechanisms from removing the bacteria on the surface of the biomaterial (Costerton, 1999). Therefore it can be argued that by preventing the adhesion of bacteria on the surface without the use of drugs would be a preferred way of preventing an infection on a biomedical implant (Campoccia et al., 2006). Typically it is understood that by reducing the surface roughness of a biomaterial, initial bacterial adhesion is also reduced, however there is now evidence that the introduction of discrete topologies on the micron-

and nano-scale, thereby increasing surface roughness, may modulate cellular attachment. Puckett et al., (2010) investigated bacterial attachment to increasing surface roughness by determining the adhesion of bacteria associated with implant infections such as *Staphylococcus aureus, Staphylococcus epidermidis* and *Pseudomonas aeruginosa* on altered titanium surfaces. Conventional titanium (nano-smooth) surfaces that possess micron size features were altered to nanorough (created by electron beam evaporation), nanotextured and nanotubular (created by anodization) surfaces as illustrated in figure 1.4. The study found that the adherence of *Staphylococcus aureus, Staphylococcus epidermidis* and *Pseudomonas aeruginosa* had was markedly reduced on the nanorough surface when compared to the conventional titanium surface, however it was also demonstrated that the adhesion of these bacteria had increased on the nanotubular and nanotextured surface. It was postulated that the bacterial attachment had increased on these surfaces because of a greater presence of fluorine on the material surface (as a product of the manufacturing process) however this can be challenged because in other studies (Yoshinari et al., 2001), it was found that fluorine possessed antibacterial activity. The findings in this study do however demonstrate that subtle alteration of surface roughness through nanotexturing has potential and further investigations are required.

Figure 1.4. SEM micrographs of Ti before and after electron beam evaporation and anodization: (a) conventional Ti; (b) nanorough Ti after electron beam evaporation; (c) nanotextured Ti after anodisation for 1 min in 0.5% HF at 20 V; (d) nanotubular Ti after anodisation for 10 min in 1.5% HF at 20 V. Scale bars =200 nm. Figure obtained from Pukett et al., 2010.
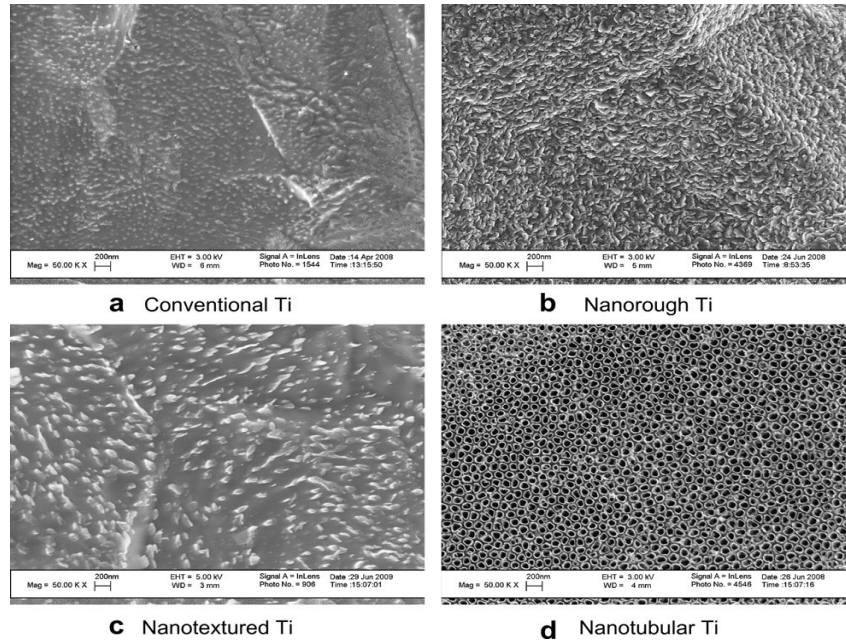
1.11.4 Antifouling Paints.

Biofouling is a process in which there is an accumulation of undesirable organisms such as microorganisms on a wetted surface. This process commonly occurs on the hulls of shipping vessels and results in the ship damage of the ship's hull. To counter this, antifouling paints have been applied to hulls as a way of reducing drag, fuel consumption and preventing biological growth. However, most of the paints used contained toxic chemicals that affected the reproductive capacity of marine organisms such as mussels (European Environmental Agency, 2006). As a result, the use of these paints has been banned, however; the development of an antifouling coating for dental implants could provide a novel system that could prevent bacterial adherence and the formation of a biofilm. In an article by Hannig and Hannig (2010), one form of an antifouling surface makes use of a nanocomposite surface

coating in which the easy-to-clean surface has a low surface energy that leads to poor protein to protein interactions and as a result, shear forces that are present in the mouth can easily remove the salivary pellicle and the bacterial biofilm from the surface of the material. If non-toxic this easy to clean surface could have potential use on the non-osseointegrating surfaces of titanium dental implants as it could prevent oral biofilms formed on the surface of the implant progressing to a pathogenic stage which could result in the peri-implantitis.

1.11.5 Improving the efficacy of antimicrobial mouth rinses with essential oils.

Essential oils are derived from the foliage of plants, through a steam or hydrodistillation process (Batish et al., 2008). Essential oils are composed of a complex mixture of monoterpenes and sesquiterpenes and a variety of constituents such as phenols, oxides, ethers, alcohols, esters, aldehydes (Batish et al., 2008; Langenheim, 2004). It is thought that in plants the presence of the volatile aroma compounds play a defensive role against herbivores, insects and pathogenic fungi (Langenheim, 1994). There is an increased interest in the use of essential oils in the role against disease, and for pest management especially because they are easily extractable, eco friendly and biodegradable (Isman, 2000; Pawar and Thakar, 2006: Abad et al., 2007). It was reported that most essential oils have low toxicity against vertebrates including fish, birds and mammals (Enan et al., 2008).

One key essential oil that has been investigated for its antibacterial and enhanced penetration properties is eucalyptus oil. The eucalyptus oil is extracted from the eucalyptus plant which belongs to a family of plants known as the Myrtacae which are native to Australia with 700 species (Brooker and Kleining, 2006). The eucalyptus family have foliage

that is rich in oil glands. The use of eucalyptus oil in the pharmaceutical, perfumery and commercial industry has meant that it is one of the world's most traded oils compared to oils extracted from other plant species (Boland et al., 1991: FAO, 1995).

The oil obtained from *Eucalyptus globulus* contains the monoterpene known as 1, 8-cineole which is the most important component (Duke, 2004 and Cimanga, et al., 2002). It has been reported that the 1,8-cineole results in an enhanced permeation of secondary molecules and in combination with chlorhexidine digluconate it leads to a synergistic antimicrobial activity against bacterial biofilms (Karpanen et al*.,* 2010), due to improved permeation and antimicrobial activity.

1.11.6 Toxicity of Eucalyptus oil and its application in vivo.

Eucalyptus oil is generally regarded as safe (GRAS) by the Federal and Drug Authority (FDA) of the United States of America (USEPA, 1993). The oil has also been given the non-toxic classification by the United Stated Environmental Agency (Batish, 2008; USEPA, 1993). The Council of Europe has given further approval in the consumption of the oil as a flavouring agent in foods of ≤ 5 mg/kg and in confectionaries with a content of ≤15 mg/kg in 1992 (Batish, 2008). Further work was carried out to determine the lethal dosage value (LD_{50}) which is a standard measurement of acute toxicity of a pesticide and is stated in mg of the pesticide per kilogram (kg) body weight (BW). The LD_{50} of Eucalyptus oil and the major constituents of the oil known as 1, 8-cineole was found to be 4440 mg/kg and 2480 mg/kg BW (Casida and Quistad, 1995).

1.12 Current applications of eucalyptus oil.

Eucalyptus oils have been used in a variety of applications such as in the fight against the hospital acquired superbugs that are resistant to commercial antimicrobials. A study carried out by Sherry et al., (2001) demonstrated that a topical application of the eucalyptus oil can eliminate methicillin resistant *Staphylococcus aureus* (MRSA). In another study by Trivedi and Hotchandani, (2004) commercially available eucalyptus oil consisting of 63% 1,8-cineole inhibited the growth of bacterial strains of *Klebsiella* spp., *Proteus* spp., *Pseudomonas* spp., *Escherichia coli,* and *Staphylococcus aureus* that were resistant to conventional antimicrobials such as tobramycin, gentamicin, amikacin, ciprofloxacin, chlorampehenicol and cefotaxime.

1.13 The use of UV light in formation oxygen radicals for the killing of bacteria.

1.13.1 Characteristics of titanium and the oxide layer.

Titanium dioxide (TiO_2) is the only naturally occurring oxide of titanium that exhibits important photocatalytic properties that exists as two main polymorphs, the metastable anatase and stable rutile. The photocatalytic properties of the metastable form of anatase are preferred to the stable rutile form because of its higher density of surface-adsorbed hydroxyl radicals (Hanaor, 2010).

1.13.2 The spectrum of UV light.

Radiometric analysis, includes the measurement of radiant energy and light in absolute power as shown below in figure 1.5. The energy of the UV light is found at a wavelength lower than visible light and is composed of UV A, B and C. The UV-A energy is found between 380 nm and 315 nm, UV-B is found in the range between 280 and 315 nm and the UV-C band

is present between the wavelengths of 280-200 nm. As UV wavelength decreases, energy increases (figure 1.5). The UV-C band gap has been found to be germicidal and research has been carried out to investigate its germicidal properties for surface decontamination (Gao et al., 2013). Clinically the UV-C could be utilised in the disinfection of dental implants pre and post placement as a means of preventing the incidence of peri-implantitis. UV-C does not penetrate the dermis of the skin and would not be harmful to cells and the tissue in the skin as shown in the figure 1.6.

Figure 1.5. An illustration of the UV wavelength spectrum which is made up of three emissions A, B and C.
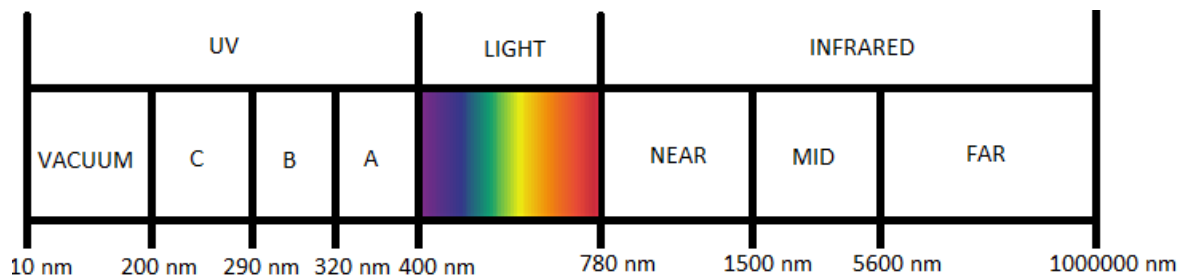
Figure 1.6. An illustration of the penetrative ability of the three bands of the UV irradiation. UVA (band gap 320 to 400 nm) irradiation is the most penetrative going down to the lower levels (Dermis) of the skin. The UVB irradiation (band gap 290 -320) penetrates the upper layers of the skin (epidermis) and UVC cannot penetrate the skin surface (band gap 200-290 nm).
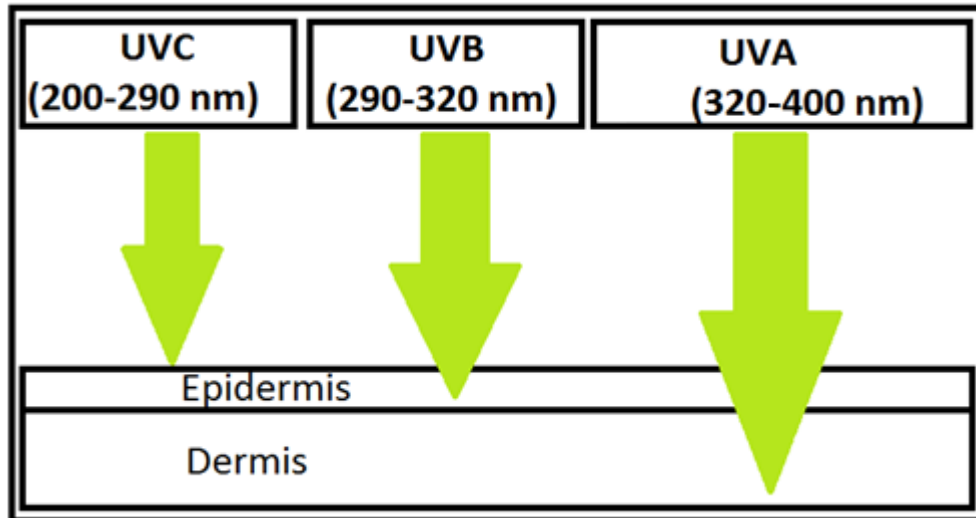
Photocatalytic activity was discovered in the 1960s when Fujishima et al., (1969) discovered electrodes coated with a photocatalytic polymorph of titanium dioxide known as anatase, could be used to "split" the water molecule to hydrogen and oxygen by photoilluminiation, termed the "Honda-Fujishima effect". The principle of the photocatalytic system involves generating active oxygen species such as $\cdot OH$, $O_2^{-\cdot}$, $HO_2^{\cdot}$, and H_2O_2 by a photocatalyst once illuminated with UV light such as the long wave UV A light (320-400 nm) (Fujishima, 2000; WHO, 2011). These oxygen species possess bactericidal properties that are able to damage the bacterial cell wall Reactive oxygen species such as those created by UV-induced photocatalytic activity decompose organic compounds, such as the bacterial membrane and are then able to enter the bacteria cell, causing the breakdown of proteins and lipids through the process of osmosis, the bacterial cells burst and die (Bekbolet, 1996). A rougher titanium surface results in more photocatalytic activity compared with a smooth titanium

surface. This is due to a larger surface area, which allows an increased reaction to light and H_2O adsorption. The effect of the UV light on the titanium oxide layer and the production of free radicals is shown in figure 1.7.

Figure 1.7. The Image illustrates the formation of the pathways in the generation of free radicals. The oxidation reaction leads to the formation of the free radical species by generating electron hole pairs from the valence band to the conductance band which generates oxygen radicals. Illustration taken from Tachikawa et al., (2010).

1.13.3 Previous investigations into using UV light in bacterial disinfection.

In a study by Suketa et al., (2005) the bactericidal properties of the photocatalytic anatase titanium dioxide (TiO_2) was investigated. The surface of CpTi disks are coated with photocatalytic anatase TiO_2 by plasma source ion implantation (PSII). The disks were seeded with *A actinomycetemcomitans* and *F nucleatum* and then exposed to UVA light and the number of viable cells present was determined. After 180 mins of exposure it was found that the number of viable bacterial cells from both types of bacteria was less than 20%; on control disks bacterial viability reduced to about 60-70%. This study demonstrated the potential of this non-invasive sterilization technique for use during dental implant procedures, however 180 mins is a very long time for a patient in the clinical setting.

In a study carried out earlier by the U.S. Environmental protection agency (Ireland et al., 1992), anatase TiO_2 was evaluated as a photocatalyst in the disinfection of *Escherichia coli* in a potable water reactor. An experimental TiO_2 photoreactor, which consisted of a steel jacket, a lamp and a photocatalytic sleeve, was made. The UV lamp on the reactor was covered with a fibreglass mesh which contained a layer of TiO_2. Once the UV lamp was turned on, it activated the TiO_2 layer and as a result produced hydroxyl radical species. Water used in the experiment was inoculated with *E.coli* and after turning on the UV lamps samples of water were then taken at regular intervals and the concentrations of colony forming units of *E. coli* were measured. The concentration of *E. coli* had reduced significantly from 3.4×10^7 CFU/mL when *E. coli* was first inoculated to 1.7×10^7 CFU/mL after 60 mins of exposure to the UV light. These findings showed the potential for the use of photocatalytic activity as a sterilization procedure in dental implants and to prevent peri-implantitis.

A study by Suketa et al., (2005) suggested that the photocatalytic system would be a useful system to pursue as a way of reducing the risk of peri-implantitis, as it was demonstrated that the number of *A. actinomycetemcomitans* and *F. nucleatum* was reduced to about 1%. However there are some issues with this technique as the photocatalytic system involves directly shining UV light onto a photocatalyst to produce active oxygen species that have bactericidal properties. This process has to be carried out at the time of implantation as the effect wears off over time (Hanoar, 2010 Another issue with the system is that it takes a long time (about 120 mins) but a higher intensity lamp could possibly be used to decrease the amount of time. Finally the effect on the process of osseointegration would need to be investigated. Sawase (2001) demonstrated that increasing the thickness of the naturally passive form of the titanium dioxide layer on the surface of the titanium implant did not

have any effect on osseointegration. However further work needs to be carried out to determine if a thick layer of anatase titanium dioxide affects the osseointegration ability of the implant.

The use of ultraviolet light has also been evaluated in a hospital setting by coating the floors with a photocatalyst; UV lights were incorporated on the room light and during the evening when the light was turned on the photocatalytic effect would kill bacteria (Norowski and Bumgardner, 2008). The use of photocatalysis for the decontamination of bacteria is advantageous because it avoids the possibility of the bacteria to develop resistance to antimicrobials (Norowski and Bumgardner, 2008).

1.13.4 Thermal oxidation treatment on the increased titanium oxide layer.

Dong et al., (1997) investigated modifying the titanium surface by increasing the TiO_2 layer through thermal oxidation to make it more resistant to wear under tribiological conditions. The study found that the morphology and density of thermally "grown" TiO_2 layer on Ti-6Al-4V is dependent on the time and temperature of exposure. It was found that a rough TiO_2 layer forms at high temperatures and long thermal oxidation treatment times.

1.13.5 Photodynamic therapy.

Photodynamic therapy involves three non-toxic components: oxygen, visible harmless light and a non-toxic photosensitiser (a photoactivatable substance) such as methylene blue (Takasaki et al., 2000). The principle action of photodynamic therapy involves applying the photosensitiser that binds to the bacterial cells and when a light with the appropriate wavelength is applied, reactive oxygen species and singlet oxygen cause bacterial cell death. Photodynamic therapy is novel in the field of dentistry and is applied to the area affected by

peri-implant disease. The affected site is mechanically debrided with the use of hand curettes and the photosensitiser injected. This is then light activated resulting in the production of reactive oxygen species that result in bacterial cell death and allowing the affected site to heal (Takasaki et al., 2000). Clinical kits are sold by Periowave ™ (Ondine Biopharma Corporation, Vancouver Canada). *In vitro* studies by Dobson and Wilson (1992) have demonstrated that the system was effective at killing bacteria. Cinical trials are in their infancy and further *in vivo* studies are needed (Meisel, 2005 and Cleplik, 2014).

1.13.6 Mechanism of microbial inactivation by photocatalysts.

It was initially thought the microbial inactivation with the use of a photocatalyst was due to the photocatalytic oxidation of the intracellular coenzyme A which is involved in the respiratory activity converting nutrients to biochemical energy (Matsunaga et al., 1985). Later Saito et al., (1992) proposed that cell death occurs due to the disruption of the cell membrane due to the leakage of Ca^{2+} ions. Further evidence of cell wall disruption was observed when an integral part of the Gram negative bacterial outer wall known as an endotoxin was shown to be degraded after photocatalysis with a TiO_2 substrate (Maness et al., 1999). The effect is consistent on both gram negative and gram positive bacteria. More recent research (Lu et al., 2003 and Kuhn et al., 2003) confirmed that bacterial cell death was caused by decomposition of the cell wall and that the leakage of the intracellular components and bacterial killing was dependent on the complexity and the density of the cell wall. The proposed mechanism for the loss of the intracellular bacterial components is illustrated in figure 1.8.

Figure 1.8. The effect of UV light on the surface of titanium sample results in the formation reactive oxygen species which in turn punches holes in the bacterial cell walls resulting in the leakage of the intracellular components of the bacterial cells. The leakage of the constituents results in the lysis of the bacterial cells.
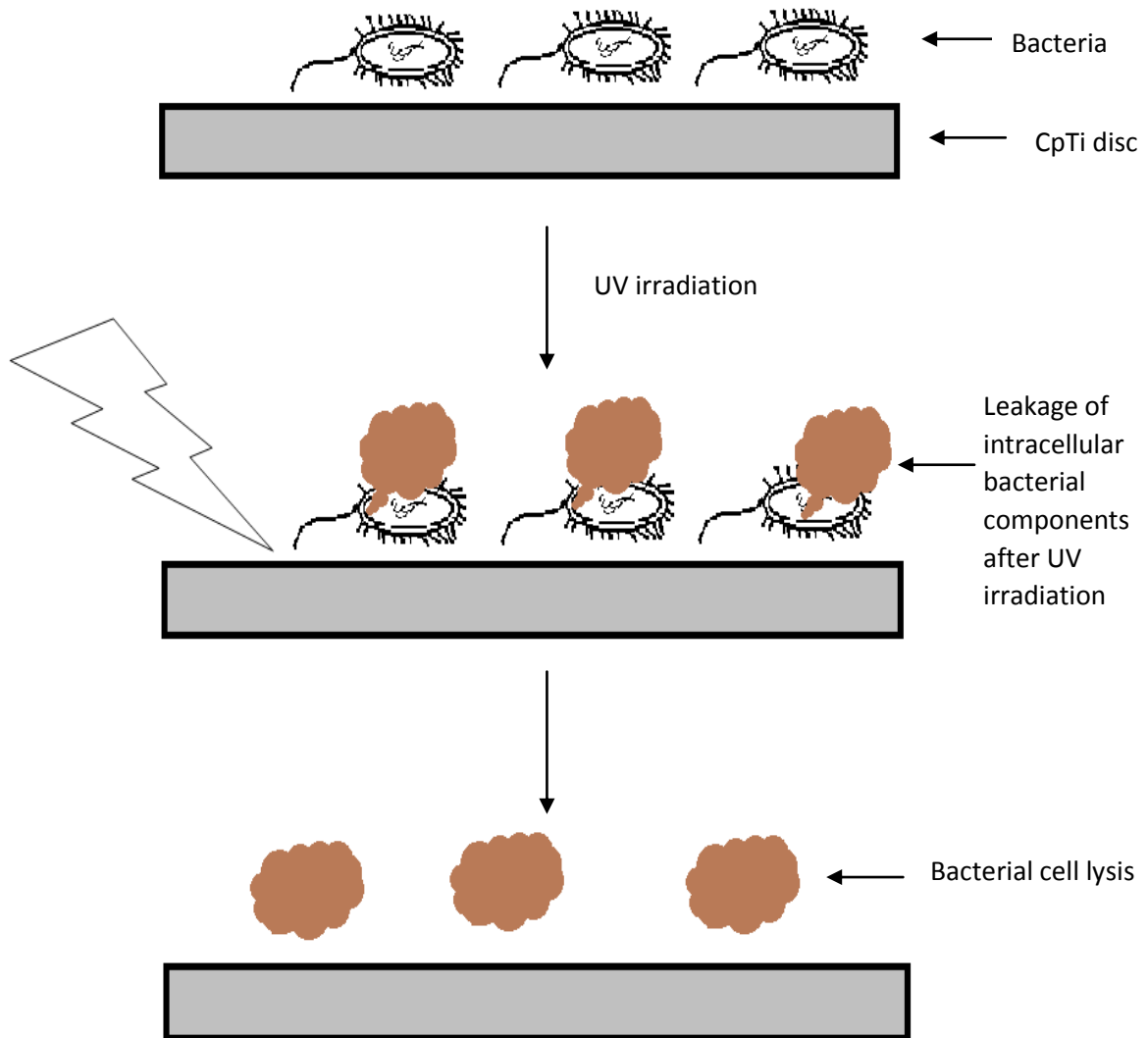
1.14 Aims and Objectives.

The initial adhesion and subsequent microbial colonisation of Ti dental implant surfaces results in peri-implant disease. Innovation is warranted to prevent the initial microbial adhesion to the Ti surface. Subsequently novel treatment modalities for the management and treatment of microbial colonisation of the Ti surface are needed. Therefore the overall aim of the study was to develop methods to prevent or treat microbial colonisation of titanium dental implant surfaces.

The specific aims of the study were as follows:

1) To systematically investigate the influence of topology on the initial bacterial attachment to the common alloy Grades of Ti that are used to manufacture dental implants.

2) To create a well characterised panel of surfaces with which to compare the effects of:

　　(i) Engineered surface topologies on initial adhesion of oral bacteria.

　　(ii) Prevention and disruption of colonisation through photocatalysis.

　　(iii) Disruption of early colonisation through chemo-mechanical methods.

CHAPTER 2: MATERIALS AND METHODS

2.1 Preparation, quality control and storage of culture media.

<u>Preparation of solid culture media.</u>

Blood agar plates (BA; Columbia agar base with 5% defibrinated horse blood and 20 mg of L-nicotinamide adenine dinucleotide (NAD)) with dimensions of 9 cm diameter and 1.3 cm thickness (bioMérieux, Hampshire, UK) were employed throughout the study to culture in-house strains of *Escherichia coli (NCTC 10401)* and *Streptococcus sanguinis* (originally obtained from Dr P. Handley, University of Manchester and previously known as *Streptococcus sanguis GWT*). Blood heart infusion (BHI) plates (Oxoid, Hampshire, UK) with dimensions of 8.5 cm diameter and 1.3 cm thickness were used to culture *Fusobacterium nucleatum* (ATCC 10953, ATCC, Middlesex, UK).

<u>Preparation of liquid culture media.</u>

Liquid media in the study were sterilised by autoclaving at 121 °C for 1 hr (Prestige Medical, Minworth, West Midlands, UK.)

Artificial saliva was used as a culture medium in studies of early bacterial adhesion and proliferation on Ti surfaces (section 2.5.7). Adopting the method described by Pratten, (1998), artificial saliva was prepared by sequentially adding to distilled water 0.35 g/L sodium chloride (NaCl), 0.2 g/L potassium chloride (KCl), 0.2 g/L calcium chloride (CaCl$_2$), 2 g/L yeast extract, 1g/L lab Lemco powder, 2.5 g/L hog gastric mucin and 5 g/L proteose peptone (reagents, suppliers and lot numbers reported in Table 2.1). Reagents were proportioned using an Ohaus T5400D precision balance accurate to 0.001 g (Ohaus

Corporation, NJ, USA) and following combination were mixed on a magnetic stir plate (Fisher Scientific, Loughborough, UK) at ambient temperature (22 ± 1 °C) for 1 hour. After autoclaving 1.25 mL of 40 % sterile filtered urea (Millex GP, 0.2 µm filter lot number R2CA91744) were added to 1 L of the prepared artificial saliva. The resultant media was wrapped with aluminium foil to exclude light and prevent protein degradation (Pachuau, Z. and Tiwari, R.C., 2008; Lodovivci, M., 2003) prior to storage at 4 ± 1 °C.

Tryptone Soya Broth (TSB) was prepared following the manufacturer's (Oxoid, Hampshire, UK) instructions by adding 30 g of the TSB to 1 L of distilled water before manually mixing to dissolve the broth. The TSB used in the inlet carboyl of the CDC biofilm reactor (Section 2.9.4.3) was a double concentration prepared by adding 60 g of TSB to 1 L of distilled water. The TSB was autoclaved 1 hr prior to use.

Table 2.1: Reagents, suppliers and lot numbers employed in the study.

Reagent	Supplier	Batch/ lot number
Acetone	Fisher Scientific, Loughborough, UK	1174369
Ammonium oxalate monohydrate	Sigma-Aldrich, Dorset, UK	Kr09003tQ
Blood agar plates	BioMérieux Ltd, Hampshire, UK	G11209
Brain Heart Infusion agar (BHI plates)	Oxoid Ltd, Bassingstoke, UK	1222557
Calcium chloride (CaCl$_2$)	AnalaR BDH, Poole, England, UK	TA748933
Carbol-fushin solution	Fluka analytical, St Gallen, Switzerland	1229737
Chlorhexidine digluconate solution (20% in H$_2$O)	Sigma-Aldrich, Dorset, UK	BCBH4944V
Crystal violet	AnalaR BDH, Poole, England, UK	K28661932

Eucalyptus oil 80-85 %	SAFC, Missouri, USA	MKBF5278V
Formaldehyde (Formalin, 37% solution)	Sigma-Aldrich, Dorset, UK	14K1269
Gluteraldehyde	Agar scientific, Essex, UK	29250
Hexamethydisilazane (HMDS)	Sigma-Aldrich, Dorset, UK	SHbb1678V
High Performance Liquid Chromatography water (HPLC)	Fisher Scientific, Loughborough, UK	1370598
Hog gastric mucin	Sigma-Aldrich, Dorset, UK	020M7011V
Hydrogen Peroxide (H_2O_2)	AnalaR BDH, Poole, England, UK	10128
Industrial denatured alcohol/ Industrial methylated spirit 99%	General medical, York, UK	01331111
L-alpha – lecithin, granular	Acros, Organic, Geel, Belgium	A0314135
Lab Lemco powder	Oxoid Ltd, Basingstoke, UK	3124346
Lugol iodine solution	Sigma-Aldrich, Dorset, UK	018k2510
Methylene Blue (MB)	Sigma-Aldrich, Dorset, UK	056K0739V
pH4 – Calibration	BDH Prolabo, Poole, England, UK	09C090509
pH7 – Calibration	BDH Prolabo, Poole, England, UK	09A160501
pH10 – Calibration	BDH Prolabo, Poole, England, UK	09B25011
Potassium chloride (KCL)	AnalaR BDH, Poole, England, UK	TA611838432
Potassium hydrogen phosphate	Sigma-Aldrich, Dorset, UK	110K026815
Potassium phosphate diabasic	Sigma-Aldrich, Dorset, UK	BCBG0398V
Proteose Peptone	Fluka Analytical, St Gallen, Switzerland	1379803
Sodium chloride (NaCl)	Sigma-Aldrich, Dorset, UK	122K0084
Sodium dihydrogen orthophosphate (H_2NaO_4P)	AnalaR BDH, Poole, England, UK	51987905
Sodium hydroxide (NaOH)	Sigma-Aldrich, Dorset, UK	4411001511

Sodium Tetraborate	Sigma-Aldrich, Dorset, UK	35H0556
Triton x - 100	Helena Biosciences Europe, Newcastle, UK	304493
Tryptone Soya Broth (TSB)	Oxoid Ltd, Bassingstoke, UK	1374133
Tween - 80	Sigma-Aldrich, Dorset, UK	52B1240V
Urea	Sigma-Aldrich, Dorset, UK	BCBG7647V
Yeast extract	Oxoid Ltd, Basingstoke, UK	121

Phosphate buffered saline (PBS) was prepared by adding 7.75 g of sodium chloride (NaCl) , 0.2 g of potassium hydrogen phosphate (K_2HPO_4) and 1.5 g of potassium phosphate dibasic to 1 L of distilled water and dissolving at room temperature by stirring. The PBS was autoclaved at 121 °C for 15 mins prior to use.

Fixative

McDowell's and Trump's 4F:1G fixative (4F:1G) was employed as a fixative in studies of bacterial adhesion to the Ti substrates. 4F:1G was prepared by sequentially combining and stirring:- 86 mL of distilled water, 10 mL of Fisher F-79 (37-40 %) formaldehyde, 4 mL of 25 % biological grade glutaraldehyde and 1.16 g of sodium dihydrogen orthophosphate (H_2NAO_4P). Approximately 0.27 g of sodium hydroxide (NaOH) was added to obtain a pH of 7.3 ± 0.1 as 1M NaOH. The pH was measured with a Jenway pH meter (3310, Essex, UK) (McDowell and Trump, 1976; Dykstra, 1993). The fixative was selected because of its long shelf life for storing and transporting biological samples.

Physiological saline.

0.85 g of NaCl was dissolved in 100 mL of distilled water and sterilised

Crystal violet solution.

The crystal violet solution was prepared by dissolving 2 g of a powdered form of crystal violet in 20 mL of ethanol. Subsequently this solution was mixed with 0.8 g of ammonium oxalate dissolved in 80 mL of distilled water. Solutions were filtered before use (Grade 1 cellulose paper, 15 mm diameter: 11 µm pore size, Whatman Ltd, Maidstone, UK).

2.2   Maintenance of test microorganisms.

2.2.1 Choice of bacteria for bacterial adhesion and proliferation.

The Gram-positive bacteria *Streptococcus sanguinis* and *Streptococcus mutans* and Gram-negative bacteria *Fusobacterium nucleatum* and *Escherichia coli* were used in the current study. *S. sanguinis* is an initial coloniser of the formed pellicle on the surface of a tooth or a Ti implant surface. *F nucleatum* acts as a significant linker between the initial colonisers and late colonisers of complex biofilms on both teeth and dental implant surfaces (Kolenbrander, 2011).

2.2.2   Storage of bacteria.

The stock microorganisms *Streptococcus sanguinis, Streptococcus mutans*, *Fusobacterium nucleatum* and *Escherichia coli* were maintained on porous beads using the PL160 Pro-Lab storage system (Pro-Lab, Texas USA) and were frozen at -20 °C. To recover a microorganism, a sterile plastic loop was used with an aseptic technique to remove a single bead from the storage tube. The bead was streaked on the surface of the solid media. This media was then

incubated (Anaerobic work station, Don Whitely Scientific, West Yorkshire, UK) at 37 °C in an atmosphere of 10 % carbon dioxide, 80-85 % nitrogen and 5-10 % hydrogen for 24 hrs.

2.3 Quality control of bacterial stock.

2.3.1 Gram stain.

A drop (approximately 0.1 mL) of the autoclaved physiological saline was placed on a microscope slide and a bacterial colony was emulsified with the use of a sterilised metal loop. The slide was heated with a Bunsen flame to fix the bacteria and stained with crystal violet solution for 30 s. The slide was then gently rinsed with water and then was re-stained with Lugol's iodine. After rinsing the microscope slide, the bacterial cells were differentiated with acetone for 2-3 s and then removed by further rinsing in water. The slide was then counter stained with carbol fuchsin solution for 30 s prior to rinsing. The slide was subsequently blotted dry using absorbent tissue paper and the bacterial cells examined under light microscope (Leitz Wetzlar, Leica Microsystems GmbH, Germany) using the oil immersion method and 1000 x magnification.

2.3.2 Catalase test.

The catalase test was performed by picking off a single bacterial colony from the culture plate with the use of a capillary tube (LG-9060-100, Lab Glass, Cambridgeshire, UK). Care was taken when picking colonies from a blood agar plate to avoid touching the media as this could potentially result in a false positive measure. The other end of the tube was inserted into a 3 % solution of hydrogen peroxide and inverted to allow the hydrogen peroxide solution to run down the tube and contact the picked colony. A positive reaction was indicated by the formation of bubbles (oxygen).

2.3.3 Storage of bacteria.

The prepared liquid media was stored at room temperature 20 ± 3.5 °C. The agar plates were resealed in their plastic and kept at 4 °C to prevent dehydration.

2.4 Preparation of Ti samples.

2.4.1 Preparation of different surface finishes.

Commercially pure Ti (CpTi) as ASTM Grade II, Grade IV and its alloy Grade V (Ti-6Al-4V) were commercially sourced (Titanium Products Ltd, Birmingham, UK) in the form of discs 14 mm in diameter and 1 mm in thickness. The upper and lower surfaces of the Ti discs were prepared by sequential polishing on a grinding and polishing machine (DAP-7, Struers, Ballerup, Denmark) with waterproof silicon carbide grit papers (Struers, Ballerup, Denmark) from P220 through P320, P500, P800, P1000, P1200, P2400 up to P4000 with distilled water as a lubricant. The diameter of the grit corresponding to the grit papers is reported in table 2.2. 10 discs of Ti Grade II, IV and V each were manufactured for each surface finish determined by the final SiC abrasive grade. Mirror-like surfaces were created by further polishing the P4000 surfaces on a MD chem disc (Struers, Ballerup, Denmark) with colloidal silica particles of 0.04 µm using water as a lubricant Struers, Ballerup, Denmark). Ti surfaces were degreased by sonicating the samples for 10 min each in acetone followed by ethanol and distilled water. The samples were air dried in a water and oil free airstream. Prior to storage the discs were sterilised by autoclaving for 1 hr.

Table 2.2: The diameter of SiC grit particles in relation to the SiC abrasive Grade.

SiC Paper Grade	Diameter (µm)
P220	68
P320	46
P500	30
P800	22
P1000	18
P1200	15
P2400	10
P4000	5

2.4.2 Engineered Ti surfaces.

2.4.3 Scanning laser melting (SLM).

An additive layer manufacturing technique was used to create micro-patterned Ti surfaces. Three 5 x 5 mm "island" textures and three linear scanning patterned samples were created by the research group (Professor Moataz Attallah, University of Birmingham, Metallurgy and Materials department) Ti-6AL-4V was used as a substrate powder and disc shaped specimens fabricated using SLM (scanning laser melting). A concept laser M2 Cusing SLM system (ES technology Ltd, Oxfordshire, UK) which utilises an ND:YAG laser with a wavelength of 1075 nm and a maximum laser output of 200 W was employed. The laser was operated at 200 W power and a scanning speed of 1300 mm/s. The prepared samples were degreased by sonicating them in an ultrasonic bath for 10 mins in acetone, ethanol and distilled water in sequence. The SLM samples were subsequently sterilised.

2.4.4 Ti Foil, compact oxide, nanopore, nanotubule and Ti samples.

A series of nano-textured anodised Ti surfaces were investigated. Specimens were prepared by a collaborating group (Professor Ales Iglic, Laboratory of Biophysics, University of

Ljubljana, Slovenia). The Ti samples exhibited a surface area of 1 cm^2 and possessed surfaces containing (i) TiO$_2$ nanotubes having diameter of 15 nm, (ii) nanotubes with a surface diameter of 50 nm, (iii) nanotubes having a diameter of 100 nm, (iv) compact oxide, (v) a nanoporous surface and (vi) Ti foil. All samples were created from Ti foils (99.6 % purity) with 0.1 mm thickness which was degreased by successive ultrasonication steps in acetone, ethanol and deionised (DI) water for 5 mins each prior to drying in a nitrogen air stream. Anodisation was performed with electrolytes containing Ethylene Glycol (EG) at various concentrations supplemented by hydrofluoric (HF) acid to create the different nanostructures. The optimal voltage utilized for the creation of the Ti structures with various surface diameters had been previously optimised by the collaborating group. The parameters utilised for the creation of the Ti surface are shown in Table 2.3.

Table: 2.3: Anodisation conditions utilized in the creation of compact oxide, nanopore (NP) and nanotubule (NT) surface diameters. The electrolyte, potential voltage (V) and the anodisation time are described.

Nanopore/Nanotube Diameter	Electrolyte	Potential (V)	Anodisation Time
Compact Oxide	1 M Phosphoric acid	20 V	15 min.
15 nm NP	EG + 6 M water + 0.2M	10 V	1 hr.
15 nm NT	EG + 8 M water + 0.2M	10 V	2.5hr.
50 nm NT	EG + 8 M water + 0.2M	20 V	2.5hr.
100 nm NT	EG + 8 M water + 0.2M	58 V	2.5hr.

2.4.5 X-ray Photoelectron spectrometry (XPS) of the Ti foil, compact oxide, nanopore, nanotubule and Ti samples.

The fluoride content of the Ti foil, Compact Oxide, 15 nm NP, 15 nm NT, 50 nm NT and 100 nm NT was determined with X-ray Photoelectron Spectrometry (XPS). The XPS measurements were commissioned from Midlands Surface Analysis Ltd, Aston University,

Birmingham to determine the fluoride content on the surface of the prepared samples. The XPS analysis was conducted in a Thermo Fisher ESCALAB 250 electron spectrometer equipped with a hemispherical sector energy analyser (Thermo Fisher Scientific Inc, Waltham, Massachusetts, USA). A monochromatic Al Kα X-ray source was used for analysis to enhance the resolution. A source excitation energy of 15 KeV, an emission current of 6 mA, an analyzer pass energy of 20 eV with step size of 0.1 eV and a dwell time of 50 ms were used throughout the experiments The base pressure within the spectrometer during examinations was always below 5 x 10^{-10} mbar which ensured that all signals recorded were from the sample surface. The area of analysis was selected to be 500 µm diameter.

XPS survey scans were first recorded for each region examined and then narrow region energy scans for all the elements identified on the surface. Narrow scans allowed determination of the chemical state of the specific element identified. To improve statistics, multiple scans were always used for all the constituents in the surface.

2.5 Storage of the prepared Ti samples.

The surfaces of the Ti discs described in section 2.4.1 prepared were dried with an air stream of nitrogen gas and stored in sealed Petri dishes prior to use in microbiological experiments or surface analysis.

2.6 Characterisation of the prepared Ti samples.

The Ti samples were characterised by using scanning electron microscopy (SEM), sessile drop contact angle measurements and surface profilometry. The characterisation enabled qualitative and quantitative measures of the surface topology in order to correlate the effects of surface finish on microbial adhesion.

2.6.1 Preparation of the Ti samples before SEM analysis.

The Ti samples were gold sputter coated to reduce the charging observed on the sample surface before SEM images were captured. An Emitech K550X (Kent, England, UK) sputter coater was employed to coat the samples for 2 mins at a current of 25 mA giving a coating thickness of approximately 15 nm.

2.6.2 SEM analysis.

The CpTi Grade II, IV and V Ti discs were imaged with SEM to compare the created surface topologies. Standardised images were obtained using a Zeiss EVO® MA10 microscope (Carl Zeiss Jena GmbH, Oberkochen, Germany) operating in high vacuum secondary electron mode at an accelerating voltage of 10-30 kV, working distance 6-10 mm. Images were captured at increasing magnifications: x100 x2000 and x8000.

2.6.3 SEM analysis of Ti substrates with increased surface oxide film thickness.

Standardised images of Ti surface topologies created by thermal oxidation or anodisation were obtained in secondary electron mode. The CpTi Grade II, IV and the alloy Grade V samples were imaged at 4 regions of the surface with a 2000x magnification. To obtain an optimum image of the substrate surface the parameters for acquiring the SEM images were a working distance of 7 mm and, an accelerating voltage of 5 kV and an I-probe current of 67 mA.

2.6.4 Surface metrology using non-contact profilometry.

Surface metrology was performed on the prepared Ti substrates using non-contact profilometry (Talysurf CLI 2000, Taylor-Hobson Precision, Leicester, UK). A chromatic length

aberration gauge with a 300 μm range and was employed with resolution of 33 picometers (pm) in the z-axis and a scanning at a speed of 500 μm/s. A central 5 x 5 mm region of the Ti disk was scanned using 1000 parallel traces each recording 1000 data points resulting in a resolution of 5 μm in the x-axis and 5 μm in the y-axis. A 0.25 mm cut-off Gaussian filter according to ISO 4287 was employed. Three samples for each Grade of the prepared substrate were scanned. The parameters obtained of the measured surface were Rp, Rv, Rz, Rc, Rt, Ra, Rq, Rsk, and the Rku. The parameters defined by the international organisation of standardisation (ISO) are defined in Table 2.4.

Table 2.4: Definitions of surface roughness profile parameters as obtained by scanning the prepared substrate surfaces with a non-contact Talysurf CLI 2000, Taylor-Hobson Precision profilometer (Taylor Hobson, Leicester, UK).

Roughness parameter	Definition
Rp	The maximum distance between the peak and the mean line in the sampling length
Rv	The maximum distance between the valley and the mean line in the sampling length
Rz	The average vertical distance, in microns, between valleys and peaks across a sample surface.
Rc	Mean height of the roughness profile elements
Rt	The maximum distance between valley and peak in the sampling length
Ra	The arithmetic mean deviation of the roughness profile from the mean line.
Rq	Root mean square of deviation (peaks and valleys) from the mean line.
Rsk	Skewness (Rsk) is a measure of the average of the first derivative of the surface (the departure of the surface from symmetry). A negative value of Rsk indicates that the surface is made up of valleys, whereas a surface with a positive skewness is said to contain mainly peaks and asperities.
Rku	Kurtosis of roughness profile is a measure of the sharpness of the profile peaks.

2.6.5 Contact angle measurements.

The contact angle measurements were carried out to determine the wettability of the substrates. The static sessile drop method was employed for the measurement of the contact angle between distilled water or artificial saliva on the prepared CpTi and Ti-6Al-4V surfaces. 20 µL of PBS or artificial saliva were pipetted on to the surface of disks using a Hamilton microtitre syringe (Hamilton, Bonaduz, Switzerland) and the media was left to equilibrate on the substrate surface for 1 min. The contact angle measurements were carried out with the rough surfaces of the Ti samples prepared by SiC polishing in parallel and perpendicular to a Hitachi CCD camera (KP-M1E-S10). Images of the droplets were recorded using Optimas software version 4 (Bioscan, Washington, USA) and the contact angle of the droplet calculated For measurements at 37 °C, the substrate temperature was kept constant using a temperature controlled hot plate (Fisher scientific, Leicestershire, UK). Temperature measurements on the substrate surface were carried out with the use of an infrared thermometer (Ebro TFI 650, Ebro Electronic GmbH, Ingolstadt, Germany) and recorded as 37 ± 2°C.

Contact angle measurements carried out on the surface of the Ti foil, compact oxide, nanopore, nanotubule with 15, 50 100 nm diameter tubules and on the other anodised Ti surfaces were obtained with the use of a Digidrop contact angle meter (GBX, Romans Sur Isère, Drôme, France) at the University of Aston, Department of Chemical Engineering and Applied Science The equipment was set according to figure 2.1. Measurements were undertaken using HPLC grade water. Three drops of the HPLC water with a volume ranging from 2- 2.5 µL were placed with a syringe tip of 0.65 mm on three different areas of the

samples. The HPLC water was left to equilibrate on to the surface for 30 s before the sequence captured by the camera was processed with the GBX Visiodrop software (GBX, Romans Sur Isère, Drôme, France). The average of the left and right angles of the droplet was analysed after 5 time points after placement onto the surface of the samples being investigated. An example of the droplet placed onto the surface of the sample and the contact angle measurement carried out on the surface is illustrated in figure 2.2.

Figure 2.1. Photograph illustrating the setup of the digidrop contact angle meter, the volume of the HPLC water placed on the surface of the sample was controlled with a syringe driver. The sample being investigated was placed on the stage and the contact angles measured on the computer with the GBX visiodrop software.

Plunger   Syringe   0.65 mm syringe tip   Stage   Computer loaded with the GBX Visiodrop software
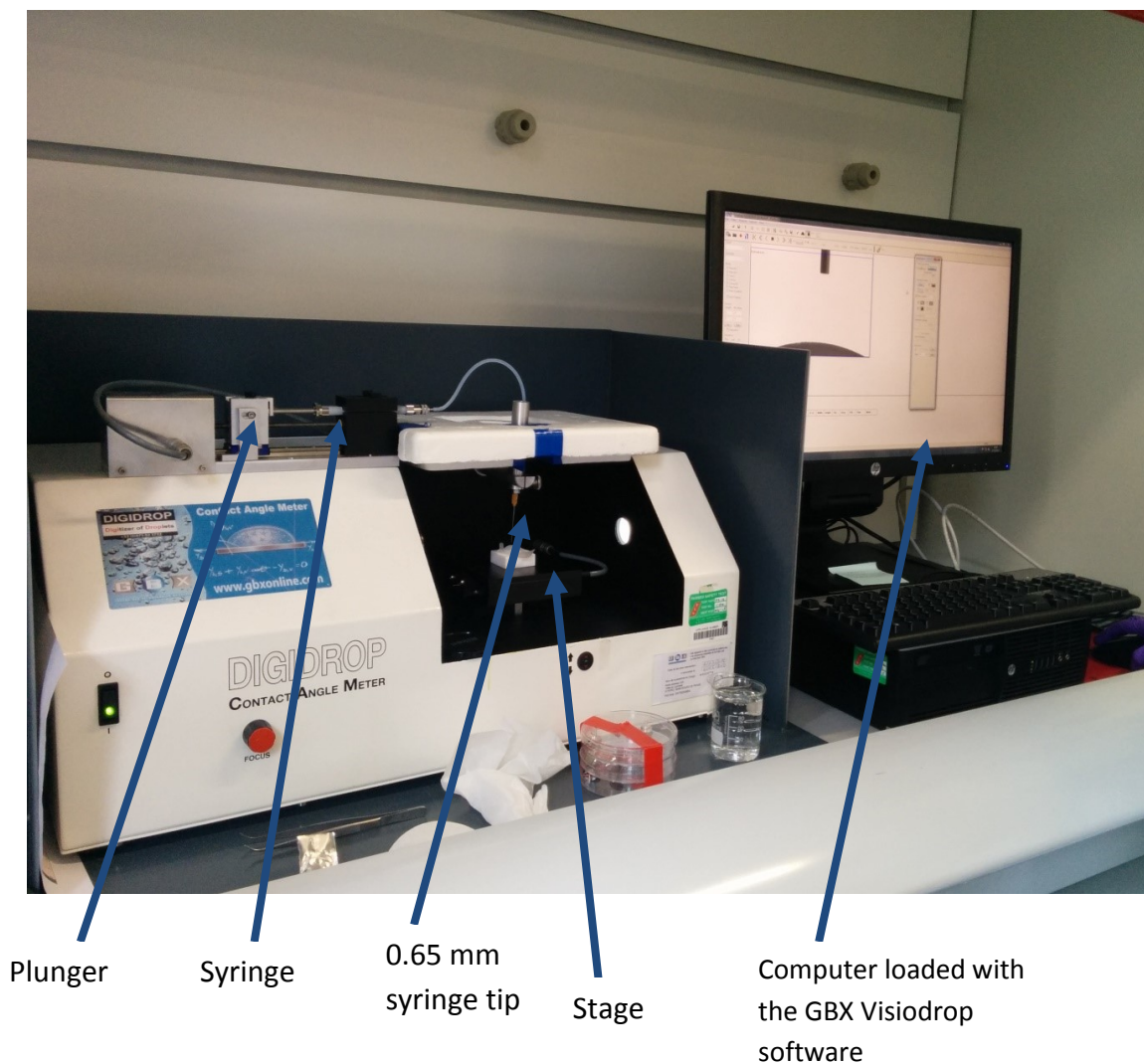
Figure 2.2. Photograph illustrating the analysis of the contact angles with the GBX Visiodrop software on the surface of the sample being investigated. The red triangle is drawn onto three edges of the droplet for the software to determine the contact angles.
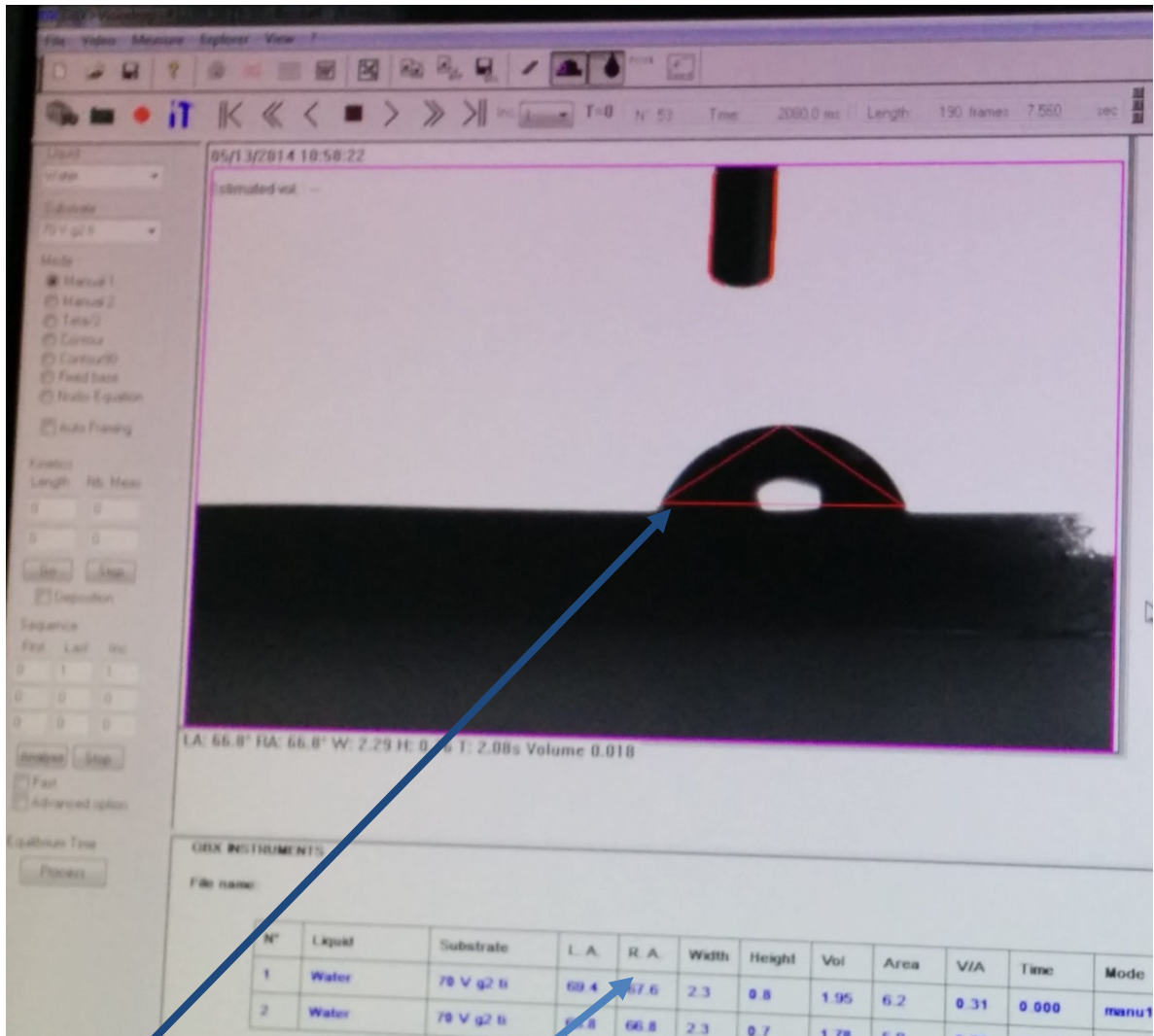
HPLC water droplet

Left and Right angles of the water droplet being calculated by the GBX Visiodrop software to determine the contact angles at 5 different time points.

2.7 Bacterial adhesion and proliferation on the prepared Ti substrates.

2.7.1 Test tube method for the adhesion of the bacteria to Ti samples with different surface roughness.

Prepared samples of CpTi Grade II, IV and the Ti-6Al-4V alloy Grade V disks (n=5) were aseptically placed (laminar flow cabinet, Bioair, B3 Aura) in disposable biosilicate culture tubes (Fisher scientific, Leicestershire, UK) with 10 mL of artificial saliva inoculated with 50 µL of an overnight culture of *S sanguinis,* F *nucleatum, E coli* or a mixture of *S sanguinis* and *F nucleatum* and incubated for 18 ± 4 hrs. As there were too many different samples to test in one run the experiment was carried out with two sets of samples with different surface roughness. Initially P220, P500, P1000, P1200, P2400 and P4000 polished Ti samples were incubated for 24 hrs with constant agitation (IKA Vibrax VXR basic) at 100 rpm in an anaerobic work station (Don Whitley Scientific, West Yorkshire, UK) with an atmosphere of 5-10% hydrogen, 10% carbon dioxide and 80-85% nitrogen. The disks (n=4) were rinsed by immersion 3 times in PBS to remove loosely adhered bacteria. A positive control disk (n=1) was then placed in 1 mL of 4F:1G fixative for an hour and prepared for SEM analysis (section 2.5.8). The test disks (n=3) were individually placed in universal tubes with 10 mL of PBS solution and were sonicated for 10 min in an ultrasonic bath (Vitasonic, Bad Säckingen, Switzerland) and vortex mixed for 15 s with a whirlimixer (Fisher scientific equipment, Leicestershire, UK) ensuring the detachment of the adherent bacteria (n=3)*.* The viable bacteria were quantified by serial dilution: 0.2 mL of the sonicated and vortexed PBS was pipetted into 1.8 mL of PBS to achieve a 1×10^{-1} dilution, and further diluted to 1×10^{-2}. 0.1 mL of the 1×10^{-2} dilution was spread on to the surface of horse blood agar plates with a sterile plastic loop and incubated overnight. The number of colonies formed on the surface of the blood agar plates was counted to determine the CFU/mL. The procedure was

repeated with disks that had a P220, P320, P800, P1200 and P4000 surface finish. A P220 finish was used as a control in both parts of the experiment to allow comparisons to be made.

2.7.2 Bacterial adhesion to Ti foil, compact oxide, nanopore, nanotubule 15 nm, nanotubule 50 nm and nanotubule 100 nm.

A colony of *S sanguinis* was inoculated into 10 mL of artificial saliva and incubated for 24 hrs at 37 ± 0.1 °C in a biosilicate glass test tube (Fisher scientific, Loughborough, UK) under anaerobic conditions. The culture was agitated at 100 rpm. The initial concentration of the bacteria was determined by carrying out a serial dilution. The bacterial culture was vortexed to separate the clumps of bacteria and diluted 1 in 10 (10 µL in 990 µL) in to fresh artificial saliva and the starting concentration of the *S sanguinis* bacteria was found to be 2 x 10^9 cells per mL. Ti foil control and test surfaces were placed face down on 5 µl of the 1/10 diluted bacterial suspension containing 2 x 10^8 CFU/mL. The samples were incubated in a Petri dish for 1 hr in an anaerobic work station (Don Anaerobic work station, Don Whitely Scientific) at 37 °C in an atmosphere of 10 % carbon dioxide, 80-85 % nitrogen and 5-10 % hydrogen for 24 hrs. The samples were rinsed by immersion in PBS three times to remove loosely bound bacteria. Four samples of each type were then placed in separate 7.0 mL bijou tubes (50mm x 20mm) containing 5 mL of sterile PBS. These were then placed in a sonic water bath (Vitasonic, Bad Säckingen, Switzerland) for 10 mins and vortex mixed for 15 s to detach the bacteria that adhered to the surfaces (n=4). 0.1 mL of the sonicated and vortexed sample was plated onto blood agar plates (BioMérieux, Hampshire, UK) and incubated for 24 hrs in an anaerobic cabinet. The number of colonies grown on the surface of the blood agar plates

was then counted to determine the number of bacteria (CFU) detached from the samples into the PBS. The experiment was repeated with *S mutans* bacteria.

2.7.3 SEM analysis on the bacteria adhered to the Ti surfaces.

Images of adherent *S sanguinis* and *S mutans* on the prepared Ti foil, compact oxide, Nanopore, Nanotubule 15, Nanotubule 50 and Nanotubule 100 surfaces were captured to compare adhesion and distribution and after detachment to confirm the removal of the bacteria from the surfaces as described in section 2.6.2.

2.8 The effect of UV irradiation on thermally oxidised Ti substrates.

2.8.1 Characterisation and calibration of the UV light engine.

The effect of UV light on the surface of the prepared Ti substrates was investigated with an Omnicure series 1000 UV light engine (Lumen Dynamics, Ontario, Canada). The UV light engine was calibrated by determining the spectral output and the absolute irradiance values. The spectral output was determined by measuring the UV output with a USB spectrophotometer (Ocean Optics, Florida, USA) at 10 % power. The spectral data was acquired with Spectrasuite software, (Ocean Optics, Florida, USA) and plotted and the absolute irradiance values were determined using Sigma Plot software (version 12, Systat Software, Chicago, USA). The correlation between power output and the absolute irradiance values was determined in a range from 1 % to 25 % power of the light engine.. Three measurements were taken from each percentage power output for the emitted spectrum using a 200 μm fibre and the data acquired with the use of a USB spectrophotometer (Ocean Optics, Florida, USA). The absolute irradiance values were determined with the Spectrasuite

software, (Ocean Optics, Florida, USA) and a calibration curve plotted. The light acquisition

equipment set up is shown in figure 2.3.

Figure 2.3. The setup of the UV light engine probe with the fibre to determine the UV emission spectrum.
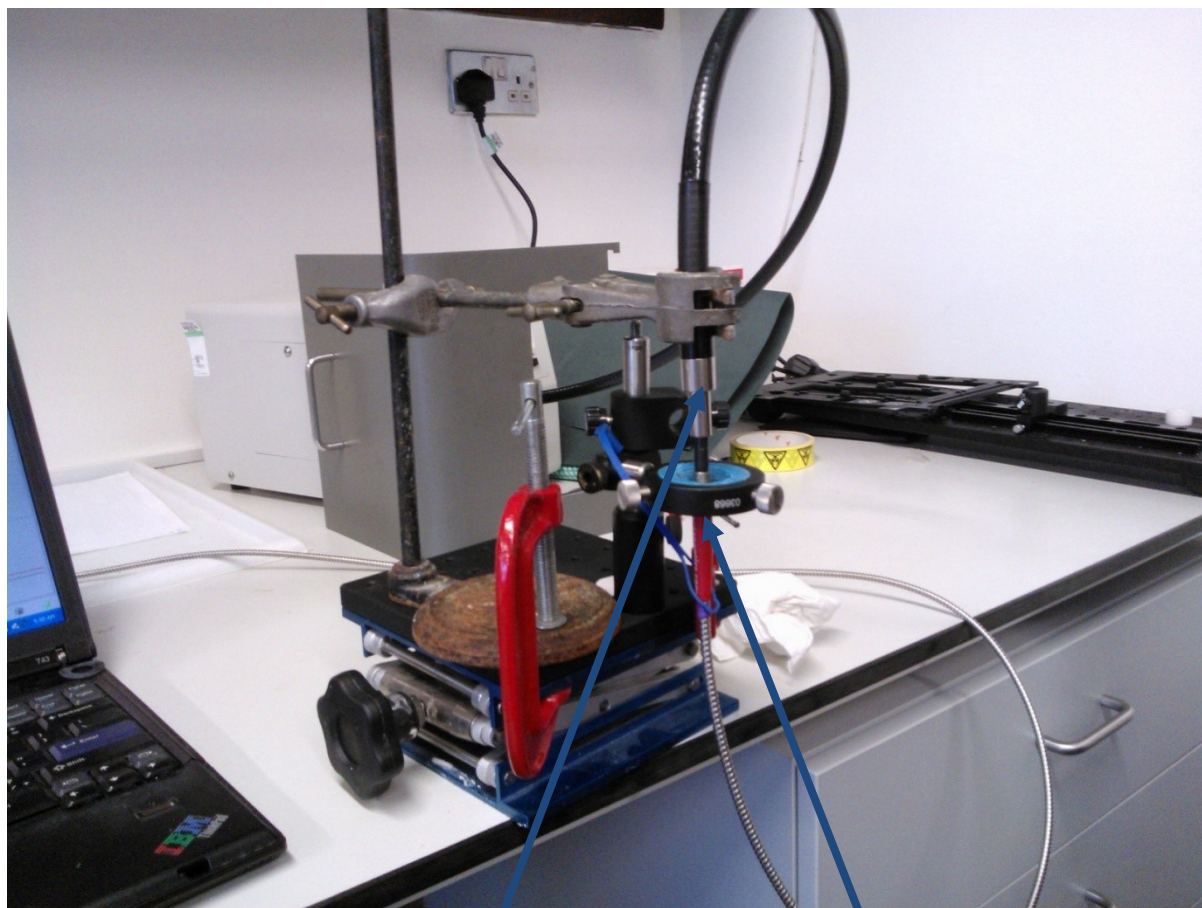
UV Probe   Spectral Acquisition
                            fibre

2.8.2 Preparation of methylene blue dye.

The degradation of MB dye was investigated in the evaluation of the photocatalytic activity

of Ti samples with different passive surface oxide layer thicknesses. A range of

concentrations of aqueous solutions of MB, ranging from 0.5 ppm-500 ppm (1.56 µM-1560

µM), were prepared from the stock solution. The pH of the solutions was reduced from pH 6

to pH 3 by incrementally adding 1M hydrochloric acid to aid the absorption of the dye onto

the surface of the prepared Ti substrate The pH change was determined by using a calibrated Jenway pH meter (3310, Essex, UK). The absorbance spectra of the methylene blue concentrations were determined with a USB spectrometer (Ocean optics, Florida, USA). An absorbance peak was identified at 665nm, which was utilised in the acquisition of data from the methylene blue degradation studies with the prepared Ti substrates.

2.8.3 Determination of the photocatalytic activity of the anodised and the thermal treated Ti samples with the use of the methylene blue dye system.

A DH-2000 deuterium tungsten halogen light source (Ocean Optics, Florida, USA) was connected to a Hellma light acquisition box (Hellma, GmbH and Co, Germany) using a 200 μm diameter fibre. The fibre was then connected to the USB spectrophotometer (Ocean Optics, Florida, USA). The system and acquisition software were calibrated by placing distilled water in a cuvette and setting the spectra suit software with an acquisition time of 173 s and a box car width of 5. To calibrate the methylene blue dye system the spectral acquisition mode on the spectra suite software was enabled, the halogen bulb from the DH-2000 light source was then switched on and the light emission stored, the light source was then turned off and the dark spectrum was then acquired. Once calibrated the software was set to acquire the emission at a wavelength of 665.03 nm.

The Ti test samples were then placed in a 12 well culture plate with 5 mL of 5 ppm methylene dye. The UV light engine fibre was set to distance of 5 cm above the sample with the use of clamps. The UV light engine was then switched on and the absorbance of the methylene blue dye was determined every 5 mins for 120 mins. The methylene blue degradation system was utilised for determining the effect of the UV light on the control

polished 50, 100, 150 hour thermal treated samples of Grade II, IV and V prepared Ti samples.

2.8.4 Preparation of the thermal treated Ti samples.

To artificially 'grow' the Ti oxide surface layer to a 1-3 μm thickness CpTi Grade II, IV and the Grade V alloy samples with a P4000 surface finish were heated in a furnace maintained at 600 °C for 50 (n=8), 100 (n=8) and 150 hrs (n=8) (Elite thermal systems LTD, Market Harborough, Leicestershire, UK), prior to slow cooling to room temperature over a period of 2-6 hrs.

2.8.5 Preparation of the anodised Ti samples.

The Ti samples were anodised by placing the samples in an electrolyte solution that consisted of 5 g/ L borax solution. The anodisation of the Ti samples was carried out with a power supply (HSYPY-120-01, China) which delivered fixed currents of 10 V (n=5), 70 V (n=5) and 120 V (n=5). A Ti rod acting as the anode was placed in the borax solution using an anode crocodile clip. The Ti discs acted as the cathode and were anodised by submerging them in the borax solution for 30 s at 23 ± 1 °C

2.8.6 Energy Dispersive X-ray spectrometry (EDX) measurements of CpTi Grade II, IV and V after anodising the samples.

The prepared anodised Ti surfaces were inserted into a Zeiss EVO MA 10 SEM microscope following the degreasing procedure (described previously in chapter section 2.5.1.3). The elemental composition of the prepared anodised surfaces was acquired in the secondary electron mode at a magnification of x2000 at a working distance of 8.0 – 8.5 mm, an I probe of 1 mA, a spot size of 548 and an accelerating voltage of 15 kV. Oxford Instruments (Oxford, UK) X-Ray detector and INCA software were used to acquire X-ray spectra and determine the

elemental composition of the samples, the acquisition time was set at 65 s with the acquisition rate of 1.50 or 15kcps.

2.8.7 The effect of UV light on the prepared Ti substrates after contamination with culture medium.

Grade IV control polished at P4000, thermal treated for 50, 100, and 150 hrs were placed into universal tubes containing 2 mL of TSB for 48 hrs and then transferred to artificial saliva for a further 24 hrs in an anaerobic chamber at 37 °C The samples were removed from the universal tubes and irradiated as described in section 2.8.6.

2.8.8 Bacterial adhesion to the Ti samples after UV irradiation.

The effect of UV irradiation and the adhesion of *S sanguinis* on the surface of the prepared Ti samples were also determined. An *S sanguinis* bacterial culture was grown for 24 hrs in 10 mL of artificial saliva. The Ti samples (n=4) were irradiated at 25 % power for 60 s before 25 μL of the bacterial culture was placed on the surface of the control polished and thermally treated samples. A sterilised glass cover slip was placed on the surface of the samples and incubated for 1 hr in the anaerobic chamber. The samples (n=3) were then immersed in sterile PBS 3 times to remove loosely bound bacteria before being placed universal tubes containing 10 mL of PBS and sonicated for 10 mins and vortexed with a whirlimixer for 15s 10 μL of the PBS were then pipetted on to the surface of the blood agar plates and spread using a sterile plastic loop. The blood agar plates were then incubated for 24 h before the bacterial colonies were counted. One sample of each prepared surface was placed in fixative (formulation was described in chapter section 2.1.2.4) to prepare the sample for SEM imaging.

2.8.9 The effect of anodised Ti and its effect on bacterial adhesion after UV irradiation.

The effect of bacterial adhesion on anodised Ti samples were determined with *S sanguinis, E coli* and *S mutans.* The methodology for bacterial adhesion is described in the chapter section 2.8.8.

2.8.10 The effect of a penetration method of eucalyptus in a Chlorhexidine Digluconate mouth-wash formulation.

The effectiveness of an oral mouth wash formulation with a potential enhanced penetrative ingredient of eucalyptus oil was determined on artificially grown bacterial biofilms. The biofilms of *S sanguinis* and *S mutans* were grown using a bioreactor and then exposed to the mouthwash.

2.8.11 Minimum inhibitory/bacterial clearance concentrations of the mouth wash formulation constituents.

A colony of the *S sanguinis* bacterium was picked using a sterile blue inoculating loops (Fisher Scientific Ltd, Loughborough, UK) and inoculated in a conical 250 mL flask containing 100 mL of sterile TSB. The conical flask was agitated constantly at 100 rpm (IKA Vibrax VXR basic, Werke Staufen, Germany) in a mini MACS anaerobic work station (Don Whitley Scientific, West Yorkshire, UK) at 37 ± 1 °C in an atmosphere of 10 % carbon dioxide, 80-85 % nitrogen and 5-10 % hydrogen for 24 h.

Individual components of IPA, CHG, EO and ethanol were added to determine their antimicrobial activity (minimum inhibitory concentration (MIC)). Double dilutions of the test agents were made in 500 µL of double strength TSB, which was inoculated with 10 µL of overnight *S. sanguinis* broth culture with a starting concentration of approximately 10^6 CFU/mL with an agitation speed of 150 rpm in an aerobic work station at 37 ± 1 °C for 18 h.

The lowest concentration that produced 10 or fewer CFU was the MIC. MICs were determined visually and more accurately with spectrophotometric readings at a wavelength of 560 nm with distilled water and TSB as a reference. The MBCs were also determined by plating the incubated MIC dilutions incubated for 18 hrs onto sterile nutrient agar plates. The plates were incubated at 37.0 ± 0.2 °C in the anaerobic workstation. The minimum bactericidal concentration (MBC) was determined as the lowest concentration which shows a log 3 (99.9%) reduction in CFU/mL of *S. sanguinis.*

2.8.12 Preparation of the CHG: EO formulation.

30 mL of the Chlorhexidine digluconate: eucalyptus oil formulation was made up as follows: 2 % eucalyptus oil (Sigma-Aldrich, Dorset, U.K.), 0.2 % chlorhexidine digluconate (Sigma-Aldrich, Dorset, U.K.), 10 % ethanol (Genta Medical, York, U.K.), 1 % tween-20 (Sigma-Aldrich, Dorset, U.K.) made up to 30 mL with sterile distilled water.

2.8.13 Preparation of the neutralising solution.

A neutralising solution was prepared with 1.17 % (w/v) lecithin, granular, molecular weight (Mw) 750 Acros Organics (Fisher Scientific, Leicestershire, U.K.), 2 % (v/v) tween-80 (Sigma-Aldrich, Dorset, U.K.), 0.785 % (w/v) sodium thiosulphate pentahydrate (BDH Ltd, Poole, U.K.) and 0.1 % (v/v) triton X-100 (Sigma-Aldrich, Dorset, U.K.), made up to 1 L with distilled water. The solution was sterilised at 121 °C for 40 mins wrapped in aluminium foil and stored at 4 °C until required.

2.8.14 The growth of an early biofilm on the surface of Grade IV Ti substrate with a CDC biofim reactor.

Bacterial biofilms of *S sanguinis* were grown on Grade IV surfaces (prepared to a P4000 SiC surface) by employing an anaerobic/sealed CDC biofilm reactor Model CBR 90-3-DH-int (Biosurface Technologies Corp, Montana, USA). The DC biofilm reactor set up is illustrated in figure 2.4 and figure 2.5. Rods of the CDC biofilm reactor were modified to include Ti samples with a diameter of 14 mm. 24 CpTi Grade IV discs were secured into 8 rods of the biofilm reactor with screws and autoclaved for sterilisation. 450 mL of TSB was added to the biofilm reactor and 1 mL of an *S sanguinis* and *S mutans* bacterial culture was pipetted into the bioreactor. Bacteria were incubated in the batch phase for 24 hrs at 37 °C before one Ti control sample was removed to determine the growth of the bacterial biofilm on the surface of the disc using SEM. The fed batch (continuous flow) of incubation was then commenced by turning on the peristaltic pump (101 U/R, Watson Marlow, Cornwall, UK) at a setting of 6 which resulted in an output of 1 mm/s into the waste carboy for 24 hrs. A control sample was removed after 48 hrs of incubation in the biofilm reactor to observe the bacterial biofilm that had grown on the surface of the Ti disc. The remaining discs were removed from the biofilm reactor after 48hrs and placed in universal tubes containing 2 mL of artificial saliva. The universal tubes were then incubated in the anaerobic chamber for 24 hrs at this stage one disc of the Grade IV Ti sample was prepared for SEM analysis. The Ti samples were then exposed to the antimicrobial solutions for 2 mins before being exposed to the CHG:EO formulation.

Figure 2.4. A photograph illustrating the setup of the CDC biofilm reactor for the growth of early bacterial biofilms on the surface of the Ti surface.
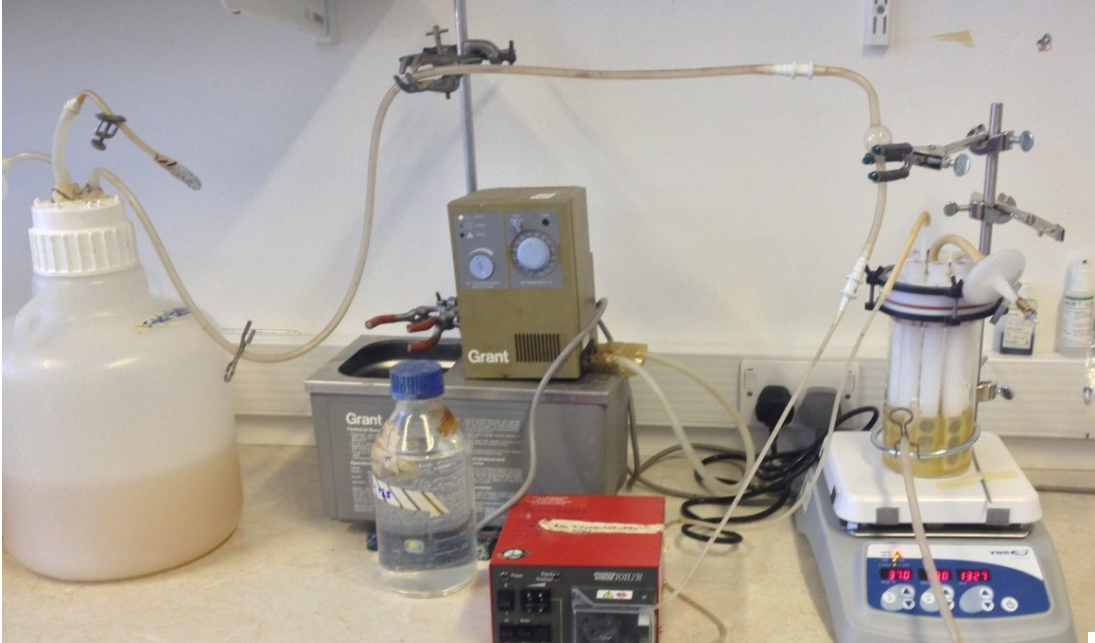
Inlet containing fresh TSB

Peristaltic pump

CDC bioreactor

Magnetic stirrer/hotplate

Waste/outlet

Figure 2.5. Schematic of the CDC biofilms reactor. The image shows the CDC biofilm reactor with spaces for 8 rods. The rod consists of three openings that allow the placement of the Ti discs. The discs are secured with screws. Image was obtained from www.biofilms.biz.
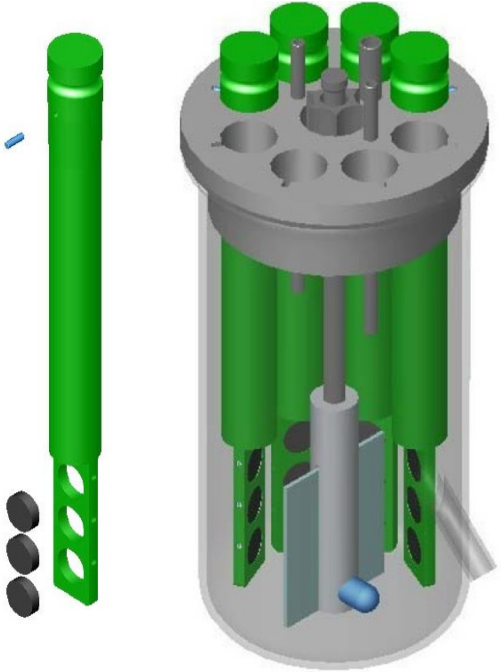
2.8.15 Bacterial viability methodology with viability counts.

The Grade IV Ti discs were removed from the rods of the biofilm reactor and placed into universal tubes containing 2 mL of the CHG:EO formulation for 2 (n=3), 15 (n=3) and 30 (n=3) mins to replicate clinically relevant time points. The control samples were exposed to sterile PBS (n=3) for similar times. After exposure the Ti discs were placed in the neutralising solution for 2 mins. The samples were rinsed by immersion in 10 mL of PBS 3 times to remove loosely bound bacteria from the surfaces and then placed in universal tubes with 10 mL of PBS before the samples were sonicated for 10 min and vortex mixed for 15 s. to detach the bacteria adhered to the surfaces. The PBS was then diluted 100 fold and 100 µl was then spread on blood agar plates and incubated in the anaerobic work station for 24 h before the number of bacterial colonies was counted.

2.8.16 Reduced exposure time for the early bacterial biofilms.

The effect of mouth-rinse formulation was further investigated on the early biofilms formed at a reduced exposure time of 30 s with increased sample numbers from n=3 to n=8. The method for this was described in section 2.8.15.

2.8.17 The effect of biofilm disruption and exposure of the CHG:EO formulation.

The biofilm on the Ti surface formed in the bioreactor after 48h was disrupted by using a cytoOne cell scraper (Starlab UK, Ltd, Milton Keynes, UK). The biofilm was scrapped twice. After disruption of the biofilm, the Grade IV CpTi surface was exposed to the CHG:EO for 30 s 2, 15 and 30 min as described in section 2.8.15. The metabolic activity of *S sanguinis* and *S mutans* following interventions was determined using an ATPase assay (Bactiter-Glo^{TM} Microbial Cell viability assay, Promega, Madison, USA) as described in 2.8.18.

2.8.18 ATPase assay.

The metabolic activity of *S sanguinis* and *S mutans* following interventions was determined using an ATPase assay (Bactiter-Glo[TM] Microbial Cell viability assay, Promega, Madison, USA). The substrate and buffer were stored at -20 °C on arrival. The reagents were thawed to room temperature and prepared for use by mixing the 10 mL of the Bactiter-Glo[TM] buffer to reconstitute the lyophilized enzyme/substrate mixture to form the BacTitre-glo[TM] reagent as described by the manufacture. The reagent was mixed by gentle vortexing and swirling. A white, opaque walled 96-multiwell plate (Costar, Corning International, New York, USA) was employed for carrying out the assay.

The assay was carried out by pipetting 100 µL of the test solution into the multiwell plate and 100 µL of the Bactiter-Glo[TM] reagent added. The plate was agitated for 5 mins to thoroughly mix the Bactiter-Glo[TM] reagent with the test solution. The luminescent signal was measured with the use of a luminometer over a period of 30 min (Tristar multimode reader, model LB2 942, Bertold technologies, Bad Wilbad, Germany). The luminiescent signal was acquired with use of the MikroWin 2000 software, version 4.4 (Mirotek labrosysteme GmbH, Overath, Germany).

2.8.19 Dehydration of substrates with adhered bacteria for SEM imaging.

A series of ethanol dilutions consisting of 20, 30, 40, 50, 60, 70, 80, 90, 95 % and 100 % ethanol (E/0650DF/17, Fisher Scientific) were prepared using distilled water. After fixation, the Ti discs were placed in each of the ethanol dilutions in turn for 10 min from the 20 % ethanol through to the 100 % ethanol. The Ti discs were then transferred to a fume cupboard and the ethanol was removed and replaced by 1 mL of

hexamethydisilazane (HMDS, Sigma-Aldrich). The HMDS was then removed and the discs were left to air dry for 24 hrs at ambient temperature in a fume cupboard.

2.8.20 SEM analysis of the bacterial biofilm present on the prepared Ti surfaces.

The distribution of the bacterial biofilm present on the surface the prepared Ti samples after 24, 48 hrs incubation in the CDC biofilm reactor and a further 24 hrs in artificial saliva was visualised with SEM. The detachment of the bacterial biofilm after sonicating for 10 mins and vortex mixing for 15 s was also visualised by SEM. four regions of the Ti disc surface were imaged as described in section 2.6.2.

2.9 Statistical Methods

Parametric statistics were used throughout these studies after preliminary testing for normality in the data produced using Analyses of Variance (ANOVA) or student t-tests using SPSS statistical software (SPSS Inc, USA). Correlation tests for metrological data and bacterial counts were undertaken using Spearman's Rank Correlation Coefficients. In all cases $\alpha = 0.05$.

CHAPTER 3: RESULTS.

3.1 The effect of surface topography on bacterial adhesion.

The surface topography of Ti dental implants may an effect on bacterial adhesion. To investigate the effect, Grade II, IV and V Ti specimens were created by polishing with SiC abrasive grit of P220, P320, P500, P800, P1000, P1200, P2400, P4000 and P4000 further polished with 0.04 µm colloidal silica. The surfaces were subsequently characterised with SEM imaging, 3D metrology measurements and contact angle measurements. The adhesion of *S sanguinis, E coli, S mutans* and *F nucleatum* were determined and the correlation between surface roughness parameters evaluated.

3.1.1 Characterisation of Ti substrates using SEM.

Figure 3.1. SEM images of Grade II CpTi surfaces prepared with a final grade of SiC abrasive paper of a) P220, b) P1000, c) P4000 or d) P4000 finished with 0.04 µm colloidal silica at x8000 magnification. a) Illustrates surface features consistent with the coarse abrasive size created on the P220 finish. b) Demonstrates uniform peaks and troughs present on the surface of a P1000 finish. The mirror-polished surfaces (c and d) are smoother but scratches or possibly impurity inclusions can be observed (indicated by the circles).
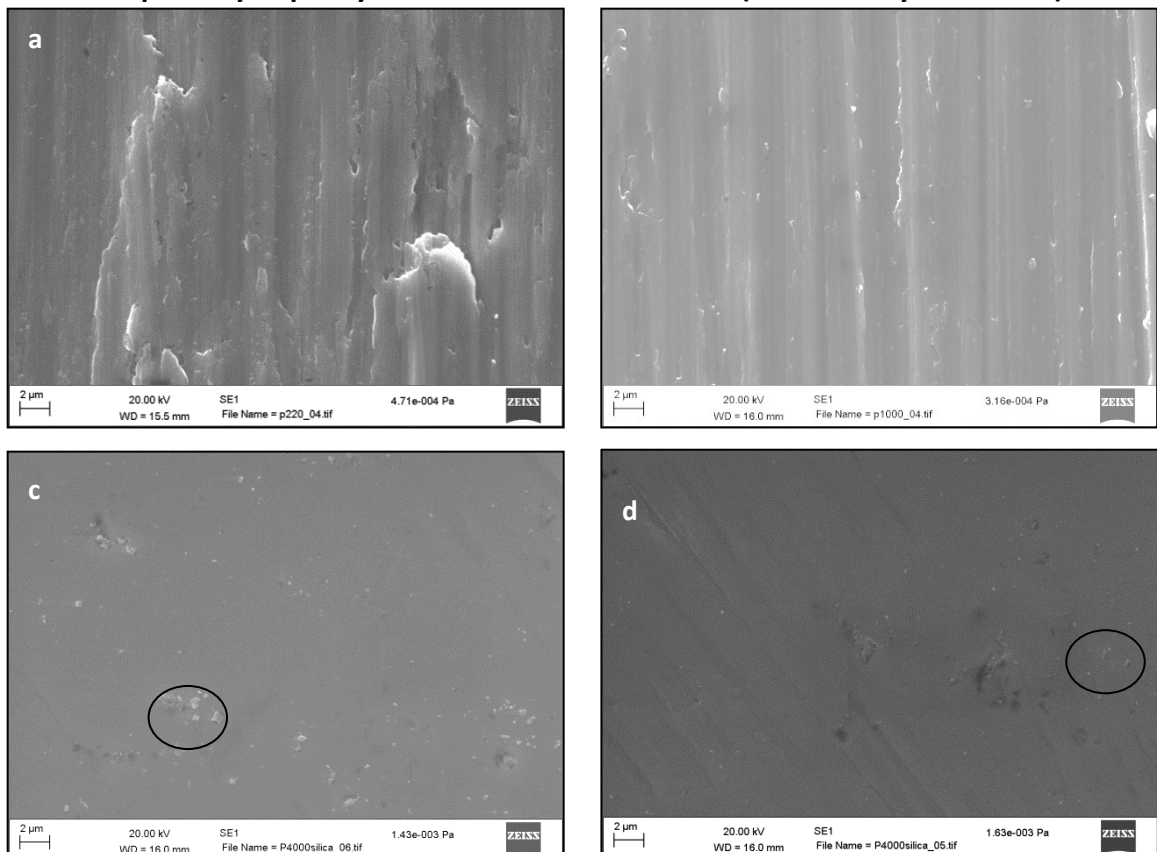
Figure 3.2. SEM images of Grade IV CpTi surfaces prepared with a final grade of SiC abrasive paper of a) P220, b) P1000, c) P4000 and d) P4000 finished with 0.04 μm colloidal silica at x8000 magnification. Features are similar to those observed for Grade II CpTi, although regular 'waviness' features related to the machining process were more pronounced in all finishes, which could be attributed to the relatively increased harness of the substrate when compared with Grade II CpTi.
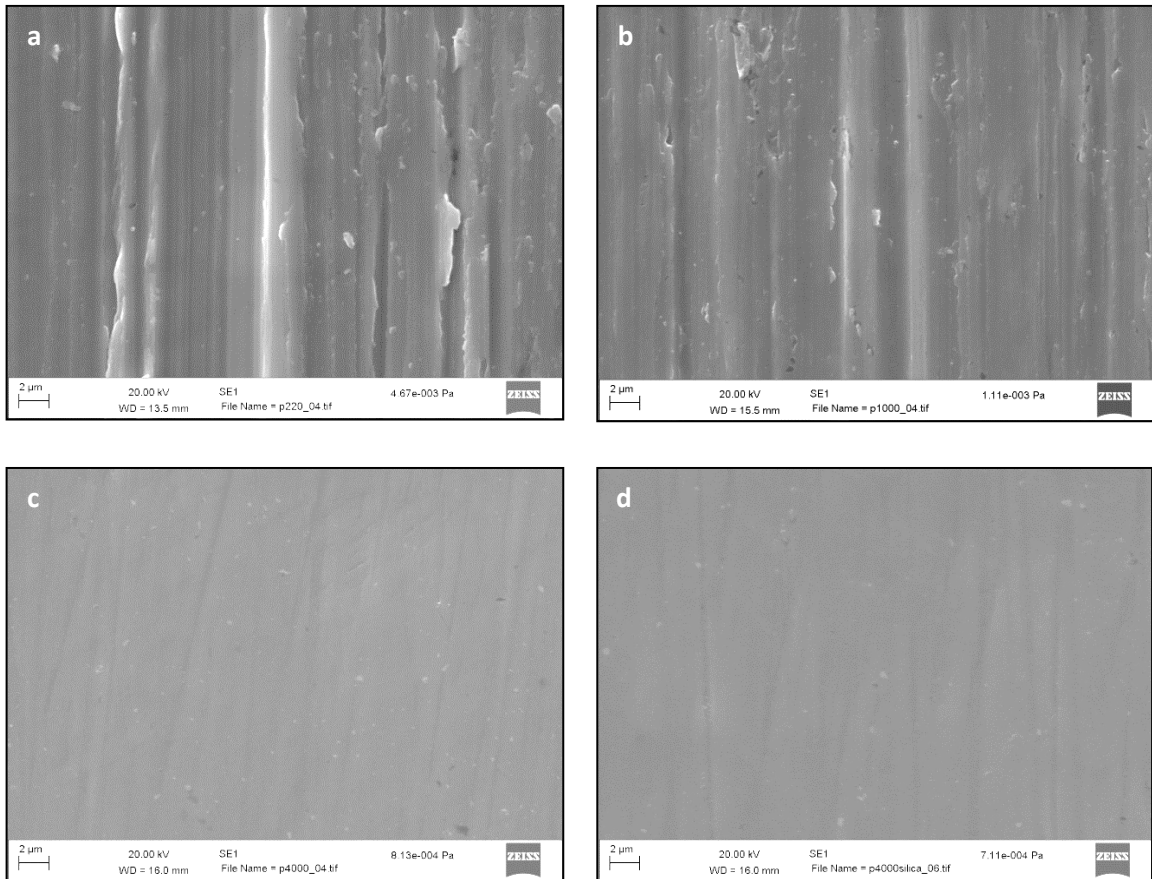
Figure 3.3. SEM images of Grade V Ti surfaces prepared with a final grade of SiC abrasive paper of a) P220, b) P1000, c) P4000 and d) P4000 finished with 0.04 μm colloidal silica at x8000 magnification. Grade V Ti has the highest hardness and machining 'waviness' was observed clearly in 3.3a and 3.3b.
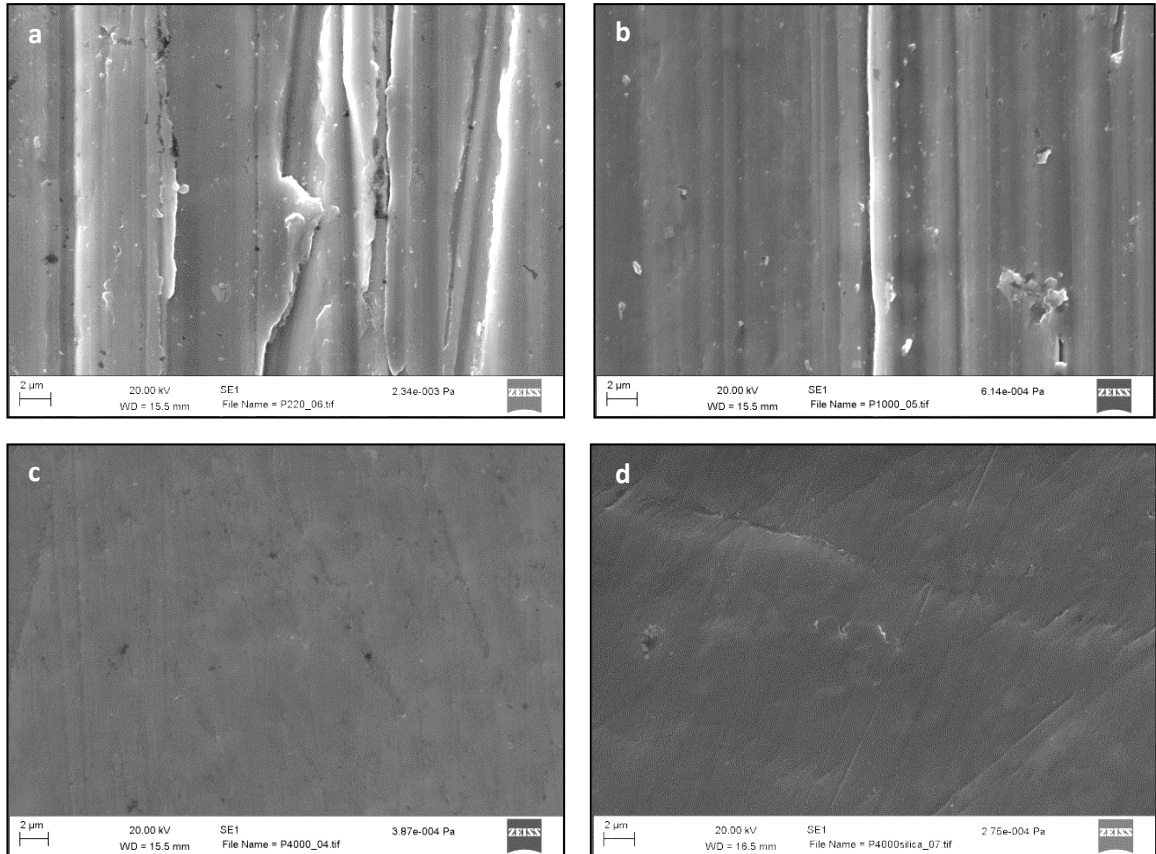
Figures 3.1, 3.2 and 3.3 illustrate the unique surface textures introduced by the different final SiC polishing papers. With the coarsest grit size P220 SiC papers an irregular surface consisting of peaks and troughs parallel to the polishing direction are clearly observed. With further polishing up to P1000 a more uniform surface finish was observed with a reduced distance between parallel features. For Grade II CpTi which has the lowest surface hardness machining features were least pronounced. This subjectively assesses rougher surface textures that have been created by P220 and P1000 SiC final abrasive grit sizes were more likely to shield bacteria from mechanical or hydraulic removal forces. The smoother surface textures that were created with silicon carbide papers of P4000 and P4000 finished with

0.04µm colloidal silica to create mirror like surfaces appear to be very smooth when visually observed however, when observed under SEM scratches or defects on a length scale larger than individual micro-organisms were observed. Grade II, IV and V Ti were utilised as they are utilised for dental implant fixtures.

3.1.2 Quantification of surface roughness using non-contact metrology.

3D surface metrology measurements were performed on the prepared Ti substrates under investigation. Multiple quantitative parameters characterising the surface topology were produced. An example of a 3D topological measurement from which roughness parameters can be calculated as illustrated in figure 3.4

Figure 3.4. 3D image of the topology produced by polishing a) Grade II CpTi, b) Grade IV CpTi and c) Grade V Ti with a P220 grit size SiC abrasive. Each image consists of 1000 individual line scans over a 5x5 mm² area at the centre of each specimen.
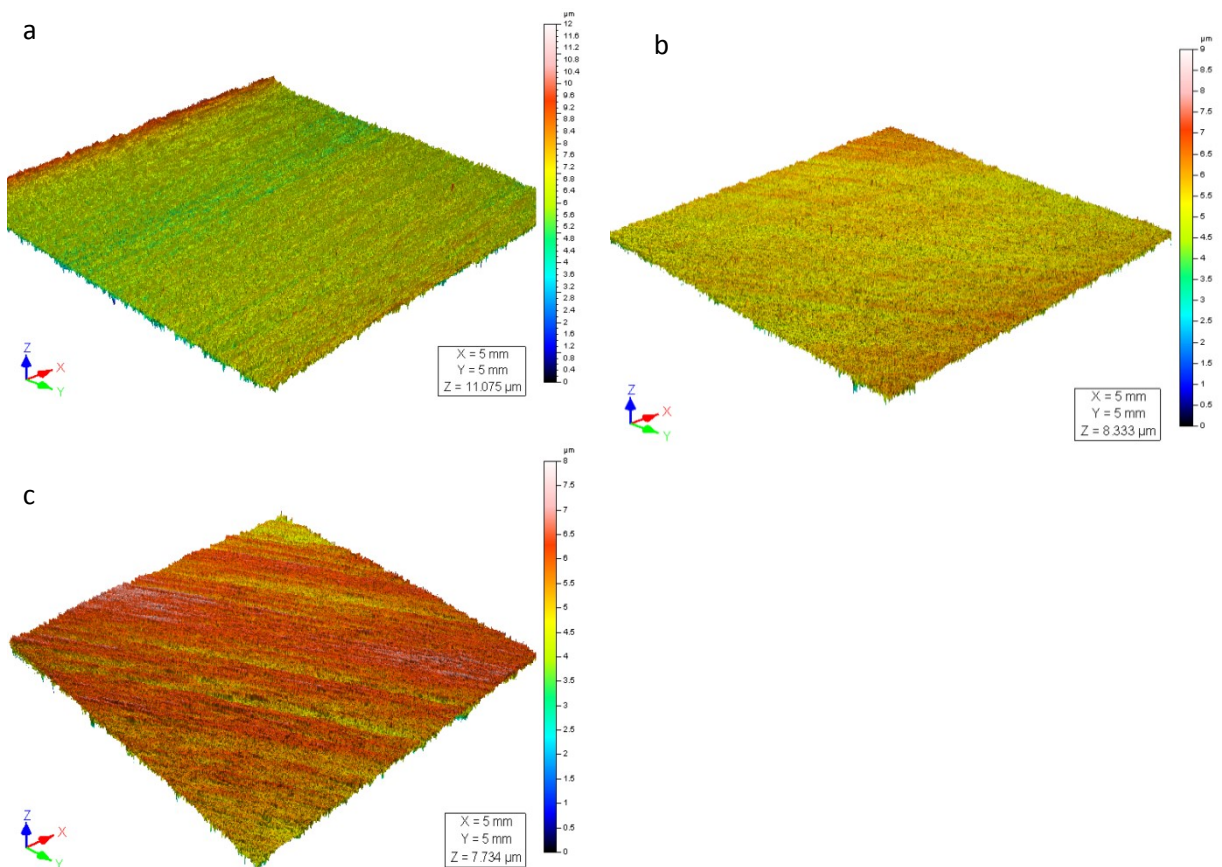
3D topological images were obtained for each surface preparation. Figure 3.4 demonstrates the difference in response of the 3 alloys to surface grinding and polishing which will be a function of the respective surface hardness. For the softest substrate CpTi Grade II, the mean z-value (maximum to minimum height of the surface profile) was 11.1 µm when compared to the CpTi Grade IV (figure 3.4b) which had a z-value of 8.3 µm. The hardest Ti alloy, Grade V exhibited the lowest z-value of 7.8 µm.

Subsequently for each Ti substrate and for each finishing grade of SiC abrasive, surface metrology parameters were calculated from the 3D measurements of the prepared surfaces.

Figure 3.5. The mean surface roughness (Ra) (µm) (and associated SDs) of Grade II, IV and V Ti surfaces prepared with P220, P320, P500, P800, P1000, P1200, P2400, P4000 grit and P4000 finished with collodial silica (n=3, * indicates statistical differences from P220 (p<0.05)).
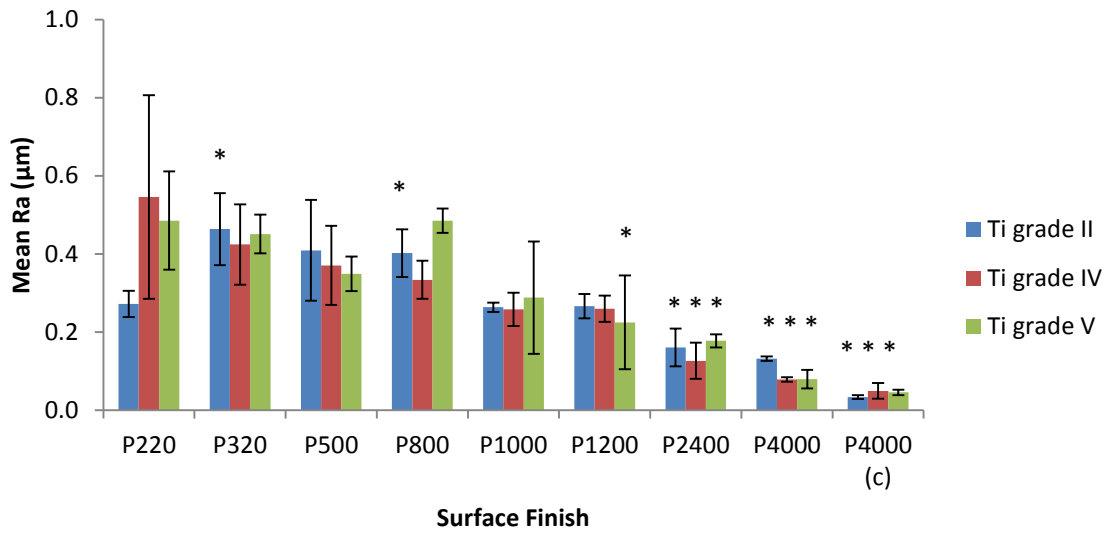
Significant decreases in Ra were observed on P2400, P4000 and P4000 (c) on Grade II, IV and V (p<0.05).

Figure 3.6. The mean of the maximum peak height Rp (μm) (and associated SDs) of Grade II, IV and V Ti surfaces prepared with P220, P320, P500, P800, P1000, P1200, P2400, P4000 grit and P4000 finished with colloidal silica (n=3, * indicates statistical differences from P220 (p<0.05)).
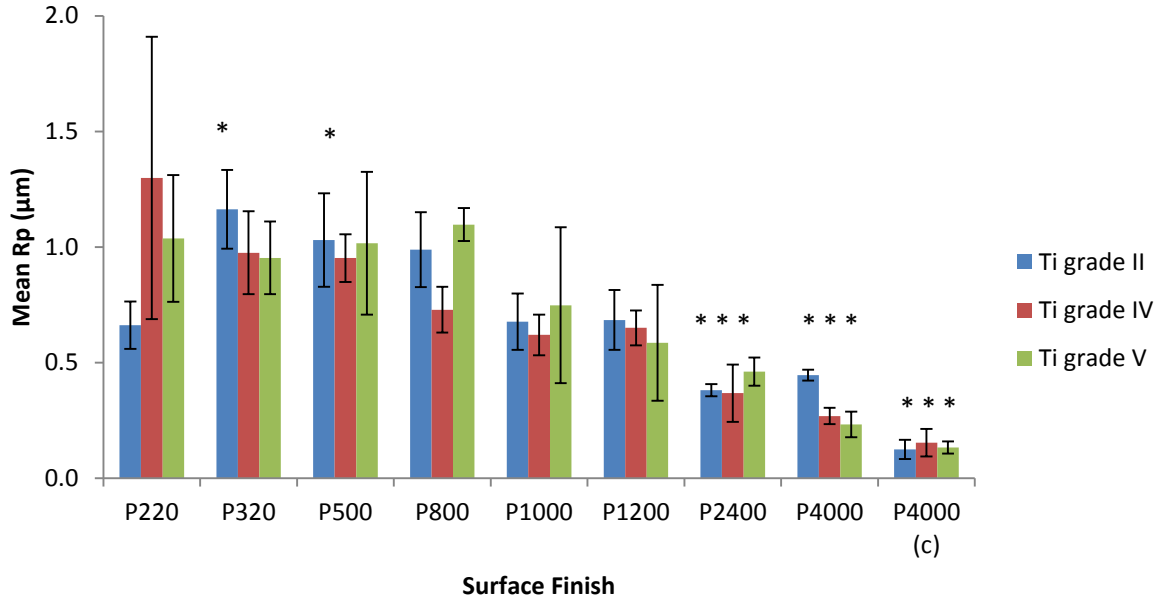
Significant decreases in Rp were observed on P2400, P4000 and P4000 (c) on Grade II, IV and V (p<0.05).

Figure 3.7. The mean of the maximum valley depth Rv (μm) and associated SDs of Grade II, IV and V Ti surfaces prepared with P220, P320, P500, P800, P1000, P1200, P2400, P4000 grit and P4000 finished with colloidal silica (n=3, * indicates statistical differences from P220 (p<0.05)).
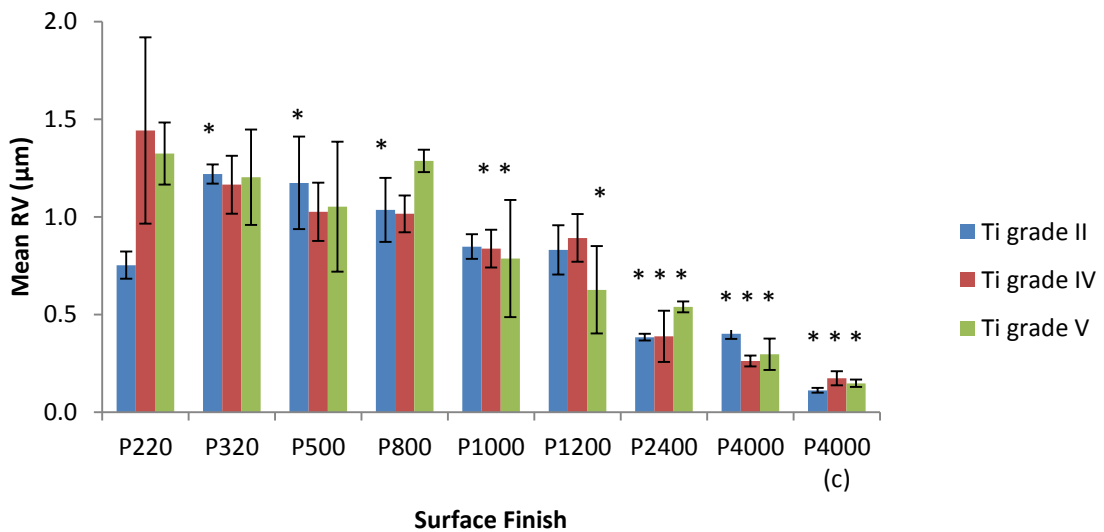
Significant decreases in Rv were observed on P2400, P4000 and P4000 (c) on Grade II, IV and V (p<0.05).

Figure 3.8. The mean of the maximum roughness height Rz (μm) and associated SDs of Grade II, IV and V Ti surfaces prepared with P220, P320, P500, P800, P1000, P1200, P2400, P4000 grit and P4000 finished with colloidal silica (n=3, * indicates statistical differences from P220 (p<0.05)).
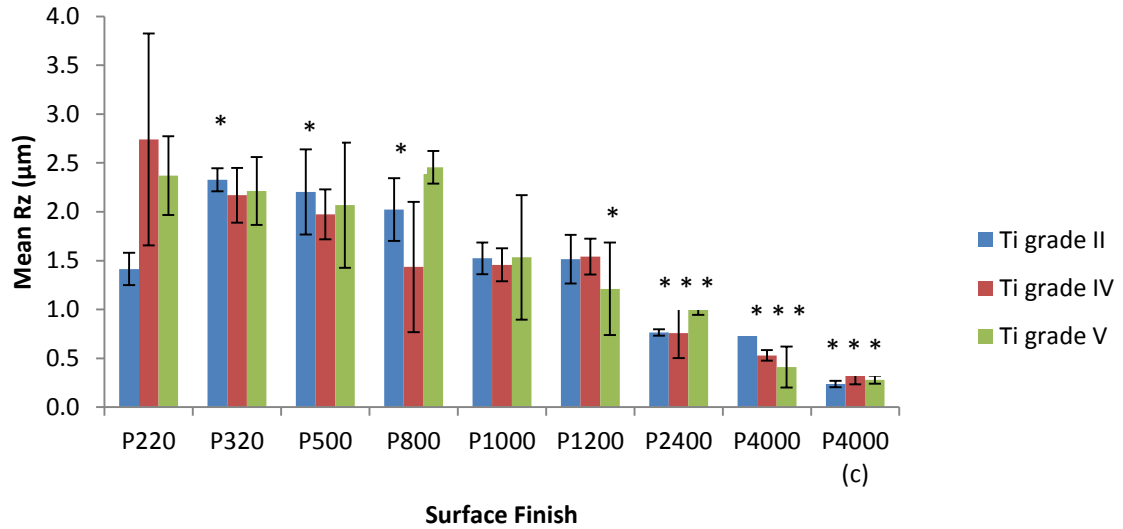
Significant decreases in Rz were observed on P2400, P4000 and P4000 (c) on Grade II, IV and V (p<0.05).

Figure 3.9. The mean height of the roughness profile elements Rc (μm) and associated SDs of Grade II, IV and V Ti surfaces prepared with P220, P320, P500, P800, P1000, P1200, P2400, P4000 grit and P4000 finished with colloidal silica (n=3, * indicates statistical differences from P220 (p<0.05)).
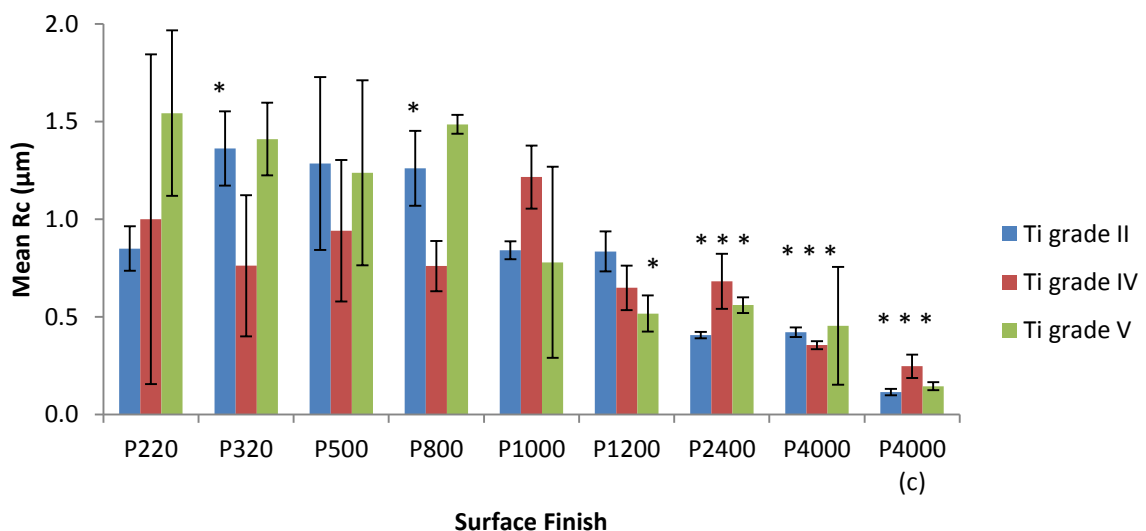
Significant decreases in Rc were observed on P2400, P4000 and P4000 (c) on Grade II, IV and V (p<0.05).

Figure 3.10. The mean maximum height of the surface profile Rt (µm) and associated SDs of Grade II, IV and V Ti surfaces prepared with P220, P320, P500, P800, P1000, P1200, P2400, P4000 grit and P4000 finished with colloidal silica (n=3, * indicates statistical differences from P220 (p<0.05)).
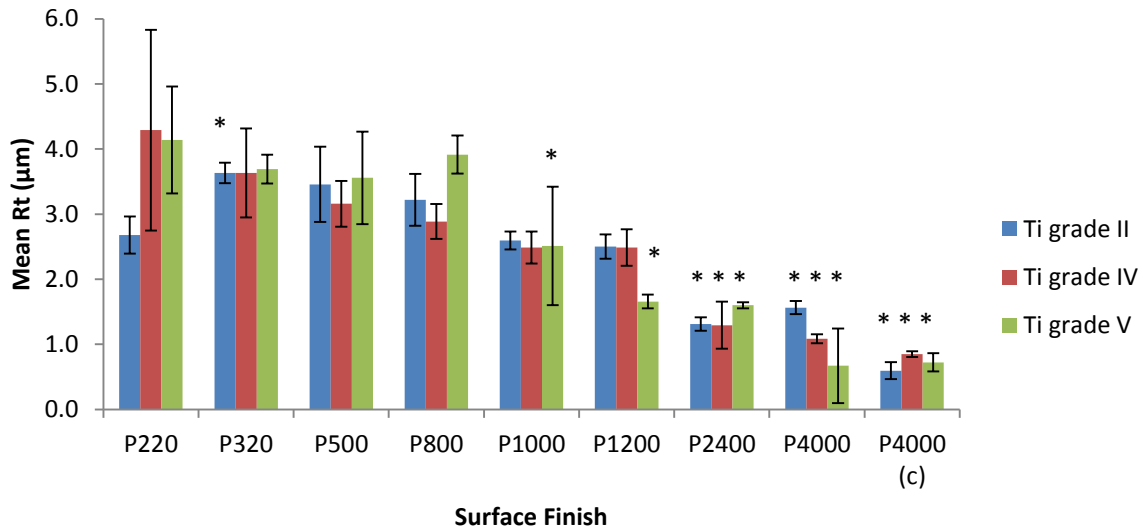
Significant decreases in Rt were observed on P2400, P4000 and P4000 (c) on Grade II, IV and

V (p<0.05).

Figure 3.11. The mean of root mean square deviation of Ti Rq (µm) and associated SDs of Grade II, IV and V Ti surfaces prepared with P220, P320, P500, P800, P1000, P1200, P2400, P4000 grit and P4000 finished with colloidal silica (n=3, * indicates statistical differences from P220 (p<0.05)).
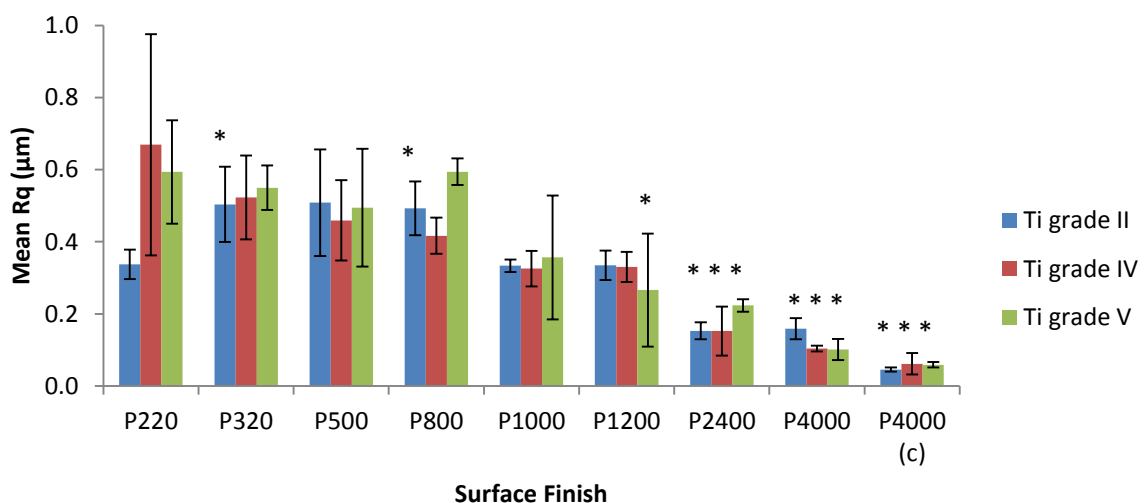
Significant decreases in R_q were observed on P2400, P4000 and P4000 (c) on Grade II, IV and V (p<0.05).

Figure 3.12. The mean skewness Rsk (µm) and associated SDs of Grade II, IV and V Ti surfaces prepared with P220, P320, P500, P800, P1000, P1200, P2400, P4000 grit and P4000 finished with colloidal silica (n=3, * indicates statistical differences from P220 (p<0.05)).
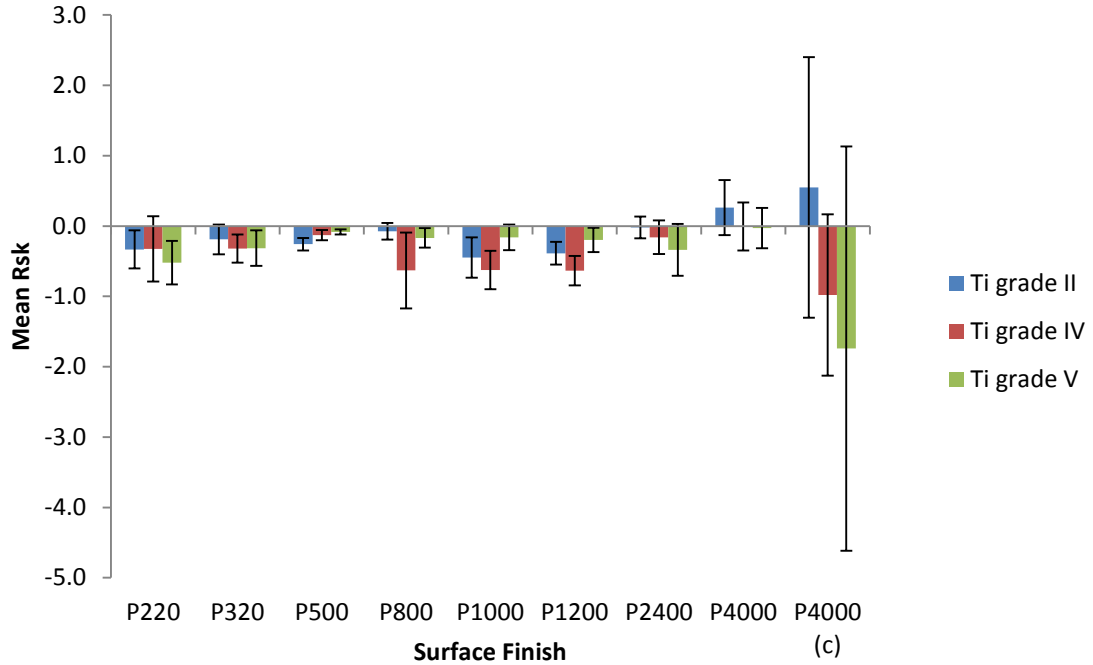
No significant differences were observed on Grade II, IV and V prepared surfaces with the mean Rsk.

Figure 3.13. The mean kurtosis values of Ti Rku (µm) and associated SDs of Grade II, IV and V Ti surfaces prepared with P220, P320, P500, P800, P1000, P1200, P2400, P4000 grit and P4000 finished with colloidal silica (n=3, * indicates statistical differences from P220 (p<0.05)).
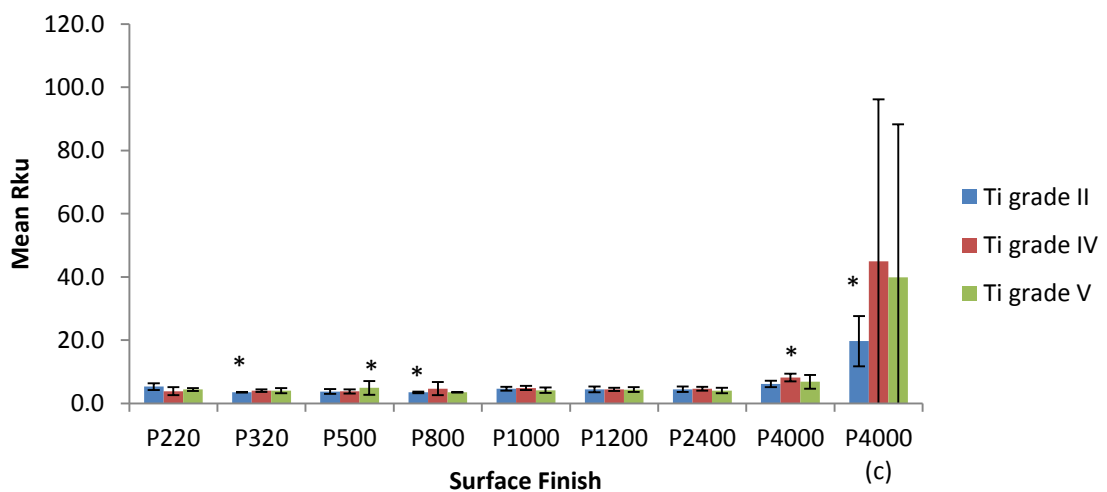
Significant increases in the Rku were observed on Grade II P320, P800 and P4000 (c) prepared surfaces (p<0.05).

71

3.1.3 Surface wettability/ contact angle measurements.

For all the Ti substrates and surfaces finishes under investigation contact angle measurements were performed at 23 ± 1 °C with artificial saliva and distilled water. A two-way ANOVA demonstrated a significant factorial effect of the contact angle medium with a reduction in the mean contact angles observed when artificial saliva was used compared with water ($p < 0.05$). No significant impact of the surface finish grade on mean contact angle was detected (figure 3.14).

Figure 3.14a. Contact angle measurements (°) of distilled water (—) and artificial saliva(—) on Grade II CpTi prepared with SiC abrasive papers to a P220, P320, P500, P800, P1000, P1200, P2400, P4000 and P4000 (c) grit size (n=3, 10 times repeat measurements) at 23 ± 1 °C. Data plotted as mean and error bars plotted as one standard deviation.
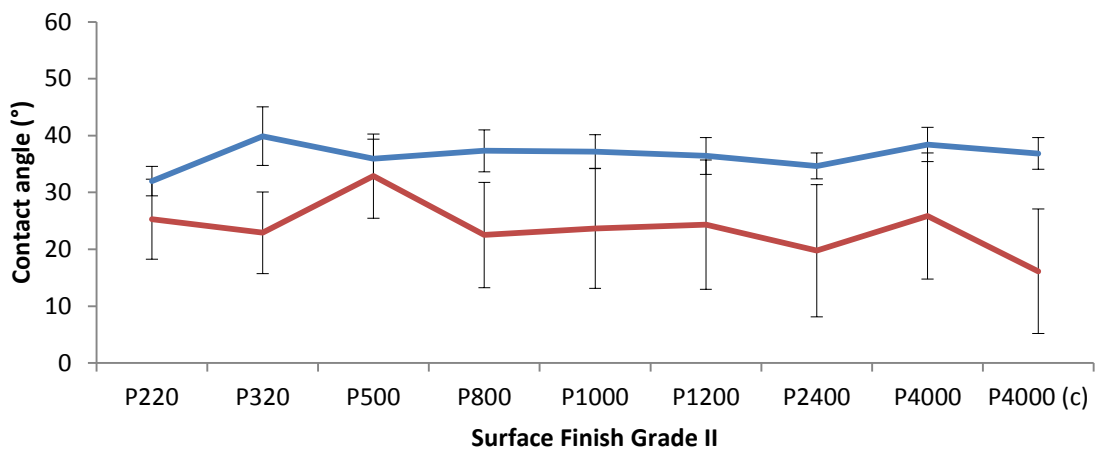
Figure 3.14b. Contact angle measurements (°) of distilled water (———) and artificial saliva(———) on Grade IV CpTi prepared with SiC abrasive papers to a P220, P320, P500, P800, P1000, P1200, P2400, P4000 and P4000 (c) grit size (n=3, 10 times repeat measurements) at 23 ± 1 °C. Data plotted as mean and error bars plotted as one standard deviation.
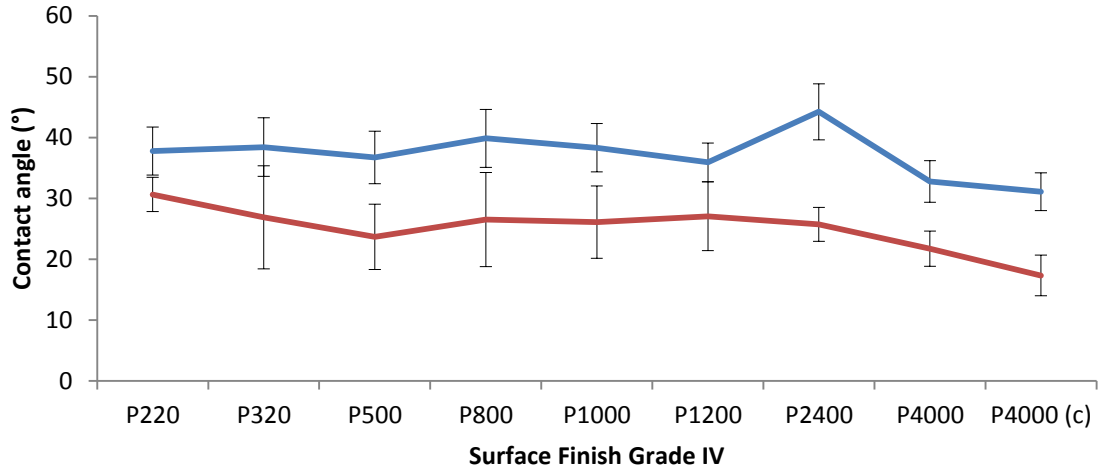
Figure 3.14c. Contact angle measurements (°) of distilled water (———) and artificial saliva(———) on Grade V CpTi prepared with SiC abrasive papers to a P220, P320, P500, P800, P1000, P1200, P2400, P4000 and P4000 (c) grit size (n=3, 10 times repeat measurements) at 23 ± 1 °C. Data plotted as mean and error bars plotted as one standard deviation.
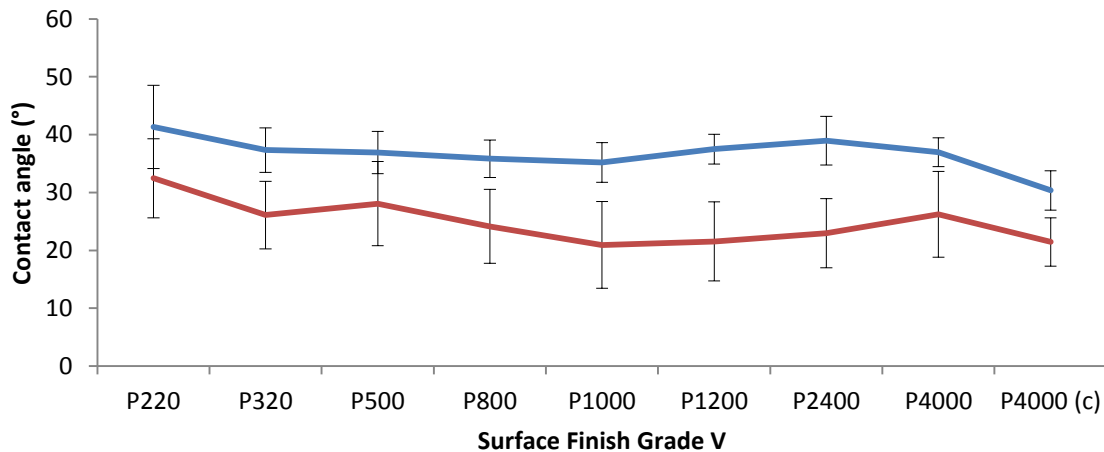
**Figure 3.14d. Contact angle measurements (°) of distilled water (━) and artificial saliva(━)
on all Grades of Ti samples (pooled) prepared with SiC abrasive papers to a P220, P320,
P500, P800, P1000, P1200, P2400, P4000 and P4000 (c) grit size (n=3, 10 times repeat
measurements) at 23 ± 1 °C. Data plotted as mean and error bars plotted as one standard
deviation.**
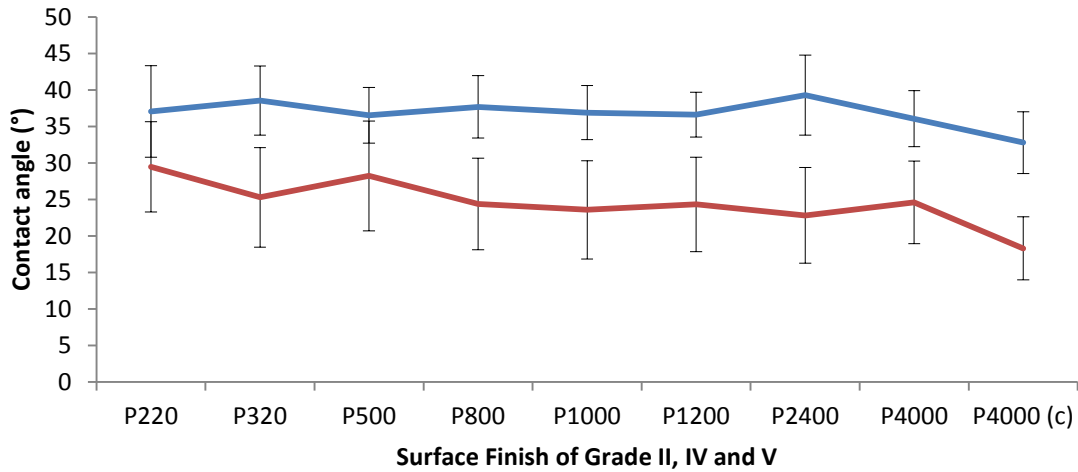
**Figure 3.14e. Contact angle measurements (°) of distilled water (━) and artificial saliva(━)
plotted against mean surface roughness (Ra-(μm)) for all Grades of Ti samples (pooled)
prepared with SiC abrasive papers to a P220, P320, P500, P800, P1000, P1200, P2400,
P4000 and P4000 (c) grit size (n=3, 10 times repeat measurements) at 23 ± 1 °C. Data
plotted as mean and error bars plotted as one standard deviation.**
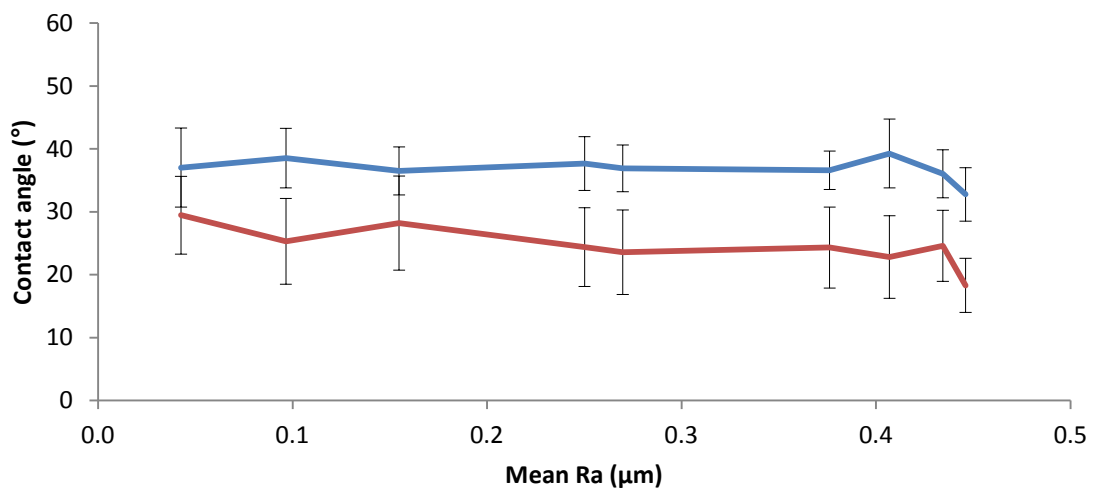
Contact angle measurements were repeated at 37 ± 3 °C with artificial saliva and with

distilled water for all the Ti substrates under investigation to provide a more representative

measurement of physiological conditions. A two-way ANOVA demonstrated a significant

reduction, in the mean contact angle when artificial saliva was used when compared with water (p=0.004). No significant impact of the surface Grade was detected (figure 3.15).

Figure 3.15a. Contact angle measurements (°) of distilled water (——) and artificial saliva(——) on Grade II CpTi prepared with SiC abrasive papers to a P220, P320, P500, P800, P1000, P1200, P2400, P4000 and P4000 (c) grit size (n=3, 10 times repeat measurements) at 37 ± 3 °C. Data plotted as mean and error bars plotted as one standard deviation.
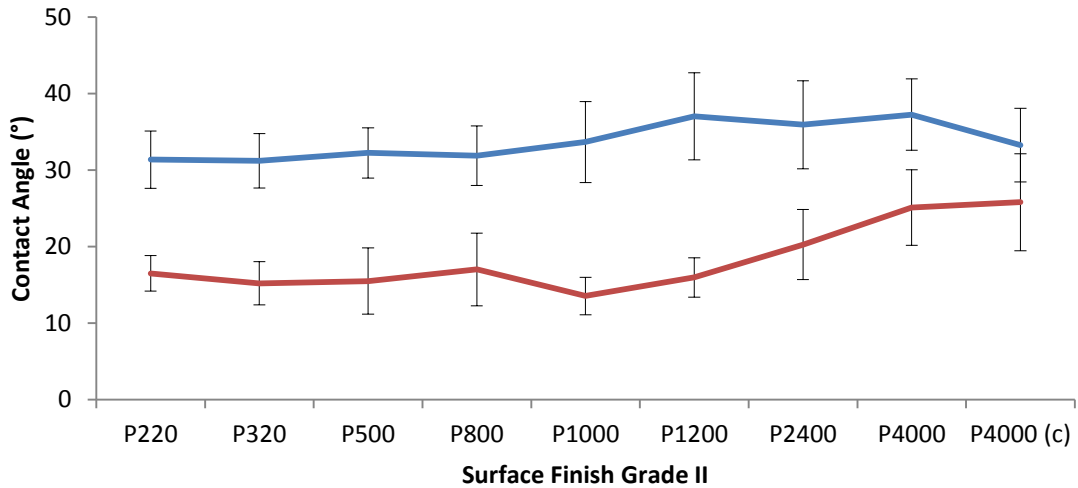
Figure 3.15b. Contact angle measurements (°) of distilled water (——) and artificial saliva(——) on Grade IV CpTi prepared with SiC abrasive papers to a P220, P320, P500, P800, P1000, P1200, P2400, P4000 and P4000 (c) grit size (n=3, 10 times repeat measurements) at 37 ± 3 °C. Data plotted as mean and error bars plotted as one standard deviation.
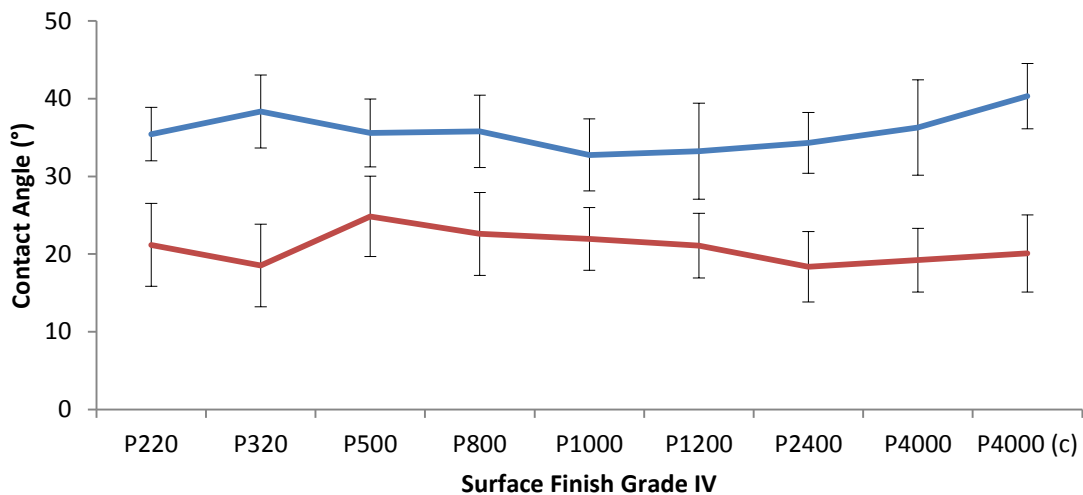
Figure 3.15c. Contact angle measurements (°) of distilled water (━) and artificial saliva(━) on Grade V CpTi prepared with SiC abrasive papers to a P220, P320, P500, P800, P1000, P1200, P2400, P4000 and P4000 (c) grit size (n=3, 10 times repeat measurements) at 37 ± 3 °C. Data plotted as mean and error bars plotted as one standard deviation.
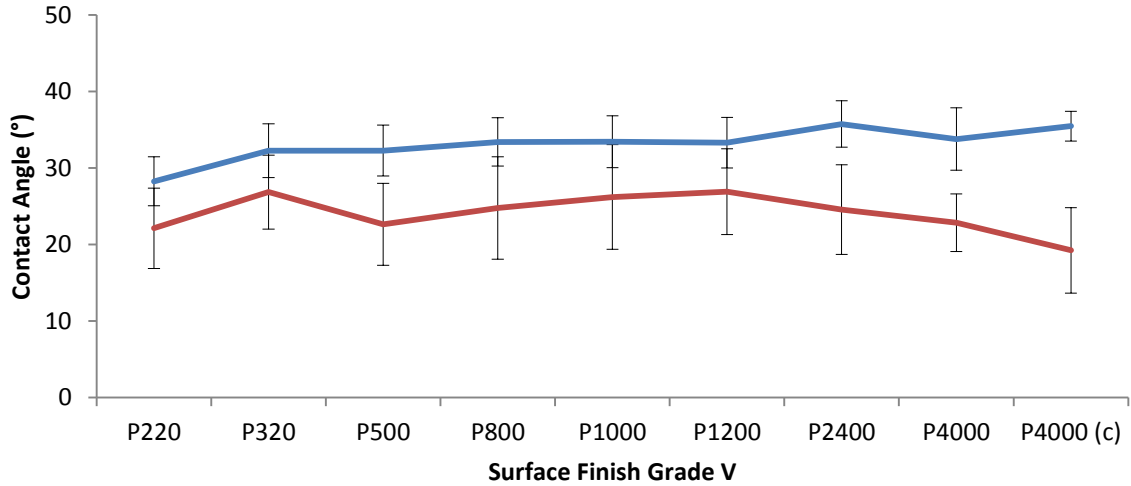
Figure 3.15d. Contact angle measurements (°) of distilled water (━) and artificial saliva(━) on all Grades of Ti samples (pooled) prepared with SiC abrasive papers to a P220, P320, P500, P800, P1000, P1200, P2400, P4000 and P4000 (c) grit size (n=3, 10 times repeat measurements) at 37 ± 3 °C. Data plotted as mean and error bars plotted as one standard deviation.
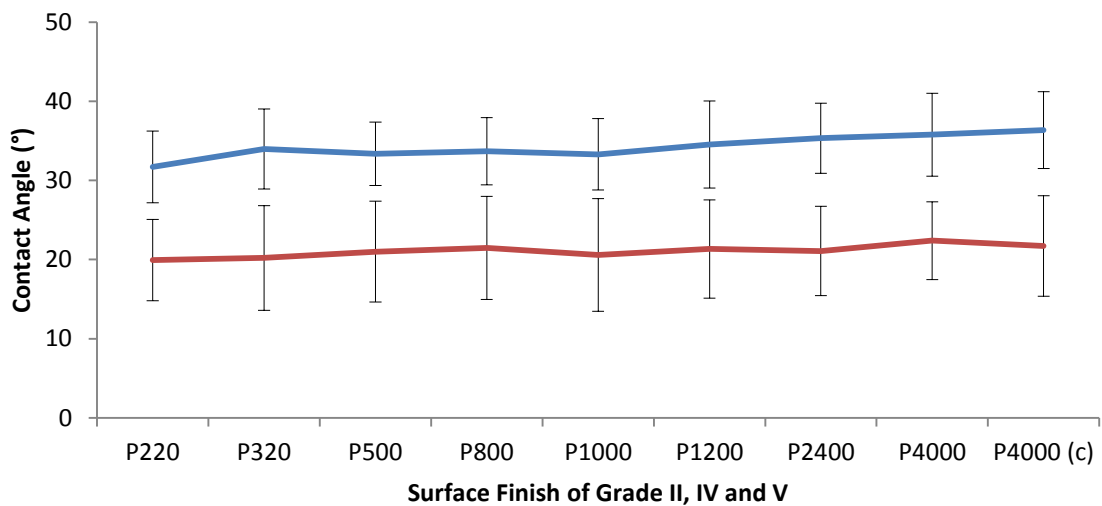
Figure 3.15e. Contact angle measurements (°) of distilled water (—) and artificial saliva(—) plotted against mean surface roughness (Ra-(µm)) for all Grades of Ti samples (pooled) prepared with SiC abrasive papers to a P220, P320, P500, P800, P1000, P1200, P2400, P4000 and P4000 (c) grit size (n=3, 10 times repeat measurements) at 37 ± 3 °C . Data plotted as mean and error bars plotted as one standard deviation.
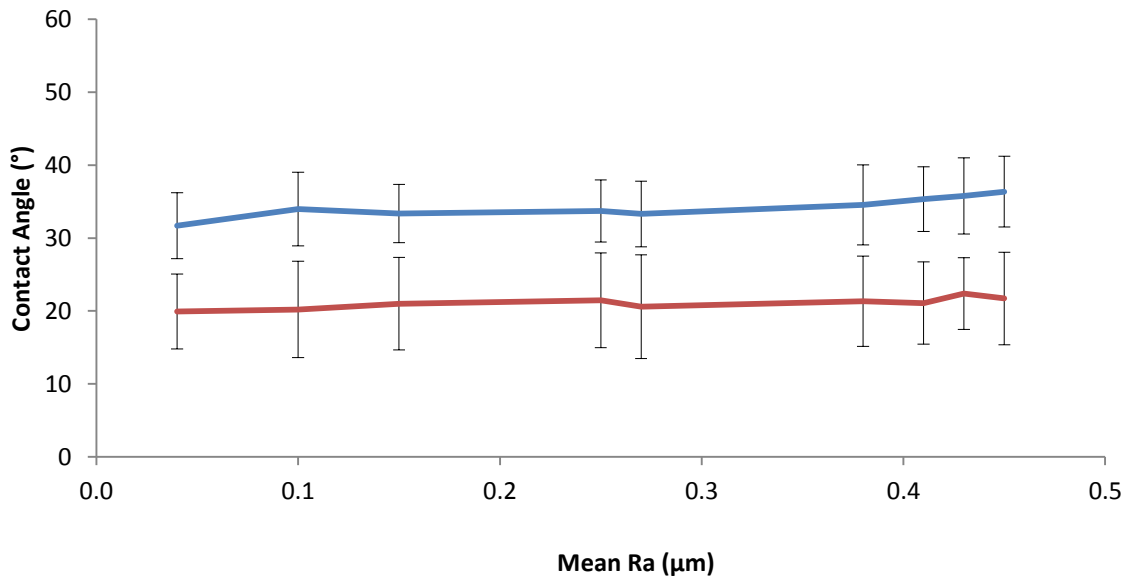
When measurements were carried out at 37 °C (in contrast to 23 °C) the contact angle values when artificial saliva was used as the medium were found to be significantly lower than those obtained for distilled water for Grade II, IV and V Ti discs (p≤ 0.005) (figures 3.14 and 3.15). The contact angles ranged from 17° at the smoothest surface finish of P4000(c) to 30° at the roughest surface finish of P220 when the measurements were carried out at ambient temperature with artificial saliva as a medium. The measurements demonstrated that as the temperature increased the artificial saliva significantly wetted the prepared Ti substrates further when compared with measurements carried out at room temperature. In contrast no significant differences were observed when compared to the distilled water. The control media of distilled water produced a mean contact angle of 32 ± 8° with the smallest angles observed on the smoother samples of P2400, P4000 and P4000(c) (figure 3.15d). At 37°C the

mean contact angle for distilled water was consistent for all the prepared Ti substrates at 32 ± 3°. Distilled water did not produce significantly different contact angles measurements between the ambient temperature and 37 °C when the data for the Ti substrates of Grade II, IV and V was combined (figure 3.15d), however the contact angles were more consistent for the prepared Ti substrates when measured at 37 °C. The mean contact angle measurements are reported in table 3.1

Table 3.1: Comparison of mean contact angle (°) measurements of distilled water and artificial saliva as a medium at 23 °C ± 1 °C and 37 °C ± 3 °C on Grade II, IV and V Ti (n=3, 10 repeat measurements).

	Mean Contact angles (°)	
Medium	**23 °C**	**37 °C**
Distilled Water	37 ± 4	34 ± 5
Artificial Saliva	25 ± 6	21 ± 6

3.2 Gram staining of bacteria to be used for early adhesion studies.

Gram staining was used as part of quality control, to confirm the morphology of the bacteria and ensure that there was no cross contamination of the bacteria. Gram positive strains of *S sanguinis, S mutans* (figure 3.16a and 3.16c) *and* Gram negative strains of *E coli, F nucleatum* (figure 3.16b and 3.16 d) were investigated in the bacterial adhesion experiments.

Figure 3.16. Light microscope images of a) *S sanguinis*, b) *E coli*, c) *S mutans* and d) *F nucleatum*.
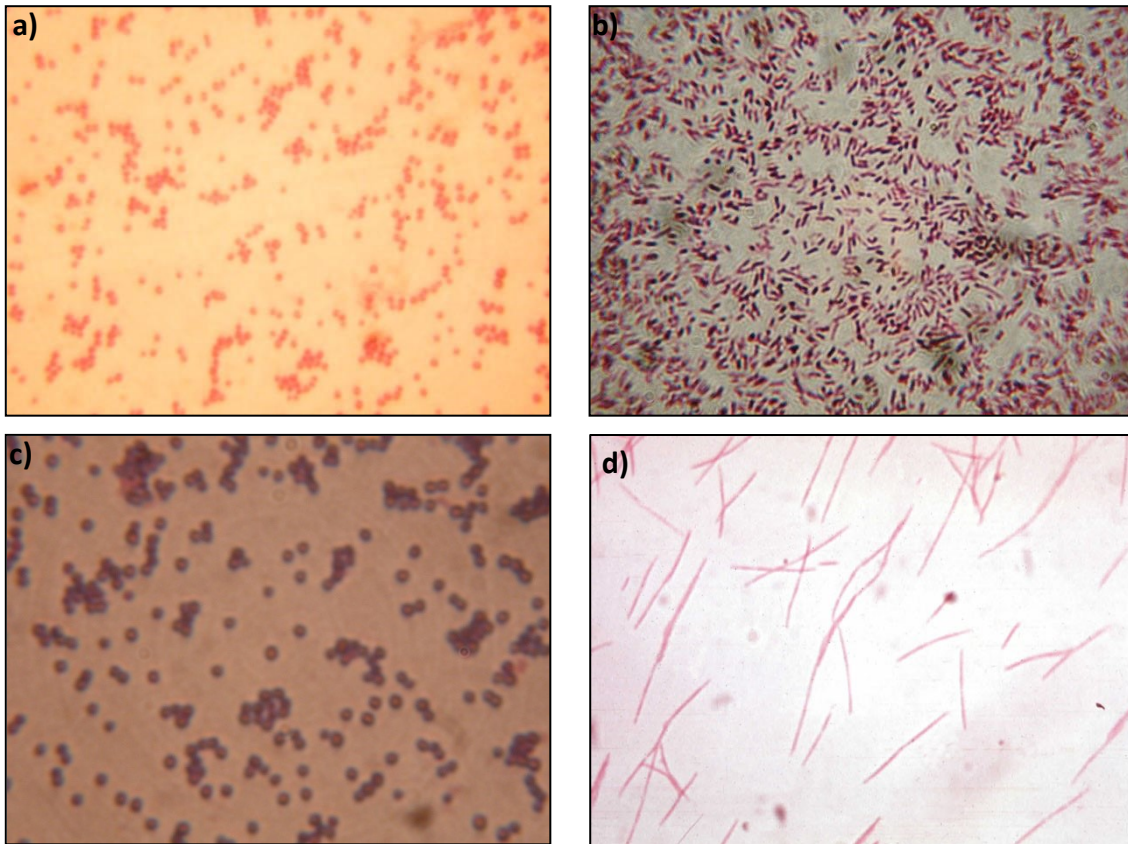
Fig 3.16a. Illustrates the morphology of coccus shaped gram positive bacteria which is a characteristic of *S sanguinis*. Fig 3.16b illustrates rod shaped gram negative *E coli* bacteria. Fig. 3.16c Illustrates the presence of gram positive coccus shaped bacteria and Fig. 3.16d illustrates the presence of gram negative (pink) cigar-shaped structures which is characteristic morphology of *F nucleatum.*

3.3 Investigation of surface adhesion and early proliferation of bacteria on prepared Ti surfaces.

3.3.1 *S sanguinis*.

S sanguinis was incubated on Grade II, IV and V surfaces for 24 h. A t-test identified no significant differences between the P220 finish samples from the two parts of the experiment (p<0.05) and therefore data could be combined. A one-way ANOVA demonstrated a significant difference of surface finish on the mean CFU/mL (p<0.05).

Figure 3.17. A histogram of mean± SD CFU/mL of *S sanguinis* (*1 x 10^5) on Grade II CpTi surfaces prepared with P220, P320, P500, P800, P1000, P1200, P2400, P4000 SiC final grit size abrasives and P4000(c) prepared with colloidal silica. (n=3, * demonstrates significant difference from P220 determined by post-hoc Tukey tests- p<0.05).
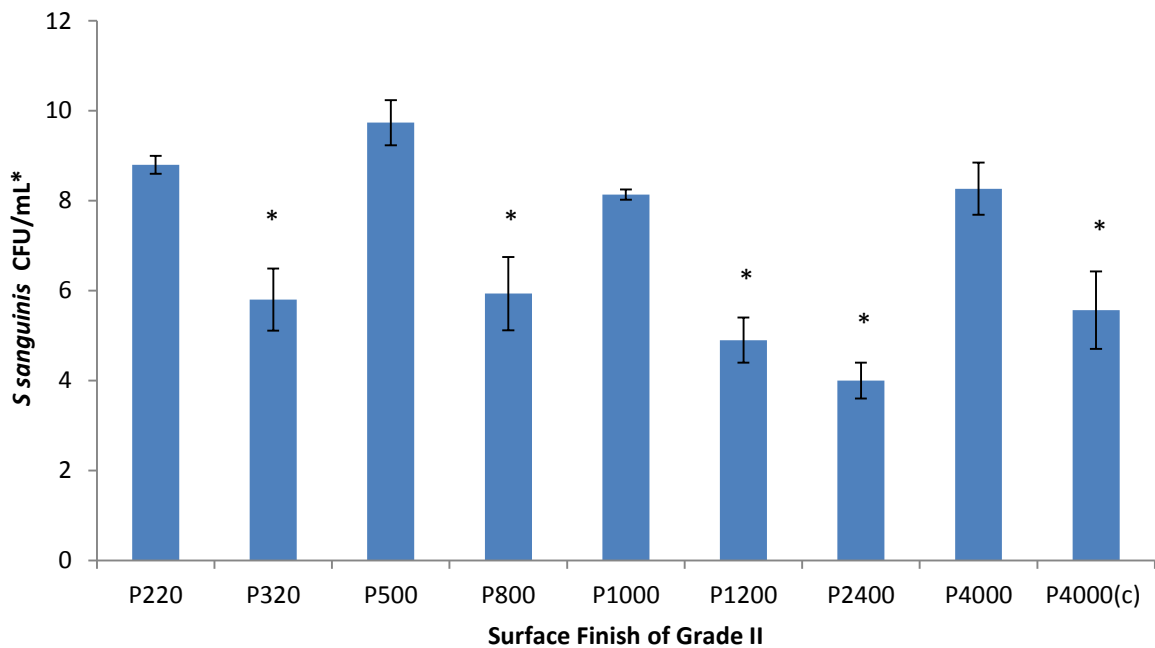
Figure 3.18. A histogram of mean ± SD CFU/mL of *S sanguinis* (*1 x 10^{5}) on Grade IV CpTi surfaces prepared with P220, P320, P500, P800, P1000, P1200, P2400, P4000 SiC final grit size abrasives and P4000(c) prepared with colloidal silica. (n=3, * demonstrates significant differences from P220 as determined by post-hoc Tukey tests - p<0.05)
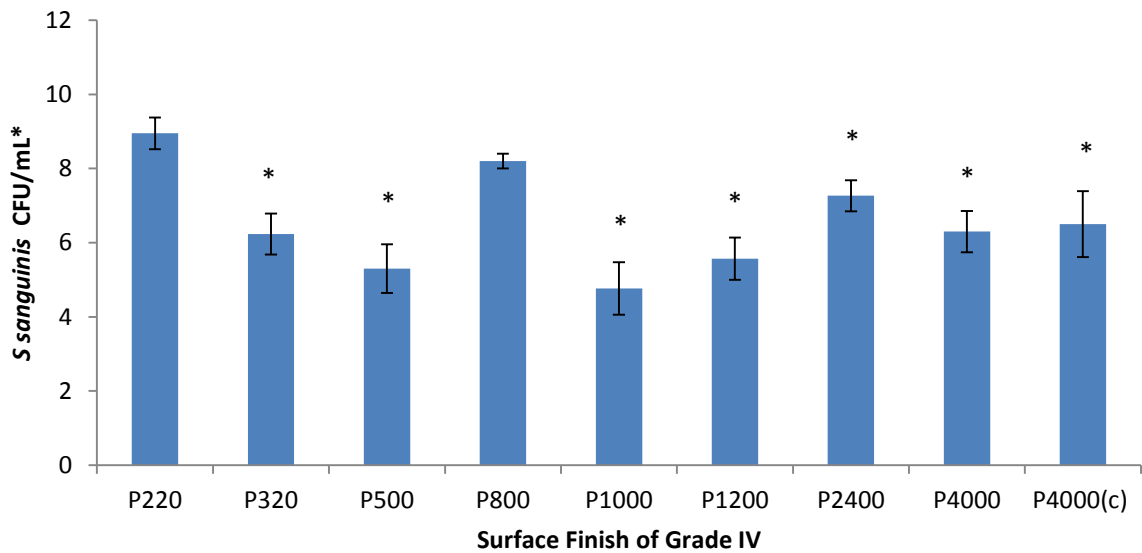
Figure 3.19. A histogram of mean ± SD CFU/mL of *S sanguinis* (*1 x 10^{5}) on Grade V CpTi surfaces prepared with P220, P320, P500, P800, P1000, P1200, P2400, P4000 SiC final grit size abrasives and P4000(c) prepared with colloidal silica. (n=3, * demonstrates significant differences from P220 as determined by post-hoc Tukey tests - p<0.05)
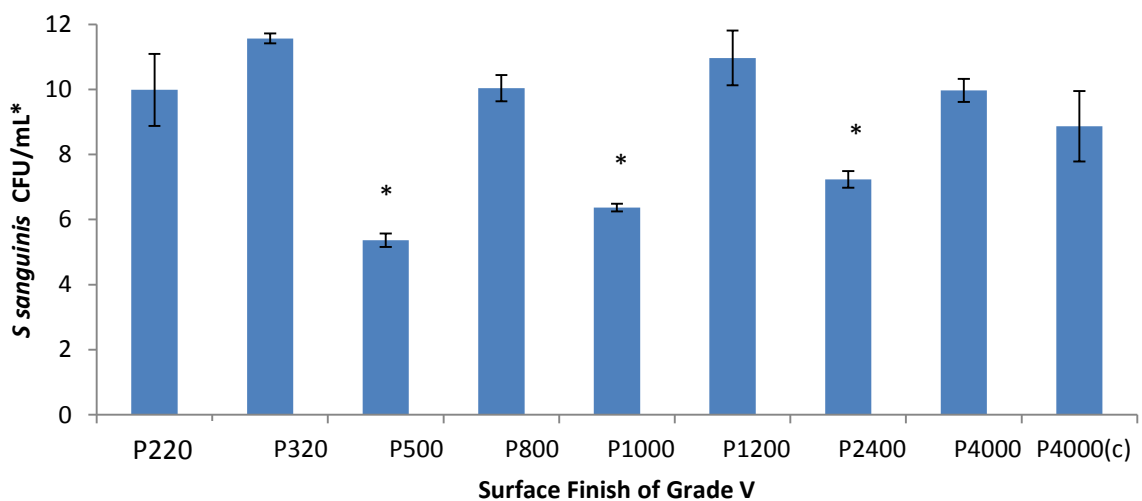
The initial bacterial biofilm coloniser *S sanguinis* possessed higher numbers of bacteria adhered to the prepared P220 surface of the Ti substrate with ~8-9x10^{5} CFU/mL of bacteria

being observed on Grade II, IV and V surfaces (figure 3.17, 3.18 and 3.19) when compared with *E coli* at ~4–7x10^5 CFU/mL (figures 3.20, 3.21 and 3.23). A significant decrease in the adhesion of *S sanguinis* was observed from the P220 prepared surface to the prepared surface textures produced by a final SiC grit of P320, P800, P1200, P2400 and P4000(c) (figure 3.17). The pattern of bacterial adhesion on the prepared Ti surfaces appeared to be largely random with no clear correlations observed. For example bacterial adhesion to the moderately rough prepared surface texture (P500) was greater at 10x10^{-5} CFU/mL than the rougher P320 prepared Ti surface at 6x10^5 CFU/mL bacteria. The smoother surfaces of P4000 and P4000(c) were in general observed to have more bacteria adhered to their prepared surface than P2400 (figure 3.17). The Grade IV prepared Ti surface illustrated a significant difference in bacterial adhesion between the P220 prepared surface and the Ti surface textures of P320, P500, P1000, P1200, P2400 P4000 and P4000(c) (figure 3.18). The number of colonies observed decreases from P220 with a CFU/mL of ~9x10^5 to P500 having a CFU/mL of 5x10^5, however there was an increase in the mean CFU/mL on the P800 created surface texture at 8x10^5. The smoother surface textures of P1200, P2400, P4000 and P4000(c) appear to have similar numbers of bacteria adhered again showing no correlation between texture and bacterial count (figure 3.18). A significant difference was observed between P220 and the prepared surface textures of P500, P1000 and P2400 on Grade V Ti alloy (figure 3.19) having lower numbers of bacterial adhesion of 4, 6 and 7x10^5. The smoother surface of P1200, P4000 and P4000(c) appeared to not affect the number of CFU/mL of *S sanguinis* adhered to the Grade V surface.

3.3.2 *E coli.*

Figure 3.20. A histogram of mean ± SD CFU/mL of *E coli* (*1 x 10^5) on Grade II CpTi surfaces prepared with P220, P320, P500, P800, P1000, P1200, P2400, P4000 SiC final grit size abrasives and P4000(c) prepared with colloidal silica. (n=3, * demonstrates significant difference from P220 determined by post-hoc Tukey tests- p<0.05).
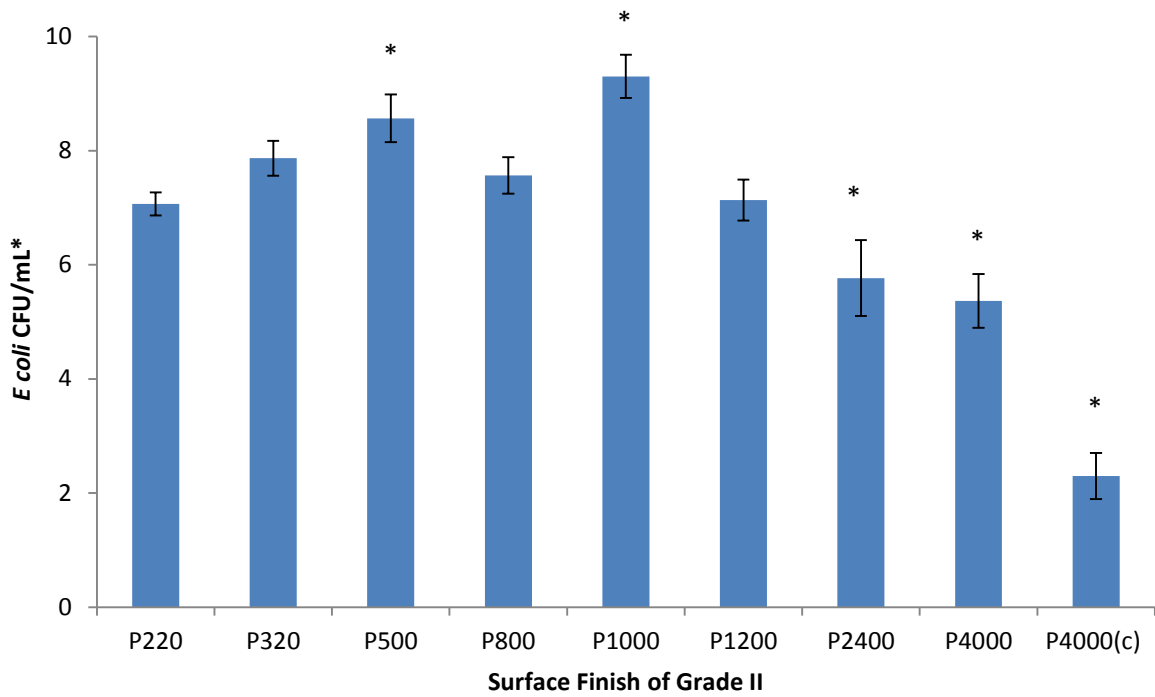
Figure 3.21. A histogram of mean ± SD CFU/mL of *E coli* (*1 x 10^5) on Grade IV CpTi surfaces prepared with P220, P320, P500, P800, P1000, P1200, P2400, P4000 SiC final grit size abrasives and P4000(c) prepared with colloidal silica. (n=3, * demonstrates significant difference from P220 determined by post-hoc Tukey tests- p<0.05).
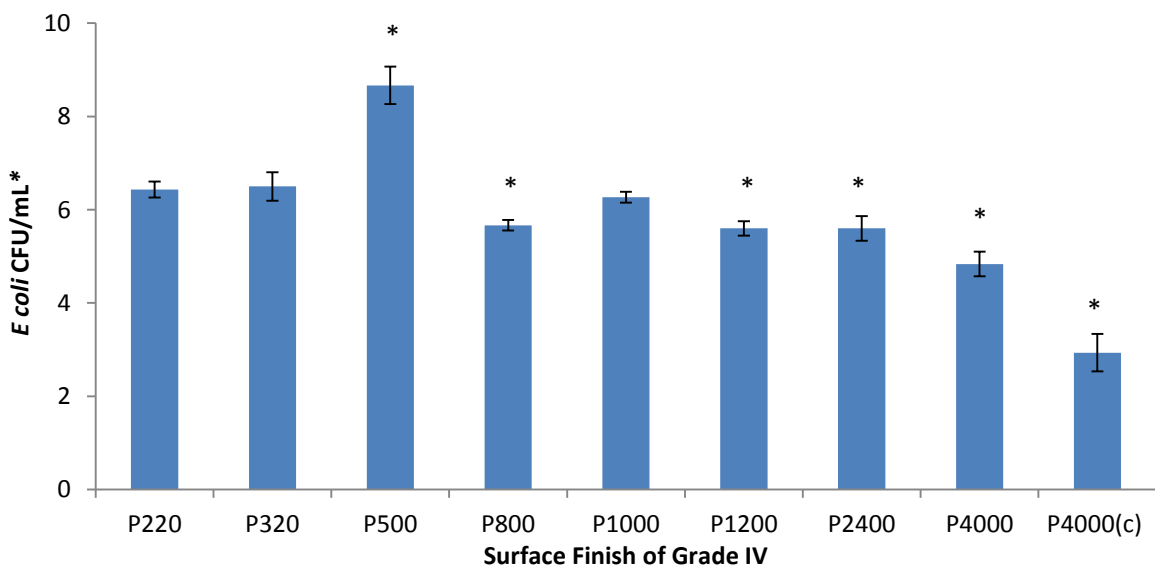
Figure 3.22. A Histogram of mean ± SD CFU/mL of _E coli_ (*1 x 10^5) on Grade V CpTi surfaces prepared with P220, P320, P500, P800, P1000, P1200, P2400, P4000 SiC final grit size abrasives and P4000(c) prepared with colloidal silica. (n=3, * demonstrates significant difference from P220 determined by post-hoc Tukey tests- p<0.05).
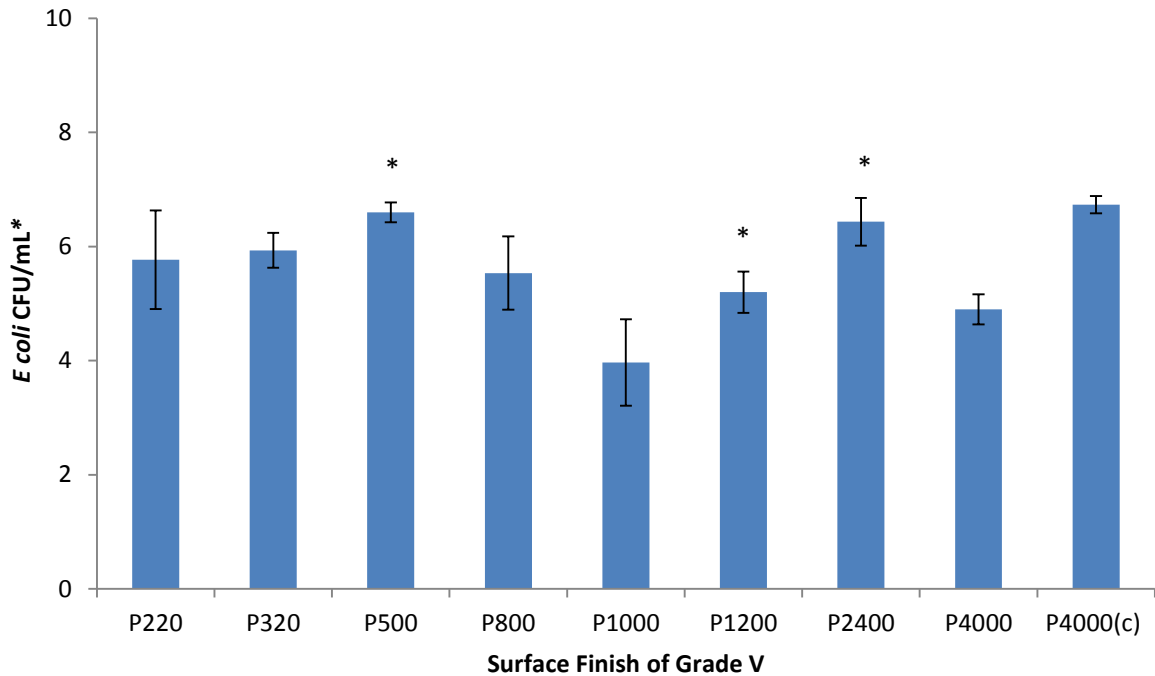
There was no significant difference observed between bacterial adhesion on the P220 surface from part one and part two of the bacterial adhesion assays for Grade II, IV and V Ti substrates (p>0.05) and hence data was combined. It was demonstrated that on Grade II CpTi there was a significant difference between _E coli_ adhesion on the P220 prepared surface and the P500, P1000, P2400, P4000 and P4000(c) surfaces as illustrated in figure 3.20. Adhesion of _E coli_ to Grade IV demonstrated a similar pattern with a significant difference being observed between the P220 prepared surface and the P500, P800, P1200, P2400, P4000 and P4000(c) surfaces. A similar number of colonies were observed on the P220 Ti substrate from all 3 Ti Grades with between 6 and 7x10^5 CFU/mL observed on Grade II, IV and V (figures 3.20, 3.21 and 3.22). A trend can be observed in bacterial adhesion on

Grade II CpTi with a gradual decrease in *E coli* numbers from the P1000 surface finish at 9×10^5 CFU/mL to 8, 6, 6 and 3×10^5 CFU/mL as the surface finish became smoother (figure 3.20). This trend was repeated on Grade IV prepared CpTi surfaces (figure 3.21). A different pattern was observed with the adhesion of *E coli* to the Grade V Ti substrate where there was an increase in the mean CFU/mL from the P1200 prepared surface to the P4000(c) prepared surface texture. The CFU/mL of *E coli* increased from 4×10^5 CFU/mL at P1000 to 5, 6, 5 and 7×10^5 on the P1200, P2400, P4000 and P4000(c) prepared surfaces respectively (figure 3.22).

3.3.3 *F nucleatum.*

Figure 3.23. A histogram of mean± SD CFU/mL of *F nucleatum* (*1 x 10^5) on Grade II CpTi surfaces prepared with P220, P320, P500, P800, P1000, P1200, P2400, P4000 SiC final grit size abrasives and P4000(c) prepared with colloidal silica. (n=3, * demonstrates significant difference from P220 determined by post-hoc Tukey tests- p<0.05).
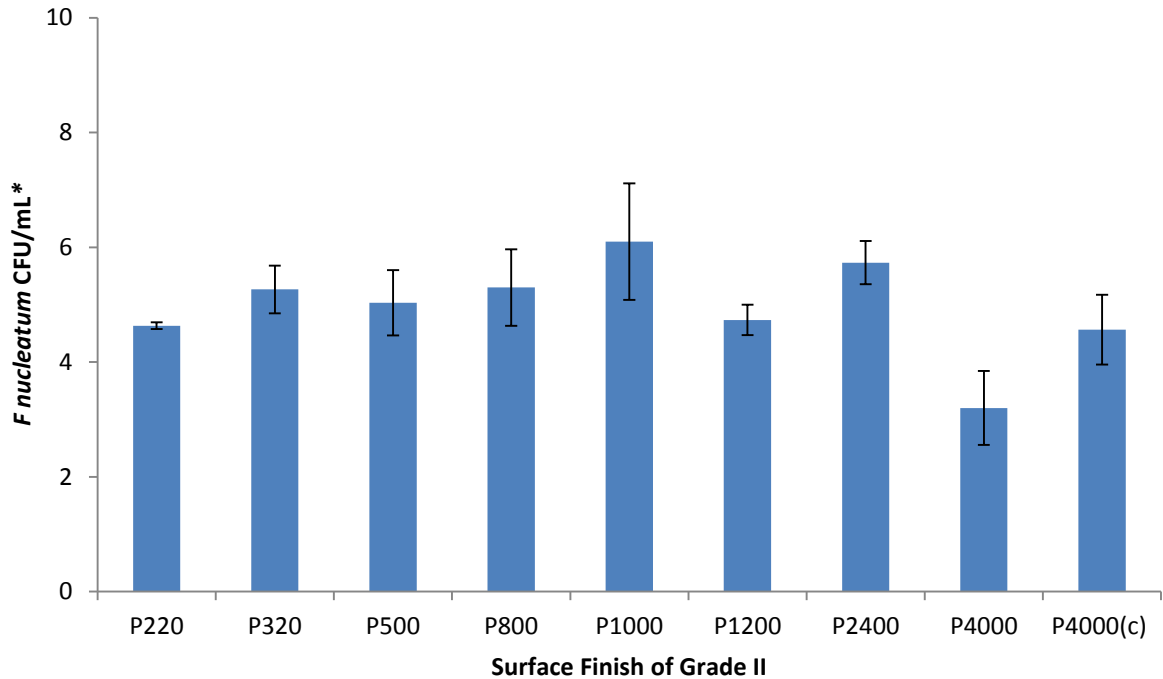
Figure 3.24. A histogram of mean± SD CFU/mL of *F nucleatum* (*1 x 10^5) on Grade IV CpTi surfaces prepared with P220, P320, P500, P800, P1000, P1200, P2400, P4000 SiC final grit size abrasives and P4000(c) prepared with colloidal silica. (n=3, * demonstrates significant difference from P220 determined by post-hoc Tukey tests- p<0.05).
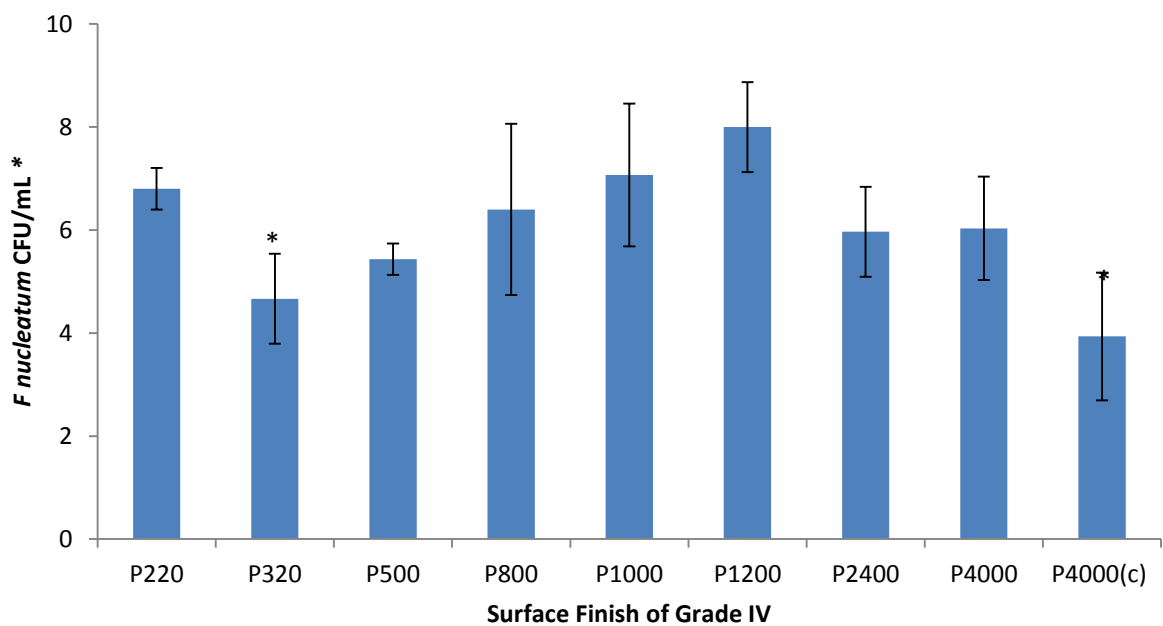
Figure 3.25. A histogram of mean± SD CFU/mL of *F nucleatum* (*1 x 10⁵) on Grade V CpTi surfaces prepared with P220, P320, P500, P800, P1000, P1200, P2400, P4000 SiC final grit size abrasives and P4000(c) prepared with colloidal silica. (n=3, * demonstrates significant difference from P220 determined by a post-hoc Tukey tests- p<0.05).
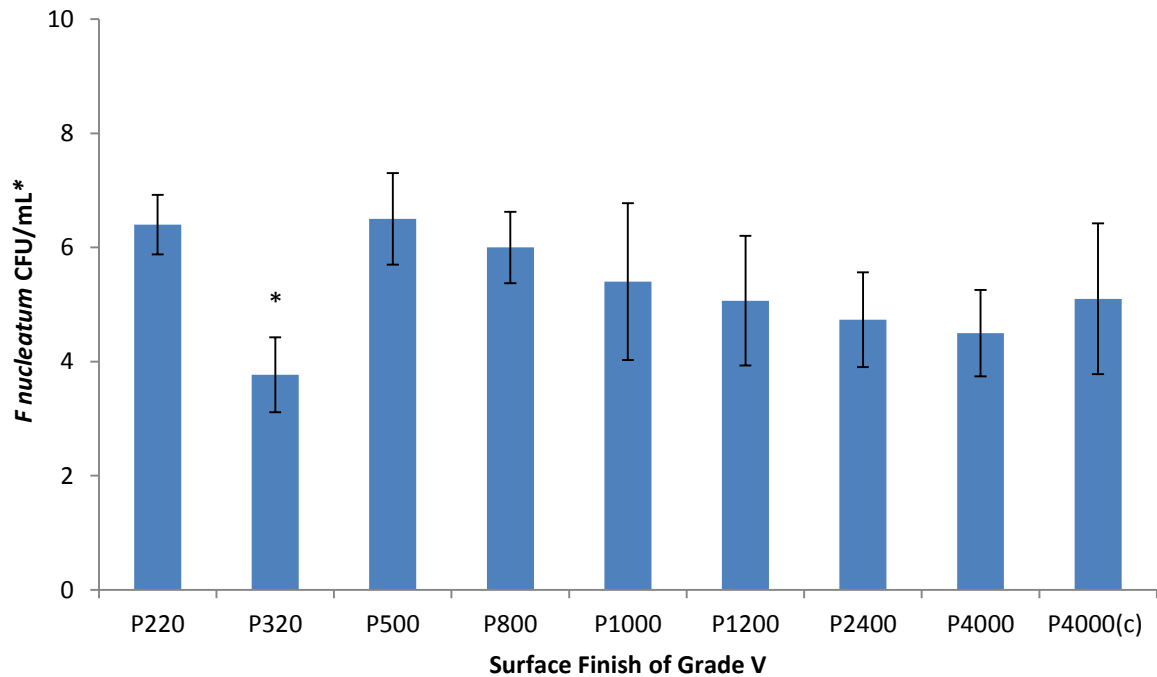
No significant differences in *F nucleatum* adhesion counts were observed between different surface textures of Grade II, IV and V Ti with a similar number of bacteria ~4-6x10⁵ CFU/mL recorded. A reduced mean CFU/mL was observed with the smoother surface texture of P4000 (figure 3.23). There was also a significant difference between the mean CFU/mL on the roughest surface of P220 and the surface textures of P320 and P4000(c) on the Grade IV surface (figure 3.24). A trend was observed between adhesion of *F nucleatum* and surface finish on the Grade IV Ti substrate. After initial bacterial adhesion on the roughest prepared Ti P220 with a bacterial count of ~7-8x10⁵ CFU/mL, the number of bacterial significantly decreased to 5x10⁻⁵ CFU/mL with further surface grinding at P320. The mean CFU/mL then increased gradually with surface finish to 8x10⁵ CFU/mL at the P1200 surface finish and then

reduced as the surface finish became smoother until P4000(c) at 4×10^5 CFU/mL (figure 3.24).

In common with Grade IV, a significant decrease in the number of bacteria adhering to the Grade V surface was observed between the roughest P220 surface and the P320 surface (figure 3.26).

3.3.4. *F nucleatum and S sanguinis.*

Figure 3.26. A histogram of mean± SD CFU/mL of *F nucleatum* and *S sanguinis* (*1 x 10^5) on Grade II CpTi surfaces prepared with P220, P320, P500, P800, P1000, P1200, P2400, P4000 SiC final grit size abrasives and P4000(c) prepared with colloidal silica. (n=3, * demonstrates significant difference from P220 determined by post-hoc Tukey tests- p<0.05).
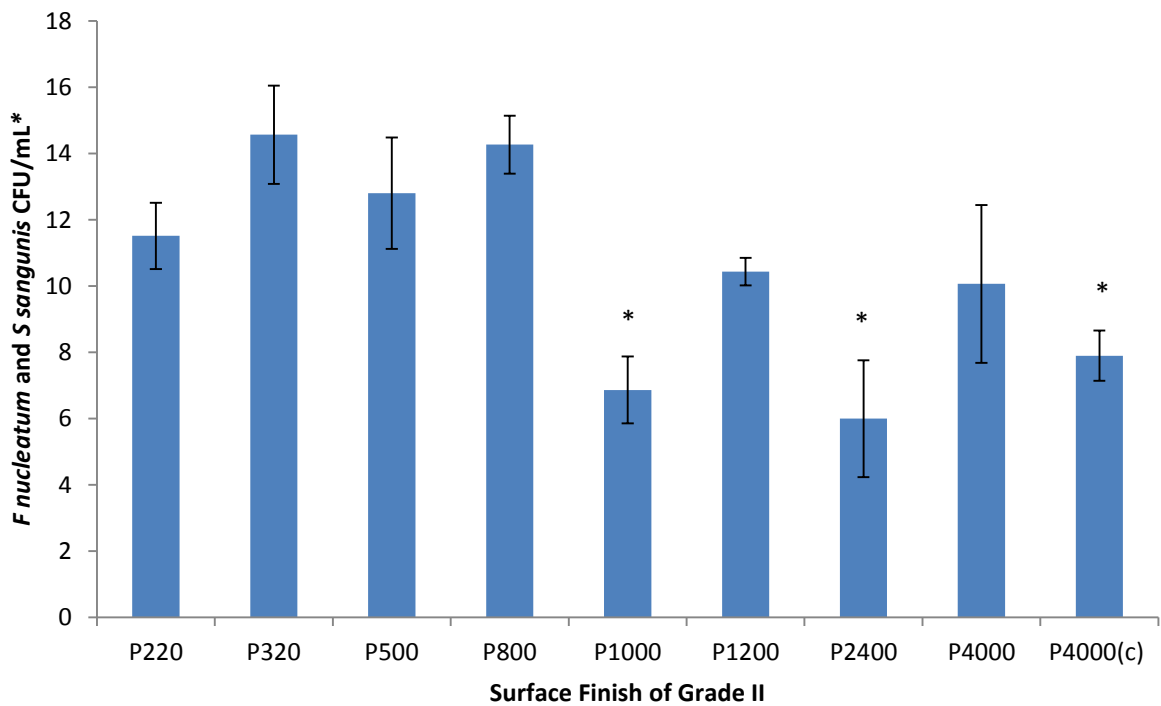
Figure 3.27. A Histogram of mean± SD CFU/mL of *F nucleatum* and *S sanguinis* (*1 x 10^5) on Grade IV CpTi surfaces prepared with P220, P320, P500, P800, P1000, P1200, P2400, P4000 SiC final grit size abrasives and P4000(c) prepared with colloidal silica. (n=3, * demonstrates significant difference from P220 determined by post-hoc Tukey tests-$p<0.05$).
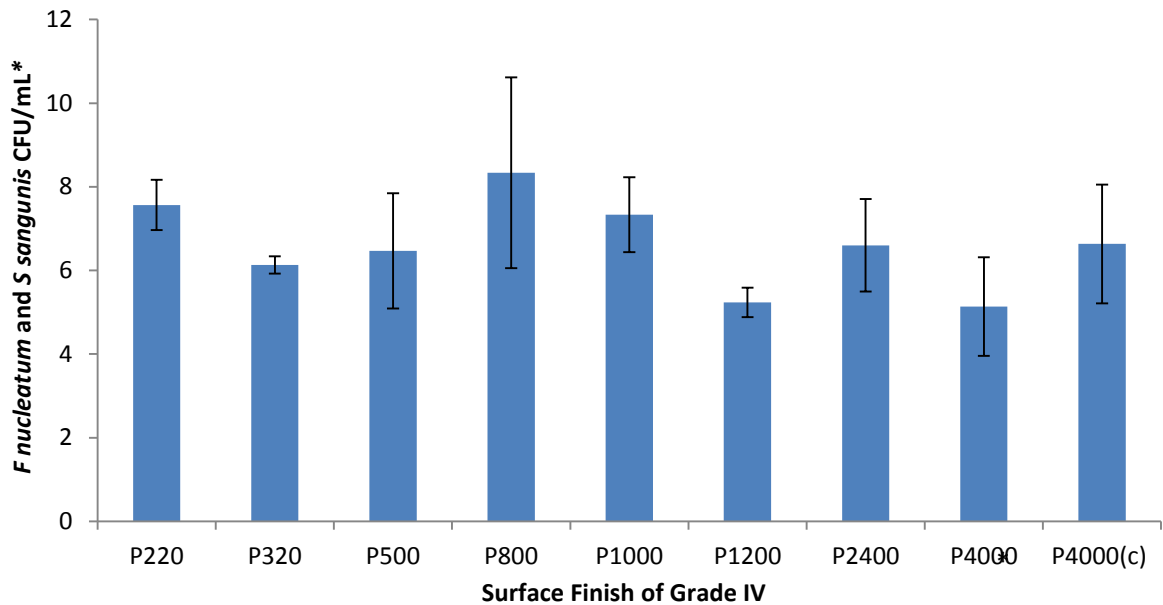
Figure 3.28. A histogram of mean± SD CFU/mL of *F nucleatum* and *S sanguinis* (*1 x 10^5) on Grade V CpTi surfaces prepared with P220, P320, P500, P800, P1000, P1200, P2400, P4000 SiC final grit size abrasives and P4000(c) prepared with colloidal silica. (n=3, * demonstrates significant difference from P220 determined by post-hoc Tukey tests-$p<0.05$).
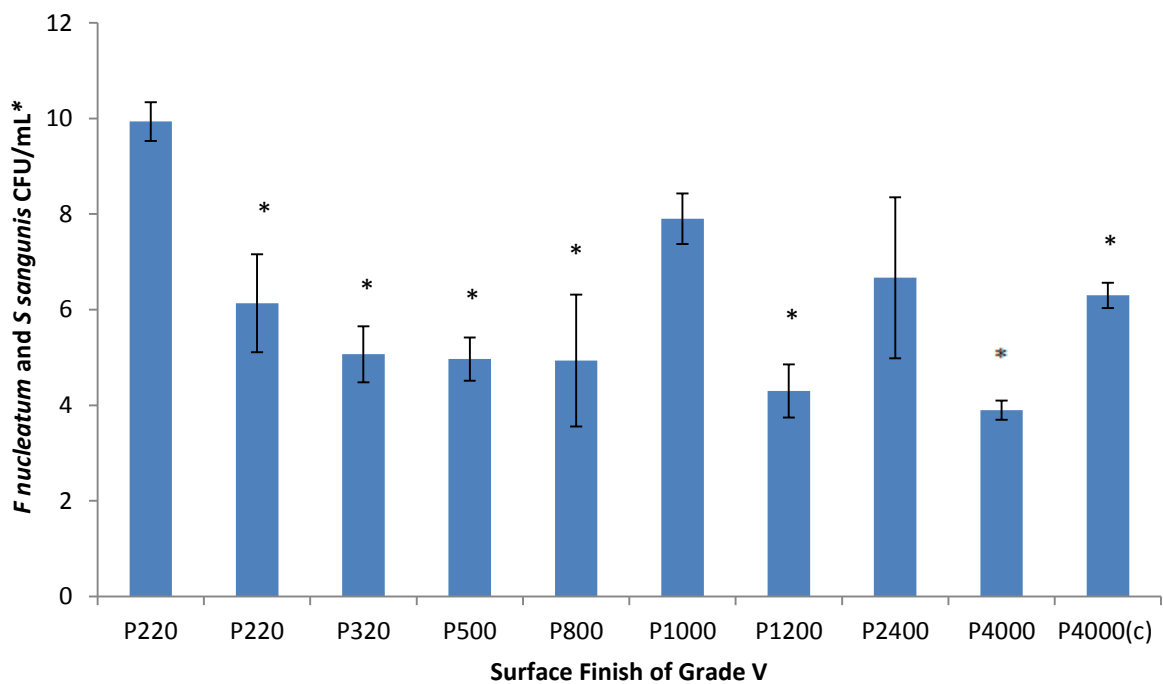
Significant differences were observed in mean CFU/mL between the surface textures of P220 and the surface textures of P1000, P2400 and P4000(c) Grade II surfaces (figure 3.26) with a tendency towards lower bacterial counts on the smoother surfaces of P1000 onwards. There were no significant differences observed in the mean CFU/mL of *F nucleatum* and *S sanguinis* on the Grade IV Ti substrate (figure 3.27). An important observation between bacterial adhesion on Grade II and IV was that there was a reduction in the number of bacteria adhered to the prepared surfaces for Grade IV in general with the mean CFU/mL on P220 Grade II at ~$12x10^5$ CFU/mL when compared with ~ $8x10^5$ CFU/mL on Grade IV Ti (figure 3.27). The adhesion of *S sanguinis* and *F nucleatum* to the Grade V alloy showed a significant difference from the P220 prepared Ti substrate from the two parts of the experiement and therefore data could not be directly compared and is indicative only (figure 3.28) however the surface texture created with the P1000 finish possessed the most bacteria with a mean count of $8x10^5$ CFU/mL.

3.3.5 Correlation between bacterial attachment/early proliferation with surface topology.
Table 3.1 displays the correlation between the bacterial adhesion of *S sanguinis*, *E coli, S mutans* and *F nucleatum* (mean CFU/mL) and the surface roughness parameters of Ra, Rp, Rv, Rz, Rt, Rq, Rc, Rsk and Rku derived from surface metrology of the prepared surfaces (Grade II, IV and V, prepared according to final SiC grit size). A value of 1 indicates a direct linear correlation whereas a value near to 0 signifies no correlation between the adhesion of the bacteria and the surface roughness parameters. The objective was to identify whether there were any specific features (defined by standard metrological measurements) of the surface topology that could be predictive of the early adhesion of relevant oral microbes.

Table: 3.2: The results of regression analyses between adhesion of *S sanguinis*, *E coli*, *S mutans* and *F nucleatum* (n=3, mean CFU/mL) on Grade II, IV V P220, P320, P500, P800, P1000, P1200, P2400, P4000 and P4000(c) prepared Ti surfaces and the surface roughness parameters of *Ra, Rp, Rv, Rz, Rt, Rq, Rc, Rsk and Rku* (µm) (Data expressed as R^2 values).

	Ra	Rp	Rv	Rz	Rt	Rq	Rc	Rsk	Rku
Grade II *S sanguinis*	0.05	0.07	0.09	0.09	0.08	0.13	0.09	0.06	0.03
Grade II *E coli*	0.66	0.65	0.75	0.72	0.68	0.73	0.69	0.79	0.72
Grade II *S mutans*	0.21	0.26	0.27	0.27	0.28	0.31	0.29	0.06	0.02
Grade II *F nucleatum*	0.05	0.05	0.07	0.07	0.07	0.14	0.08	0.14	0.07
Grade II *F nucleatum and S sanguinis*	0.62	0.66	0.55	0.60	0.64	0.61	0.62	0.05	0.15
Grade IV *S Sanguinis*	0.23	0.23	0.16	0.25	0.23	0.23	0.16	0.05	0.02
Grade IV *E coli*	0.27	0.22	0.33	0.17	0.28	0.28	0.09	0.003	0.25
Grade IV *S mutans*	0.19	0.14	0.24	0.15	0.23	0.20	0.05	0.10	0.01
Grade IV *F nucleatum*	0.16	0.17	0.23	0.19	0.16	0.16	0.26	0.01	0.36
Grade V *S sanguinis*	0.01	0.00	0.00	0.00	0.07	0.00	0.00	0.05	0.02
Grade V *E coli*	0.13	0.01	0.10	0.01	0.46	0.09	0.66	0.20	0.31
Grade V *S mutans*	0.23	0.20	0.21	0.20	0.18	0.21	0.21	0.03	0.0
Grade V *F nucleatum*	0.01	0.01	0.00	0.01	0.01	0.01	0.01	0.00	0.00

It was found that there was a weak correlation between the surface roughness parameters and the numbers of bacteria adhered to the Ti prepared surfaces of P220, P320, P500, P800, P1000, P1200, P2400, P4000 and P4000(c). No specific parameter was consistently associated with bacterial cell count for the Ti surfaces and species examined. The strongest correlations were observed was between a number of surface roughness parameters and the polyculture of *F nucleatum* and *S sanguinis* prepared on a Grade II surface (Ra =0.62, Rp = 0.66, Rv = 0.55, Rz = 0.60, Rt= 0.64, Rq= 0.61, Rc= 0.62, Rsk =0.05 and the Rku of 0.15 µm). The weakest correlation was observed on the Grade V surface with *F nucleatum* where the surface roughness parameters demonstrate almost zero correlation with cell numbers.

3.3.6 The effect of bacterial adhesion on P220, P1220 and P400 with increased sample numbers.

Given the lack of obvious correlations between surface metrology parameters and microbial adhesion to prepared Ti surfaces, the adhesion of *Sanguinis, F nucleatum, E coli* and *S mutans* was further investigated with increased sample numbers on the roughest P220, smoothest P4000 and the P1200 prepared surface which had an intermediary surface roughness in order to provide better statistics.

Figure 3.29. A histogram of *S sanguinis* adhesion (mean± SD CFU/mL -(seeded at *5 x 10^1) on Grade II CpTi surfaces prepared with to a final P220, P1200 and P4000 grit size (n=5, *= differences in significance at p<0.05).
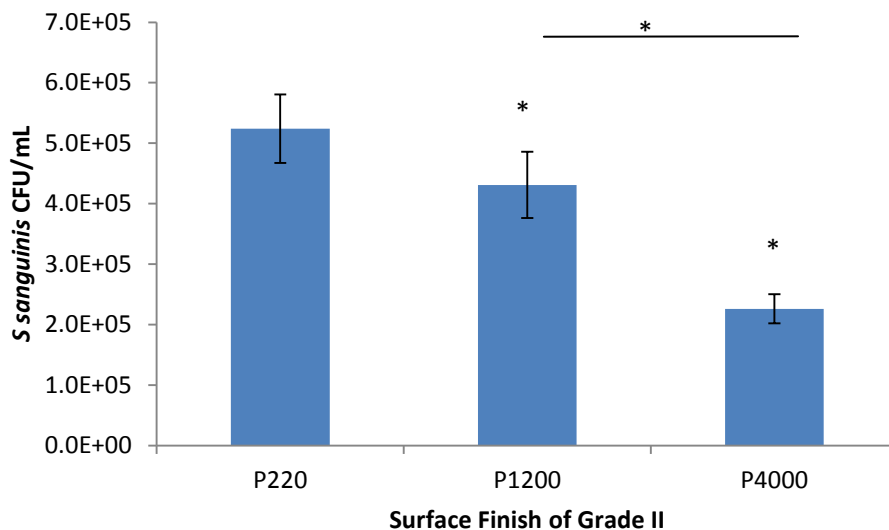
A significant reduction in mean CFU/mL was observed from the P220 prepared surface to the P1200 finished Grade II surface (p=0.01). It was further observed that there were significant differences in bacterial count between the P220 and the P4000 surfaces (p<0.001). There was a similar reduction in bacterial adhesion observed between the P1200 prepared surface and the P4000 prepared surface (p<0.001).

Figure 3.30. A histogram of *E Coli* adhesion (mean± SD CFU/mL -(seeded at *5 x 10^1) on Grade II CpTi surfaces prepared with to a final P220, P1200 and P4000 grit size (n=5, *= differences in significance at p<0.05).
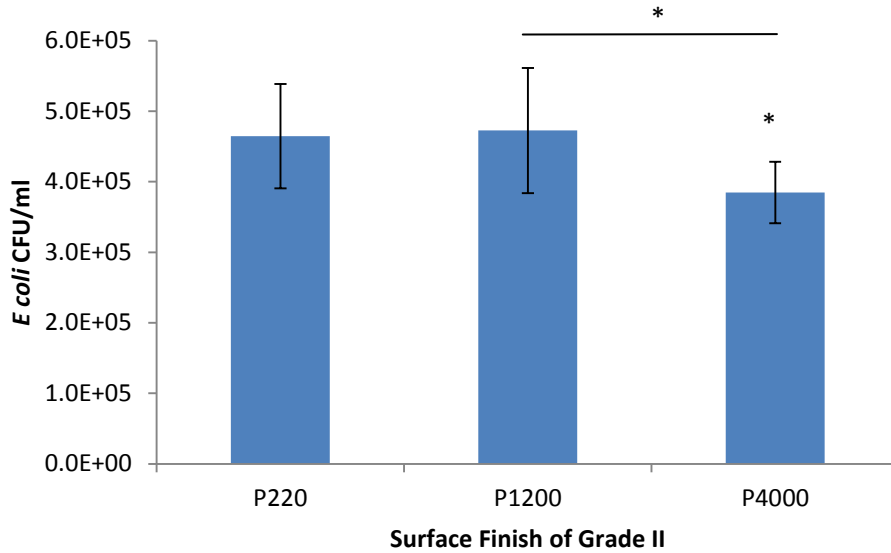
No significant difference was observed in the mean CFU/mL of *E coli* between the P220 and P1200 Grade II prepared surfaces (p>0.05). There was a significant reduction in the mean CFU/mL of *E coli* between the P220 prepared surface and the P4000 surface (p<0.05). A further significant reduction was between the P1200 and P4000 prepared surfaces (p<0.05).

Figure 3.31. A histogram of *S mutans* adhesion (mean± SD CFU/mL -(seeded at *5 x 10^1) on Grade II CpTi surfaces prepared with to a final P220, P1200 and P4000 grit size (n=5, *= differences in significance at p<0.05).
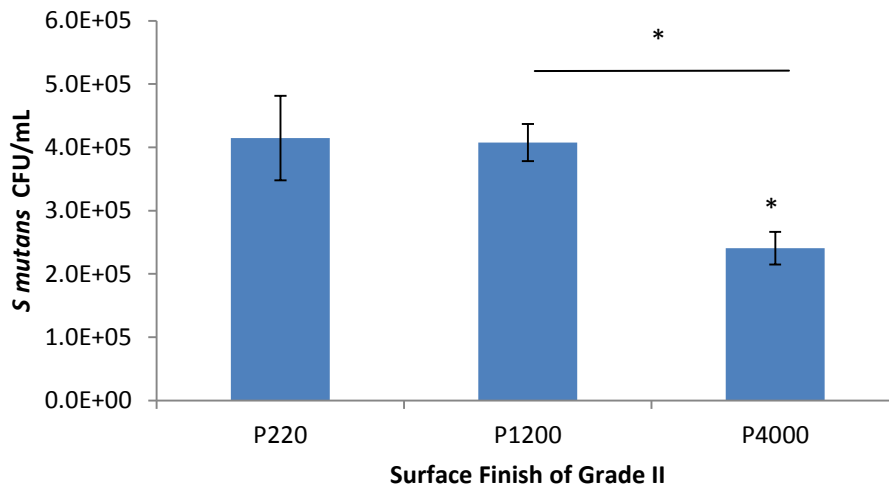
For *S mutans* there was a significant increase in the bacterial adhesion to Grade IV CpTi as the surface roughness decreased from P220 to P1200 (p<0.05) and from P1200 to P4000 (p<0.05)

Figure 3.32. A histogram of *F nucleatum* adhesion (mean± SD CFU/mL -(seeded at *5 x 10^1) on Grade II CpTi surfaces prepared with to a final P220, P1200 and P4000 grit size (n=5, *= differences in significance at p<0.05).
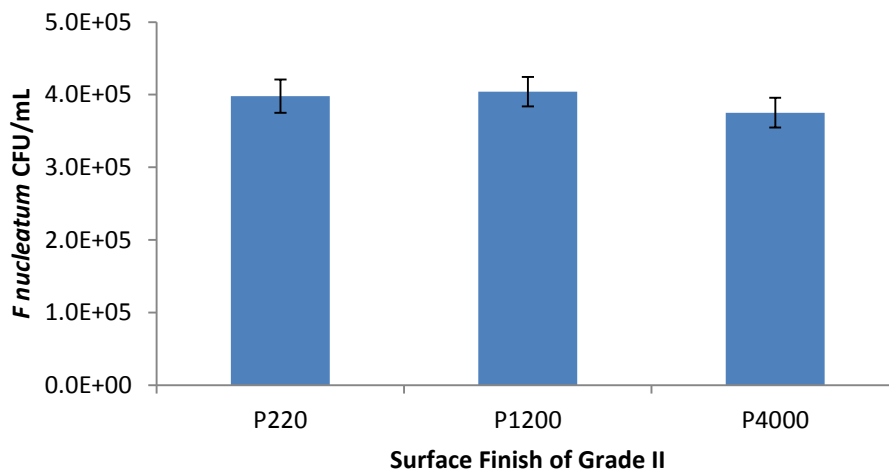
No significant differences in the mean CFU/mL of *F nucleatum* on the surface of prepared Grade IV surfaces was observed (p<0.05) (figure 3.32).

Figure 3.33. A histogram of *S sanguinis* adhesion (mean± SD CFU/mL -(seeded at *5 x 10^1) on Grade IV CpTi surfaces prepared with to a final P220, P1200 and P4000 grit size (n=5, *= differences in significance at p<0.05).
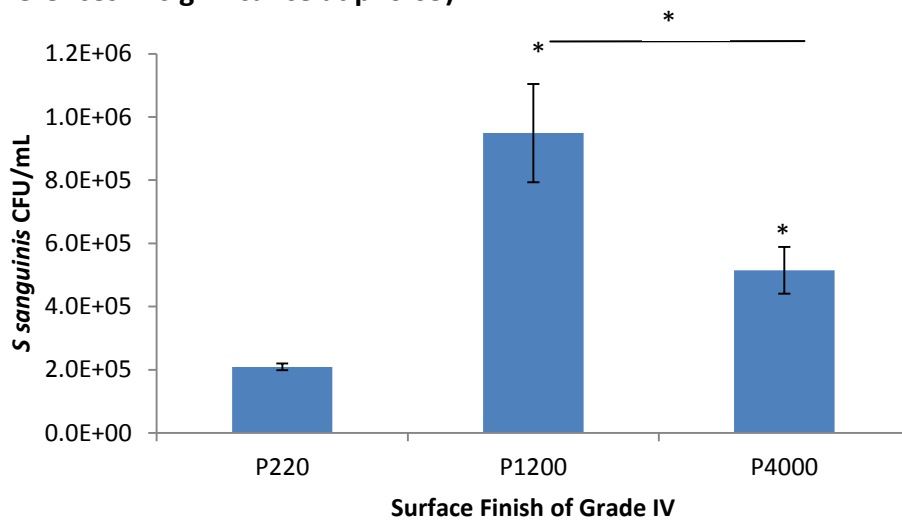
No significant difference in the adhesion of *S sanguinis* between the P220 prepared surface and the P1200 finished Grade V surface was observed (p>0.05) however there was a significant increase in *S sanguinis* adhesion between the P220 and the P4000 surfaces (p<0.001) and between P1200 prepared and the P4000 prepared surfaces (p<0.05).

Figure 3.34. A histogram of *E Coli* adhesion (mean± SD CFU/mL -(seeded at *5 x 10^1) on Grade IV CpTi surfaces prepared with to a final P220, P1200 and P4000 grit size (n=5, *= differences in significance at p<0.05).
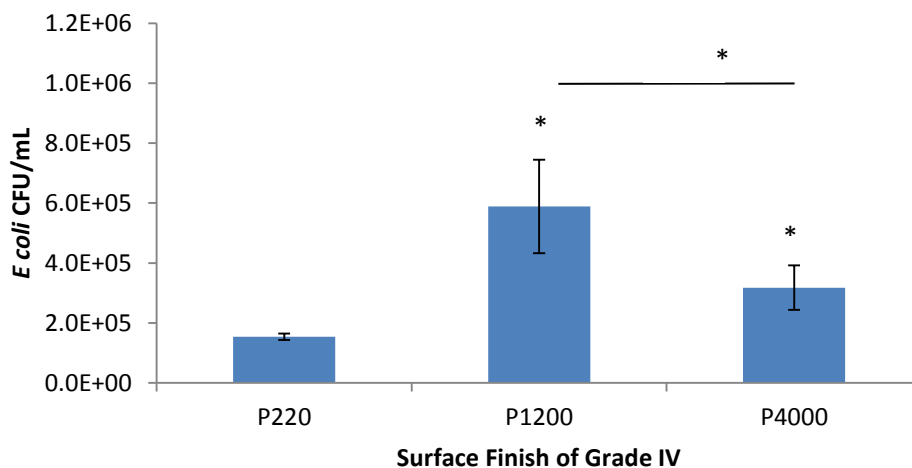
E coli adhesion on the prepared Grade V surfaces of P220, P1200 and P4000 finish (figure

3.34) significantly decreased as the surface roughness decreased from P220 to P1200

(p<0.001) and from P1200 to P4000 (p<0.001).

Figure 3.35. A histogram of *S mutans* adhesion (mean± SD CFU/mL -(seeded at *5 x 10^1) on Grade IV CpTi surfaces prepared with to a final P220, P1200 and P4000 grit size (n=5, *= differences in significance at p<0.05).
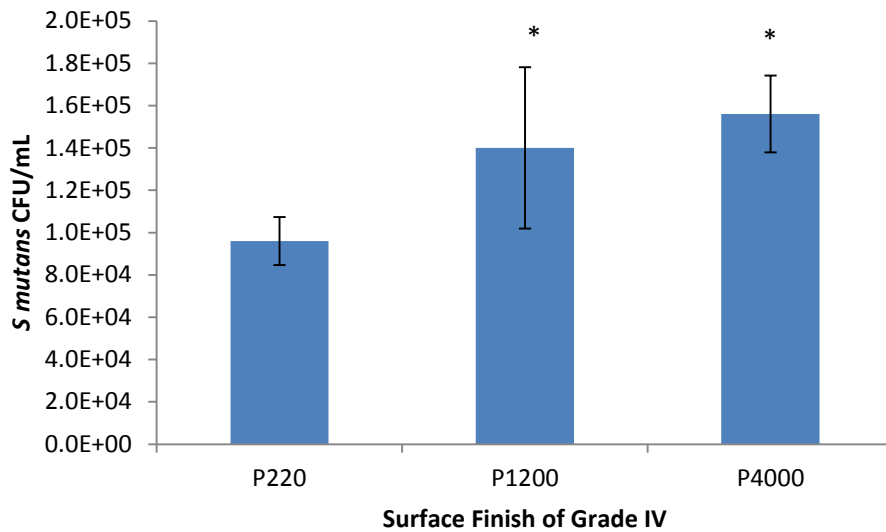
S mutans adhesion to Grade V surfaces prepared to a P220, P1200 and P4000 finish

significantly from P220 to P1200 (p<0.05). A further significant reduction was observed

between the P220 Grade V prepared surface and the P4000 prepared surface (p<0.001).

Figure 3.36. A histogram of *F nucleatum* adhesion (mean± SD CFU/mL -(seeded at *5 x 10^1) on Grade IV CpTi surfaces prepared with to a final P220, P1200 and P4000 grit size (n=5, *= differences in significance at p<0.05).
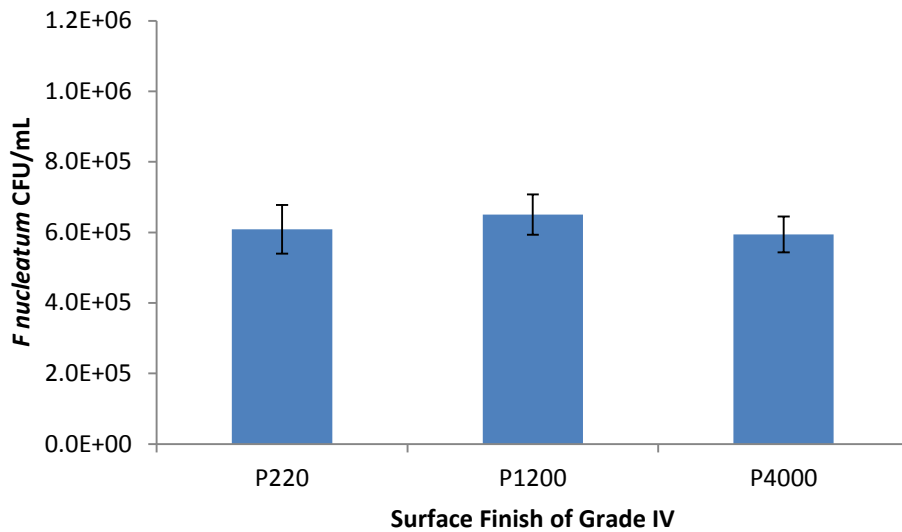
No significant differences in the mean CFU/mL of *F nucleatum* on the surface of prepared

Grade IV surfaces was observed (p<0.05)(figure 3.36)

Figure 3.37. A histogram of *S sanguinis* adhesion (mean± SD CFU/mL -(seeded at *5 x 10^1) on Grade V CpTi surfaces prepared with to a final P220, P1200 and P4000 grit size (n=5, *= differences in significance at p<0.05).
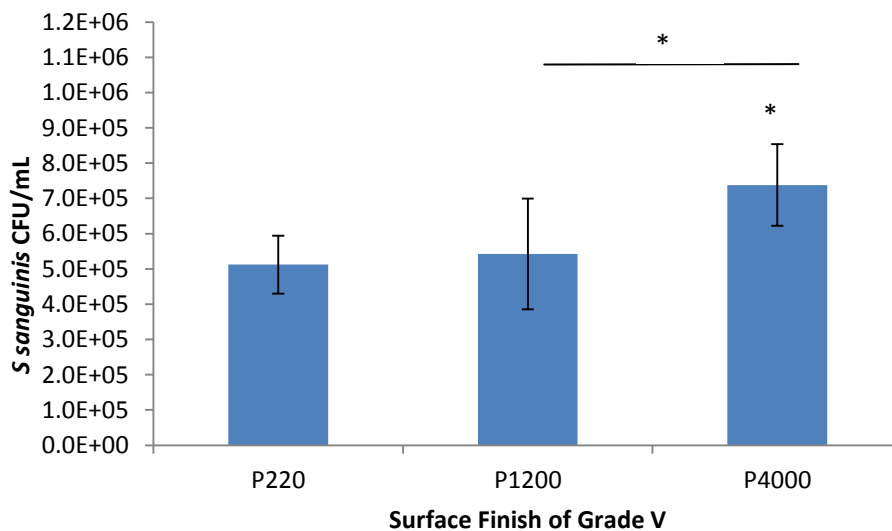
No significant difference in the adhesion of *S sanguinis* between the P220 prepared surface

and the P1200 finished Grade V surface was observed (p>0.05) however there was a

significant increase in *S sanguinis* adhesion between the P220 and the P4000 surfaces

(p<0.001) and between P1200 prepared and the P4000 prepared surfaces (p<0.05).

Figure 3.38. A histogram of *E coli* adhesion (mean± SD CFU/mL -(seeded at *5 x 10^1) on Grade V CpTi surfaces prepared with to a final P220, P1200 and P4000 grit size (n=5, *= differences in significance at p<0.05).
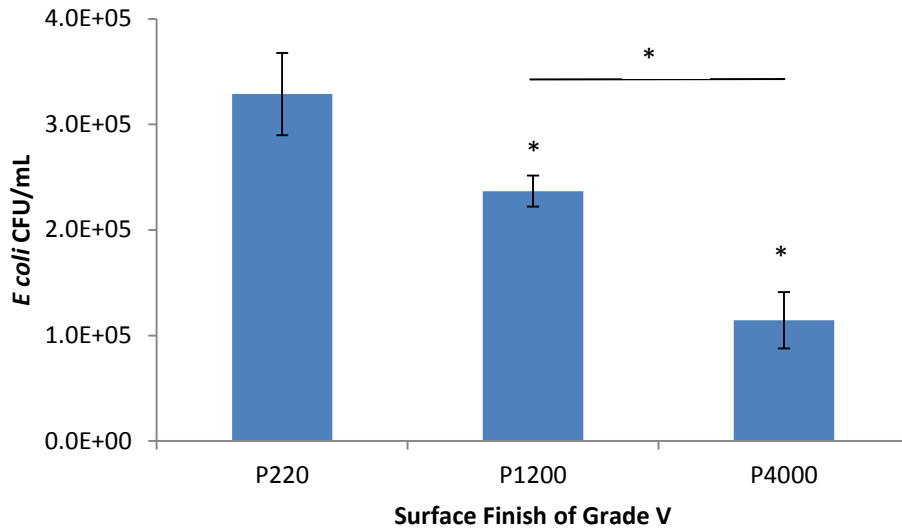
E coli adhesion on the prepared Grade V surfaces of P220, P1200 and P4000 finish (figure

3.53) significantly decreased as the surface roughness decreased from P220 to P1200

(p<0.001) and from P1200 to P4000 (p<0.001).

Figure 3.39. A histogram of *S mutans* adhesion (mean± SD CFU/mL -(seeded at *5 x 10^{1}) on Grade V CpTi surfaces prepared with to a final P220, P1200 and P4000 grit size (n=5, *= differences in significance at p<0.05).
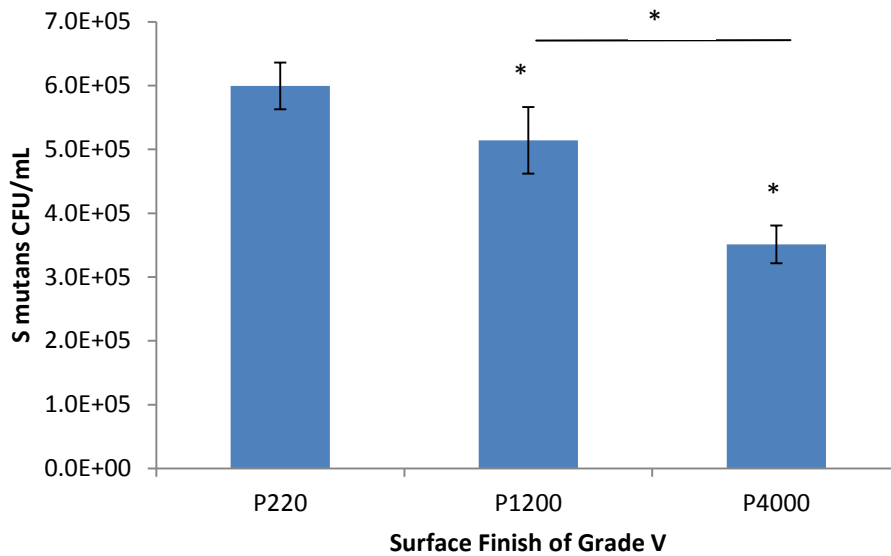
S mutans adhesion to Grade V surfaces prepared to a P220, P1200 and P4000 finish

significantly from P220 to P1200 (p<0.05). A further significant reduction was observed

between the P220 Grade V prepared surface and the P4000 prepared surface (p<0.001).

Figure 3.40. A histogram of *F nucleatum* adhesion (mean± SD CFU/mL -(seeded at *5 x 10^{1}) on Grade V CpTi surfaces prepared with to a final P220, P1200 and P4000 grit size (n=5, *= differences in significance at p<0.05).
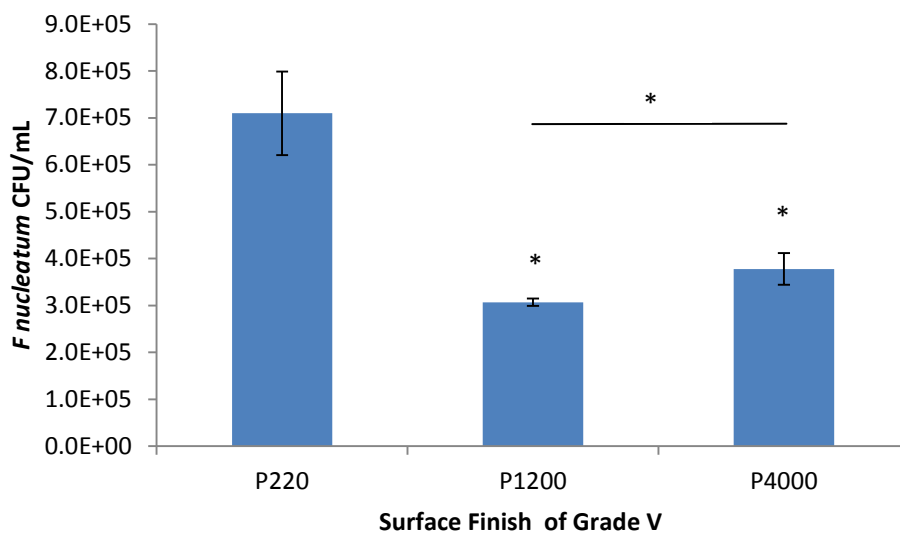
The adhesion of *F nucleatum* to the surface of prepared Grade V surfaces (figure 3.40) was observed to follow a different pattern when compared with adhesion on Grade II and Grade IV substrates (figure 3.32 and 3.36). A significant reduction in *F nucleatum* adhesion was observed ($p<0.001$).

3.3.7 The correlation between bacterial adhesion and surface roughness parameters with on P220, P1200 and P4000 Grade II, IV and V prepared Ti surfaces with increased sample numbers.

The relationship between mean bacterial adhesion (CFU/mL) and surface metrology parameters was explored to identify potential predictive correlations.

Table: 3.3: The correlation between *S sanguinis*, *E coli*, *S mutans* and *F nucleatum* (n=5) adhesion on Grade II, IV, V P220, P1200 and P4000 prepared Ti surfaces against the surface roughness parameters of Ra, Rp, Rv, Rz, Rt, Rq, Rc, Rsk and Rku (data expressed as the R^2 value).

	Ra	Rp	Rv	Rz	Rt	Rq	Rc	Rsk	Rku
Grade II *S sanguinis*	0.91	0.85	0.78	0.81	0.92	0.97	0.91	0.86	0.41
Grade II *E coli*	0.99	1.00	0.99	0.99	0.99	0.95	0.99	1.00	0.78
Grade II *S mutans*	1.00	0.99	0.96	0.97	1.00	0.99	1.00	0.99	0.68
Grade II *F nucleatum*	0.96	0.99	1.00	1.00	0.95	0.88	0.95	0.98	0.87
Grade IV *S sanguinis*	0.28	0.30	0.14	0.27	0.21	0.23	0.27	0.34	0.001
Grade IV *E coli*	0.24	0.26	0.12	0.21	0.18	0.19	0.23	0.36	0.002
Grade IV *S mutans*	0.98	0.99	0.91	0.96	0.96	0.96	0.98	0.07	0.63
Grade IV *F nucleatum*	0.01	0.01	0.08	0.04	0.034	0.03	0.08	0.92	0.36
Grade V *S sanguinis*	0.60	0.79	0.684	0.77	0.41	0.64	0.69	0.69	0.98
Grade V *E coli*	0.80	0.94	0.86	0.92	0.83	0.87	0.63	0.87	0.88
Grade V *S mutans*	0.87	0.98	0.92	0.97	0.90	0.93	0.72	0.93	0.81
Grade V *F nucleatum*	0.84	0.66	0.78	0.70	0.81	0.77	0.96	0.77	0.12

It was found that there was a stronger correlation between bacterial adhesion to prepared Ti surfaces and the surface roughness parameters when discrete surface roughnesses were studied (P220, P1200 and P4000). The correlation observed was stronger when compared with Table 3.1 especially for the Grade II prepared surfaces. The strongest correlation was

observed with the adhesion of Grade II *E coli* with the metrology parameters Ra = 1.00, Rp = 1, Rt =0.99, Rq = 0.99, Rc = 0.99 and Rsk =1.00 The weakest correlations were between *F nucleatum* adhesion and roughness parameters for the Grade IV CpTi surface.

3.4 Engineered Ti surfaces.

3.4.1 Bacterial adhesion on SLM surfaces.

The engineered Ti SLM "5 x 5 mm" and the SLM "flat" surfaces were characterised by SEM and contact angles measurements. Characterisation identified the surface topology and wettability. The SLM surfaces were subsequently tested for the adhesion of *S sanguinis, E coli, S mutans* and *F nucleatum.* In addition the SLM prepared surfaces were placed in a CDC bioreactor to study S *sanguinis* attachment under biofilm conditions which was visualised using SEM.

Figure 3.41 Image of the SLM flat and the SLM "5 x 5 mm" checkerboard patterned surface
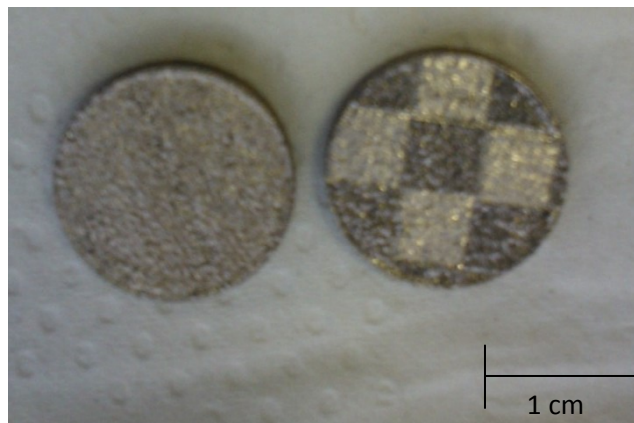
Figure 3.41 illustrates the two distinct surface textures created -smooth (left on the image) and the SLM "5 x 5 mm" patterned surface on the right.

3.4.2 SEM studies of Grade IV P220, P4000, and SLM Ti surface.

SEM was employed to compare the topology of the SLM "5 x 5 mm" and the SLM "flat"

surfaces (figure 3.43 and 3.44) with the control previously characterised Grade II P220 and

P4000 prepared surfaces (figures 3.42 and 3.45).

Figure 3.42. SEM images illustrating two regions of a Grade II surface prepared with a final P220 SiC grit at x2000 magnification (for comparison).
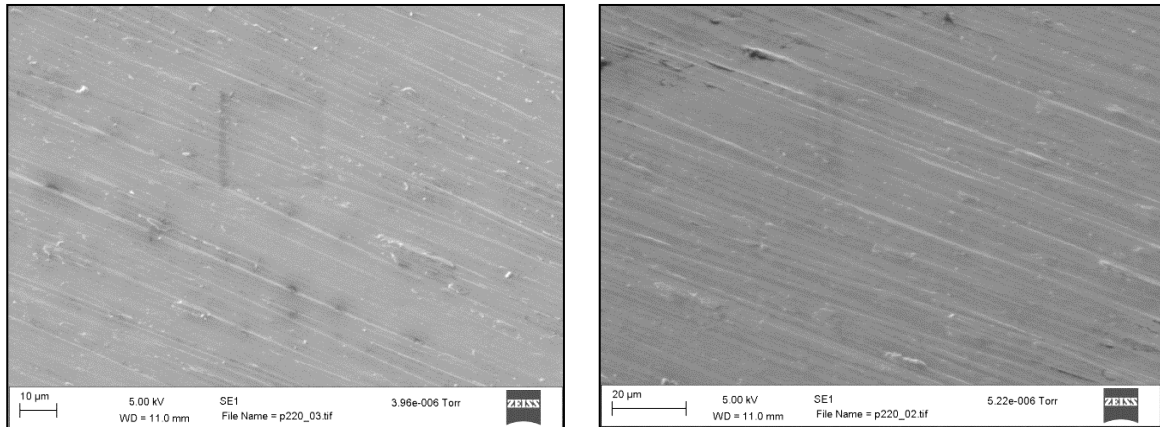
Images demonstrate the topography which is composed of consistent regular repeated small

amplitude peaks and valleys throughout the surface of the Grade II Ti rough surface.

Figure 3.43. SEM images illustrating the surface topography of the "5 x 5 mm" SLM grid patterned surface at x 2000 magnification. The circles highlight pores created on the island samples surface.
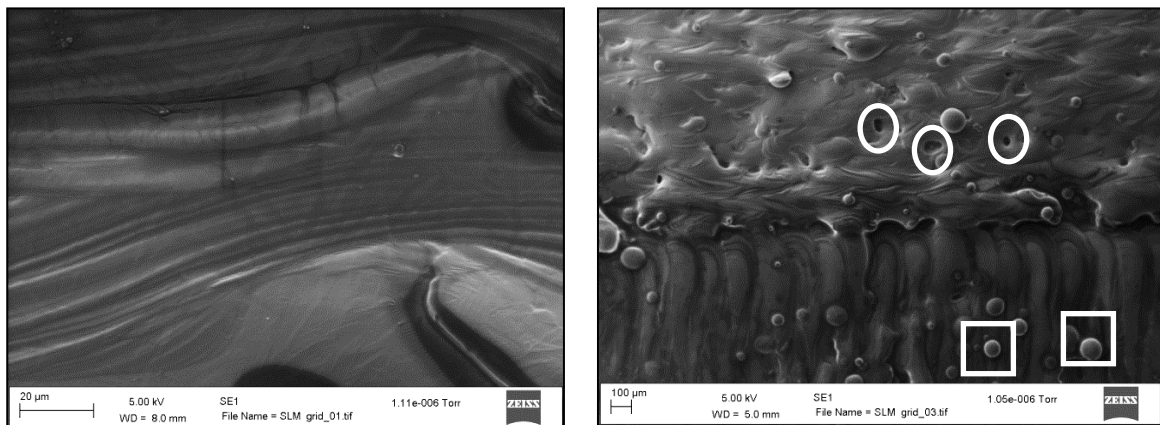
The images demonstrate the surface of the SLM "5 x 5 mm" patterned surface which exhibited a variable surface topography with the presence of areas which are relatively flat compared to areas that resemble slope like contours. The textures created within the comprised of repeating orientated patterns with the presence of residual Ti powder indicated by squares in the image.

Figure 3.44. SEM images illustrating the SLM flat surface topography at x2000 magnification.
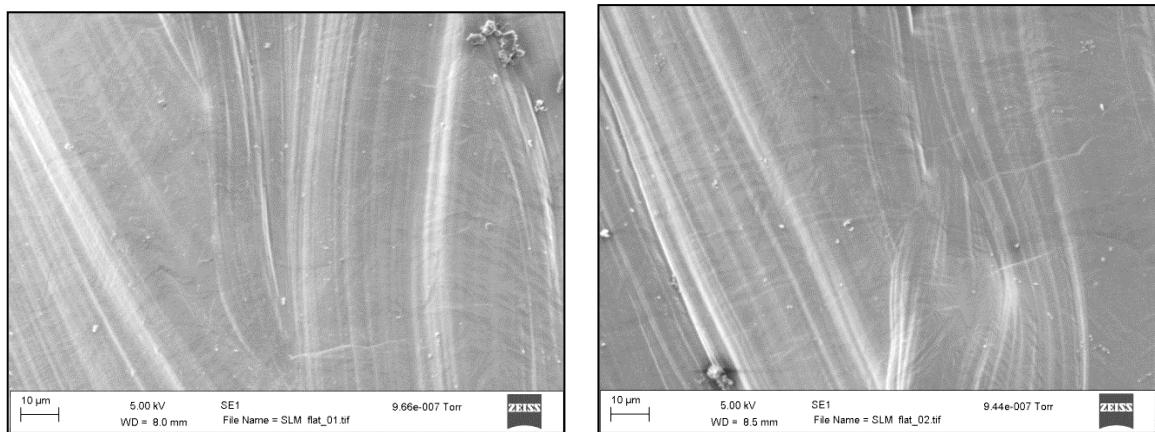
Figure 3.44 illustrates the SLM "flat" surface and demonstrates the consistent contours with low amplitude slopes and valleys being present. The surface topology was consistent across the whole surface.

Figure 3.45. SEM images illustrating two regions of the Grade II surface topography prepared with P4000 SiC grit at x2000 magnification (for comparison).
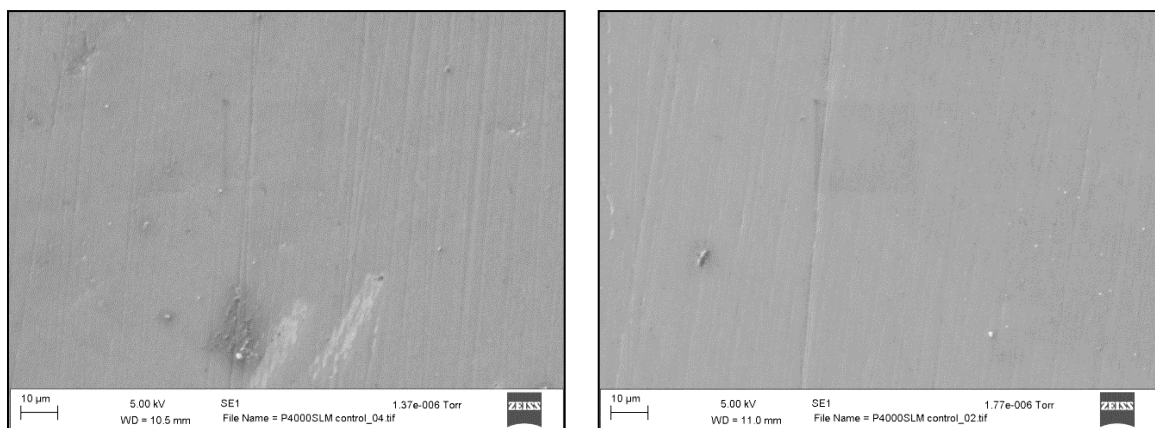
Figure 3.45 illustrates the two regions on the surface of the Grade II Ti P4000 polished surface. The surface contains scratches and imperfections that were not removed even using the finest polishing steps.

3.4.3 Contact angle measurements of the SLM engineered surfaces.

Contact angle measurements performed on the SLM "5 x 5 mm" and the SLM "flat" surfaces at 23 ± 1° however contact angles were relatively high suggesting a low degree of wettability.

Figure 3.46. Contact angle measurements performed at 23 ± 1 °C on the SLM prepared Ti samples prepared with SiC abrasive papers to a P220, P1200 and P4000 grit size (mean ± SD, n=3, *= P<0.05).
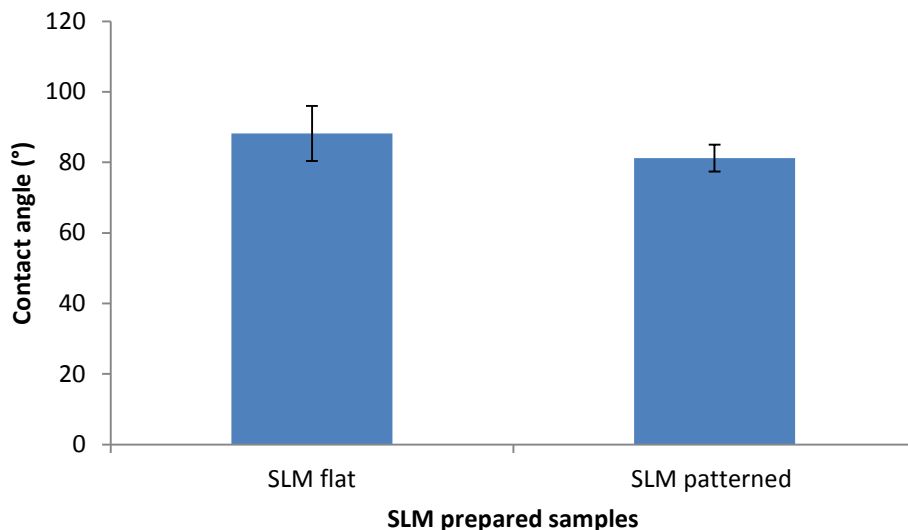
The contact angle measurements performed on both the SLM flat and the SLM "5 x 5 mm" surfaces using distilled water as a probing medium did not show any significant differences between the two surface conditions (p>0.05).

3.4.4 *S sanguinis, E coli, S mutans* and *F nucleatum* adhesion to SLM surfaces.

The adhesion of *S sanguinis, E coli, S mutans* and *F nucleatum* was determined on the SLM flat and the SLM "5 x 5 mm" surfaces. Controls of Grade II P220 and P4000 were included for comparison with previous data.

Figure 3.47. A histogram demonstrating *S sanguinis* adhesion to the prepared SLM "5 x 5 mm" and the SLM flat Ti surfaces with the controls of Grade II prepared with SiC abrasive papers to a P220 or P4000 grit size (mean ± SD, n=3, *= P<0.05).
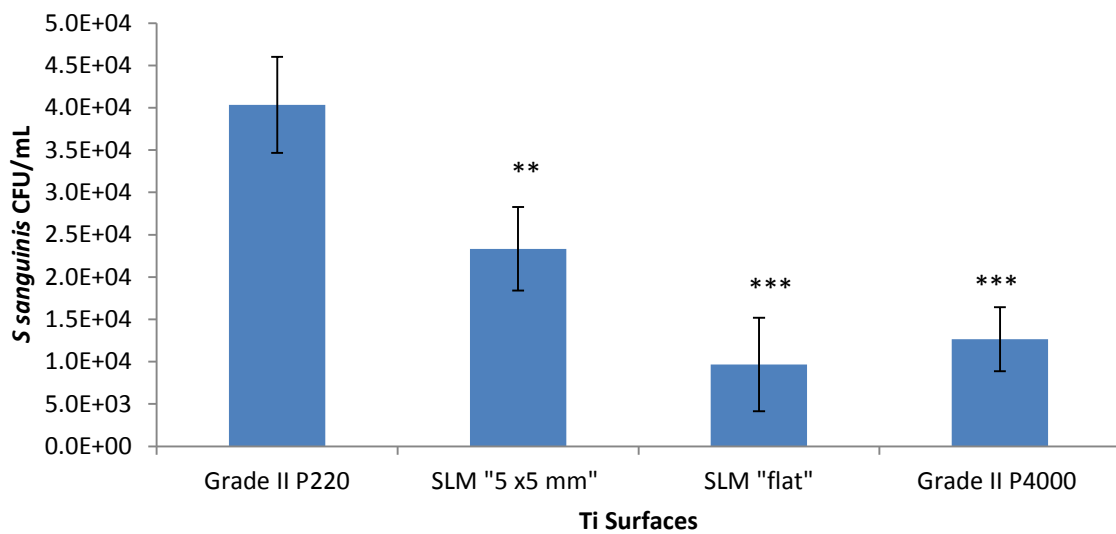
The Grade II P220 polished and the Grade II P4000 polished surfaces were used as well characterised control surfaces. A one-way ANOVA demonstrated a significant difference between the mean CFU/mL of *S sanguinis* on the different surfaces. Post-hoc Tukey tests identified that there was reduced bacterial adhesion for both SLM surfaces when compared to the P220 control (SLM "5 x 5" mm island samples (p=0.008) and the SLM "flat" surface (p=0.001)). There was no significant difference observed in *S sanguinis* adhesion between the SLM "flat" and the Grade II P4000 prepared surface. Further bacterial adhesion testing was determined with the bacteria of *E coli, S mutans* and *F nucleatum* (figure 3.48, 3.49 and 3.50).

Figure 3.48. A histogram demonstrating *E Coli* adhesion to the prepared SLM "5 x 5 mm" and the SLM flat Ti surfaces with the controls of Grade II prepared with SiC abrasive papers to a P220 or P4000 grit size (mean ± SD, n=3, *= P<0.05).
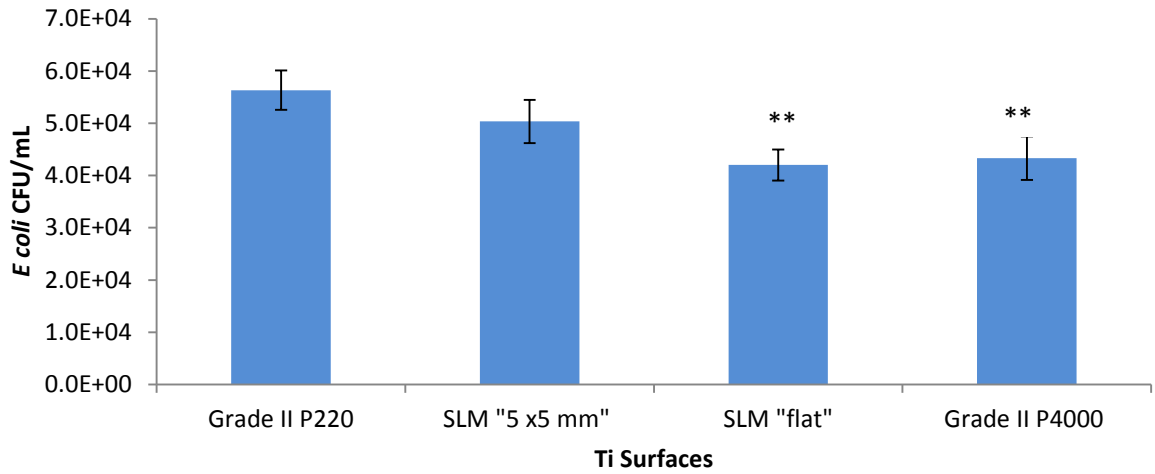
No significant differences were observed in the mean CFU/mL for *E coli* between the Grade II P220 and the SLM "5 x 5 mm" island prepared samples (p=0.07), however there was a significant reduction in bacterial adhesion between the Grade II P220 surface and the SLM "flat" surface (P=0.003).

Figure 3.49. A histogram demonstrating *S mutans* adhesion to the prepared SLM " 5 x 5 mm" and the SLM flat Ti surfaces with the controls of Grade II prepared with SiC abrasive papers to a P220 and P4000 grit size (mean ± SD, n=3, *= P<0.05).
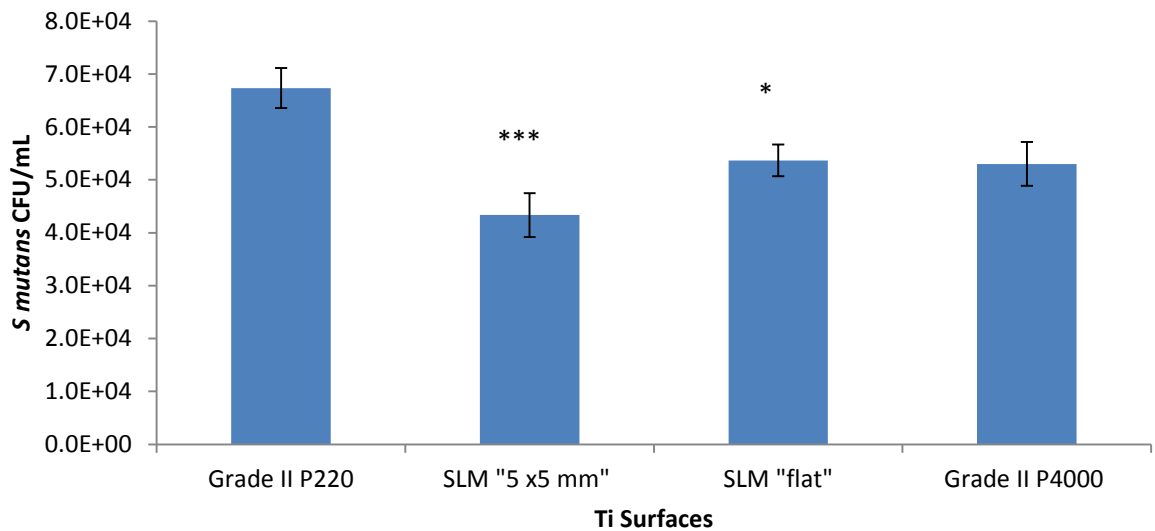
A significant reduction in *S mutans* adhesion (mean CFU/mL) to the SLM "5 x 5 mm" island prepared samples (p=0.001) and the SLM "flat" surface (p=0.006) was observed when compared with the Grade II P220 control. No significant difference was observed between the SLM surfaces and the P4000 controls (p>0.05).

Figure 3.50. A histogram demonstrating *F nucleatum* adhesion to the prepared SLM " 5 x 5 mm" and the SLM flat Ti surfaces with the controls of Grade II prepared with SiC abrasive papers to a P220 and P4000 grit size (mean ± SD, n=3, *= P<0.05).
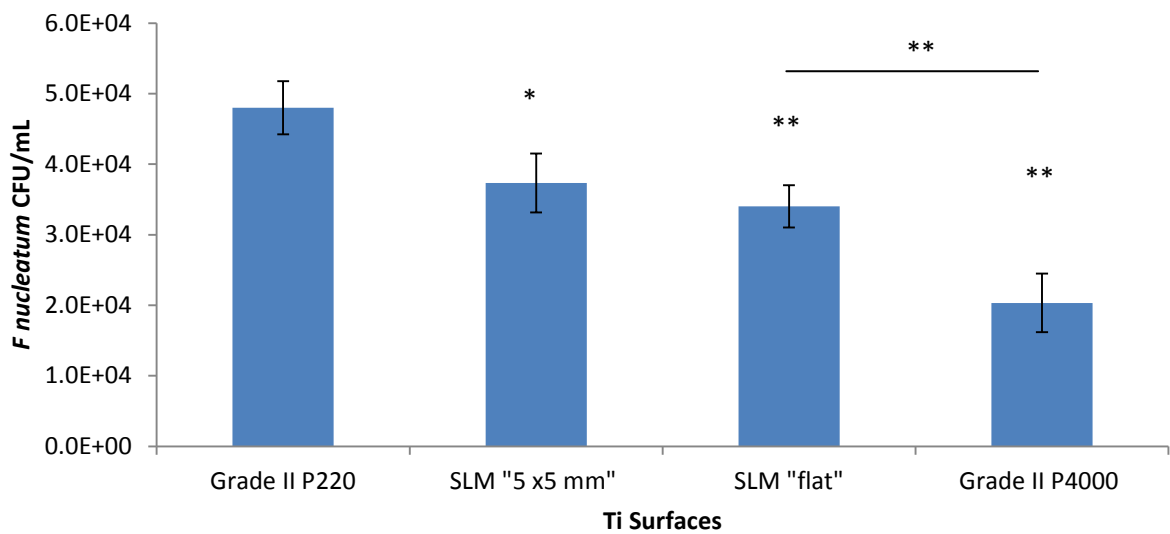
A significant decrease in mean *F nucleatum* CFU/mL was observed when compared with the P220 control for the SLM "5 x 5 mm" island prepared samples (p=0.02) and the SLM "flat" surface (p=0.006). A significant difference was further observed between the SLM "flat" surface and the Grade II P4000 prepared surface (p=0.002). The Grade II P4000 surface demonstrated significantly reduced bacterial attachment of *S sanguinis*, *E coli, S mutans* and *F nucleatum* when compared to the Grade II P220 control surfaces (p<0.05) (figures 3.47, 3.48, 3.49 and 3.50), but interestingly significantly reduced CFU/mL were observed for the SLM surfaces.

3.4.5 *S sanguinis* biofilm formation on SLM surfaces.

Three SLM "Flat" and three SLM "5 x 5 mm" samples were placed in the CDC bioreactor for

48 hrs to characterise the formation of *S sanguinis* biofilms on the SLM surfaces.

Figure 3.51. SEM images illustrating the distribution of *S sanguinis* on the surface of a SLM "flat" specimen x350 magnification demonstrating the SLM "flat" surface was entirely covered with *S sanguinis* bacteria with no obvious pattern being observed.
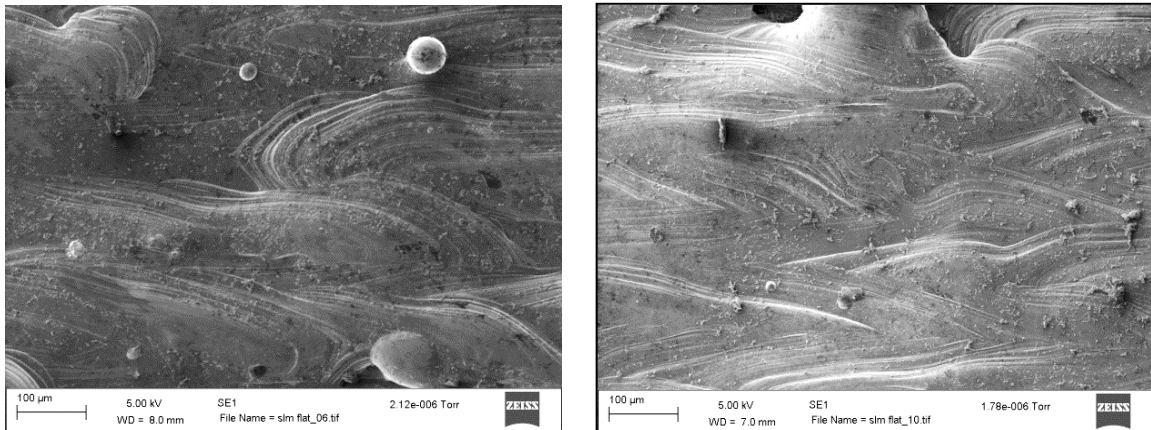
Figure 3.52. SEM images illustrating the distribution of *S sanguinis* on the surface of a second SLM "flat" specimen x350 magnification demonstrating an accumulation of *S sanguinis* biofilm adhered at the top of the contours.
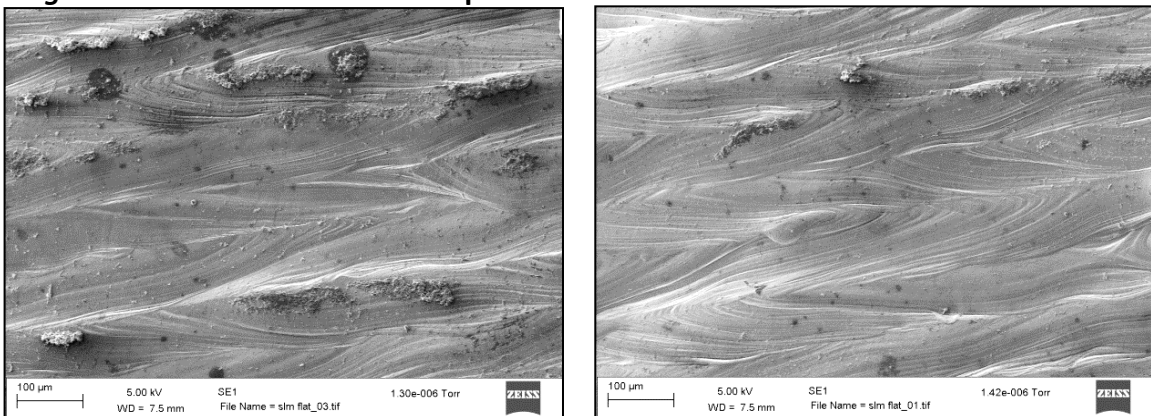
Figure 3.53. SEM images illustrating the distribution of *S sanguinis* on the surface of a third SLM "flat" specimen x350 magnification demonstrating the accumulation of the *S sanguinis* biofilms on the entire surface with further accumulation being observed around the powder that was left on the surface of the sample as part of manufacturing.
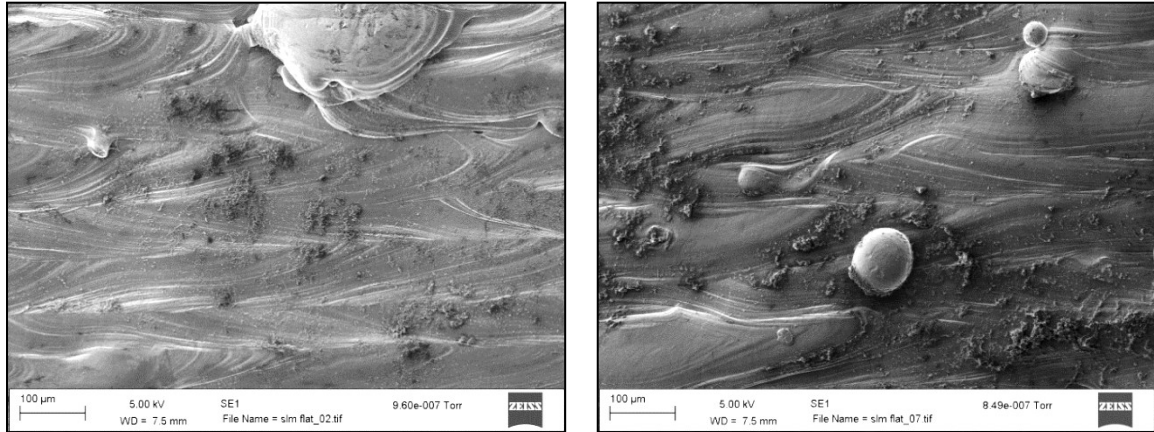
Figure 3.54. SEM images illustrating the distribution of *S sanguinis* on the surface of a SLM "5 x 5 mm" patterned specimen x350 magnification demonstrating a low number of cells of *S sanguinis* adhered to the surface with no obvious pattern being observed.
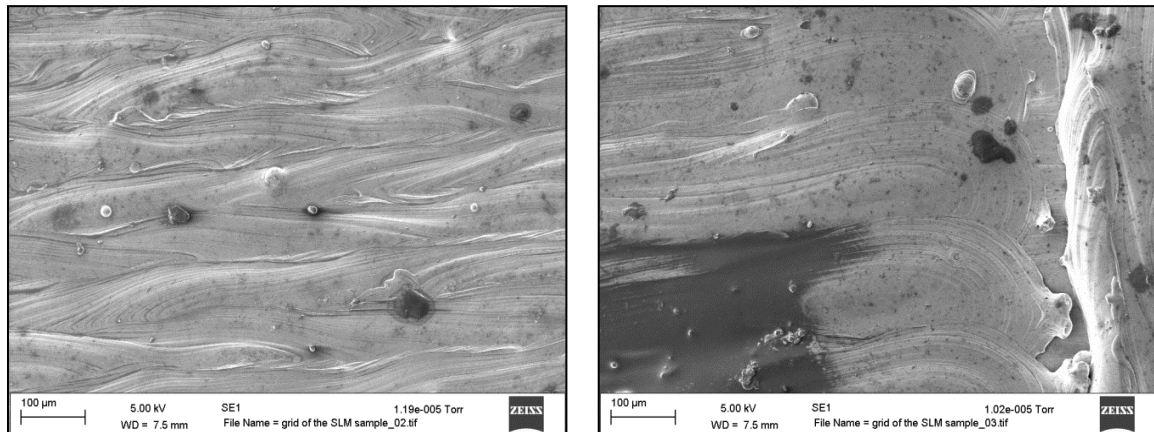
Figure 3.55. SEM images illustrating the distribution of *S sanguinis* on the surface of a second SLM "5 x 5 mm" patterned specimen x350 magnification demonstrating a high number of cells of *S sanguinis* adhered to the surface with no obvious pattern being observed

110
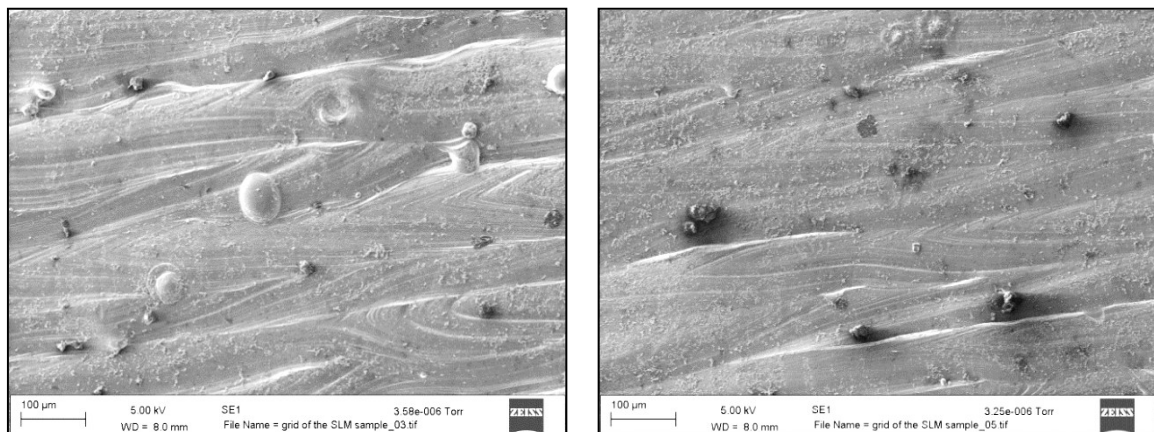
Figure 3.56. SEM images illustrating the distribution of *S sanguinis* on the surface of a third SLM "5 x 5 mm" patterned specimen x350 magnification demonstrating the formation of thick biofilm structures formed on the entire surface.
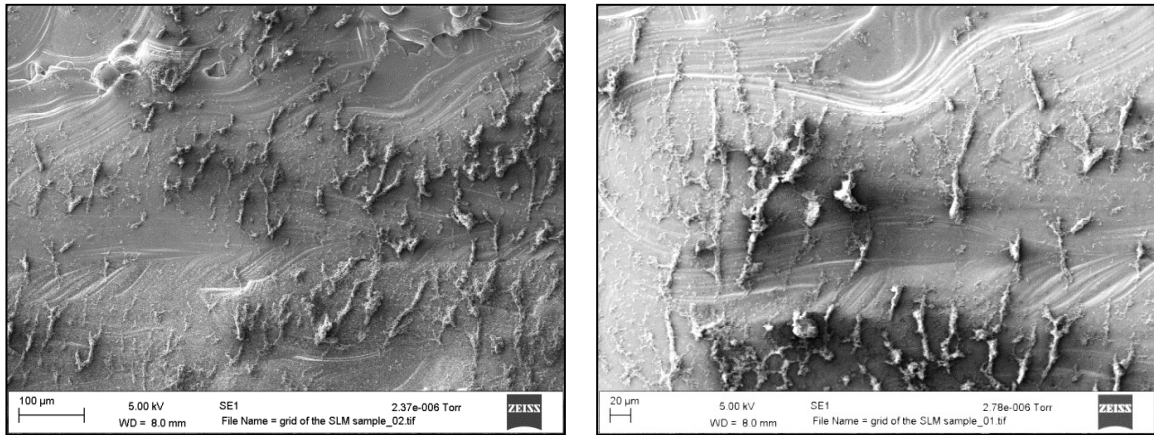
The SEM images illustrate the distribution of *S sanguinis* biofilm on the surface of the SLM flat and the SLM "patterned" surfaces after incubation in a CDC biofilm reactor. Although there was inconsistency between samples it was evident the *S sanguinis* biofilm appeared to be more dense at the peak of contours of the engineered topography. The SEM figures 3.54, 3.55 and 3.56 there is no obvious patterns on the surface of the "5 x5 mm" SLM surface as the *S sanguinis* biofilm covers the while surface topography.

3.4.6 The effect of Nanopore and Nanotubule surfaces on bacterial adhesion.

The engineered surfaces of Ti foil, Compact oxide (CO), Nanopore (NP), Nanotubule (NT) 15 nm, NT 50 nm and 100 nm diameter surfaces were initially characterised by contact angle measurements to determine the surface wettability and subsequently the adhesion of *S sanguinis* and *S mutans* was determined. X-ray photoelectron spectrometry (XPS) was performed on the engineered Ti surfaces to determine the Fluorine content.

3.4.7 Contact angle measurements.

Figure 3.57. Histogram illustrating the contact angles (°)performed at 23 ± 1 °C on the Ti foil, CO, NP, NT with 15 nm, 50 nm and 100 nm diameter surfaces with distilled water (Mean ± SD, n=3, *= P<0.05).
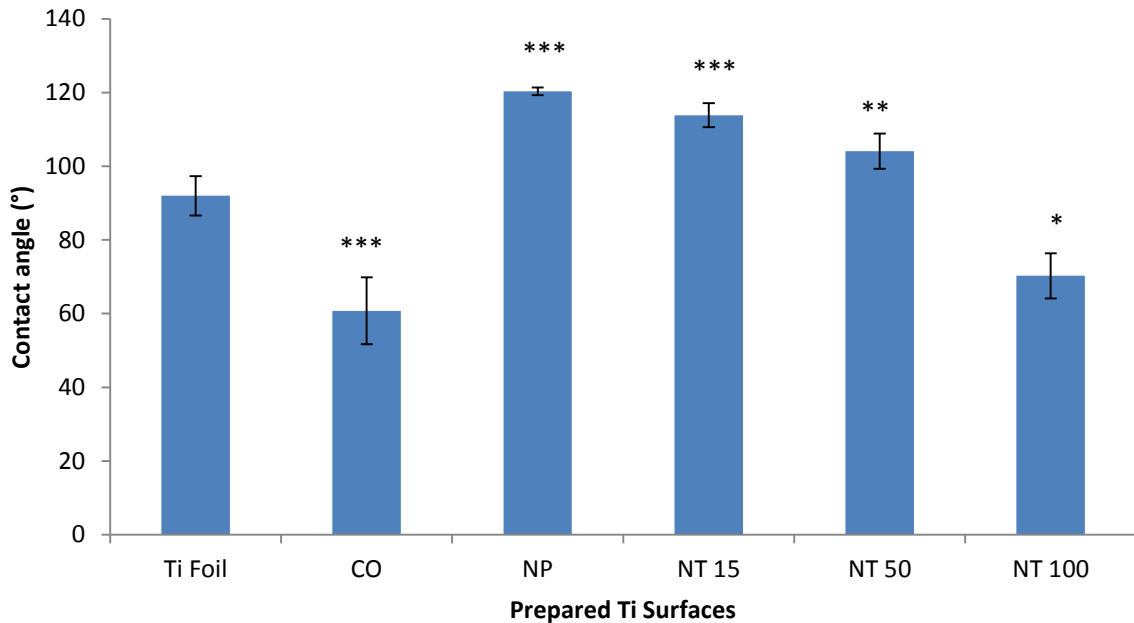
Contact angle measurements were performed to determine the wettability of the engineered Ti surfaces and demonstrated that the CO and the NT 100 nm surfaces demonstrated the most wettability whilst the Ti Foil, NP, NT 15 nm, NT 50 nm were more hydrophobic.

3.4.8 Adhesion of *S sanguinis* and *S mutans* to Ti foil, CO, NP and NT surfaces.

The adhesion of *S sanguinis* and *S mutans* was evaluated on the Ti foil, CO, NP, NT with 15 nm, 50 nm and 100 nm diameter surfaces. It was demonstrated that there was a significant increase in the adhesion of *S sanguinis* and *S mutans* to the NT 50 nm and NT 100 nm diameter surfaces compared to the Ti foil control (figures 3.58 and 3.59).

Figure 3.58. A histogram illustrating the *S sanguinis* attachment to the Ti Foil, CO, NP, NT with 15 nm, 50 nm and 100 nm diameter surfaces (Mean ± SD, n=3, *= P<0.05).
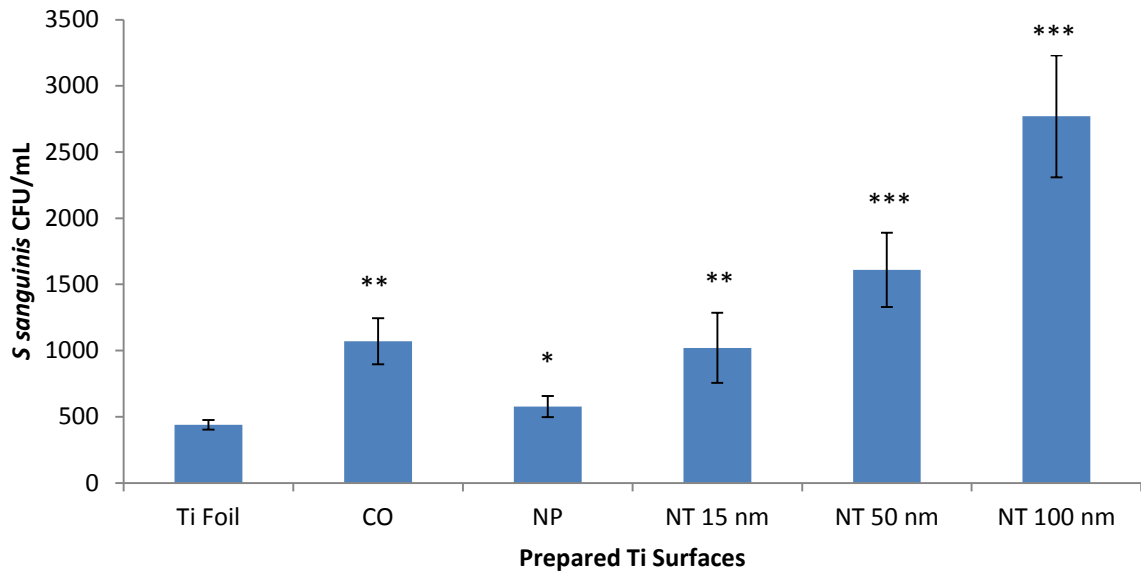
Three control samples were included in the study (Ti Foil, CO, NP) to compare the adhesion of *S sanguinis* to the prepared nanotube Ti samples of NT 15 nm, NT 50 nm and NT 100 nm diameter (figure 3.58). Significant differences were observed between the Ti Foil (440 CFU/mL), CO (1070 CFU/mL) (p<0.05) and NP (578 CFU/mL) (p<0.01). It was also observed that there was significantly reduced adhesion of *S sanguinis* on the Ti foil surface (440 CFU/mL) when compared with NT 15 nm (578 CFU/mL) (p<0.05), NT 50 nm (1610 CFU/mL) (p=0.001) and NT 100 nm (2770 CFU/mL) (p=0.001). The data demonstrated that as the NT size increased from 15 nm, 50 nm to 100 nm there was also a concomitant increased adhesion of *S sanguinis*.

Figure 3.59. Histogram illustrating *S mutans* attachment to the Ti Foil, CO, NP, NT with 15 nm, 50 nm and 100 nm diameter surfaces (Mean ± SD, n=3, *= P<0.05).
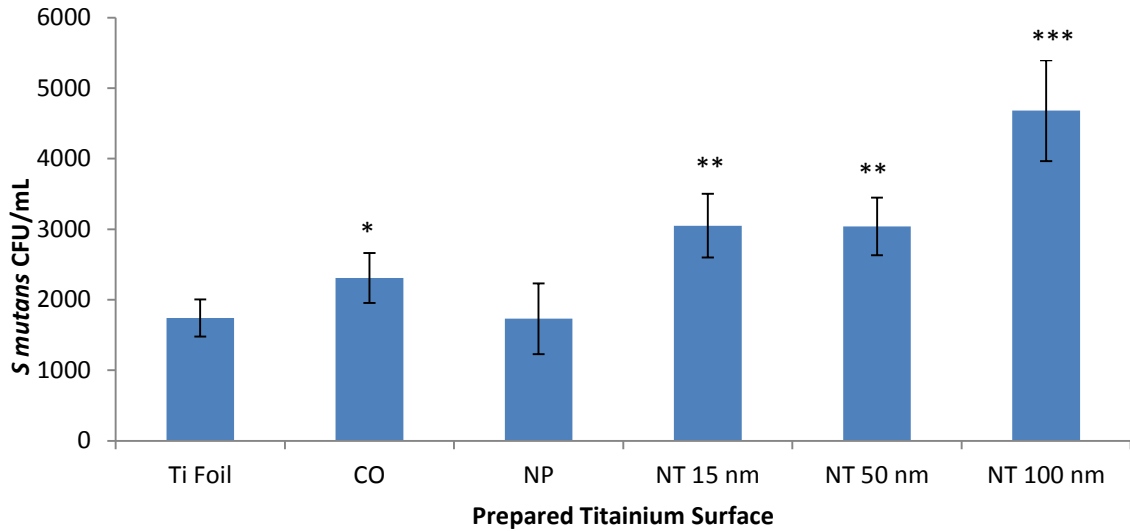
Three control samples were included in the study (Ti Foil, CO, NP) and the adhesion of *S mutans* was compared to these surfaces was compared with the prepared Ti samples of NT 15 nm, NT 50 nm and NT 100 nm (figure 3.59). It was demonstrated that there were significant differences between the mean CFU/mL on the Ti Foil (1740 CFU/mL) and CO (2310 CFU/mL) (p>0.05) however there was no significant difference between the Ti foil control and the NP (1730 CFU/mL) (p<0.01) surfaces. It was also observed that there was significantly increased adhesion of *S mutans* on the Ti foil (1740 CFU/mL) when compared with the NT 15 nm surface (3050 CFU/mL) (p=0.01), the NT 50 nm surface (3040 CFU/mL) (p<0.01) and the NT 100 nm surface (4680 CFU/mL) (p=0.001). The data demonstrated that as the NT size increased from 15 nm, 50 nm to 100 nm there was also an increased adhesion of the *S mutans.* A similar pattern of bacterial adhesion to *S sanguinis* was observed (figure 3.58) however; there were increased bacterial counts for *S mutans* (figure 3.59).

3.4.9 XPS measurements on Ti Foil, CO, NP, NT with 15 nm, 50 nm and 100 nm diameter surfaces.

XPS measurements were performed to determine the fluorine content on the surface of the

Ti Foil, CO, NP, NT with 15 nm, 50 nm and 100 nm diameter surfaces to isolate its possible

effect on the adhesion of *S sanguinis* or *S mutans*. The XPS measurements demonstrated an

increase in the fluorine (%) on the NP, NT 15 nm, NT 50 nm and NT 100 nm surfaces (Table

3.3).

Table 3.4. Atomic concentration of the fluorine and Ti concentrations obtained with XPS measurements on Ti foil, CO, NP, NT15 nm, NT50 nm, NT 100 nm. Not all Atomic concentrations shown.

Sample	Fluorine (%)	Ti (%)
Ti Foil	-	17.9
CO	-	16.4
NP	1.6	16.5
NT 15 nm	3.1	15.8
NT 50 nm	5.8	19.4
NT 100 nm	7.0	20.4

The Table illustrates that there was no atomic fluorine (%) present on the Ti Foil and the CO

samples. The fluorine (%) concentration increases from 1.6 on the NP sample with increasing

NT tube diameter with the highest concentration found on the NT 100 sample (Table 3.4).

3.5 The effect of UV irradiation on bacterial adhesion and viability on increased TiO$_2$ surfaces.

The photocatalytic effect of UV irradiation on Grade II, IV and V Ti surfaces and with increased thickness TiO$_2$ surfaces was investigated. Initially an Omnicure series 1000 UV light engine was characterised and subsequently a methylene blue dye photocatalytic assay was optimised. Grade II, IV and V thermally treated Ti samples at 50, 100 and 150 hrs were prepared and characterised by SEM before determining their photocatalytic activity. The adhesion of *S sanguinis* on the thermally treated Ti surfaces and the effect of time on *S sanguinis* adhesion and viability were also determined.

3.5.1 UV light engine calibration.

The photocatalytic assays were developed by initially calibrating the Omnicure Series 1000 light engine. It was demonstrated that the spectral output of the UV light engine was composed of 5 peaks at 313, 335, 365, 407 and 440 nm which overlap with the absorption spectra of TiO$_2$ (figure 3.60).

Figure 3.60. The spectral output of the Omnicure series 1000 light engine at 10 % power illustrated that the spectral output is made up peaks at 313, 335, 365, 407 and 440 nm.
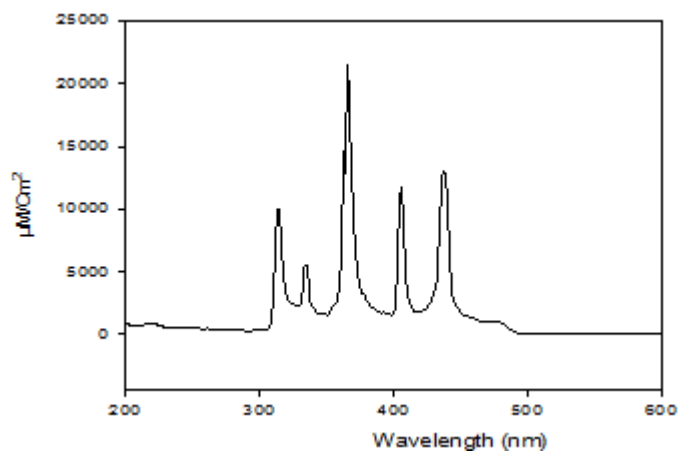
The relationship between increased light engine power and any possible modifications in the spectral output was studied. A satisfactory 'linear' correlation between absolute irradiance and light engine power was observed. (figure 3.60).

Figure 3.61. The absolute irradiance (mW/cm^2) against Power of the Light Engine. The trend line intercept was set at 0 and an R^2 value of 0.7962 was obtained.
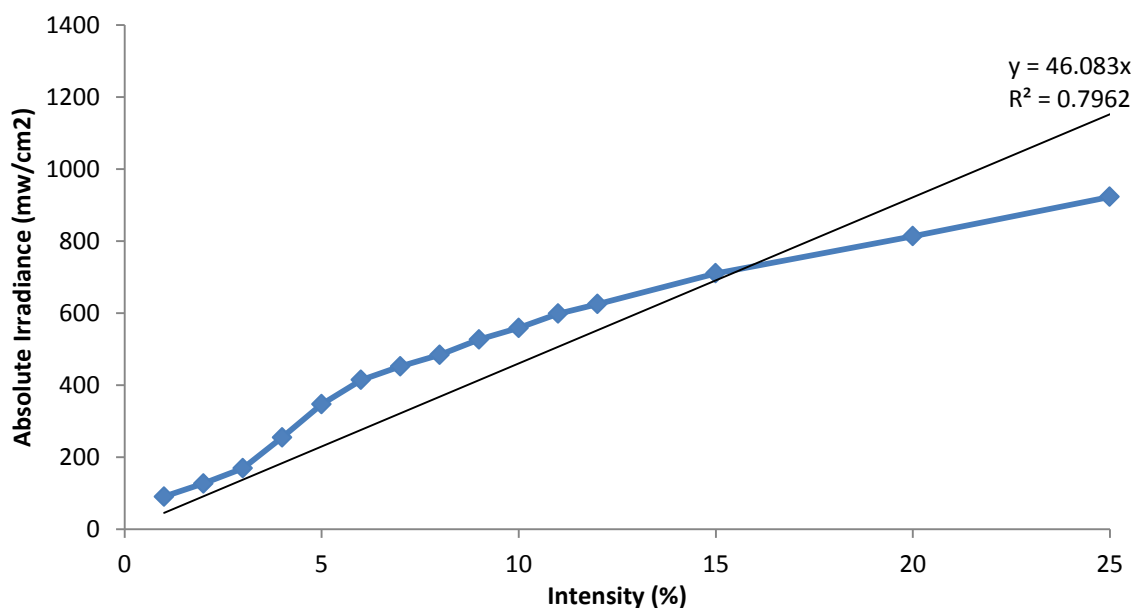
The Omnicure series 1000 light engine was calibrated to determine the correlation between the absolute irradiance values (mW/cm^2) and the increasing intensity. It was observed that the absolute irradiance at 25 % power was 923 mW/cm^2.

3.5.2 Determination of methylene blue dye concentration for the photocatalytic assay.

The concentration of methylene blue dye to utilise for the photocatalytic degradation assays was determined by preparing concentrations ranging from 1 ppm to 500 ppm and initially determining the spectral absorbance.

Figure 3.62. The absorbance spectra from methylene blue concentrations ranging from 1 ppm to 500 ppm. A primary absorption peak can be observed at a wavelength of 665 nm.
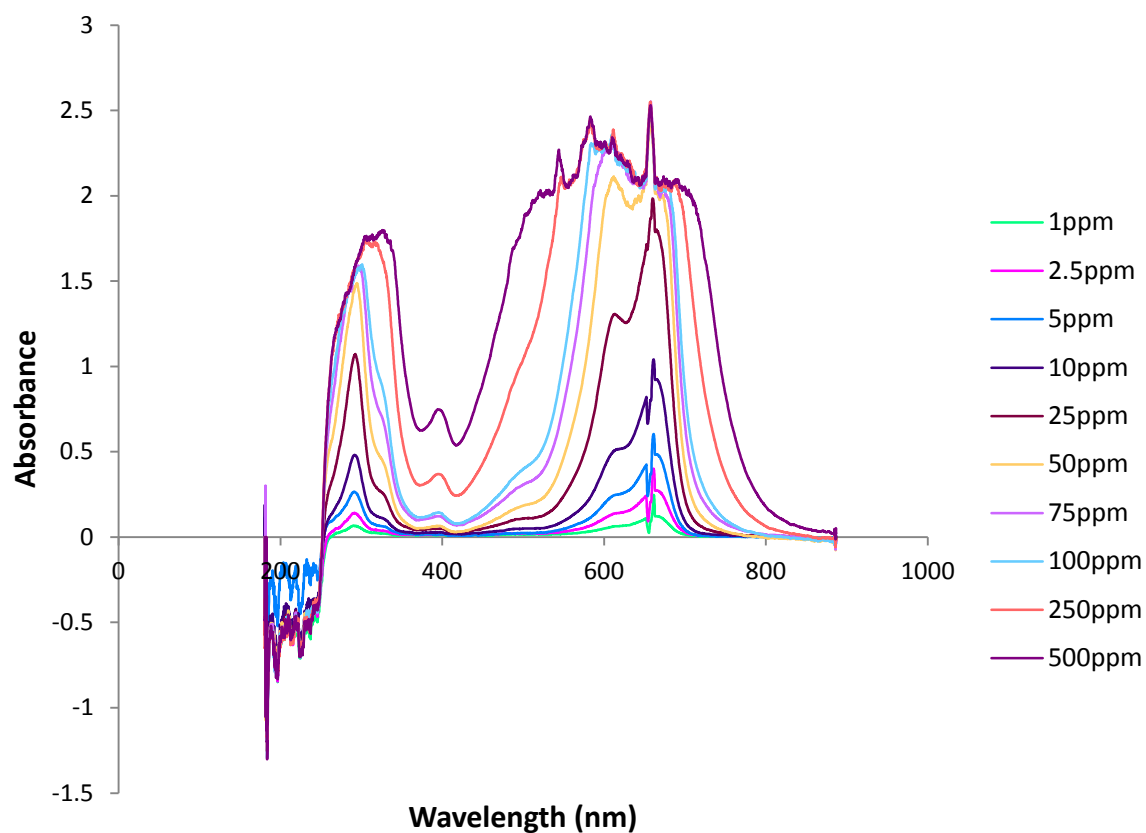
The primary absorbance peak of 665 nm was detected for all the concentrations of methylene blue used and was therefore used to monitor methylene blue degradation in the further studies (figure 3.62).

Figure 3.63. Line plot demonstrating the relationship between an increased concentration of methylene blue (µM) and absorbance at 665 nm.
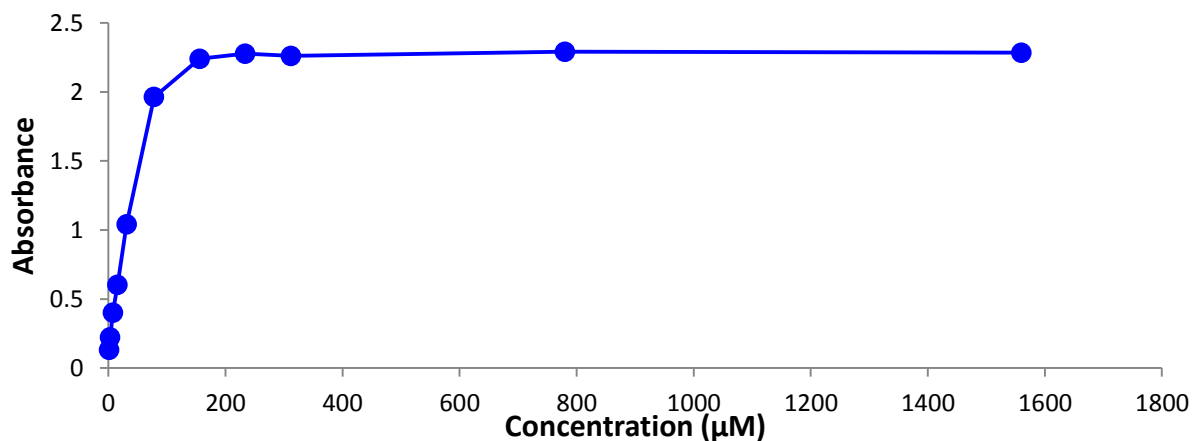
Figure 3.64. A linear correlation can be observed between the lower concentration of methylene blue and absorbance which is described by the Beer-Lambert law.
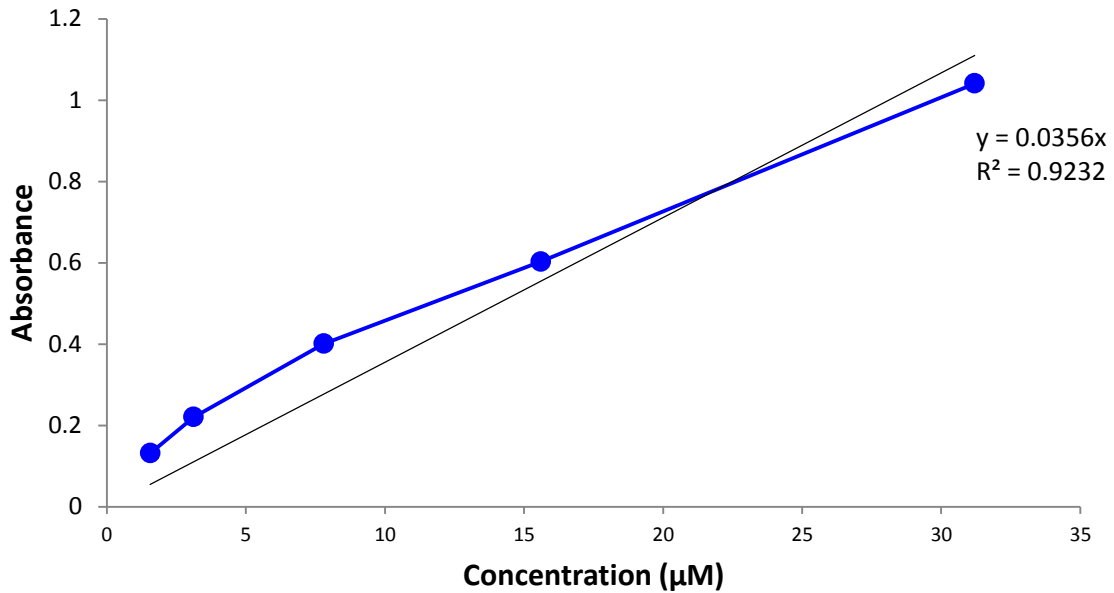
A low concentration of methylene blue dye exhibited a strong correlation with absorbance and therefore a concentration of 3.12 μM was utilised for the photocatalytic degradation assays

3.5.3 SEM characterisation of the thermal oxidation of Ti surfaces.

Grade II, IV and V Ti samples prepared to P4000 SiC grit surface finish and were thermally oxidised at 600 °C for 50, 100 and 150 hrs. The surfaces were then characterised by SEM imaging which demonstrated a roughening associated with thermal treatment. (figures 3.65, 3.66 and 3.67).

Figure 3.65. a) SEM images illustrating the topography of the thermally treated Grade II CpTi disk surface after 50 hrs thermal treatment at x2000 magnification, illustrating the Grade II surface after 50 hrs is rougher compared to the P4000 prepared SiC grit.
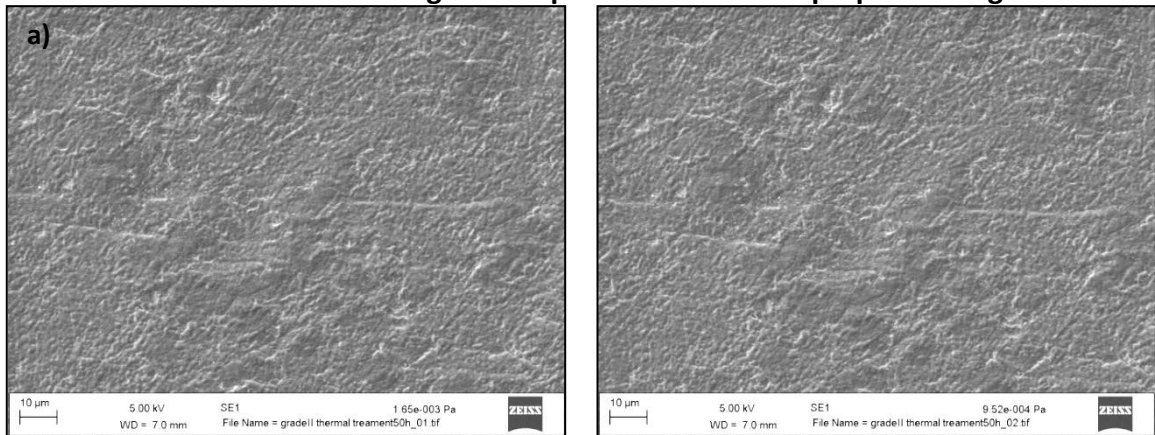
Figure 3.65. b) SEM images illustrating the topography of the thermally treated Grade II CpTi disk surface after 100 hrs thermal treatment at x2000 magnification illustrating a rougher topography compared to 50 hrs treatment.
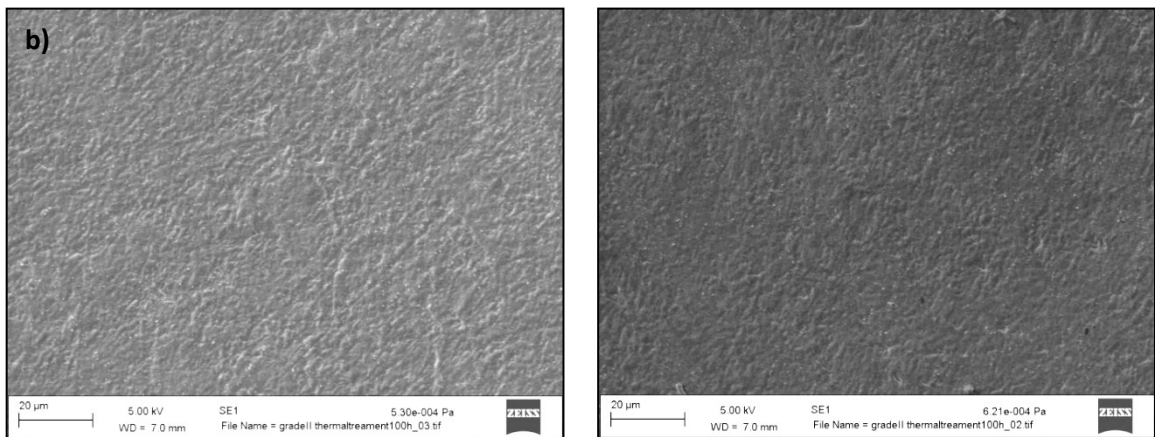
Figure 3.65. c) SEM images of the Grade II surface after 150 hrs thermal treatment illustrating a rougher topography compared to 50 and 100 hrs treatment with the raised features observed on the sample surface.
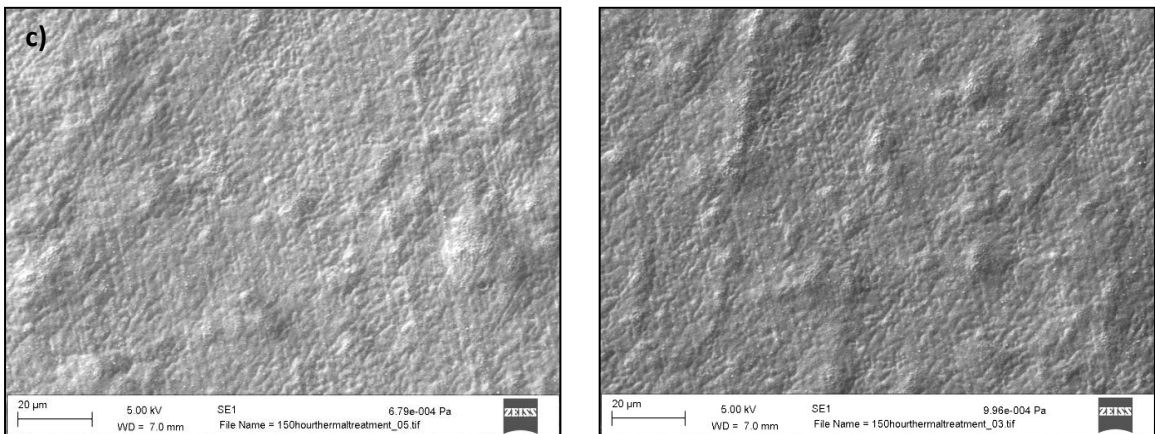
Figure 3.66. a) SEM images illustrating the topography of the thermally treated Grade IV CpTi disk surface after 50 hrs thermal treatment at x2000 magnification, illustrating the Grade II surface after 50 hrs is rougher compared to the P4000 prepared SiC grit.
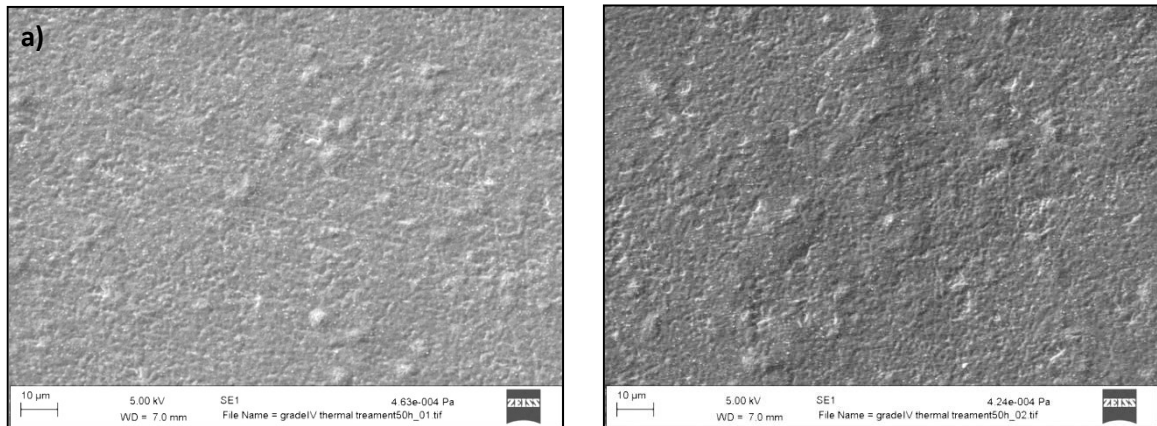
Figure 3.66. b) SEM images illustrating the topography of the thermally treated Grade IV CpTi disk surface after 100 hrs thermal treatment at x2000 magnification illustrating a rougher topography compared to 50 hrs treatment.
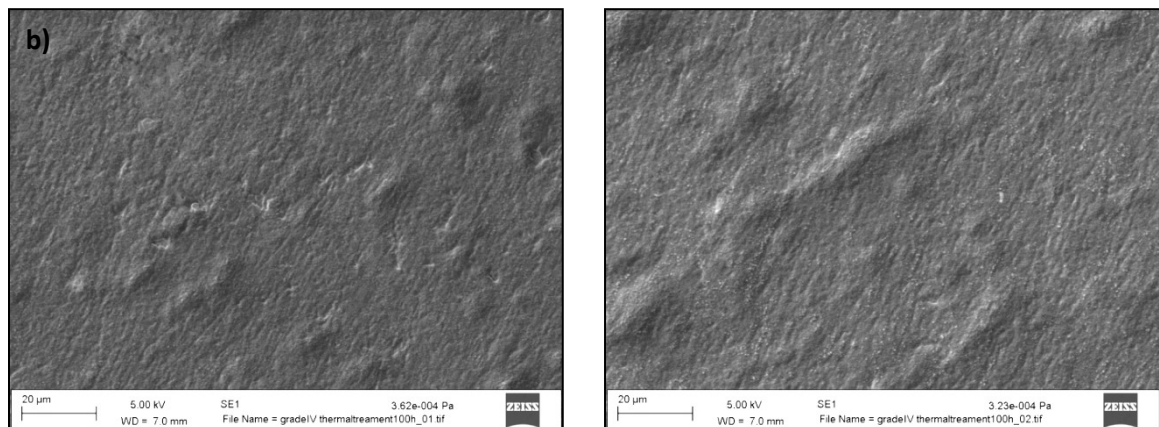
Figure 3.66. c) SEM images of the Grade IV surface after 150 hrs thermal treatment illustrating a rougher topography compared to 50 and 100 hrs treatment with the raised features and craters observed on the sample surface.
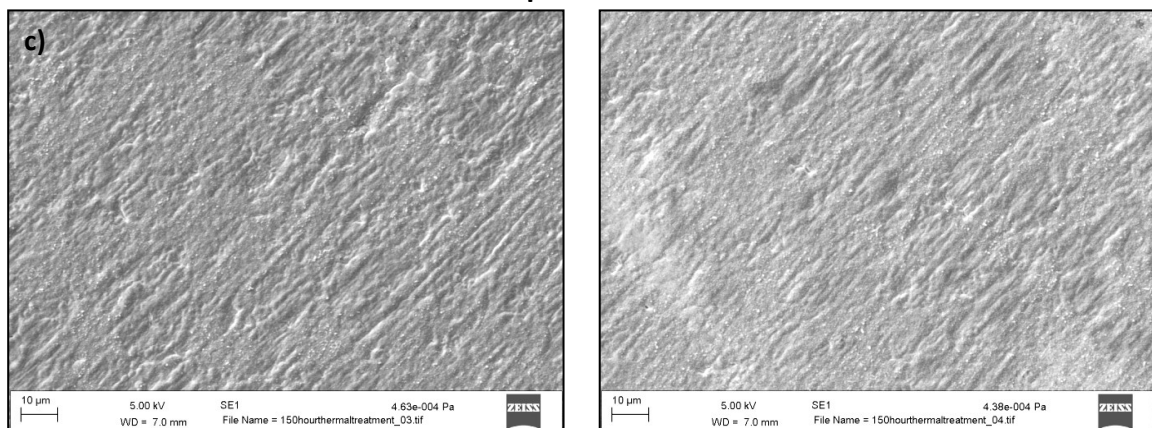
Figure 3.67. a) SEM images illustrating the topography of the thermally treated Grade V CpTi disk surface after 50 hrs thermal treatment at x2000 magnification, illustrating the Grade II surface after 50 hrs is rougher compared to the P4000 prepared SiC grit.
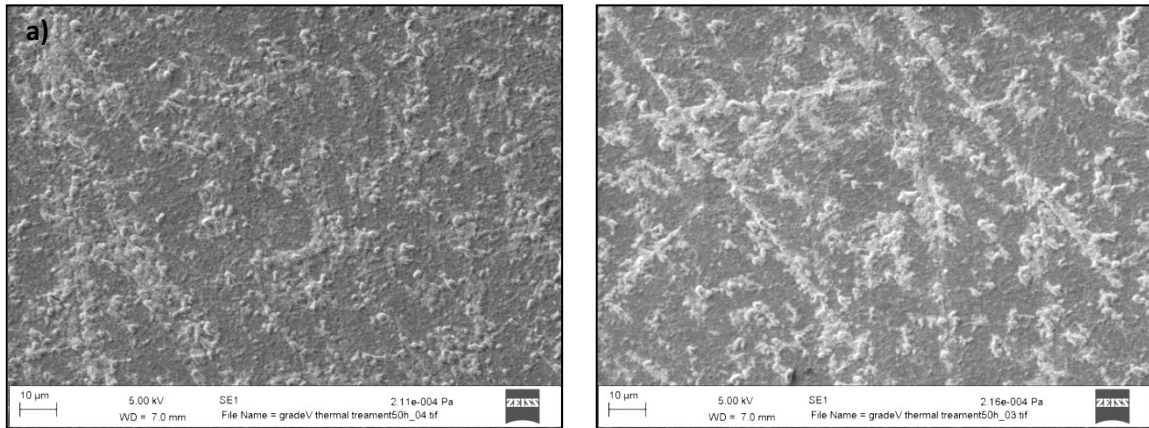
Figure 3.67. b) SEM images illustrating the topography of the thermally treated Grade V CpTi disk surface after 100 hrs thermal treatment at X 2000 magnification
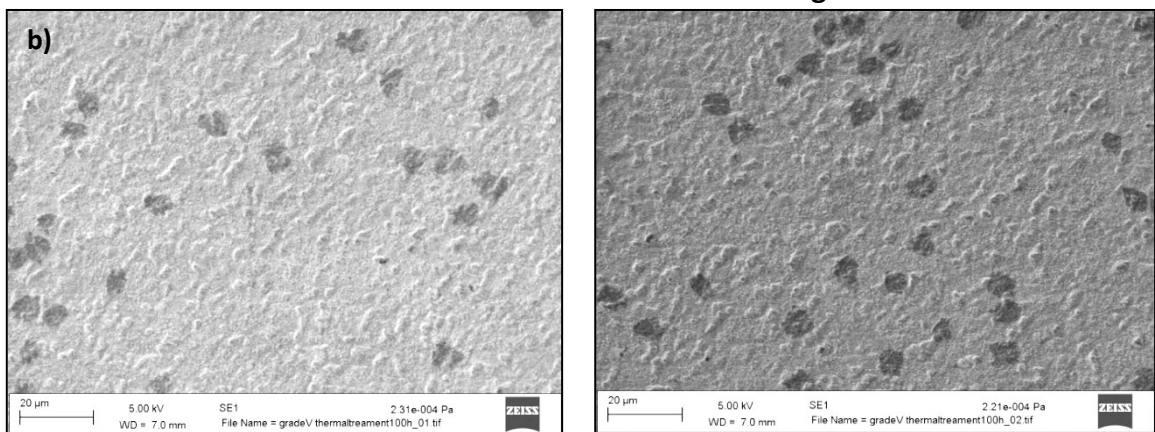
Figure 3.67. c) SEM images illustrating the topography of the thermally treated Grade V CpTi disk surface after 150 hrs thermal treatment at X 2000 magnification.
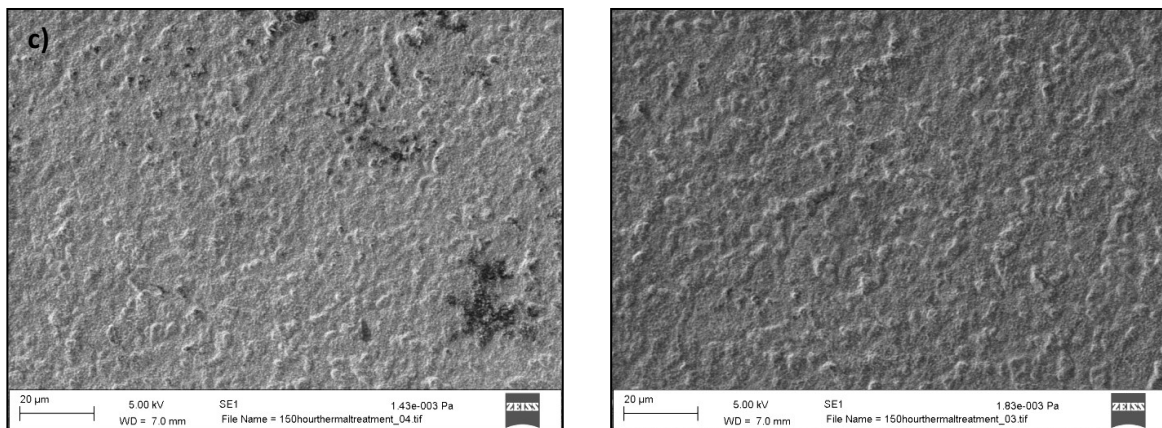
The surface topography of the thermally treated samples becomes noticeably rougher with the appearance of raised surface morphologies such as isolated raised morphologies. The change in surface morphology is most prominent on the Grade V surface, (figure 3.67 c), Grade II thermal treated for 150 hours and (figure 3.66 b), Grade IV 100 hour thermal treated (figure 3.66 b).

3.5.4 Photocatalytic assays.

The photocatalytic effect of the thermally treated Grade II, IV and V Ti surfaces after 50, 100 and 150 hrs thermal treatment was determined with methylene blue degradation assays. It was observed that the Grade II, IV and V samples thermally treated for 100 and 150 hrs demonstrated the greatest methylene blue degradation after 120 mins using a light intensity of 923 mW/cm^2 (figures 3.68, 3.69 and 3.70). The photocatalytic effect was also determined on the Grade IV Ti surface after contamination with TSB and artificial saliva, the assays demonstrated that photocatalysis was still effective (figure 3.71).

3.5.4.1 Methylene blue degradation on Grade II Ti.

Figure 3.68. Line chart showing the degradation of methylene blue after irradiation with UV light at an irradiance of 923 mW/ cm^2 (25% intensity). The chart shows the effect of UV light on the methylene blue dye degradation without a Ti disc, polished, non-thermal treated, 50, 100 and 150 hrs thermal treated Grade II CpTi samples. Readings were taken in triplicate every five mins for 120 mins (Mean ± SD, n=1).
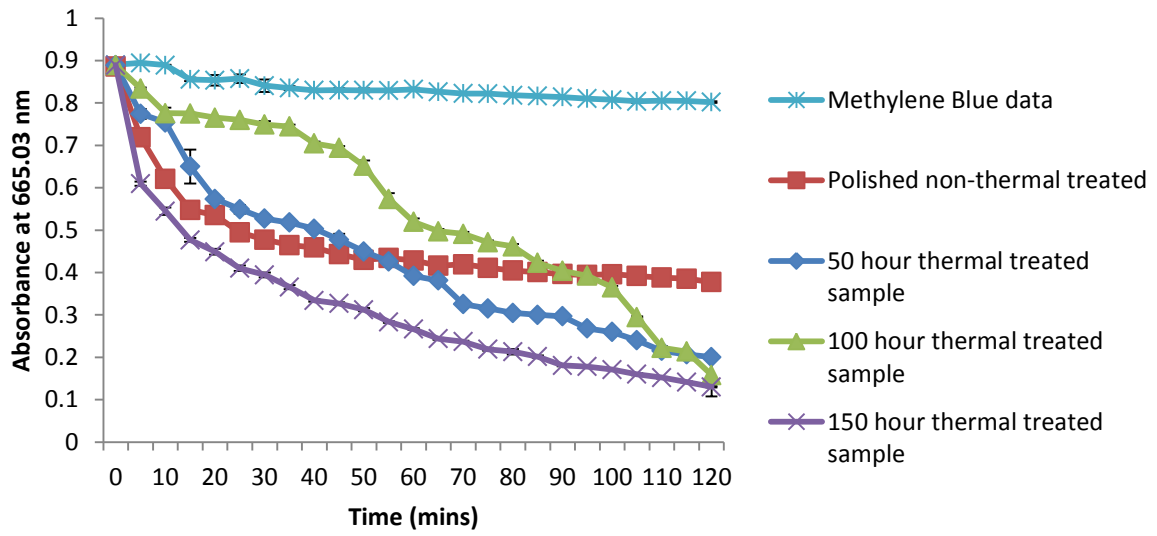
The Grade II CpTi samples were submerged in methylene blue dye and irradiated at 923 mW/cm^2 for 120 mins. It was observed that the controls of methylene blue and the polished non-thermally treated sample had degraded by 9 % and 57%, respectively after 120 min irradiation with UV at a light intensity of 923 mW/cm^2. Thermal treatment of samples for 50, 100 and 150 hrs led to a degradation of 77 %, 82 % and 85 % of methylene blue, respectively after 120 mins of irradiation (figure 3.68).

Figure 3.69. Line chart showing the degradation of methylene blue after irradiation with UV light at an irradiance of 923 mW/ cm^2 (25% intensity). The chart shows the effect of UV light on the methylene blue dye degradation without a Ti disc, polished, non-thermal treated, 50 hr thermal treated, 100 hour thermal treated and 150 hour thermal treated Grade IV CpTi samples. Readings were taken in triplicate every five mins for 120 mins (Mean ± SD, n=1).
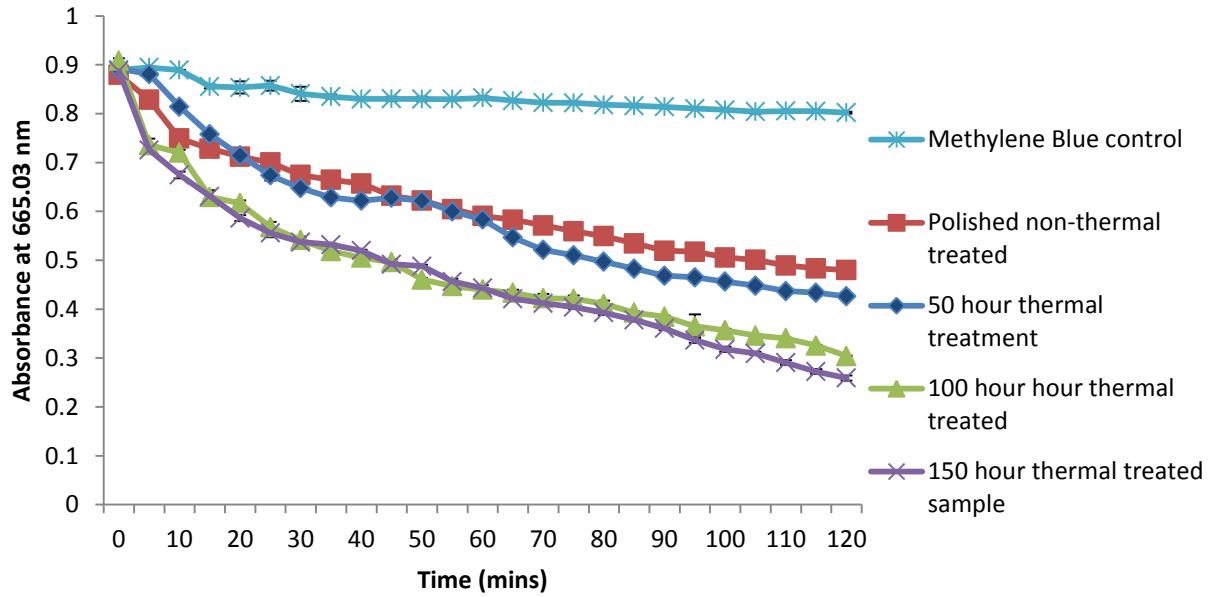
The Grade IV CpTi samples were submerged in methylene blue dye and irradiated at 923 mW/cm^2 for 120 mins. The methylene blue control and the polished non-thermally treated sample degraded 9 % and 45%, respectively after 120 mins irradiation whereas the samples thermally treated for 50, 100 and 150 hrs led to a degradation of 52 %, 66 % and 70 % of methylene blue after 120 mins irradiation, respectively (figure 3.69).

Figure 3.70. Line chart showing the degradation of methylene blue after Grade V Ti6-Al-4V alloy was irradiated with UV light at an irradiance of 923 mW/ cm^2 (25% intensity). The chart shows the effect of UV light on the methylene blue dye degradation without a Ti disc, polished, non-thermal treated, 50 hr thermal treated, 100 hr thermal treated and 150 hr thermal treated Grade V Ti-6Al-4V samples. Readings were taken in triplicate every five mins for 120 mins (Mean ± SD, n=1).
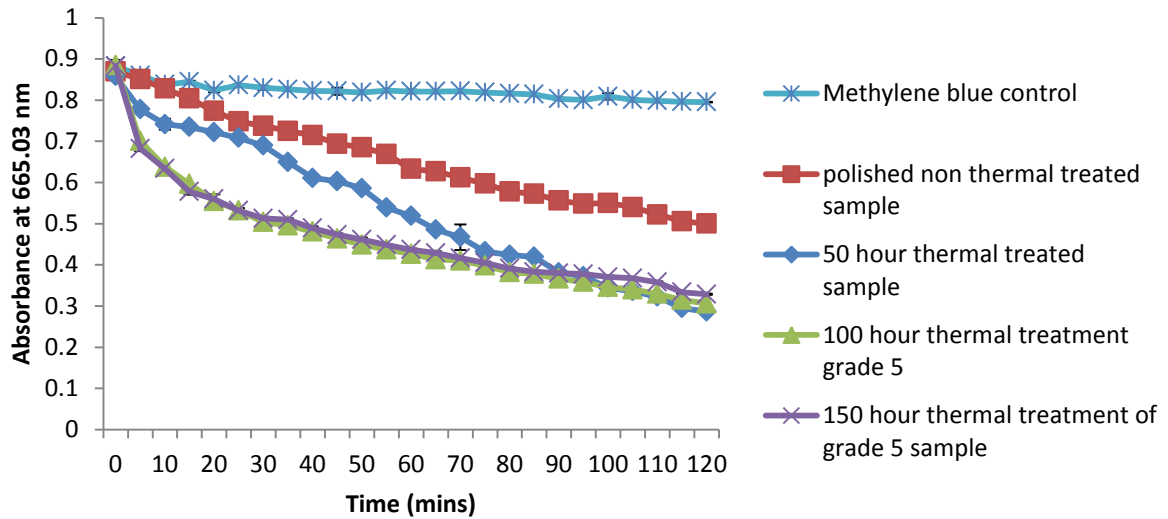
The Grade V CpTi samples were submerged in methylene blue dye and irradiated at 923 mW/cm^2 for 120 mins. It was observed that the controls of methylene blue and the polished non-thermally treated sample had degraded 9 % and 42% after 120 mins irradiation whereas the thermally treated samples (50, 100 and 150 hrs thermal treatment) led to a degradation of 66 %, 65 % and 62 % of methylene blue respectively, after 120 mins irradiation (figure 3.70).

Figure 3.71. Line chart showing the degradation of methylene blue after the Grade IV CpTi was irradiated sample was contaminated with TSB for 48 hrs and artificial saliva after a further 24 hrs were with UV light at an irradiance of 923 mW/ cm^2 (25% intensity). The chart shows the effect of UV light on the methylene blue dye degradation without a Ti disc, polished, non-thermal treated, 50, 100 and 150 hrs thermal treated Grade IV CpTi samples. Readings were taken in triplicate every five mins for 120 mins (Mean ± SD, n=1).
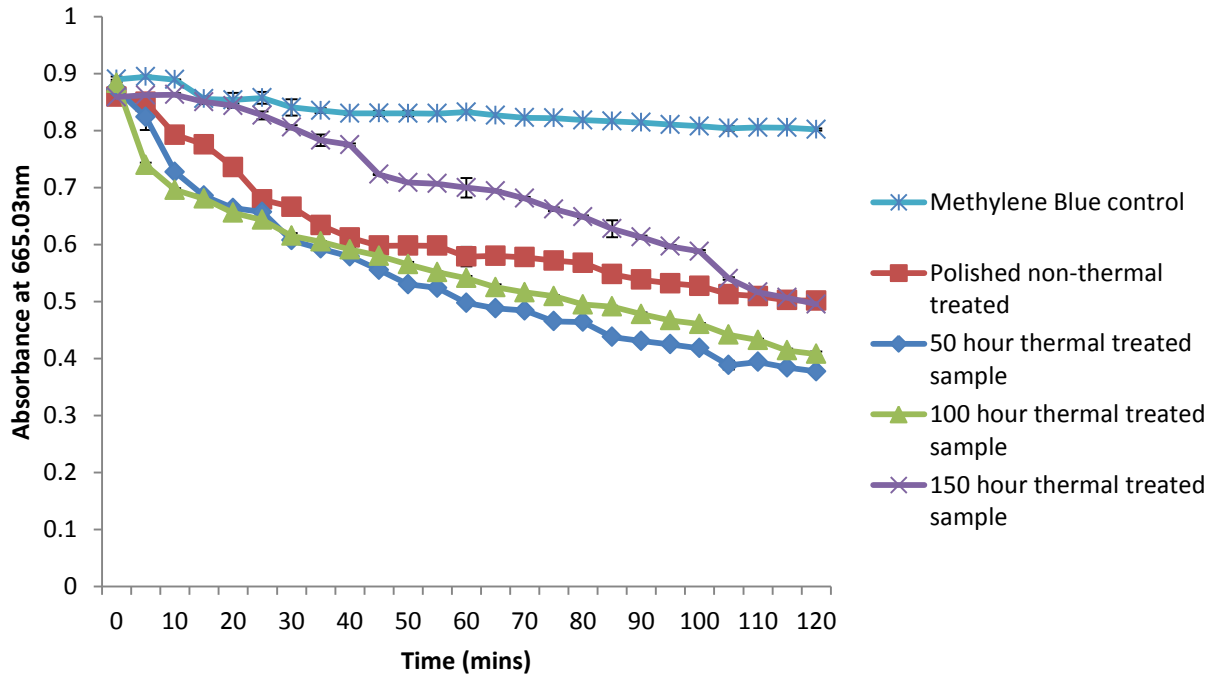
The Grade IV Ti sample contaminated with the TSB and artificial saliva for 72 hrs was observed to still produce methylene blue degradation. The controls of methylene blue and the polished non-thermal treated sample degraded by 9% and 42%, respectively after 120 mins irradiation with UV at an intensity of 923 mW/cm^2. It was also observed that samples thermally treated for 50, 100 and 150 hrs degraded the methylene blue by 56 %, 53 % and 42 %, respectively after 120 mins irradiation (figure 3.71).

3.5.4.2 The effect of *S sanguinis* adhesion on Grade IV and V Ti surfaces after 60 s UV irradiation.

The effect of UV irradiation on the Grade IV and V Ti surfaces after 50, 100 and 150 hrs of thermal treatment was determined.

Figure 3.72. A histogram illustrating the effect of irradiating the Grade IV Ti surface for 60 s on *S sanguinis* adhesion. The P4000 polished, non-thermal treated Grade IV sample, 50 hour thermal treated, 100 hr thermal treated and 150 hr thermal treated Grade IV CpTi samples were irradiated at an irradiance of 923 mW/ cm^2 (25% intensity) for 60 s (Mean ± SD, n=3, *=P<0.05). A significant reduction in bacterial adherence was observed on the 50 hrs thermal treated sample compared to the control P4000 polished Ti (p=0.03). No significant difference was observed between the P4000 polished, non-thermal treated and the thermal treated 100 hr and 150 hr samples.
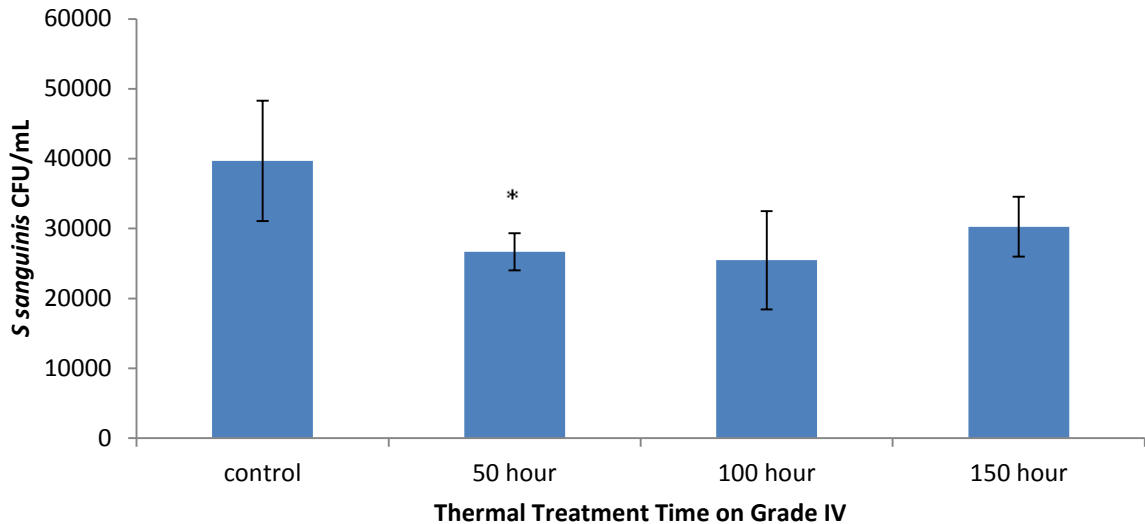
The attachment of *S sanguinis* to the thermally prepared CpTi Grade IV surface was reduced from the P4000 polished control when compared to the 50, 100 and 150 hr thermally treated surfaces however the only significant reduction was on the 50 hr thermally treated specimens.

A similar trend in the data was observed on the Grade V surface with the mean CFU/mL significantly reduced from the P4000 control for the 50 hr thermally treated samples only (p=0.003).

Figure 3.73. A Histogram illustrating the effect of irradiating Grade V Ti surface for 60 s on *S sanguinis* adhesion. The P4000 polished, non-thermal treated Grade V sample, 50 hr thermal treated, 100 hr thermal treated and 150 hr thermal treated Grade V Ti-6Al-4V alloy samples were irradiated at an irradiance of 922 mW/ cm^2 (25% intensity) for 60 s (Mean ± SD, n=3, *=P<0.05). A significant reduction in bacterial adherence was observed on the 50 hr thermal treated sample compared to the control P4000 polished Ti (p=0.003). No significant difference was observed between the P4000 polished, non-thermal treated and the 100, 150 hrs thermal treated samples.
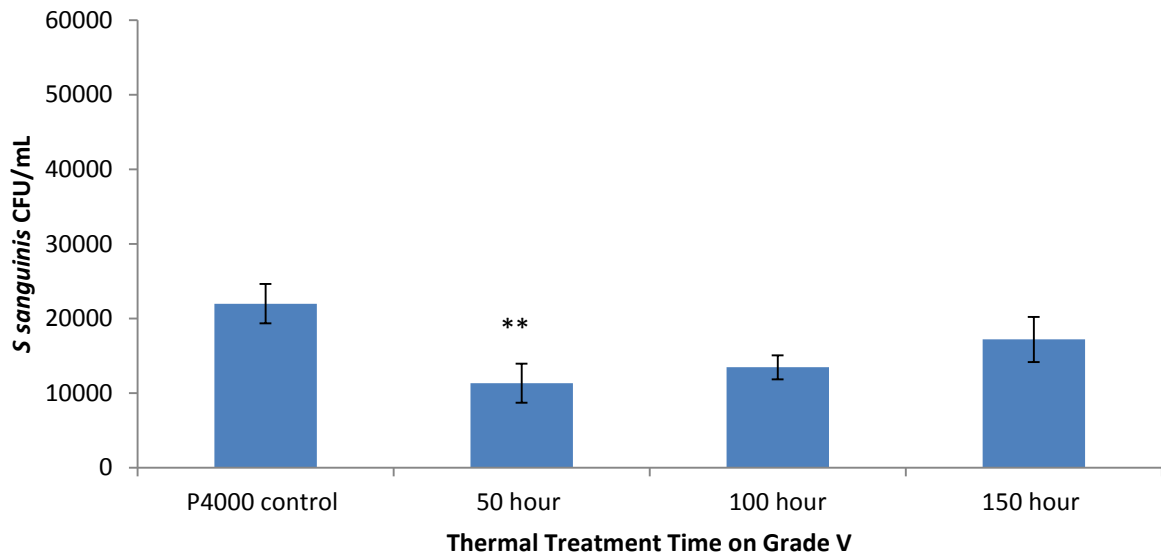
3.5.4.3 The effect of UV irradiation intensity on the adhesion of *S sanguinis* on thermally oxidised Grade II samples at 50, 100 and 150 hrs.

The effect of UV irradiation intensity on *S sanguinis* adhesion was determined on samples thermally treated for 50, 100 and 150 hrs. Irradiation intensities of 0, 559 and 923 mw/cm^2 were studied. Significant reductions of *S sanguinis* (mean CFU/mL) were observed on the 100 and 150 hrs thermally oxidised samples after UV irradiation when compared with non-irradiated samples (p<0.05) (figure 3.74).

Figure 3.74. A histogram demonstrating the effect of UV irradiation of Grade II CpTi (non-thermal treated, 50 hrs, 100 hrs and 150 hrs thermal treated samples) on *S sanguinis* adhesion (Mean ± SD, n=3, *=P<0.05).
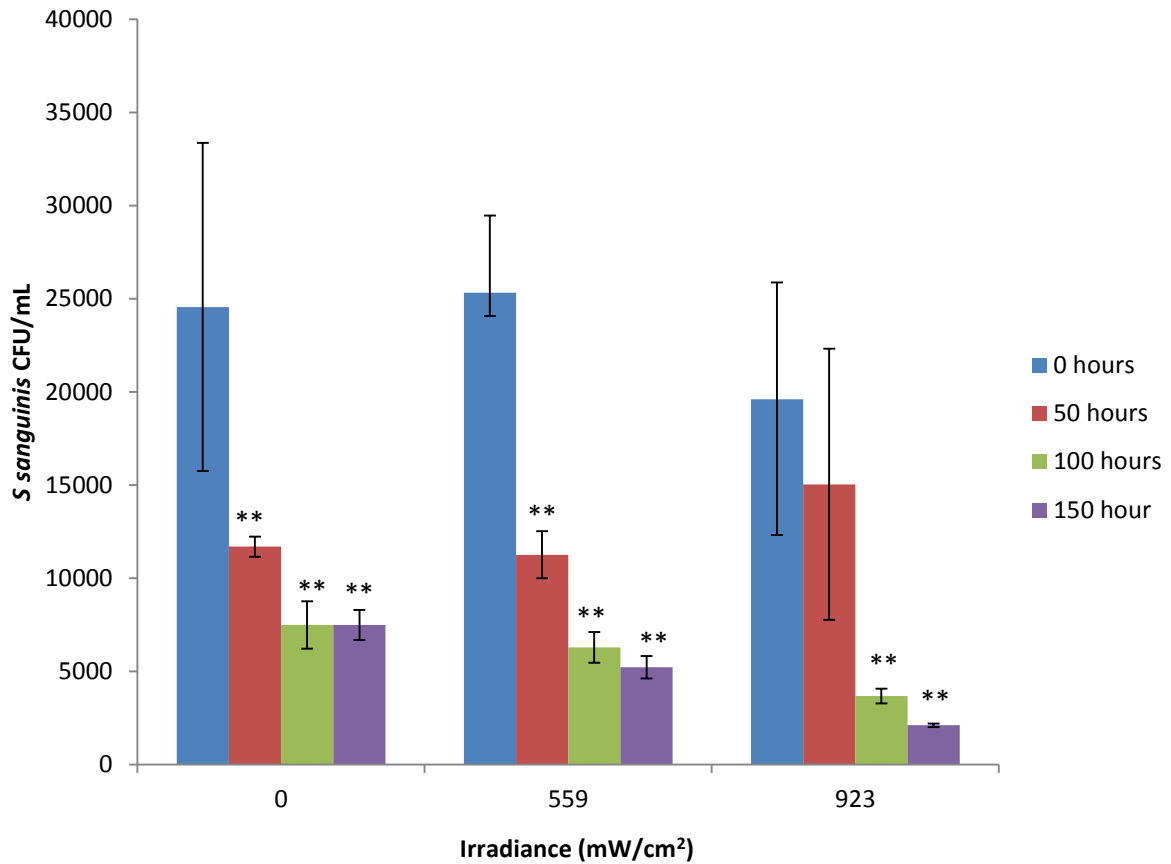
The prepared Ti samples received no UV light irradiation or were treated with UV at 559 or 923 mW/ cm^2 power for 60 s. A one-way ANOVA identified no significant difference between the mean CFU/mL of *S sanguinis* attached to the non-thermally treated Grade II CpTi with or without irradiation (p<0.05). Furthermore there was no significant difference in the adhesion of *S sanguinis* to the 50 hr thermally treated surface with or without UV light irradiation (p> 0.05). After 100 hr of thermal treatment UV irradiation at 923 mW/cm^2 of the surface significantly reduced the mean CFU/mL of *S sanguinis* (p= 0.003). Similarly after 150 hr of thermal treatment subsequent irradiation at 923mW/cm^2 also significantly reduced the mean CFU/mL (p=0.004). Significant differences were also observed at each irradiation level

which demonstrated that the thermal treatment resulted in a significant reduction in mean

CFU/mL (p<0.01) which was increased with Ti thermal treatment time.

3.5.4.4 The effect of UV irradiation time.

The effect of UV irradiation for 1 min, 5 mins and 10 mins on the adhesion of *S sanguinis* to a

Grade II CpTi surface which had been thermally oxidised for 100 hrs was subsequently

determined. It was demonstrated that after 5 and 10 mins of UV irradiance at 923 mW/cm^2,

there was a significant reduction of *S sanguinis* adhesion to the thermally treated Ti surface

(figure 3.75).

Figure 3.75. A histogram illustrating the effect of UV irradiation at 923 mW/cm^2 on the adhesion of *S sanguinis* to the 100 hrs thermally treated Grade II Ti surface after 1, 5 and 10 mins (Mean ± SD, n=3, *=P<0.05).
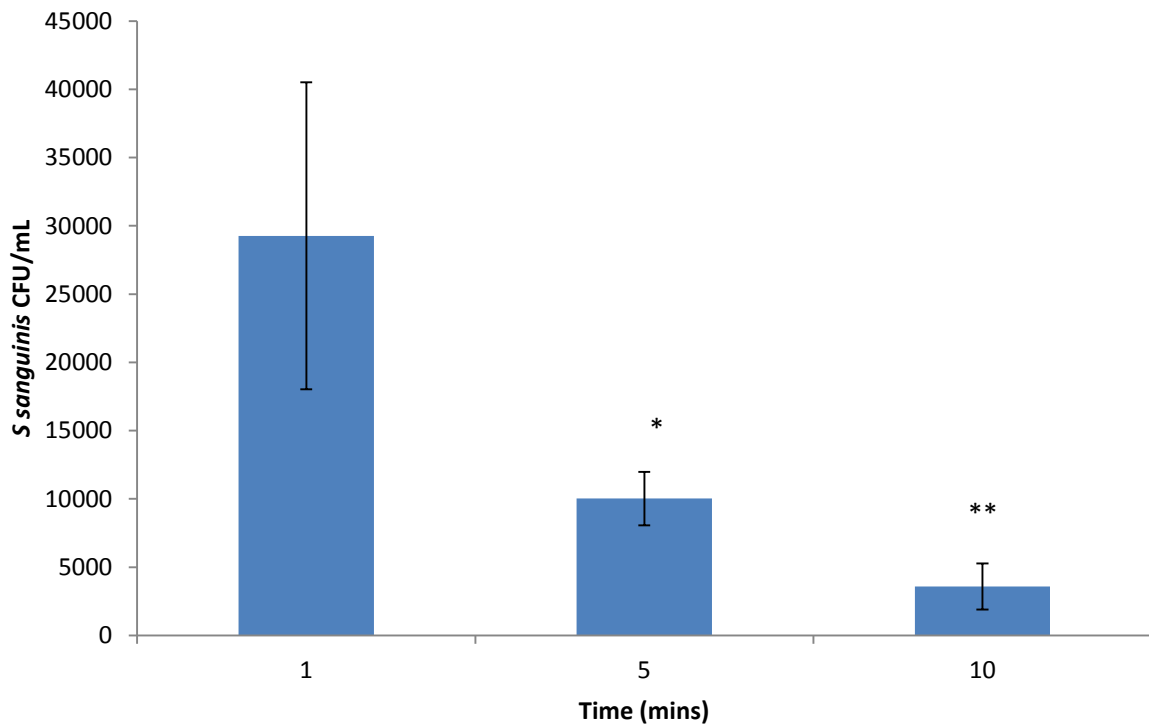
A one-way ANOVA demonstrated a significant reduction in the adhesion of *S sanguinis* to the Ti surface after 5 (p=0.002) and 10 mins (p=0.008) of UV light irradiation. At increased irradiation times there was significantly decreased the adhesion of *S sanguinis* (figure 3.75).

3.5.4.5 SEM characterisation of *S sanguinis* adhesion to the thermally oxidised surfaces.

SEM was used to characterise the adhesion of *S sanguinis* to the control P4000 non-thermally treated Ti surfaces and to the thermally prepared Grade V Ti surfaces treated for 50, 100 and 150 hrs. The appearance of the *S sanguinis* population was observed to change from a unicellular covering on the control surface to being chained and bunched on the 50 and 100 hrs thermally treated surfaces. There were no bacterial cells observed on the 150 hrs thermally treated samples.

Figure 3.76a. SEM images illustrating the adhesion of *S Sanguinis* to the control non-thermally treated Grade V surface after irradiation with 923 mW/ cm^2 (25% intensity) for 60 s (x2000 magnification).
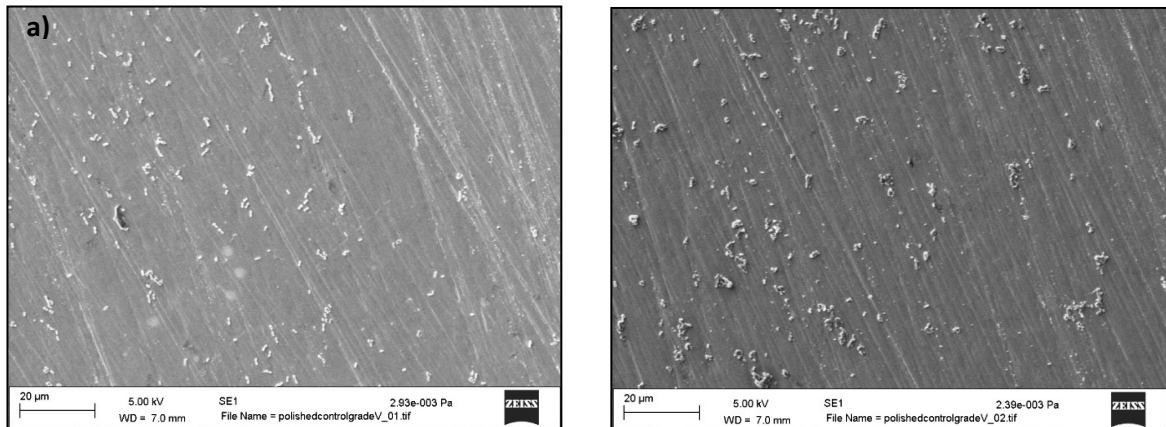
The *S sanguinis* bacteria were spread evenly on the surface of the Grade V P4000 polished surface with no obvious preferential attachment pattern.

Figure 3.76b. SEM images illustrating the adhesion of *S sanguinis* to the 50 hrs thermally treated Grade V surface after irradiation with 923 mW/ cm^2 (25% intensity) for 60 s (x2000 magnification).
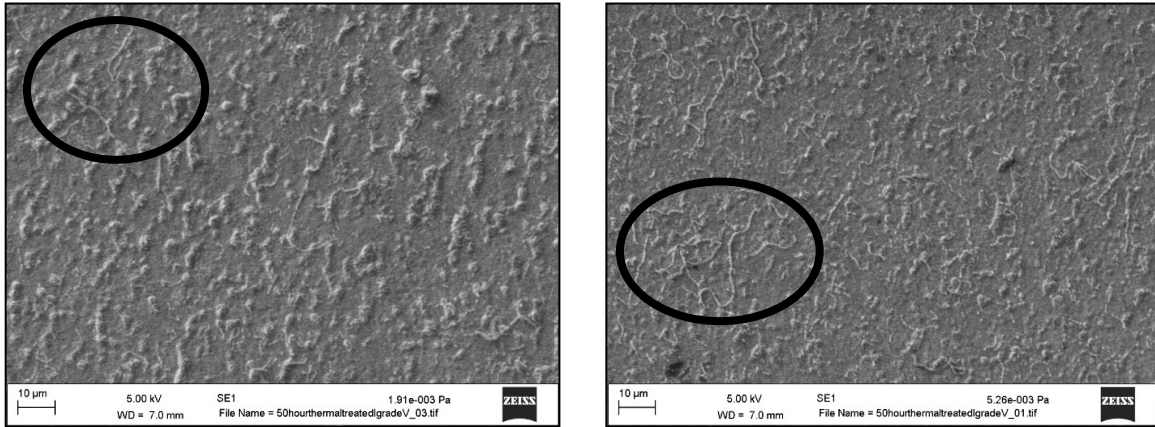
The *S sanguinis* bacteria are observed agglomerated and in chains on the Grade V surface

thermally oxidised for 50 hrs, highlighted with the circles.

Figure 3.76c. SEM images illustrating the adhesion of *S sanguinis to* the 100 hrs thermally treated Grade V surface after irradiation with 923 mW/ cm^2 (25% intensity) for 60 s (magnification of x2000).
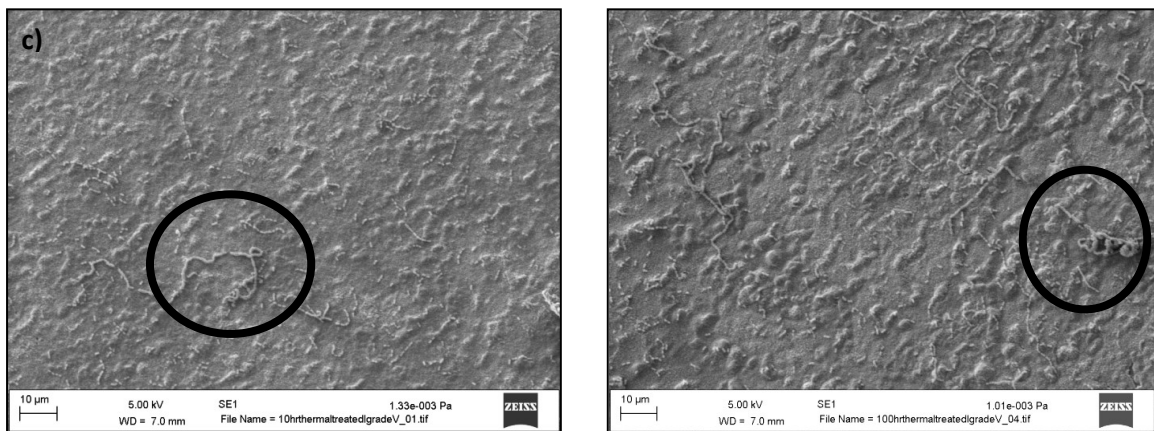
The *S sanguinis* bacteria are observed bunched up in chains on the surface of the Grade V

thermally oxidised surface, highlighted by the circles (figure 3.76c).

Figure 3.76d. SEM images illustrating the adhesion of *S sanguinis* to the 150 hrs thermally treated Grade V surface after irradiation with 923 mW/ cm^2 (25% intensity) for 60 s (magnification x2000).
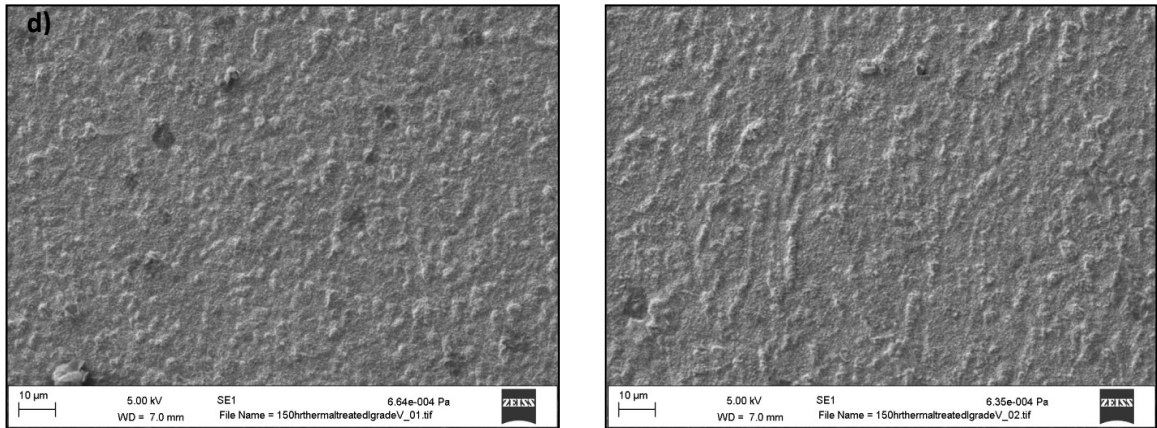
On the surface of the 150 hrs thermally treated Grade V surface no adhesion of *S sanguinis* was observed.

3.5.5 UV irradiation of anodic oxidised Grade II, IV and V Ti surfaces

Grade II, IV and V Ti substrates were prepared by anodic oxidation at 10 V, 70 V and 120 V in a sodium tetraborate electrolyte solution. The samples were characterised using EDX analysis, SEM imaging and contact angle measurements to determine the wettability of the surface. Methylene blue degradation assays were carried out to determine the photocatalytic activity the prepared surfaces and the early adhesion of *S sanguinis, E coli, S mutans* and *F nucleatum* with and without UV irradiation was then determined.

3.5.5.1 Appearance of the Ti samples prepared by anodic oxidation.

The Grade II, IV and V Ti surfaces were prepared with 0 V, 10 V, 70 V and 120 V. Anodisation resulted in a surface colour change dependent on the Voltage used (gold colour at 10 V, blue at 70 V and a "pink-blue" coloured surface at 120 V) (figure 3.77).

Figure 3.77. Macroscopic image illustrating the colours of the Ti surface after anodisation. The samples include Grade IV polished P4000, 10 V, 70 V and 120 V anodised Ti.

3.5.5.2 Oxygen content on the surface of the Grade II, IV and V anodised surfaces.

The oxygen content of the Grade II, IV and V Ti surfaces after anodic oxidation was determined using EDX analysis. A significant increase in the Oxygen weight % was observed with increasing with the anodising voltage (figure 3.78).

Figure 3.78. A histogram illustrating the oxygen weight% for Grade II, IV and V Ti surfaces polished and then anodised at 10, 70 or 120 V (Mean ± SD, n=3, *=P<0.05).
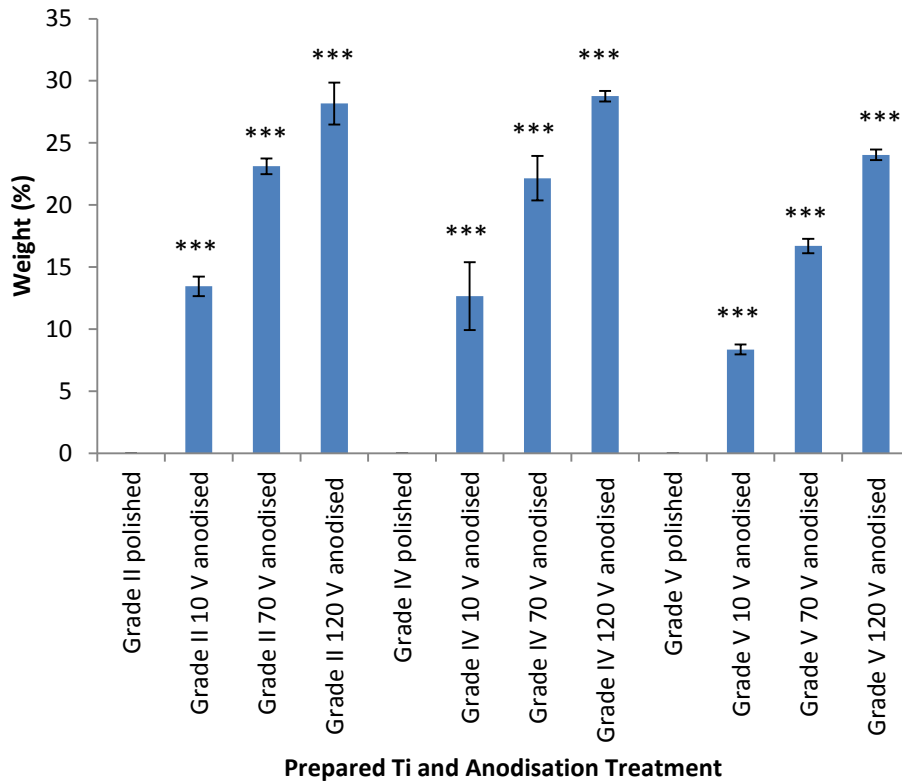
The oxygen weight percentage obtained with EDX measurements of the surfaces of Grade II, IV and V anodised Ti demonstrated a clear pattern indicative of a thickening of the surface oxide film. In the polished condition where the oxide film is 8-10 nm thickness the measurements were below the detection limit of the EDX instrument for all Ti Grades. The oxygen weight % on the Grade II surface increased from 0 to 13.5, to 23.1 to 28.2% when the Grade II Ti surface was anodised at 0, 10, 70 and 120 V respectively. A similar pattern that was observed for both the Grade IV Ti surface where the oxygen weight % increased from 0 % from the polished control to 12.7, 22.2 and 28.8 % for the samples being anodised at 10 V, 70 V and 120 V. The correlation between the oxygen weight (%) was confirmed on the

surface of the Grade V anodised Ti surfaces. The oxygen weight increased from 0 % for the Grade IV polished surface to 8.4, 16.7 and 24.0 % for the samples anodised at 10 V, 70 V and 120 V. (figure 3.78). Significant increases of oxygen weight (%) were observed on grade II, IV and V anodised specimens compared to the controls (p<0.001).

3.5.5.3 SEM imaging of Grade II, IV and V anodised Ti surfaces.

The SEM images of the Grade II, IV and V Ti surface prepared by anodic oxidation at 10 V, 70 V and 120 V demonstrated that the surface became noticeably rougher with distinct raised surface features observed at 120 V (figures 3.79 to 3.80).

Figure 3.79. SEM image of a Grade II CpTi surface anodised at 10 V (x2000 magnification), demonstrating increased prominence of the surface scratches introduced during the polishing process.
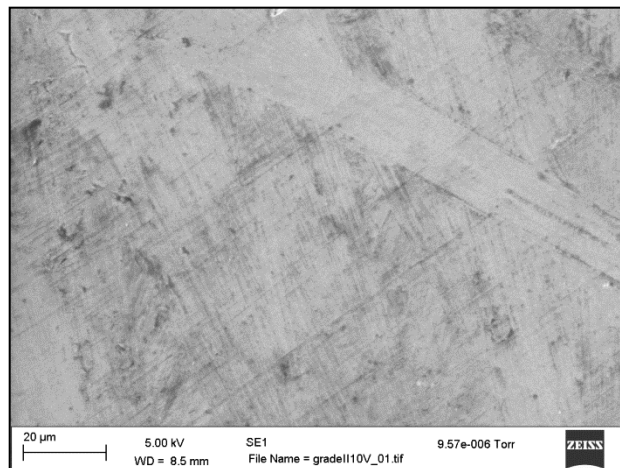
Figure 3.80. SEM image of a Grade II CpTi surface anodised at 70 V (x2000 magnification), demonstrating a heterogeneously raised surface appearance.
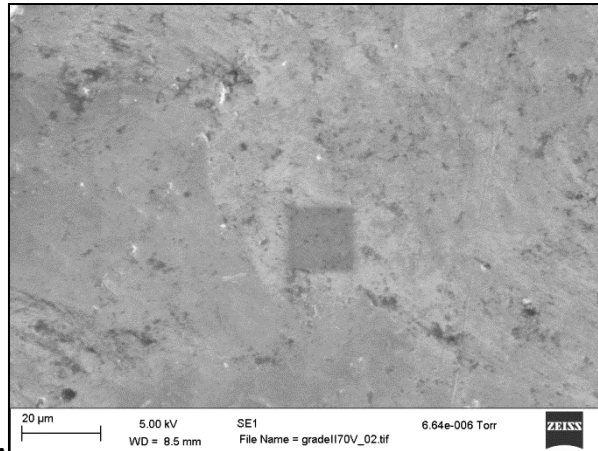
Figure 3.81. SEM image of a Grade II CpTi surface anodised at 120 V (x2000 magnification), demonstrating distinct raised surface features highlighted in circles.
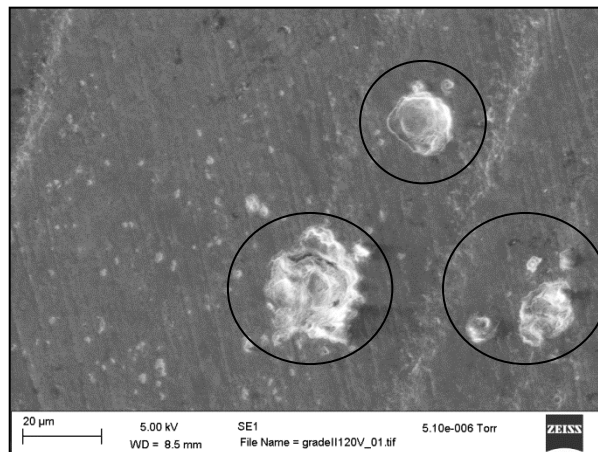
Figure 3.82. SEM image of a Grade IV Ti surface anodised at 10 V (x2000 magnification), demonstrating raised features which are consistent with machining features introduced during surface polishing.
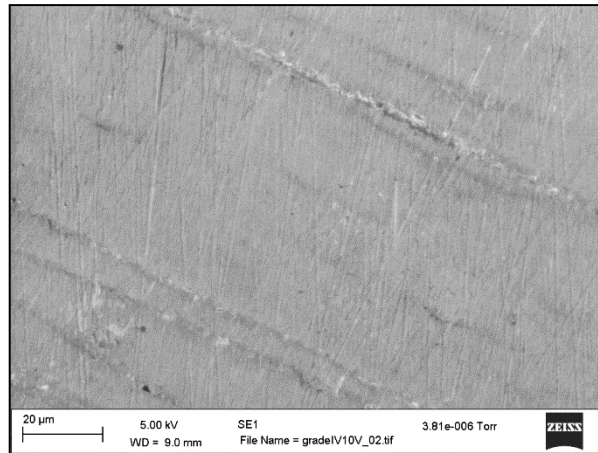
Figure 3.83. SEM image of a Grade IV Ti surface anodised at 70 V (x2000 magnification), demonstrating heterogeneous thickening of the surface and visibly increased surface roughness.
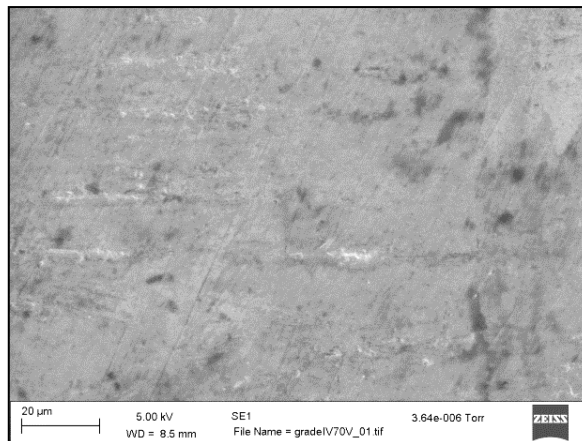
Figure 3.84. SEM image of a Grade IV Ti surface anodised at 120 V (x2000 magnification), demonstrating raise parallel ridges on the surface of the samples, highlighted by circles.
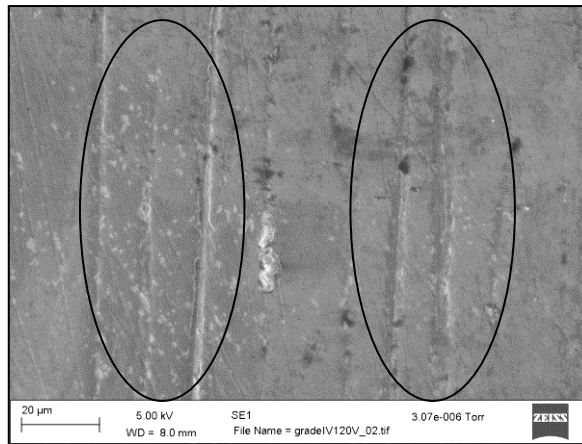
Figure 3.85. SEM image of a Grade V Ti surface anodised at 10 V (x2000 magnification), demonstrating increased clarity of the remnant polishing features introduced by processing.
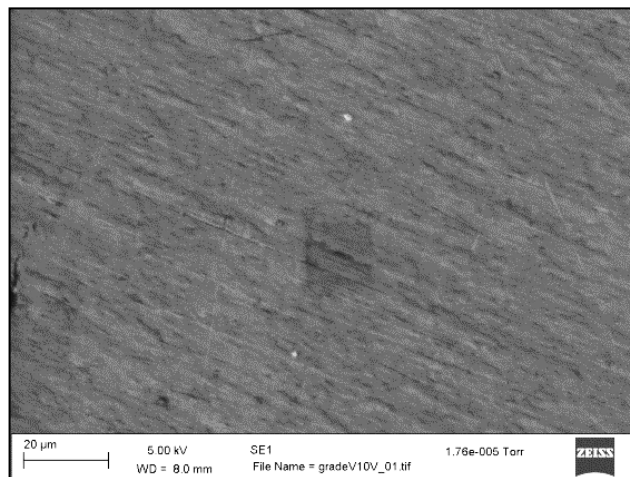
Figure 3.86. SEM image of a Grade V Ti surface anodised at 70 V (x2000 magnification), demonstrating polishing features introduced by the initial surface processing.
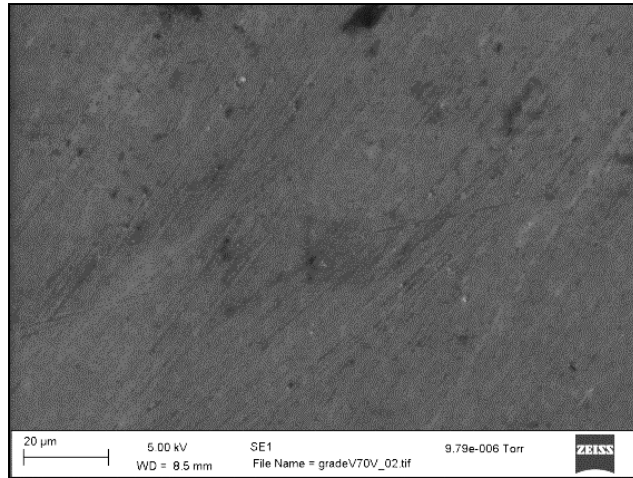
Figure 3.87. SEM image of a Grade V Ti surface anodised at 120 V (x2000 magnification), demonstrating increased surface roughness characterised by peaks and surface defects.
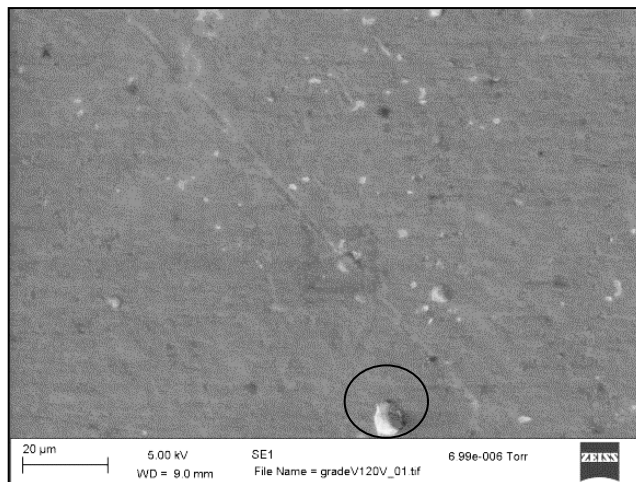
The SEM images figures 3.85, 3.86 and 3.87 illustrate the surface topography for the Grade V Ti surfaces anodised at 10, 70 and 120 V. figure 3.86 illustrates the roughening of Ti surface with the presence of valleys and peaks on the surface of the Ti providing a distinct texture. figure 3.87 illustrates a different surface texture compared with figure 3.86 which illustrates the formation of different surface textures at different voltages being applied. The figure 3.88 illustrates the presence of distinct isolated features formed on the surface at increased voltages which may be related to the presence of impurity inclusions within the alloy itself.

3.5.5.4 Contact angle measurements on anodically oxidised Ti surfaces.

Contact angle measurements were performed on Grade II, IV and V Ti surfaces prepared with anodic oxidation at 10 V, 70 V and 120 V using distilled water at 23 ± 1°C. The surfaces prepared by anodic oxidation exhibited no significant change in mean contact angle when compared with non-oxidised surfaces ($p > 0.05$) although a slight increase in contact angle was observed with increasing anodising voltage (figures 3.88, 3.89 and 3.90).

Figure 3.88. A histogram illustrating the mean contact angle measurements on Grade II CpTi surfaces anodised at a voltage of 0V, 10 V, 70 V and 120 V (Mean ± SD, n=3, 5 repeat measurements *=p<0.05).
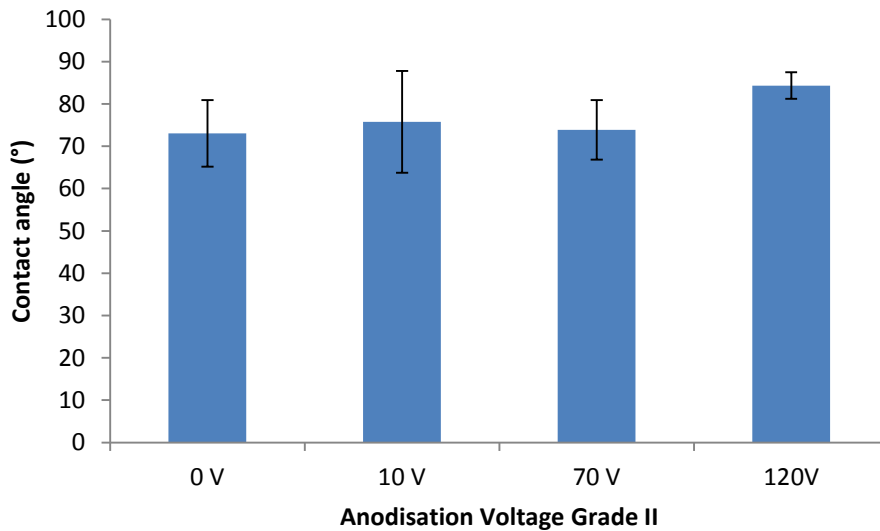
Figure 3.89. A histogram illustrating the mean contact angle measurements on Grade IV CpTi surfaces anodised at a voltage of 0V, 10 V, 70 V and 120 V (Mean ± SD, n=3, 5 repeat measurements *=P<0.05).
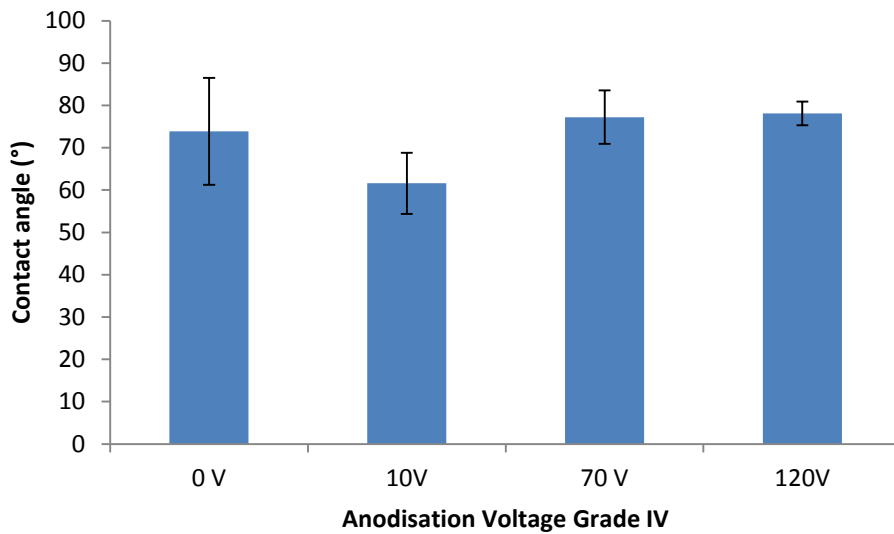
The mean contact angles were in the same range as for Grade II CpTi although less of a trend with increasing anodisation voltage was observed.

Figure 3.90. A histogram illustrating the mean contact angle measurements on Grade V CpTi surfaces anodised at a voltage of 0V, 10 V, 70 V and 120 V (Mean ± SD, n=3, 5 repeat measurements *=P<0.05).
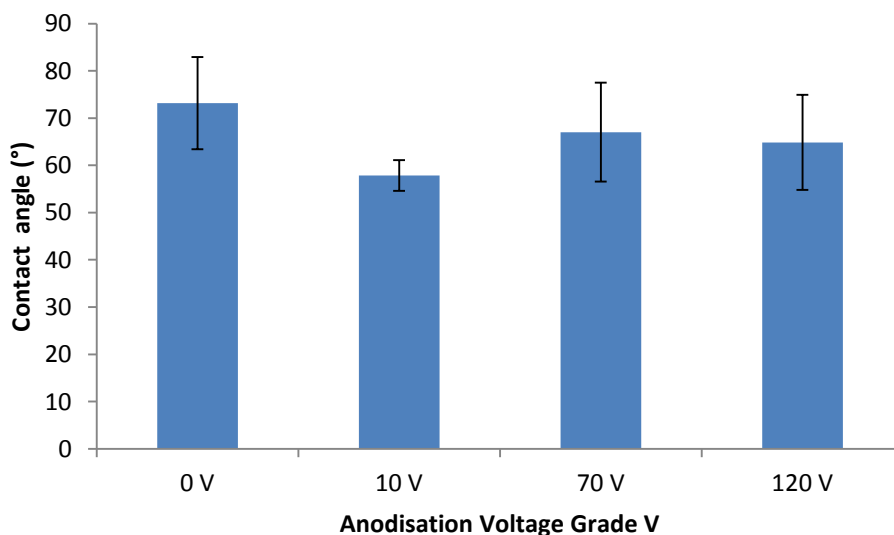
The contact angles determined on Grade V (figure 3.90) prepared Ti surfaces demonstrated a similar pattern to CpTi Grade IV.

3.5.5.5 Photocatalytic degradation by anodised Ti surfaces

Methylene blue degradation assays were carried out on the surfaces of Grade II, IV and V Ti anodised at 0V, 10 V, 70 V and 120 V. It was observed that the 70 V and 120 V anodic oxidised Ti surfaces were the most photocatalytic after 120 mins when irradiated at an intensity of 923 mW/cm^2 (figures 3.91, 3.92 and 3.93).

Figure 3.91. Line chart illustrating the degradation of methylene blue on Grade II CpTi discs after irradiating with UV light at 923 mW/cm^2 (25% intensity). The chart shows the effect of UV light on the methylene blue dye degradation without a Ti disc, and in the presence of 0V, 10 V, 70 V and 120 V anodised Grade II CpTi samples. Readings were taken in triplicate every five mins for 120 mins (Mean ± SD, n=1).
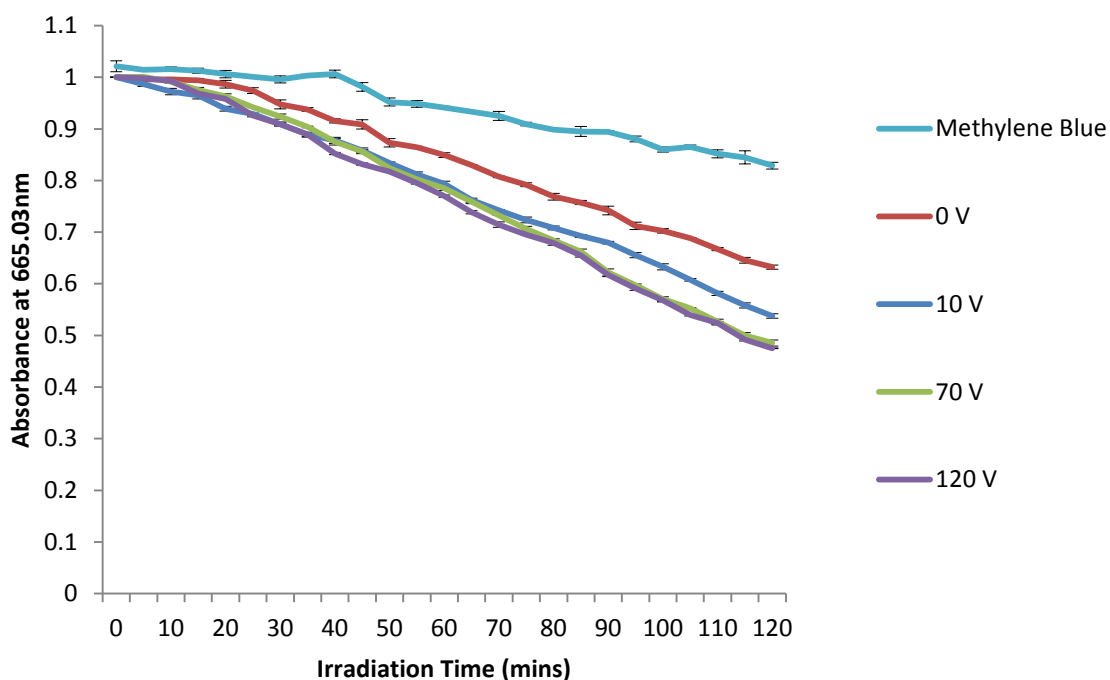

The Grade II CpTi samples were submerged in methylene blue dye and irradiated at 923 mW/Cm2 for 120 mins. The control methylene blue degraded by approximately 19 % whereas the polished Ti control resulted in a 37 % degradation after 120 mins of irradiation.

Grade II Ti samples anodised at 10, 70 and 120 V led to a degradation of 46 %, 51 % and 52

%, respectively of methylene blue after 120 mins (figure 3.91).

Figure 3.92. Line chart illustrating the degradation of methylene blue on Grade IV CpTi discs after irradiating with UV light at 923 mW/cm^2 (25% intensity). The chart shows the effect of UV light on the methylene blue dye degradation without a Ti disc, and in the presence of 0V, 10 V, 70 V and 120 V anodised Grade II CpTi samples. Readings were taken in triplicate every five mins for 120 mins (Mean ± SD, n=1).
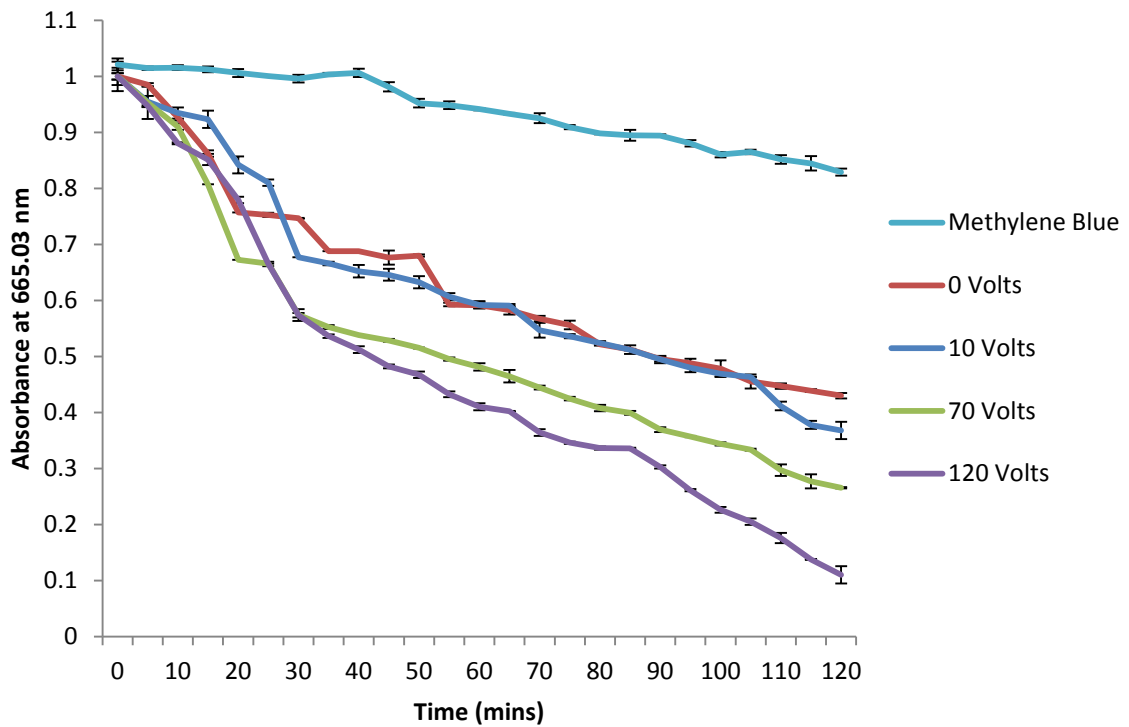
The control of methylene blue degraded by 19 % after 120 mins irradiation with UV at an

intensity of 923 mW/cm^2 whereas the polished control and Ti specimens anodised at 10, 70

and 120 V led to a degradation of methylene blue of 57, 63, 73, and 88 % respectively after

120 mins irradiation (figure 3.92).

Figure 3.93. Line chart illustrating the degradation of methylene blue on Grade V CpTi discs after irradiating with UV light at 923 mW/cm^2 (25% intensity). The chart shows the effect of UV light on the methylene blue dye degradation without a Ti disc, and in the presence of 0V, 10 V, 70 V and 120 V anodised Grade II CpTi samples. Readings were taken in triplicate every five mins for 120 mins (Mean ± SD, n=1).
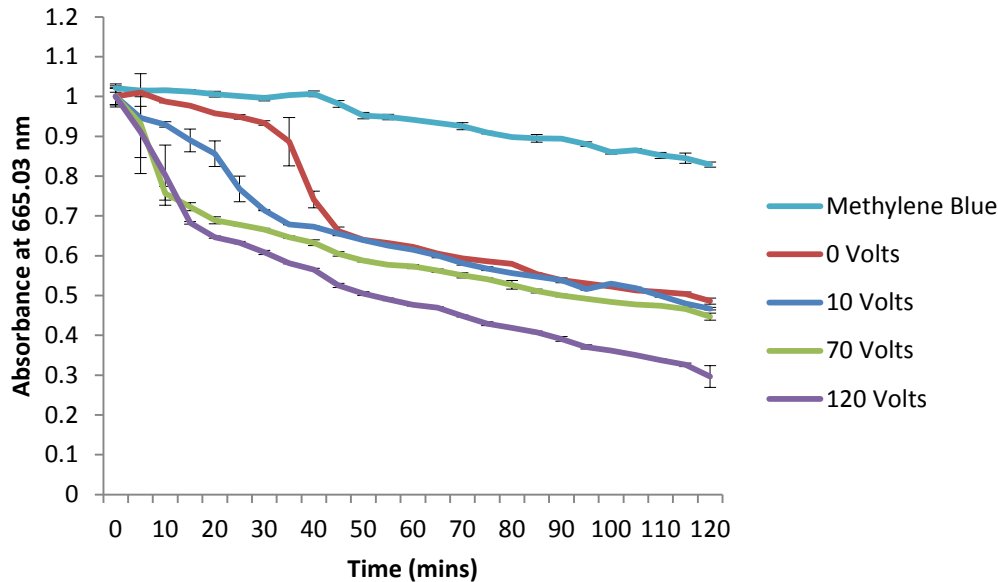
The control of methylene blue degraded by 19 % after 120 mins irradiation with UV at an intensity of 923 mW/cm^2 whereas the polished control and Ti specimens anodised at 10, 70 and 120 V led to a degradation of methylene blue of 51, 53, 55, and 70 % respectively after 120 mins irradiation (figure 3.93).

From the methylene blue degradation studies it was observed that by increasing the voltage when generating the anodised samples, there was a significant increase in the degradation of the methylene blue dye after 120 mins irradiation with 923 mW/cm^2. The increased degradation rate was observed on Grade II, IV and V Ti substrates with the highest degradation being observed on the Grade IV anodised Ti that was created at 120 V (88 % degradation of methylene blue after 120 mins at intensity of 923 mW/cm^2 (figure 3.93)).

3.5.5.6 The effect of UV irradiation of prepared Ti surfaces on bacterial adhesion and viability

The effect of pre-treating anodised Ti surfaces with UV at an intensity of 923 mW/cm^2 on the adhesion and viability of *S sanguinis*, *E coli*, *S mutans* and *F nucleatum* was determined on the Grade II, IV and V Ti samples (prepared by anodic oxidation at 10 V, 70 V and 120 V).

Figure 3.94. A histogram summarising the effect of UV irradiation at 923 mW/ cm^2 (25% intensity) for 1 min on the viability of *S sanguinis* on Grade II Ti surfaces anodised at 0 V, 10 V,70 V and 120 V (Mean ± SD, n=5, *=P<0.05).
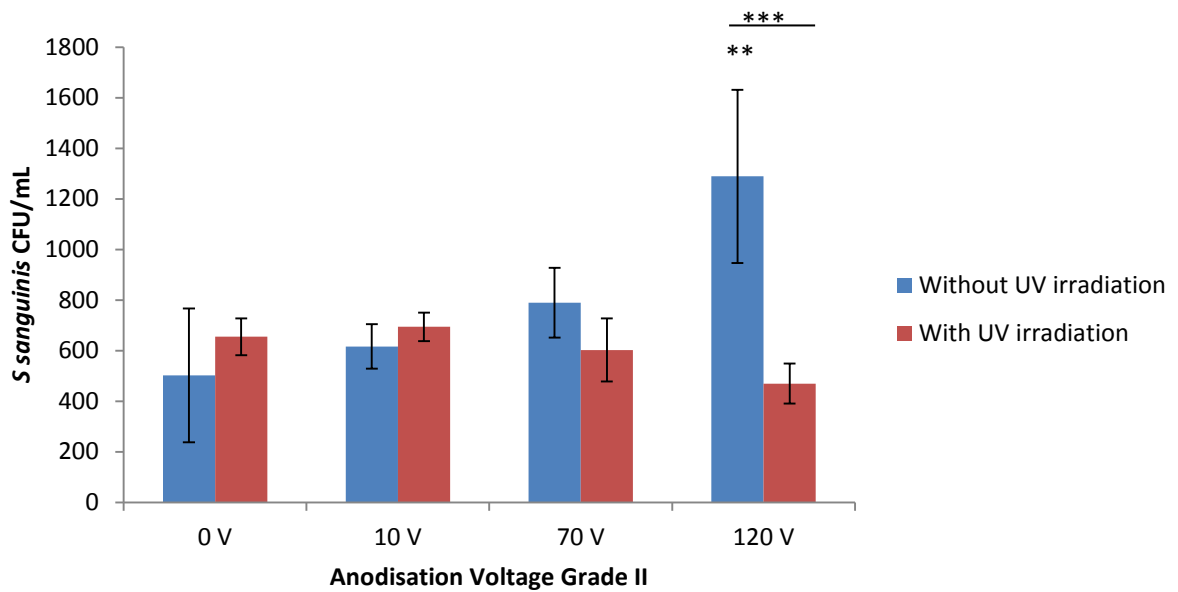
In the absence of UV irradiation, increased bacterial counts were observed with increasing anodising voltage, significant increase was observed on the 120 V specimens (P<0.01). Following UV irradiation for 1 min a modification of the observed pattern occurred with a significant reduction in mean CFU/mL observed on the 120 V anodised specimen which had a significantly lower count than the control samples (P<0.001).

Figure 3.95. A histogram summarising the effect of UV irradiation at 923 mW/ cm^2 (25% intensity) for 1 min on the viability of *S sanguinis* on Grade IV Ti surfaces anodised at 0 V, 10 V,70 V and 120 V (Mean ± SD, n=5, *=P<0.05).
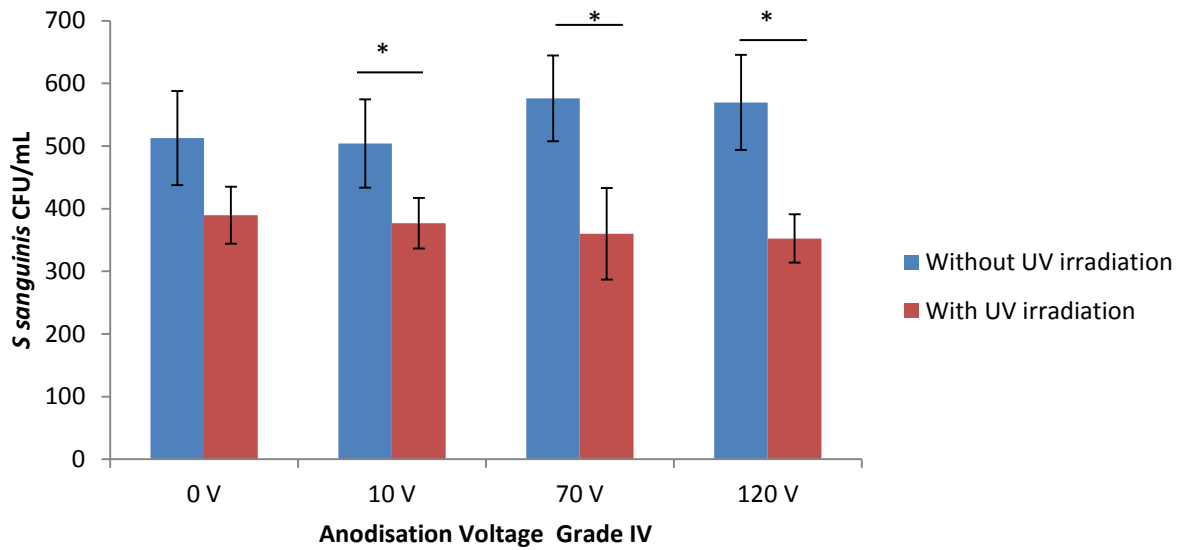
Following anodisation the mean CFU/mL of *S sanguinis* increased when compared with the control surface but was not significant (p>0.05). Following UV irradiation the mean CFU/mL of *S sanguinis* was significantly decrease on all surfaces with the greatest decrease observed on the Ti surface anodised at 120V (p<0.05).

Figure 3.96. A histogram summarising the effect of UV irradiation at 923 mW/ cm^2 (25% intensity) for 1 min on the viability of *S sanguinis* on Grade V Ti surfaces anodised at 0 V, 10 V,70 V and 120 V (Mean ± SD, n=5, *=P<0.05).
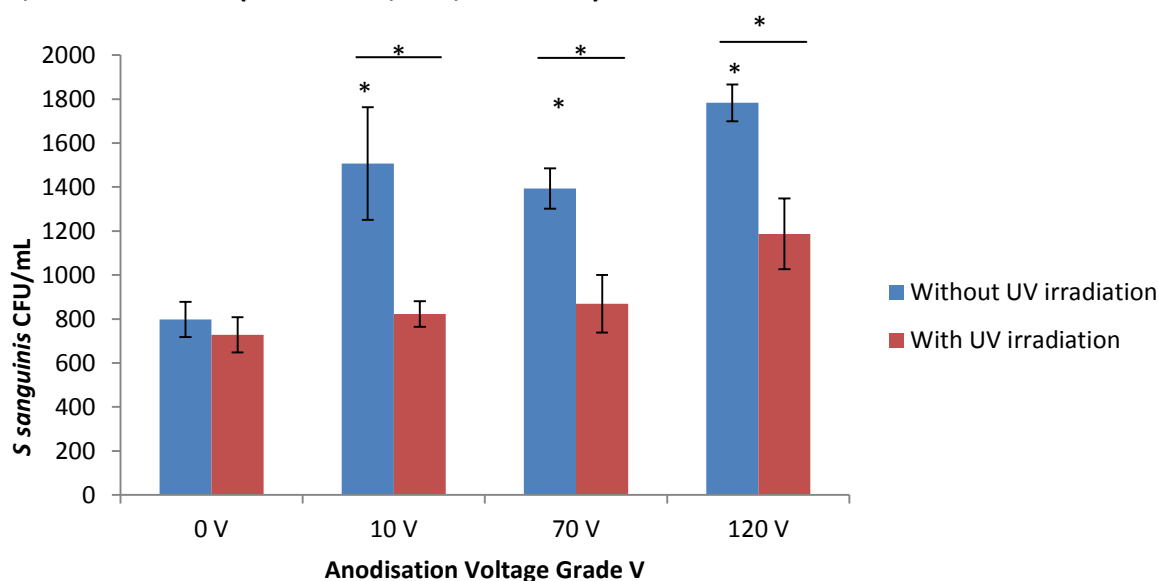
On Grade V surfaces there was a significant increase of mean CFU/mL of *S sanguinis* as the anodising voltage was increased (p<0.05). UV irradiation resulted in a decrease in mean CFU/mL for all surfaces with similar magnitudes of decrease observed on all anodised surfaces (p<0.05).

Figure 3.97. A histogram summarising the effect of UV irradiation at 923 mW/ cm2 (25% intensity) for 1 min on the viability of *E coli* on Grade II Ti surfaces anodised at 0 V, 10V, 70 V and 120 V (Mean ± SD, n=5, *=P<0.05).
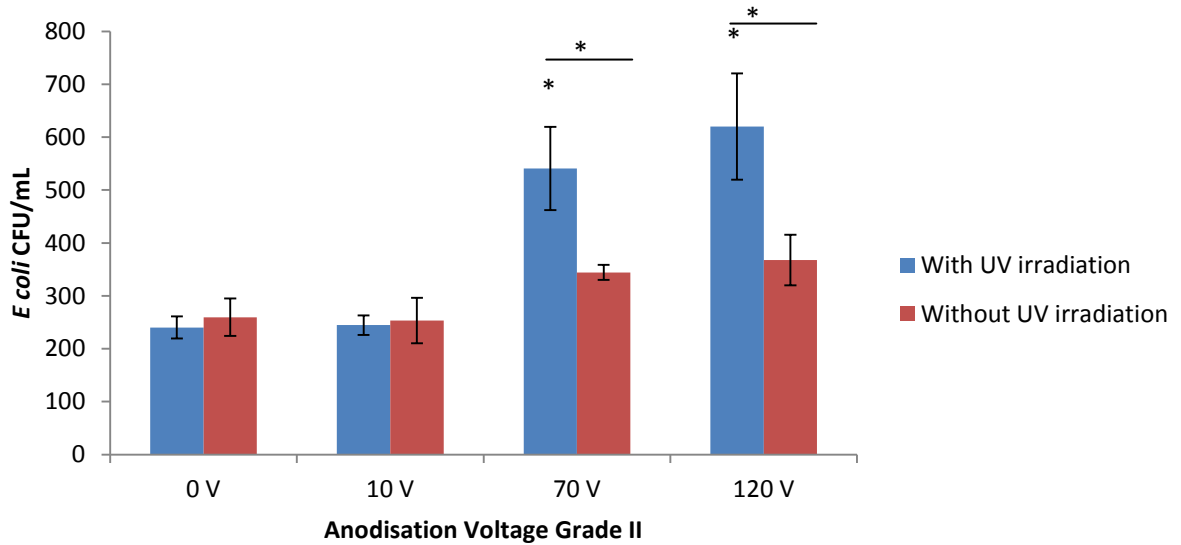
In the absence of UV irradiation, significant increases of mean CFU/mL were observed on Grade II 70 and 120 V anodised specimens (P<0.05). Following UV irradiation for 1 min a modification of the observed pattern occurred with a significant reduction in mean CFU/mL observed on the 70 and 120 V anodised specimens which had a lower count than the control samples (p<0.05).

Figure 3.98. A histogram summarising the effect of UV irradiation at 923 mW/ cm^2 (25% intensity) for 1 min on the viability of *E coli* on Grade IV Ti surfaces anodised at 0 V, 10 V,70 V and 120 V (Mean ± SD, n=5, *=P<0.05).
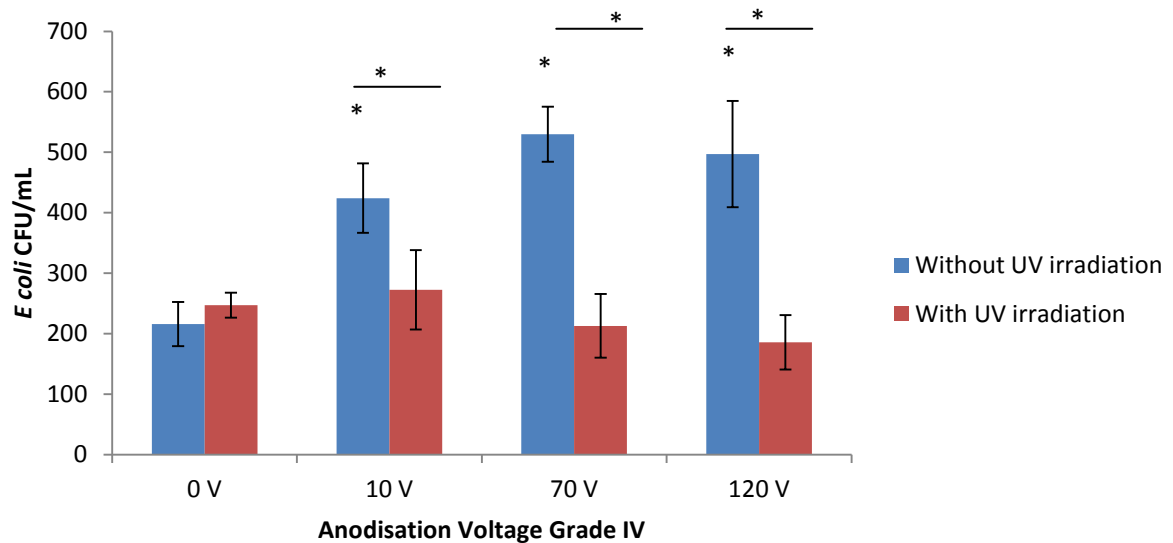
On Grade IV surfaces there was a significant increase of mean CFU/mL of *E coli* as the anodising voltage was increased (p<0.05). UV irradiation resulted in a decrease in mean CFU/mL for all surfaces with similar magnitudes of decrease observed on all anodised surfaces (p<0.05).

Figure 3.99. A histogram summarising the effect of UV irradiation at 923 mW/ cm² (25% intensity) for 1 min on the viability of _E coli_ on Grade V Ti surfaces anodised at 0 V, 10 V, 70 V and 120 V (Mean ± SD, n=5, *=P<0.05).
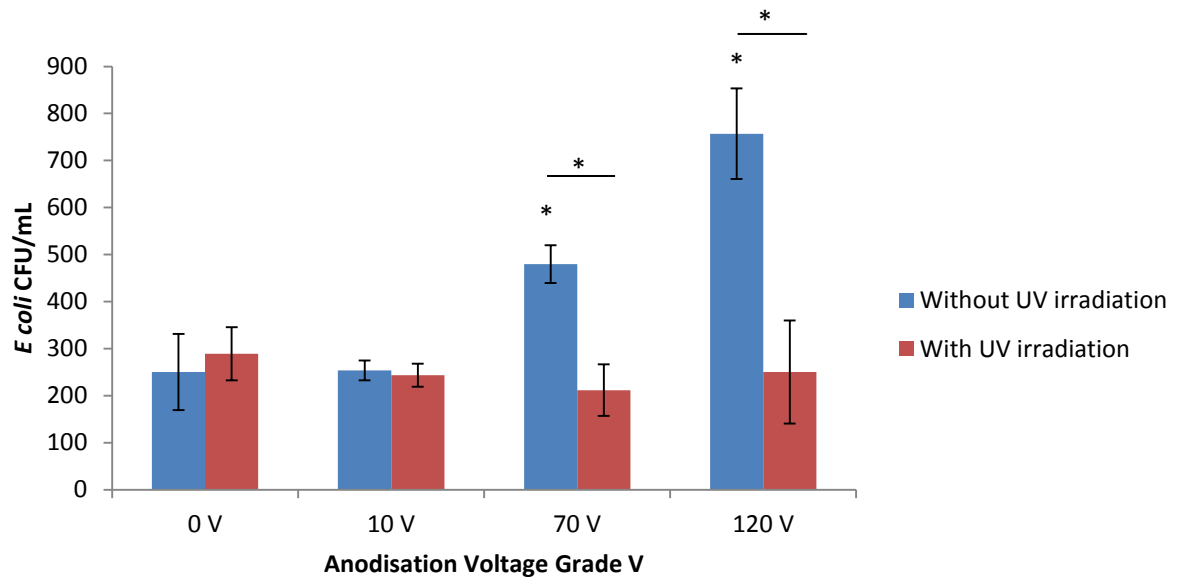
On Grade V surfaces there was a significant increase of mean CFU/mL of _E coli_ as the anodising voltage was increased (p<0.05). UV irradiation resulted in significant decreases in mean CFU/mL for all surfaces with similar magnitudes of decrease observed on the 70 and 120 V anodised specimens (p<0.05).

Figure 3.100. A histogram summarising the effect of UV irradiation at 923 mW/ cm^2 (25% intensity) for 1 min on the viability of _S mutans_ on Grade II Ti surfaces anodised at 0 V, 10 V,70 V and 120 V (Mean ± SD, n=5, *=P<0.05).
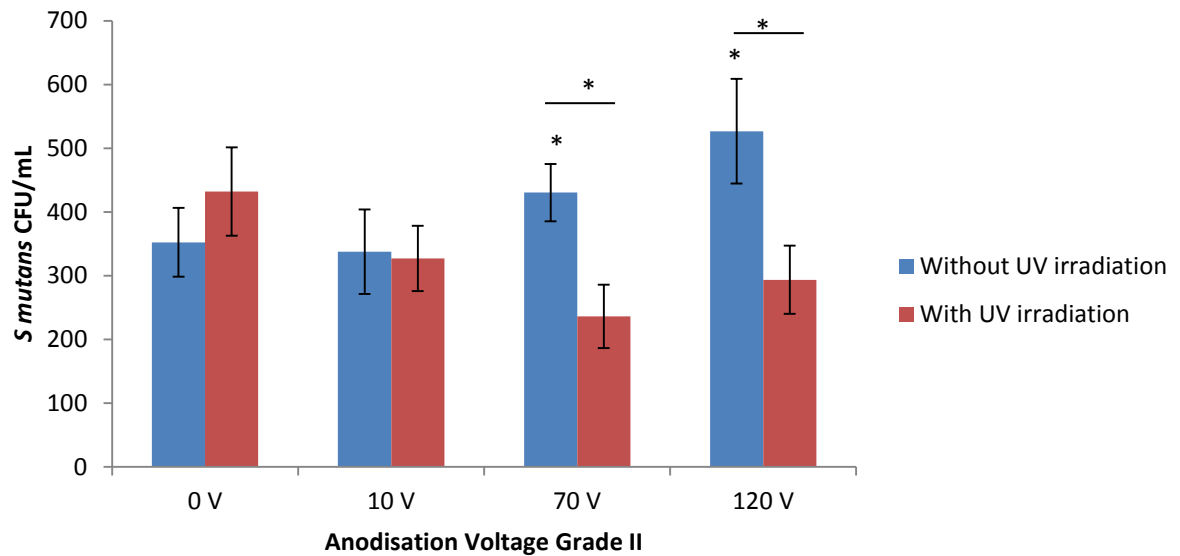
On Grade II surfaces there was a significant increase of mean CFU/mL of _S mutans_ with Grade II 70 and 120 V anodised specimens (p<0.05). UV irradiation resulted in significant decreases in mean CFU/mL for the 70 V and 120 V anodised specimens (p<0.05).

Figure 3.101. A histogram summarising the effect of UV irradiation at 923 mW/ cm^2 (25% intensity) for 1 min on the viability of _S mutans_ on Grade IV Ti surfaces anodised at 0 V, 10 V,70 V and 120 V (Mean ± SD, n=5, *=P<0.05).
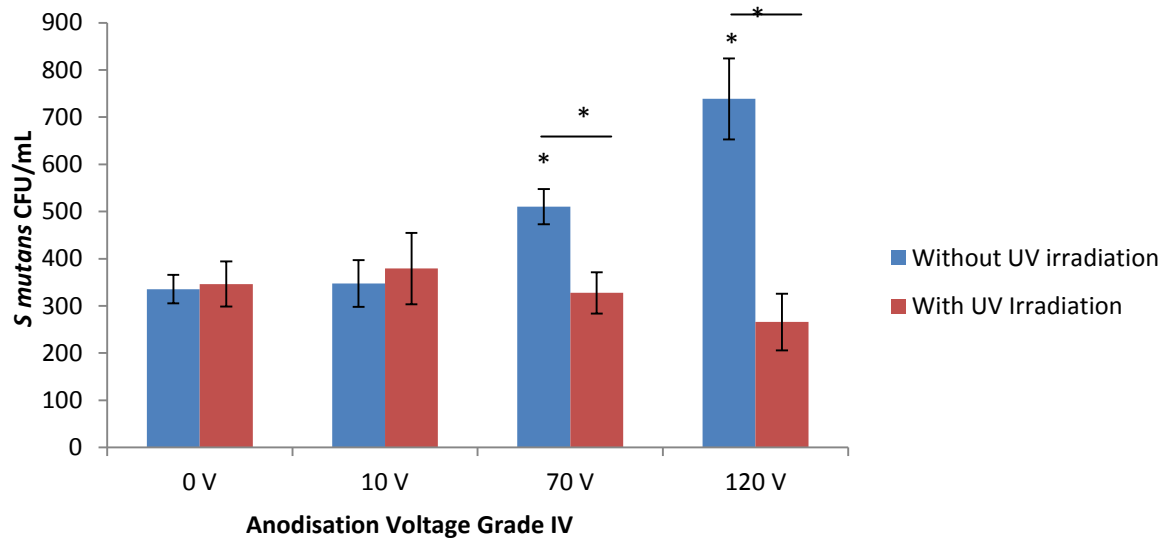
On Grade IV surfaces there was a significant increase of mean CFU/mL of _S mutans_ with Grade IV 70 and 120 V anodised specimens (p<0.05). UV irradiation resulted in significant decreases in mean CFU/mL for the 70 V and 120 V anodised specimens (p<0.05).

Figure 3.102. A histogram summarising the effect of UV irradiation at 923 mW/ cm^2 (25% intensity) for 1 min on the viability of *S mutans* on Grade V Ti surfaces anodised at 0 V, 10 V, 70 V and 120 V (Mean ± SD, n=5, *=P<0.05).
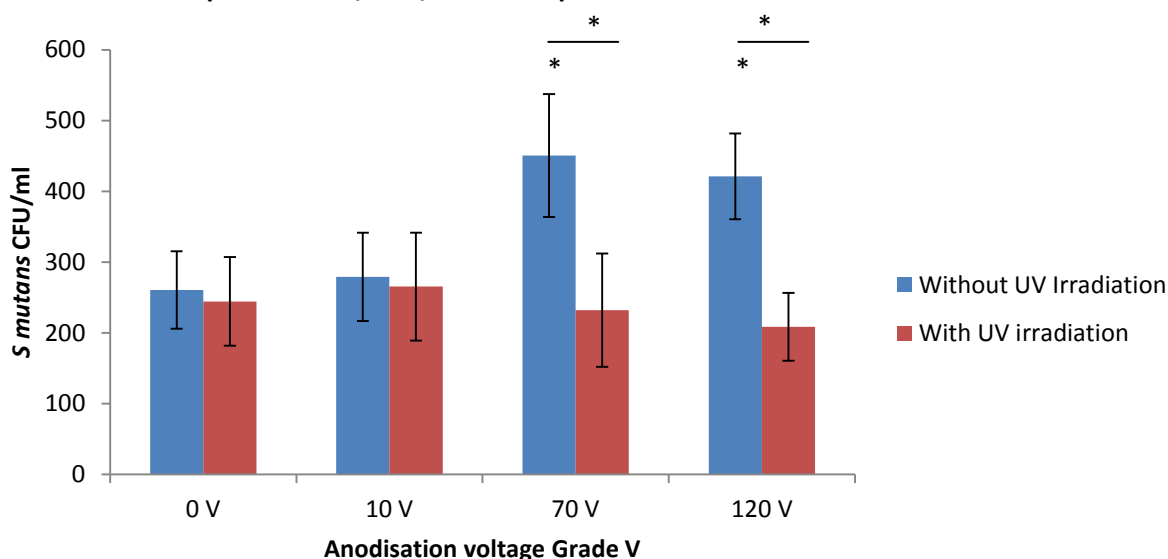
On Grade V surfaces there was a significant increase of mean CFU/mL of *S mutans* with Grade IV 70 and 120 V anodised specimens (p<0.05). UV irradiation resulted in significant decreases in mean CFU/mL for the 70 V and 120 V anodised specimens (p<0.05).

3.6 The effect of EO in the enhanced penetration Chlorhexidine Digluconate based mouth wash formulations.

Previous work by Hendry et al., 2008 and Karpanen et al., 2010 demonstrated enhanced penetration of bacterial biofilms on the skin surface with the IPA:EO biocide formation. The formulation was adapted and developed as a mouthwash formulation to determine its effectiveness against oral bacteria associated with peri-implant disease.

The MIC and the MBC of the constituents of the IPA:EO formulation was determined against the *S sanguinis* and *S mutans* bacteria. The effectiveness of the IPA: EO biocide formulation was determined on *S sanguinis* biofilms grown in a CDC biofilm reactor. The IPA:EO

formulation was adapted by replacing the IPA for ethanol and the exposure times on *S sanguinis* and *S mutans* determined.

3.6.1 The minimum inhibitory concentration and minimum bacterial clearance assays on *S sanguinis*

The minimum inhibitory clearance assays for isopropanol (IPA), chlorhexidine gluconate (CHG), Eucalyptus oil (EO) and ethanol were carried out to determine the bacteriostatic or bactericidal effect on *S sanguinis*.

Table 3.5: The minimum bacterial clearance assay for Isopropanol (IPA) with concentrations ranging from 70% through to 0.14%. (TMTC= Too many to count).

Plate no	1	2	3	4	5	6	7	8	9	10
IPA (%)	70	35	17.5	8.8	4.4	2.2	1.1	0.55	0.27	0.14
CFU/mL	0	0	0	TMTC	TMTC	TMTC	TMTC	TMTC	TMTC	TMTC

Concentrations of IPA from 70 % through to 17.5 % were found to prevent the growth of *S sanguinis.* At the concentrations of 8.8 % volume and lower there was no antibacterial activity and a lawn of *S sanguinis* was observed to have grown on the surface of the agar plate.

Table 3.6: The minimum bacterial clearance assay results of chlorhexidine digluconate concentrations ranging from 0.02 % to 10 %. (TMTC= Too many to count).

Plate no	1	2	3	4	5	6	7	8	9	10
CHG (%)	10	5	2.5	1.3	0.6	0.31	0.16	0.78	0.04	0.02
CHG (µg/mL)	100000	50000	25000	12500	6250	3125	1562.5	781.25	390.63	195.31
CFU/mL	0	0	0	0	0	0	TMTC	TMTC	TMTC	TMTC

Concentrations of CHG from 10 % (100000 µg/mL) through to 0.31 % (3125 µg/mL) were found to prevent the growth of *S sanguinis.* At the concentrations of 0.16% volume and lower there was no antibacterial activity and a lawn of *S sanguinis* was observed to have grown on the surface of the agar plate.

Table 3.7: The minimum bacterial clearance assay for Eucalyptus oil on *S sanguinis*. The concentrations of EO being tested ranged from 1 % (455 g/mL) through to 0.002 % (0.89 µg/mL). The EO did not show any antibacterial activity at the concentrations tested (TMTC = Too many to count).

Plate no	1	2	3	4	5	6	7	8	9	10
EO (%)	1	0.5	0.25	0.13	0.06	0.03	0.02	0.01	0.004	0.002
EO (µg/mL)	455	227.5	113.75	56.88	28.44	14.22	7.11	3.55	1.78	0.89
CFU/mL	TMTC	TMTC	TMTC	TMTC	TMTC	TMTC	TMTC	TMTC	TMTC	TMTC

The EO concentrations ranging from 1% (455 µg/mL) through to 0.002 % (0.89 µg/mL) were demonstrated to have no antibacterial activity with lawns of *S sanguinis* being observed on the surface of all the agar plates.

Table 3.8: The minimum bacterial clearance assay for ethanol on *S sanguinis*. The concentrations tested ranged from 70% through to 0.14%. The MBC was found to be at an ethanol concentration of 17.5 % (TMTC = Too many to count).

Plate no	1	2	3	4	5	6	7	8	9	10
Ethanol (%)	70	35	17.5	8.75	4.38	2.19	1.09	0.55	0.27	0.14
CFU/mL	0	0	0	TMTC	TMTC	TMTC	TMTC	TMTC	TMTC	TMTC

It was observed that an ethanol concentration ranging from 70 % through to 17.5% was bactericidal with concentrations of 8.75% and below having no antibacterial effect with bacteria being observed on the surface of the agar plate.

The doubling dilutions of the constituents of the IPA : EO biocide formulation demonstrated that the MBC for IPA was 8.75%, CHG was 0.165%, EO was found not to have a bactericidal effect and ethanol was 8.75 % (Tables 3.5, 3.6, 3.7 and 3.8).

3.6.2 The minimum inhibitory clearance and minimum bacterial clearance assay on *S sanguinis* with reduced concentrations.

The initial MIC/MBC assays performed by double dilutions resulted in large concentration ranges of the constituents for a possible mouthwash formation against the *S sanguinis* bacteria. The MIC/MBC assays were repeated with ethanol concentrations of 6% to 15%, eucalyptus oil 1% to 5%, Tween 0.25% to 2% on *S sanguinis* and *S mutans* (Table 3.8 and Table 3.9).

Table 3.9: The minimum bacterial clearance assay on *S sanguinis* bacterium with the components of the mouth rinse formulation.

Plate no	Constituent and concentration of the mouth wash formulation (v/v)	*S sanguinis* CFU/mL
1	Ethanol 15%	Growth
2	Ethanol 14%	Growth
3	Ethanol 13%	Growth
4	Ethanol 12%	Growth
5	Ethanol 11%	TMTC
6	Ethanol 10%	TMTC
7	Ethanol 9%	TMTC
8	Ethanol 8%	TMTC
9	Ethanol 7%	TMTC
10	Ethanol 6%	TMTC
11	Eucalyptus oil 5% (145.6 mg/mL)	TMTC
12	Eucalyptus oil 4% (72.8 mg/mL)	TMTC
13	Eucalyptus oil 3% (36.4 mg/mL)	TMTC
14	Eucalyptus oil 2% (18.2 mg/mL)	TMTC
15	Eucalyptus oil 1% (9.1 mg/mL)	TMTC
16	Tween 2%	TMTC
17	Tween 1%	TMTC
18	Tween 0.5 %	TMTC
19	Tween 0.25%	TMTC
20	Tween 0.125%	TMTC
21	CHG 0.5% (1 mg/mL)	No Growth
22	CHG 0.4% (0.8 mg/mL)	No Growth
23	CHG 0.3% (0.6 mg/mL)	No Growth
24	CHG 0.2% (0.4 mg/mL)	No Growth
25	CHG 0.1% (0.2 mg/mL)	Growth

It was observed that the various concentrations of Tween, EO and ethanol used did not have an antimicrobial effect on the *S sanguinis* bacterium with bacterial colonies still being observed on the surface of the agar plate. At concentrations ranging from 0.2 to 0.5 % of CHG there was no bacterial growth however at the lower concentration of 0.1% of the CHG, there was no bactericidal effect on the *S sanguinis bacterium.*

3.6.3 The minimum inhibitory clearance and minimum bacterial clearance assay on *S mutans*.

Table 3.10: The minimum bacterial clearance assay on *S mutans* bacterium with the components of the mouth rinse formulation.

Plate no	Constituent and concentration of the mouth wash formulation (*v/v*)	*S mutans* CFU/mL
1	Ethanol 15%	Growth
2	Ethanol 14%	Growth
3	Ethanol 13%	Growth
4	Ethanol 12%	Growth
5	Ethanol 11%	Growth
6	Ethanol 10%	Growth
7	Ethanol 9%	Growth
8	Ethanol 8%	Growth
9	Ethanol 7%	TMTC
10	Ethanol 6%	TMTC
11	Eucalyptus oil 5% (145.6 mg/mL)	TMTC
12	Eucalyptus oil 4% (72.8 mg/mL)	TMTC
13	Eucalyptus oil 3% (36.4mg/mL)	Growth
14	Eucalyptus oil 2% (18.2 mg/mL)	Growth
15	Eucalyptus oil 1 % (9.1 mg/mL)	Growth
16	Tween 2%	TMTC
17	Tween 1%	TMTC
18	Tween 0.5 %	TMTC
19	Tween 0.25%	TMTC
20	Tween 0.125%	TMTC
21	CHG 0.5% (1 mg/mL)	No Growth
22	CHG 0.4% (0.8 mg/mL)	No Growth
23	CHG 0.3% (0.6 mg/mL)	No Growth
24	CHG 0.2% (0.4 mg/mL)	No Growth
25	CHG 0.1% (0.2 mg/mL)	No Growth

The minimum bacterial clearance assay was repeated with *S mutans* (Table 3.10). It was observed that the antibacterial component of the formulation was CHG which ranged in concentration from 0.1 to 0.5%. The concentrations of Tween, EO and ethanol used in the study did not possess bactericidal properties with the presence of bacteria growing on the surface of the agar plates as lawns or high number of colonies after incubation with the

constituents for 24 hrs. The MBC data was included in the study because it is considered to be more reliable when compared with the MICs.

The MIC/MBC assays performed on *S sanguinis* and *S mutans* demonstrated that the concentrations of ethanol, Tween and EO did not possess antibacterial properties whereas the concentrations of CHG ranging from 0.1 to 0.4 % were bactericidal against both *S sanguinis* and *S mutans* (Table 3.7 and 3.8).

3.6.4 Bacterial biofilms growth on the surface of the prepared Ti substrates on the CDC biofilm reactor.

To determine the effectiveness of the IPA: EO and CHG:EO formulations on *S sanguinis* and *S mutans,* biofilms on the surfaces of Grade IV Ti were grown within a CDC bioreactor. The biofilms were then exposed to the formulations before being detached and incubated on blood agar plates to determine the bacterial viability. The SEM images illustrate the formation of the *S sanguinis* biofilms on Grade IV P220 prepared surfaces after 24, 48 hrs incubation in a CDC bioreactor with TSB as a nutrient source and further incubation for 24 hours in artifical saliva for conditioning (figures 3.104 a, b and c) and compared with the adhesion of *S sanguinis* on a healing abutment sample.

Figure 3.103a. SEM images of different stages of *S sanguinis* growth on control Grade IV CpTi discs polished with P220 grit at x2000 magnification. The SEM image illustrates two images captured of *S sanguinis* bacterial growth on the surface of the P220 polished Grade IV surface after 24 hrs in the CDC biofilm reactor. The circle highlights the bacterial biofilm formed on the surface and the arrows indicate the dark areas of proteins adhered to the surface.
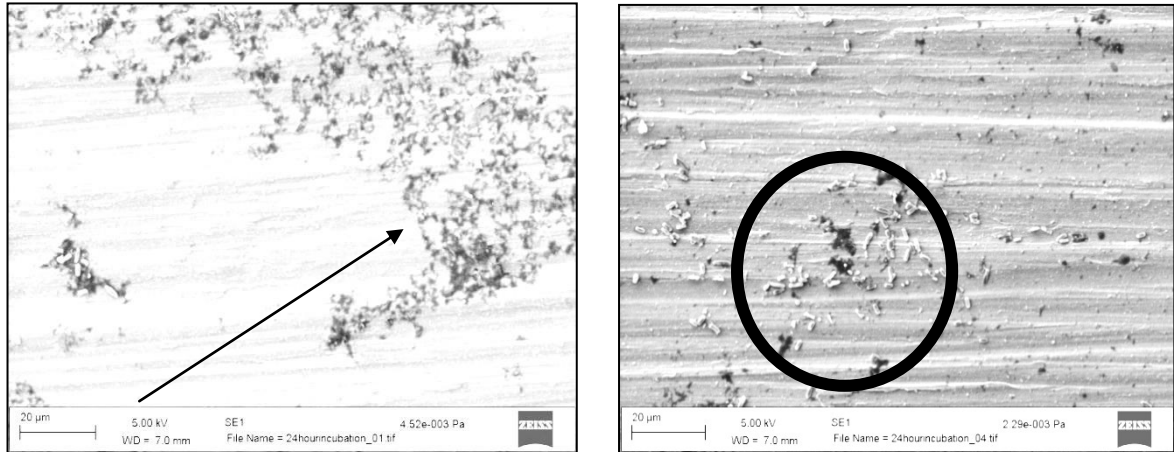
The CDC biofilm reactor was employed to grow biofilms of *S sanguinis* on the Grade IV

surface of the polished P4000 surface. It was found that after 24 hrs that bacterial cells of *S*

sanguinis had adhered to the control P220 polished surface as illustrated in figure 3.103a.

Figure 3.103b. Two SEM images illustrating *S sanguinis* bacterial growth on the surface of the P220 polished Grade IV surface after 48 hrs in the CDC biofilm reactor. The circle highlights the bacterial biofilm formed on the surface.
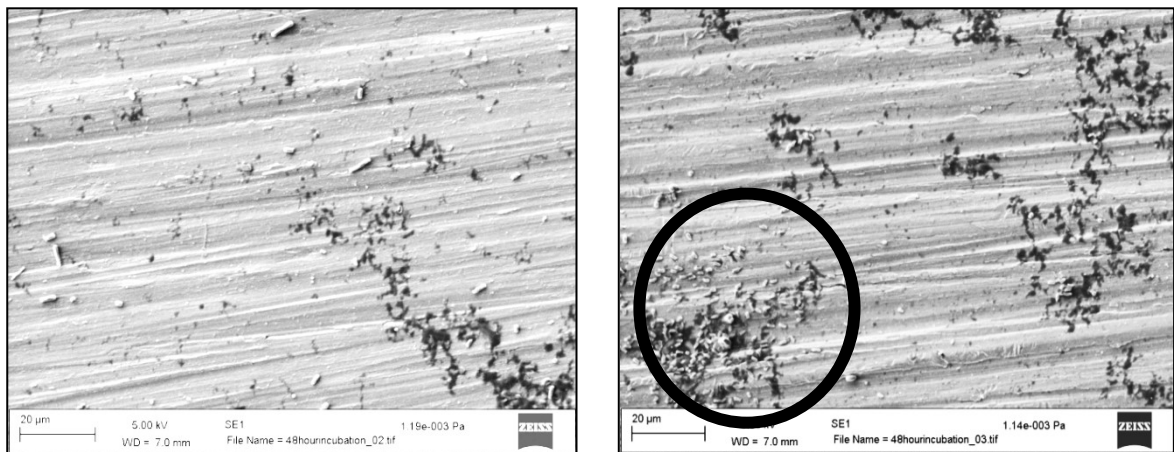
It was observed that after a further 24 hrs under continuous flow phase of the biofilm reactor that pockets of *S sanguinis* biofilms could be observed on the P220 Ti surface. The Ti surface was also found to have proteins and constituents of the tryptone soya broth adhered to the Ti surface.

Figure 3.103c. Two SEM images illustrating two SEM images captured of the *S sanguinis* bacterial growth on the surface of the P220 polished Grade IV surface after conditioning with artificial saliva for 18 hrs. The circle highlights the presence of a biofilm Ti surface.
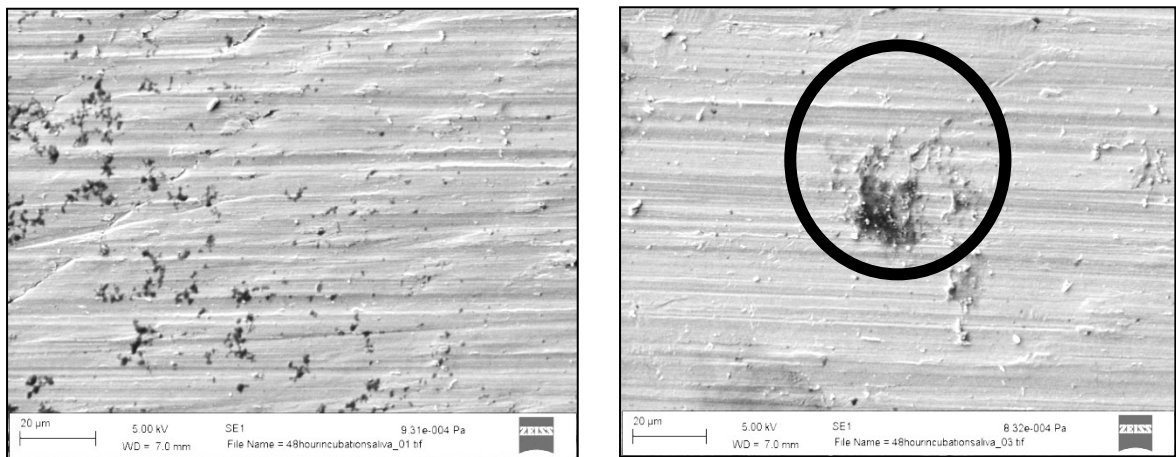
The Ti samples were incubated for a further 24 hrs with artificial saliva as a means of conditioning the surface with artificial saliva proteins and increasing the *S sanguinis* biofilm layer. An isolated *S sanguinis* biofilm can be observed in figure 3.103c.

Figure 3.103d. SEM images illustrates the adhesion of *S sanguinis* on the surface of a healing abutment, magnification x12 and x1300.
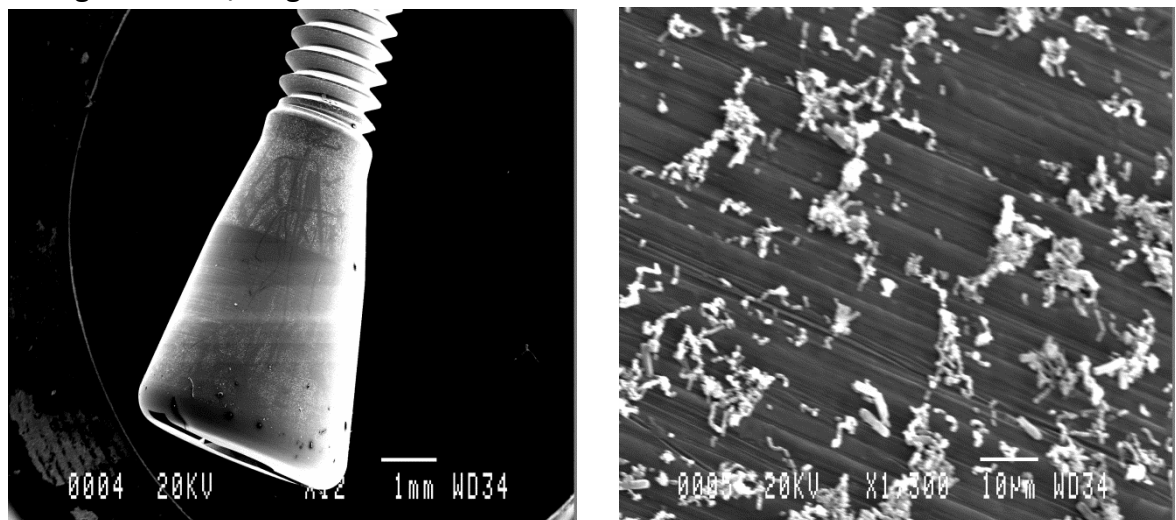
The images illustrate (figure 3.103 d) the *S sanguinis* bacterial cells adhered to the surface of the healing abutment and demonstrates a similar distribution pattern when grown in the CDC biofilm reactor (figures 3.103 a and b).

3.6.5 The effect of the IPA:EO formulation on biofilms formed on the Ti disc surface.

The effect of the IPA: EO biocide formulation was determined on *S sanguinis* biofilms grown on the P220, P1000 and P4000 surfaces. The IPA:EO formulation resulted in a significant decrease in the CFU/mL of *S sanguinis* grown on the P1000 and P4000 Grade IV Ti surface when compared to their controls ($p < 0.05$).

Figure 3.104. A histogram of mean CFU/mL before and following exposure for 2 mins to CHG mouth wash formulations containing 70 % IPA, 2 % EO, 2 % CHG, 1 % Tween on Grade IV CpTi P1000, P1000 and P4000 finish surfaces (mean ± SD, n=3, *=P < 0.05).
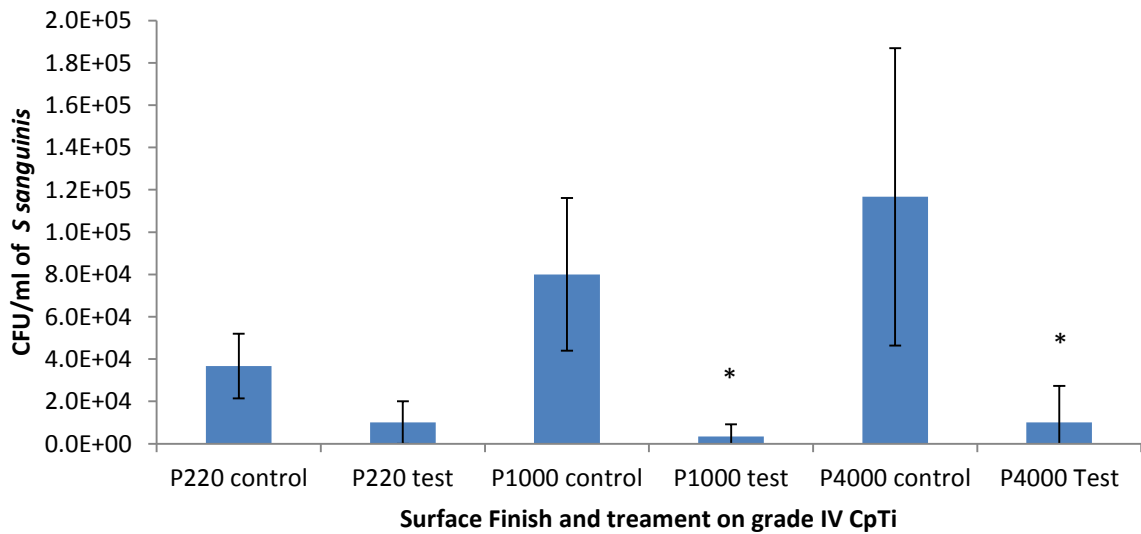
3.6.6 The effect of a reduced IPA content on the *S sanguinis* biofilm.

The concentration of IPA in the formulation was subsequently reduced to 35 % and 17.5 %.

Figure 3.105. Histogram illustrating the mean CFU after exposure for 2 mins to CHG mouth wash formulations containing 35% and 17.5 % IPA on P220 and P4000 finish surfaces prepared with SiC grit (Mean ± SD, n=3, *=P < 0.05). Control is distilled water.
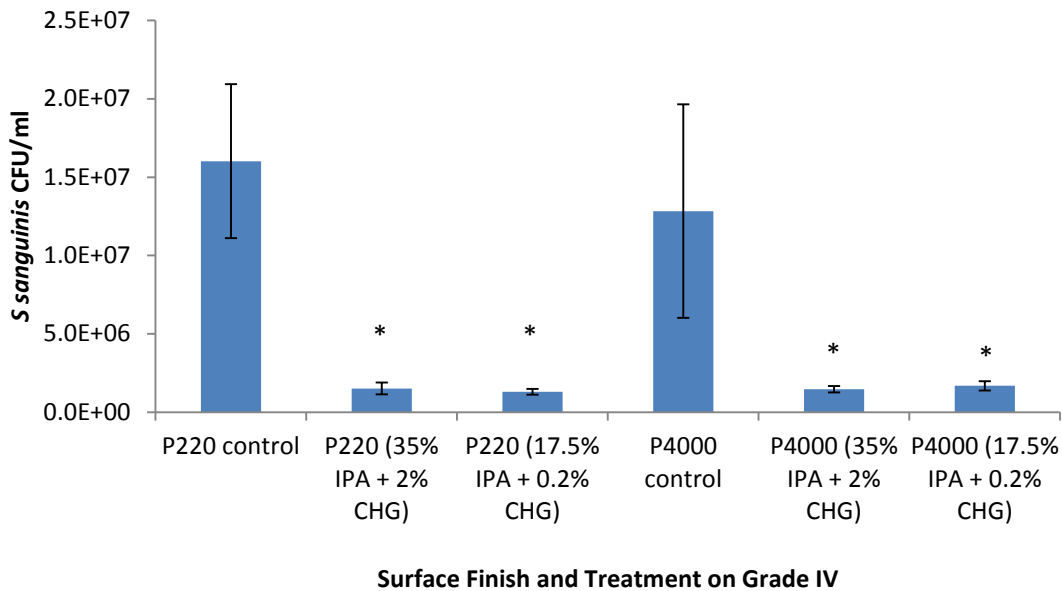
There was no significant difference in the mean CFU/mL on the P220 control and P4000 control surface (p= 0.3). Significant differences were observed in the mean CFU/mL between the P220 control formulation (distilled water) and the formulation consisting of 35% IPA and 17.5 % IPA (p=0.02). (figure 3.105).

To determine the effect of the formulation described by Hendry et al (2009) consisting of 70 % IPA, 2% EO, 2% CHG and 1 % Tween, tests on antimicrobial activity on *S sanguinis* biofilms formed on the prepared Grade IV P220, P1000 and P4000 Ti surfaces were conducted (figure 3.106). The data observed from this assay illustrated that the formulation was effective as an antimicrobial however; the formulation consisted of a very high IPA concentration. A high

IPA concentration could potentially be harmful to and therefore further studies were

conducted to identify whether it could be replaced.

3.6.7 The effect of replacing the IPA in the formulation to ethanol and a reduced ethanol concentration.

IPA was replaced with ethanol to make the formulation more clinically relevant. It was

observed that the CHG:EO formulation containing 10 and 20 % ethanol significantly reduced

the mean CFU/mL of *S sanguinis*.

Figure 3.106. A histogram illustrating the mean CFU/mL after the Grade IV P220 and P4000 finish surfaces with a *S sanguinis* biofilm were exposed for 2 mins to the control CHG and the novel antimicrobial formulations (Mean ± SD, n=3, *=P < 0.05).
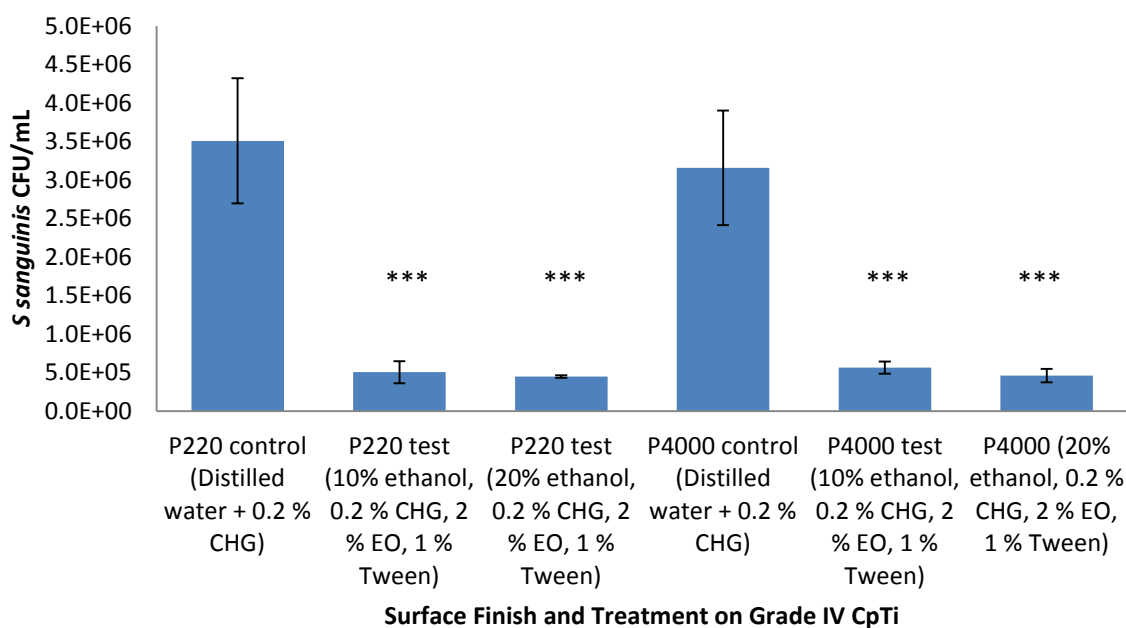
There was no significant difference in the mean CFU/mL on the P220 control and P4000

control surfaces (P= 0.3) (figure 3.107). Significant differences in mean CFU/mL were

observed between the P220 control surface and the formulations containing 10 and 20 %

ethanol (p=0.001). Significant differences were also observed in mean CFU/mL were

observed between the P4000 control surface and the formulations containing 10 and 20 % ethanol (p=0.001).

3.6.8 The effect of exposure time for the EO:CHG formulation on the *S sanguinis* biofilm.

It was confirmed that the CHG: EO formulation containing ethanol was effective on *S sanguinis* biofilms and few differences existed between the rough P220 surface and the smooth P4000 surface (figure 3.106) For further experiments the Grade IV P4000 prepared surface was employed only as the surface finish could be consistently manufactured (highlighted by Ra-measurements in figure 3.107). The effect of the CHG: EO formulation with and without EO was determined.

Figure 3.107. A histogram illustrating the mean Ra values of 5 x 5 mm regions on three of the P4000 polished CpTi Grade IV samples obtained with a non-contact profilometry demonstrating a highly consistent surface finish. No significant difference on the mean Ra was observed (p>0.05)
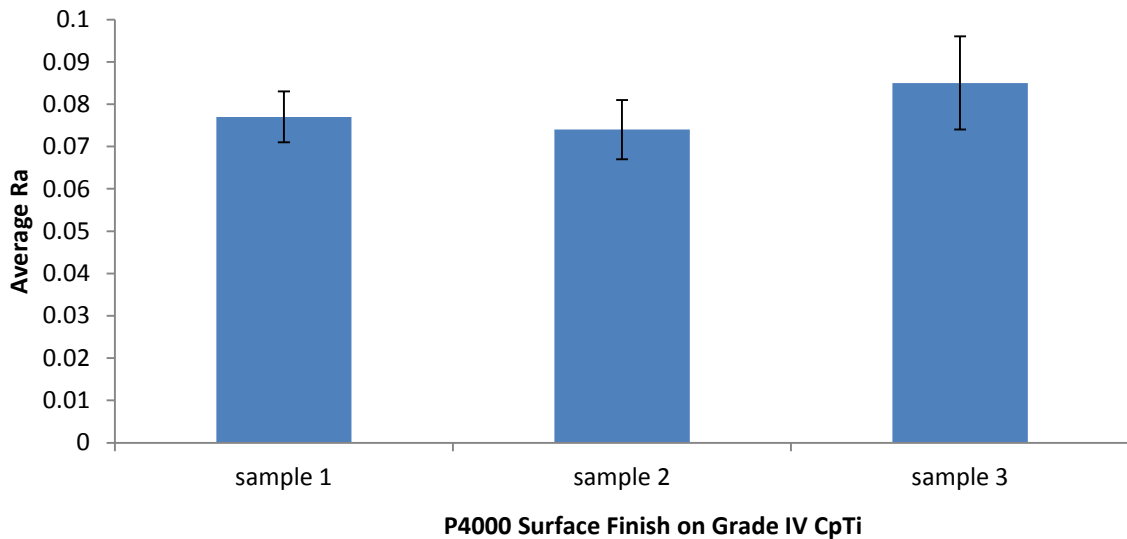
Figure 3.108. SEM image showing the presence of an early *S sanguinis* biofilm grown on the surface of a P4000 polished CpTi surface after incubation in a biofilm reactor for 48 hrs.
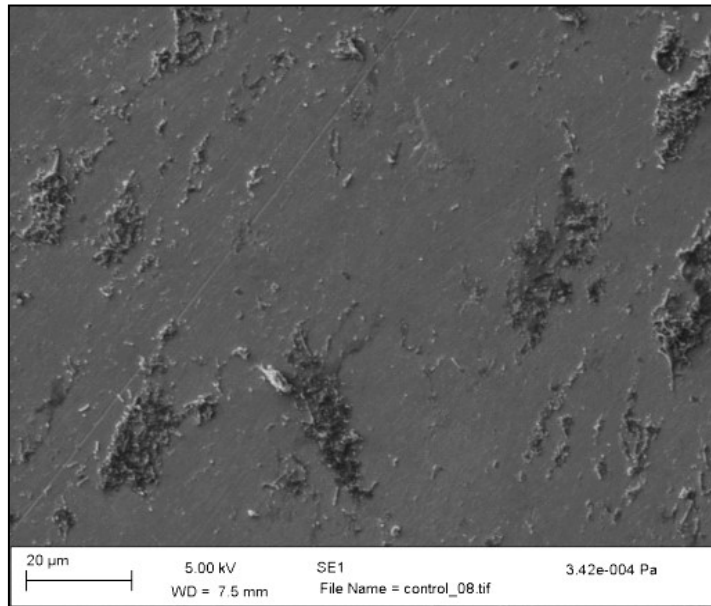
After 48 hrs there was formation of an early "patchy" biofilm that covers the surface of the P4000 surface. The *S sanguinis* bacteria appear as isolated clumps on the surface (figure 3.108).

Figure 3.109. SEM image illustrating the surface of the P4000 polished CpTi Grade IV after sonicating the *S sanguinis* biofilm for 10 mins and vortexing for 15 s demonstrating complete removal of the attached biofilm.
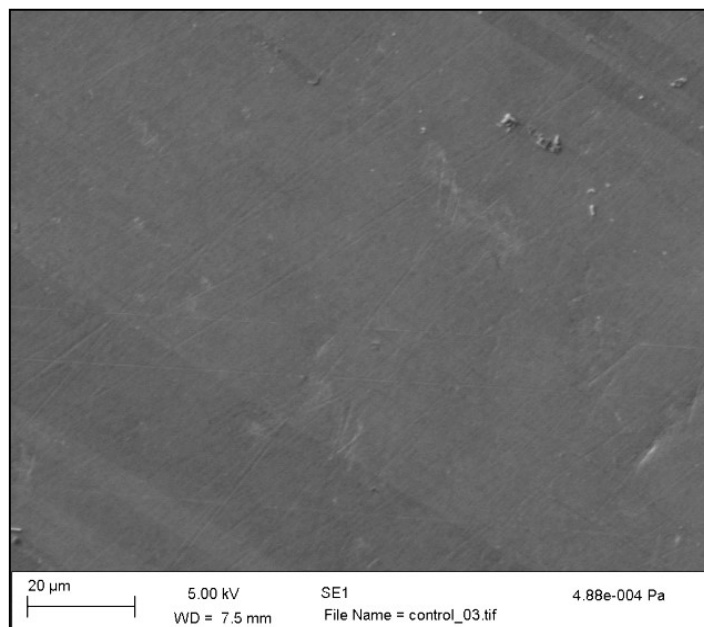
Figure 3.110. A histogram illustrating the mean CFU/mL on the Grade IV CpTi P4000 surface after a formed *S sanguinis* biofilm was exposed to the mouth wash formulations consisting with and without EO for 2, 15 and 30 mins (mean ± SD, n=3, *=P < 0.05).
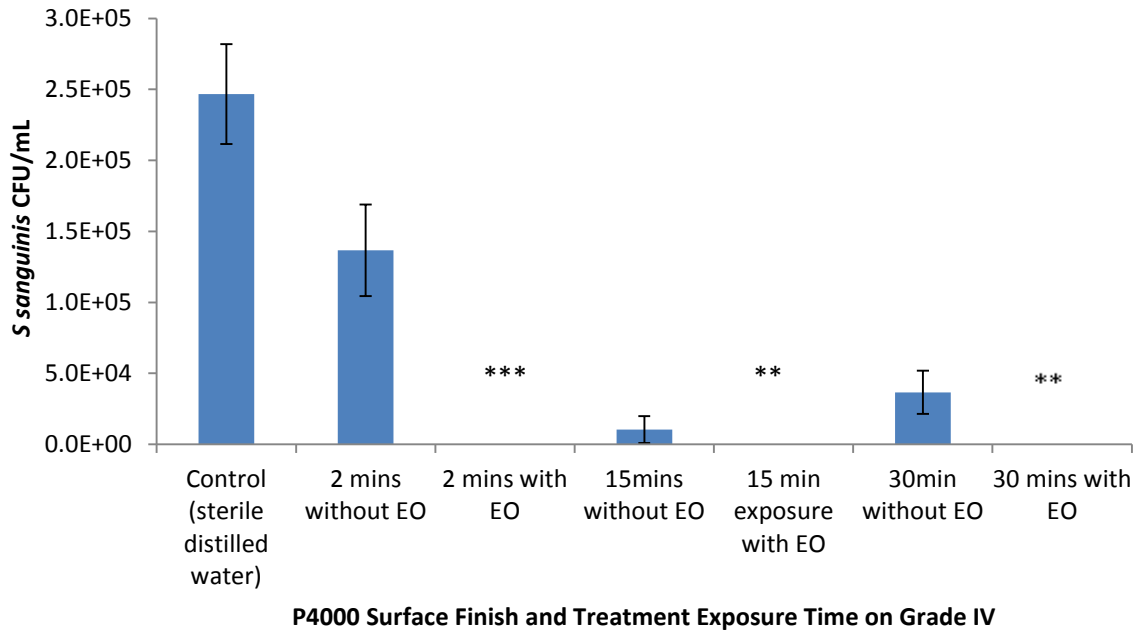
Significant differences were observed in the number of viable bacterial cells between the exposure with the formulation with EO and without EO for 2 (p=0.001), 15 (p=0.01) and 30 mins (p=0.01) (figure 3.110).

Figure 3.111. Histogram illustrating the RLU from the ATPase assay from the exposure of the mouth wash formulations consisting with and without EO for 2, 15 and 30 mins on Grade IV CpTi P4000 surface with a formed *S sanguinis* biofilm (mean ± SD, triplicate measurements n=3, *=P < 0.05).
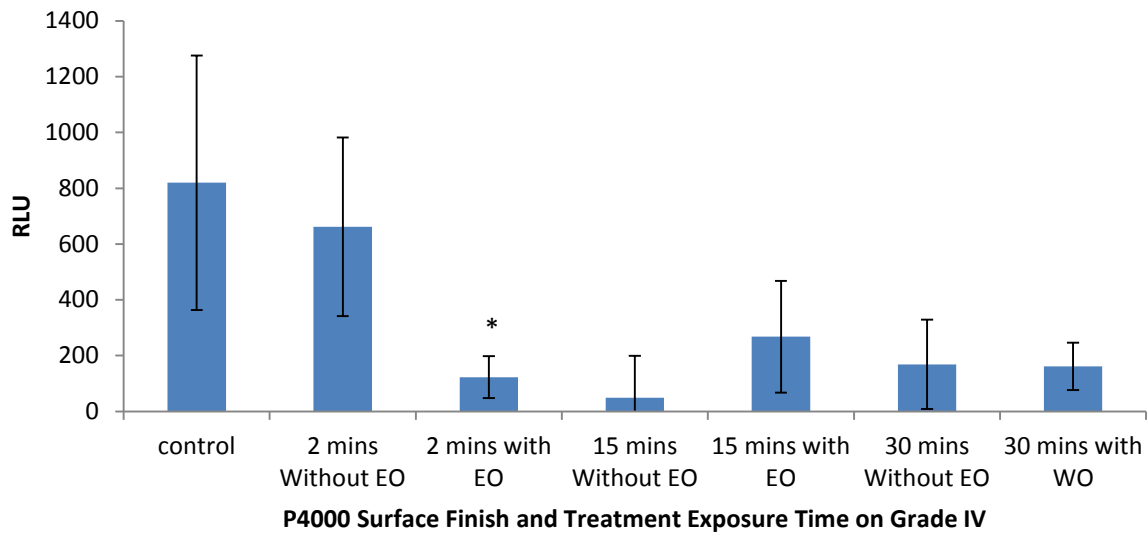
A significant reduction in the mean RLU was observed following a 2 min exposure with the formulation with EO (p=0.001). No significant difference was observed between the number of viable bacterial cells after the biofilm was exposed to the formulation that did and did not contain EO at 15 and 30 mins (p>0.05) figure 3.111.

3.6.9 The effect of exposure time for the CHG:EO formulation on the *S mutans* biofilm.

The effectiveness of the CHG:EO formulation on *S mutans* after 2, 15 and 30 mins without and without EO was studied. It was observed that significant reductions in mean CFU/mL occurred when compared to the matched controls (p <0.05). The ATPase assay also illustrated a trend in the reduction in the mean RLU derived from *S mutans* however no reductions were significant when compared to the matched controls (p<0.05) (figure 3.114).

Figure 3.112. A histogram illustrating the effect the CHG:EO mouth wash formulation on the mean CFU/mL of *S mutans* grown as a biofilm on Grade IV CpTi for 2, 15 and 30 mins (Mean ± SD, n=3, *=P < 0.05).
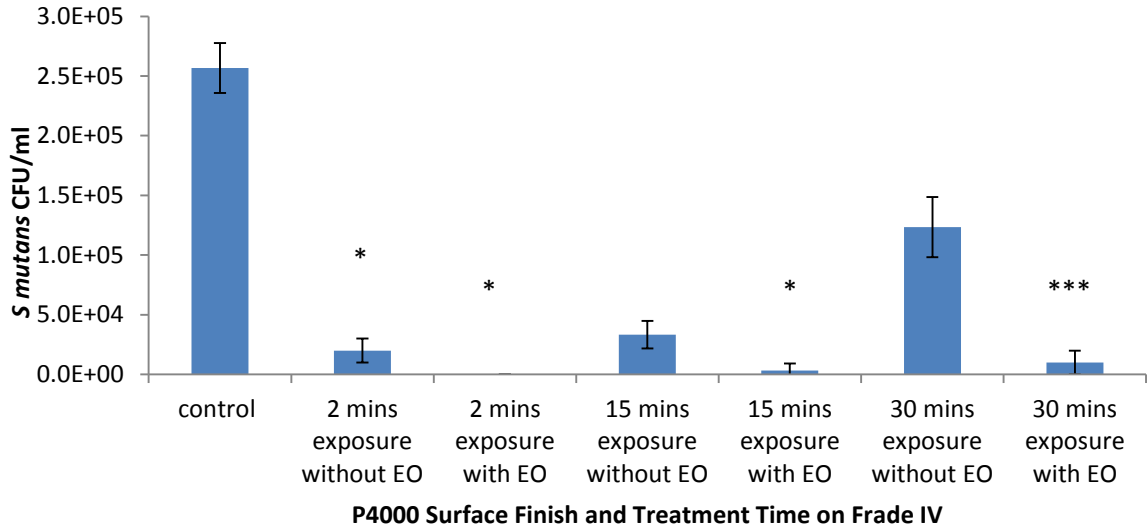
A significant reduction was observed between the bacterial count on the control surfaces following a 2 min exposure to the CHG:EO formulation (p <0.001). The inclusion of EO significantly reduced the mean CFU/mL at all time points (p<0.001) (figure 3.112).

Figure 3.113. A histogram illustrating the mean RLU (ATPase assay) from *S mutans* following growth of a biofilm on Grade IV CpTi P4000 surfaces that were subsequently non-exposed or exposed to the mouth wash formulations with and without EO for 2, 15 and 30 mins (Mean ± SD, triplicate measurements n=3, *=p < 0.05).
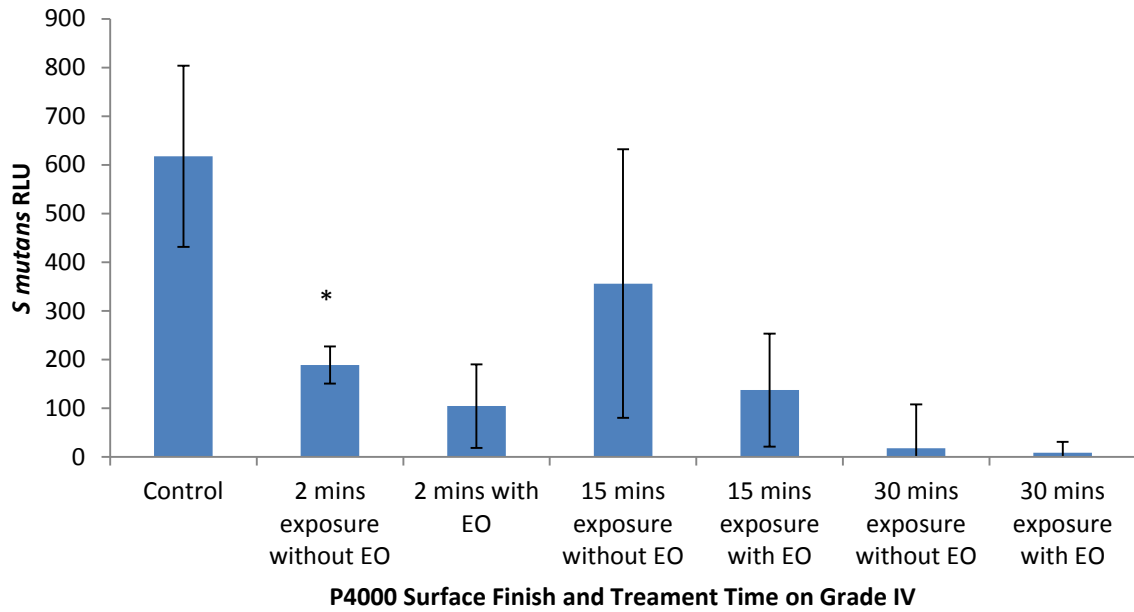
3.6.10 Effectiveness of the CHG:EO at reduced exposure times.

The exposure time was decreased to 30 s and the sample numbers were increased to 8 to determine the mouthwash formulation efficacy (figure 3.114). After 30 s exposure times, EO incorporation significantly reduced the mean CFU/mL.

Figure 3.114. A histogram demonstrating the effect of the control (distilled water), 30 s exposure without EO and 30 s exposure with EO on *S sanguinis* biofilms formed on the P4000 polished surface (mean ± SD, n=8, *=p<0.05).
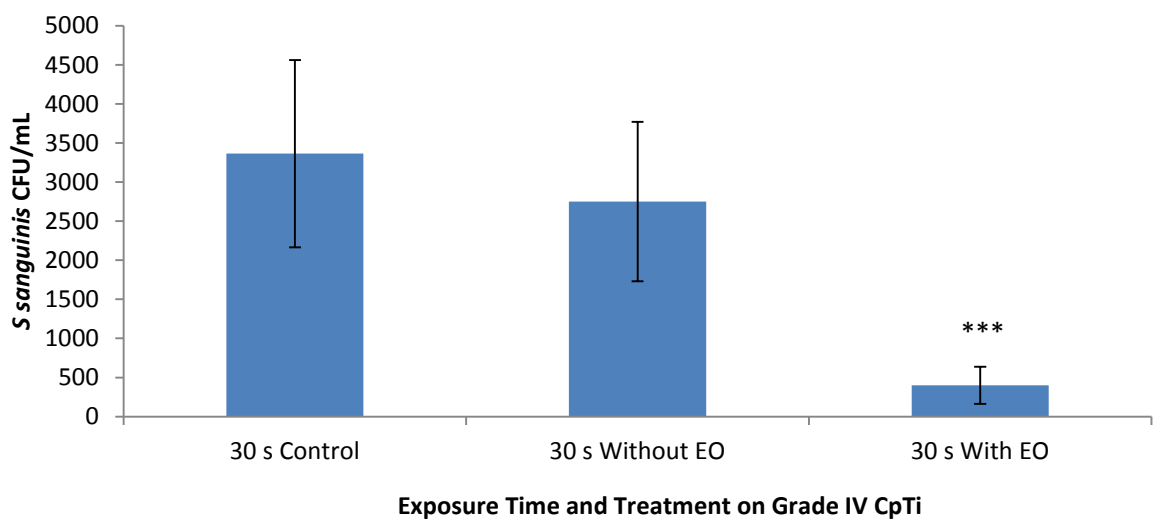
A significant difference of a 1 log reduction was observed in the mean CFU/mL of *S sanguinis* exposed to the EO formulation when compared with the control and non-EO mouthwash (p < 0.001).

Figure 3.115. A histogram demonstrating the mean RLU signal from the control (distilled water), 30 s exposure without EO and 30 s exposure with EO on *S sanguinis* biofilms formed on the surface of Grade IV titanium (mean ± SD, Triplicate repeats n=3, *=p<0.05).
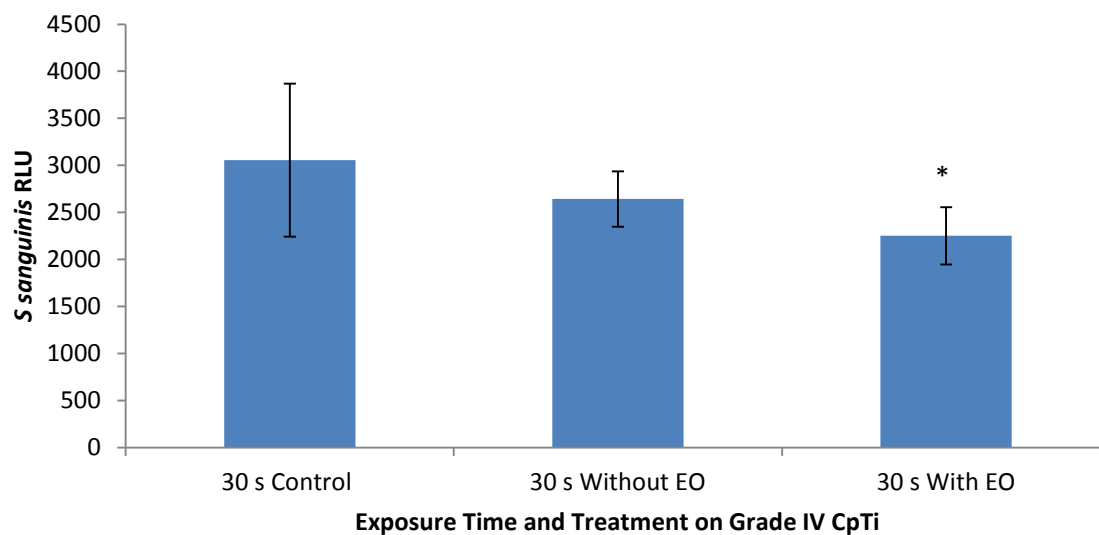
A significant reduction in the mean RLU from *S sanguinis* exposed to the control formulation and the EO mouth wash formulation was observed (p=0.03) although no significant differences were observed between the control the 30 s w/o EO exposures (p=0.06). (figure 3.115).

Figure 3.116. A histogram demonstrating the effect of the control (distilled water), 30 s exposure without EO and 30 s exposure with EO on *S mutans* biofilms formed on the P4000 polished surface (mean ± SD, n=8, *=p<0.05).
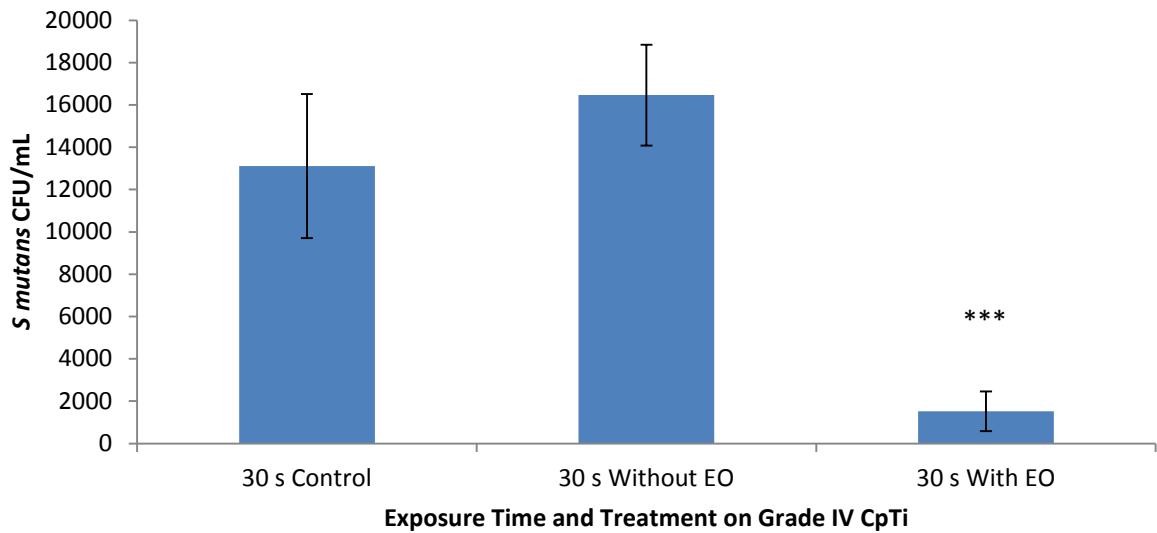
Exposure of *S mutans* biofilms to CHG in the presence of EO resulted in a significant decrease of 1 log reduction in mean CFU/mL after 30 s exposure (p<0.001). No significant difference was observed between the control (sterile distilled water and the 30 s w/o EO) (figure 3.116).

Figure 3.117. A histogram demonstrating the mean RLU signal from the control (distilled water), 30 s exposure without EO and 30 s exposure with EO on *S mutans* biofilms formed on the surface of Grade IV titanium (mean ± SD, Triplicate repeats n=3, *=p<0.05).
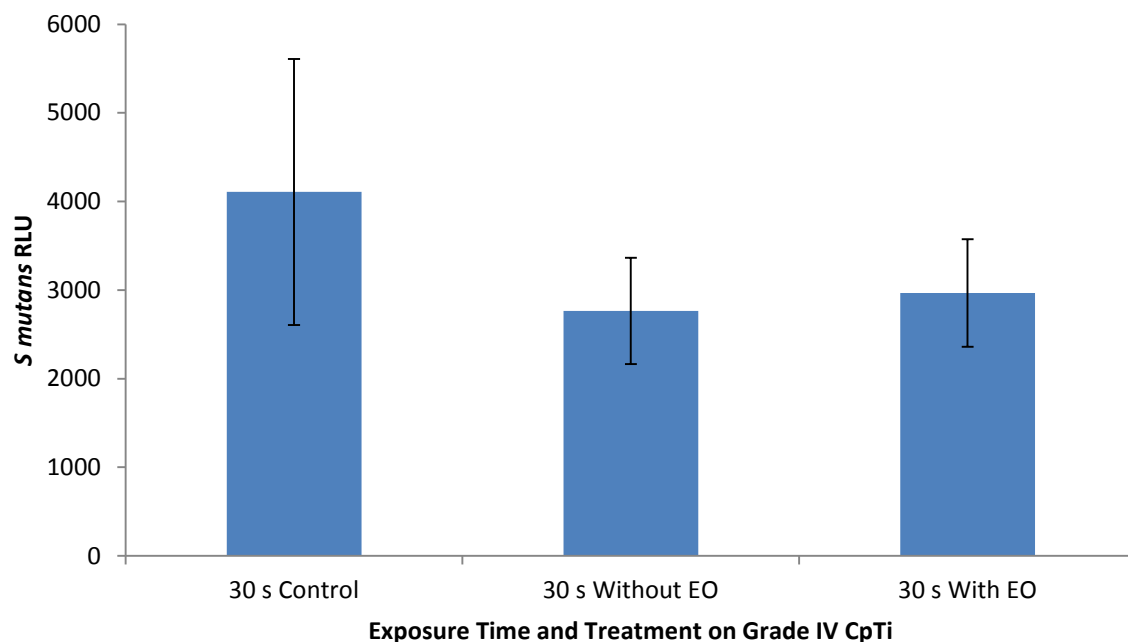
There was a significant decrease in the mean RLU between the *S sanguinis* exposed to the control formulation and both mouth-wash formulations however, no significant differences were observed between formulations with and without EO (p>0.05) (figure 3.117).

3.6.11 The effect of biofilm disruption and exposure of the CHG:EO formulation.

The *S sanguinis* and S *mutans* biofilms were disrupted and exposed with the CHG:EO

formulation to determine viability.

Figure 3.118. A histogram illustrating the effect of *S sanguinis* viability after scraping of the control, 30 seconds without EO and 30 seconds with EO on the surface of Grade IV Ti (mean ± SD, n=8, *=p<0.05).
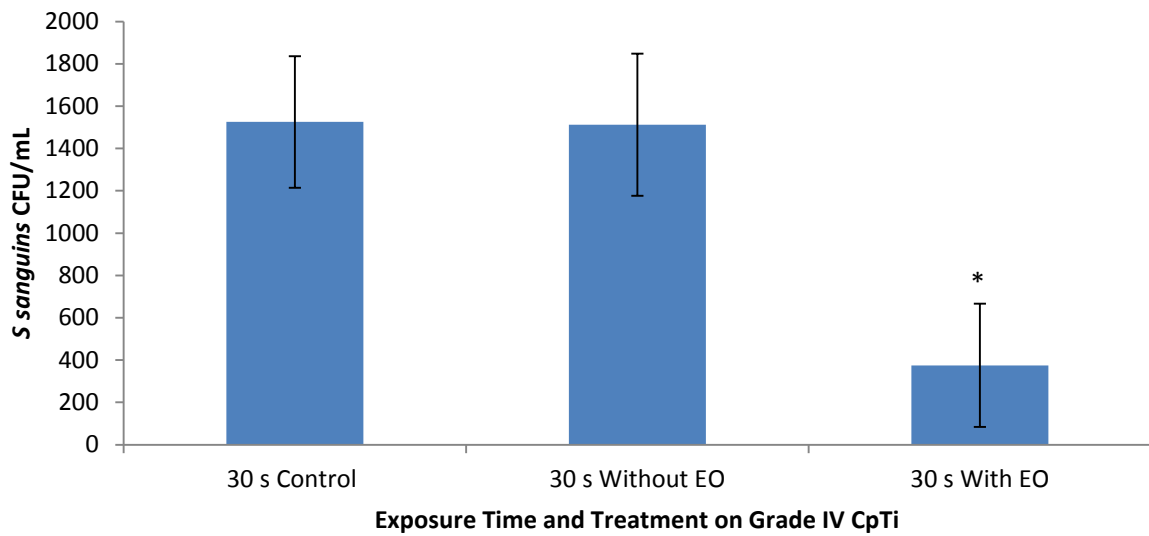
There is a significant difference of a 1 log reduction in the bacterial viability between the *S*

Sanguinis after scraping and exposing to the control formulation and the mouth wash

formulation (p<0.05). There is no significant difference observed between the control

exposure of sterile distilled water and 30 seconds with EO (p>0.05) (figure 3.118).

Figure 3.119. A histogram illustrating the *S sanguinis* viability after scraping of the control, 30 seconds without EO and 30 seconds with EO on the surface of Grade IV titanium. (mean ± SD, n=8, *=p<0.05).
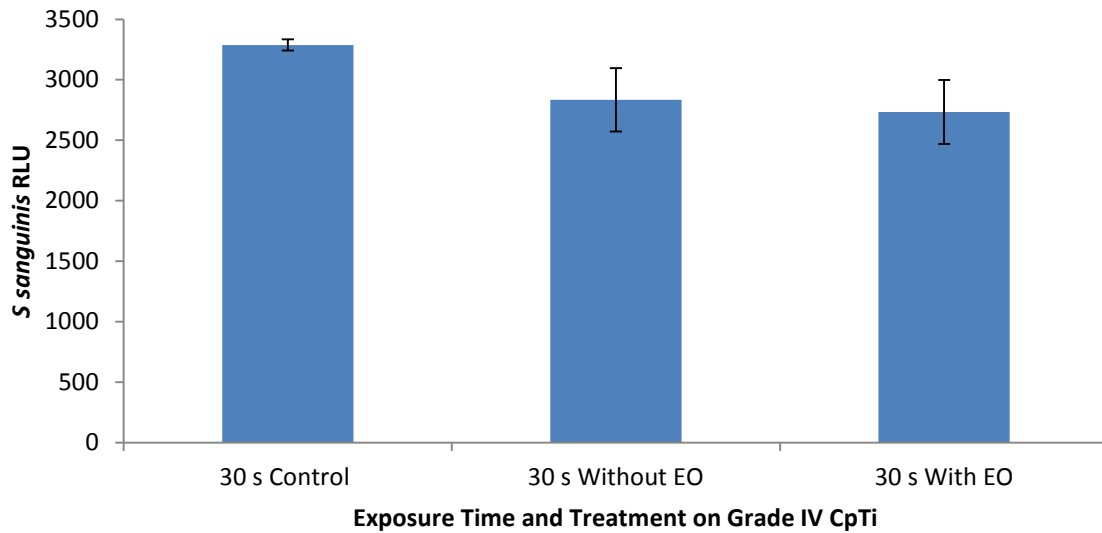
There were no significant differences in the RLU signal when the 300 sec Wo EO, 30 sec W

EO were compared to 30 sec control (p>0.05) (figure 3.119).

Figure 3.120. A histogram illustrating the effect of the control, 30 seconds without EO and 30 seconds with EO on the surface of Grade IV titanium (mean ± SD, n=8, *=p<0.05).
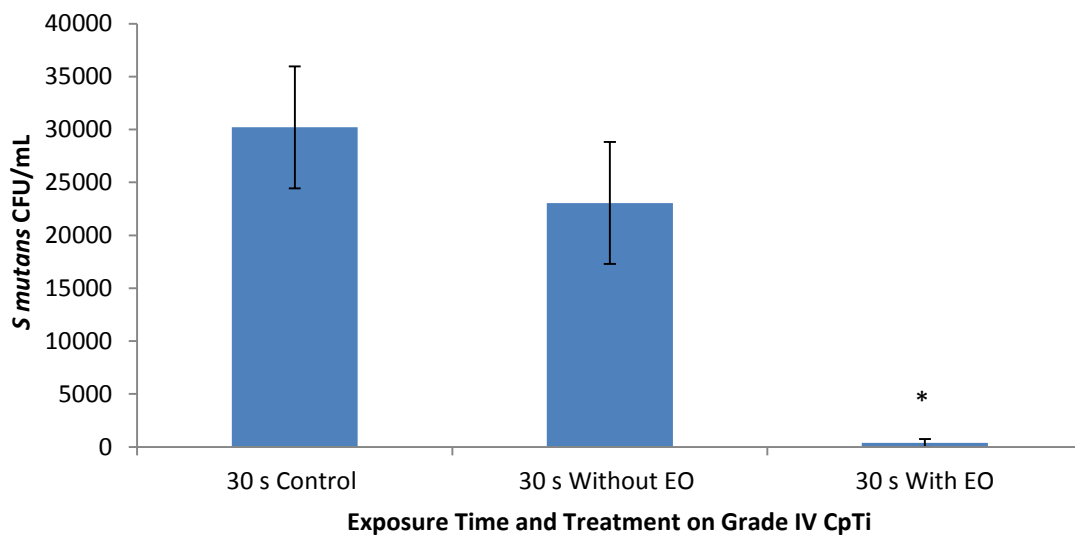
There is a significant difference in the bacterial viability between the *S mutans* after scraping and exposing to the control formulation and the mouth wash formulation (p<0.05), a log 2 reduction. There is no significant difference observed between the control exposure of sterile distilled water and 30 seconds with EO (p>0.05) (figure 3.120).

Figure 3.121. A Histogram illustrating the RLU signal from the control, 30 seconds without EO and 30 seconds with EO on the surface of Grade IV titanium. (mean ± SD, n=8, *=p<0.05).
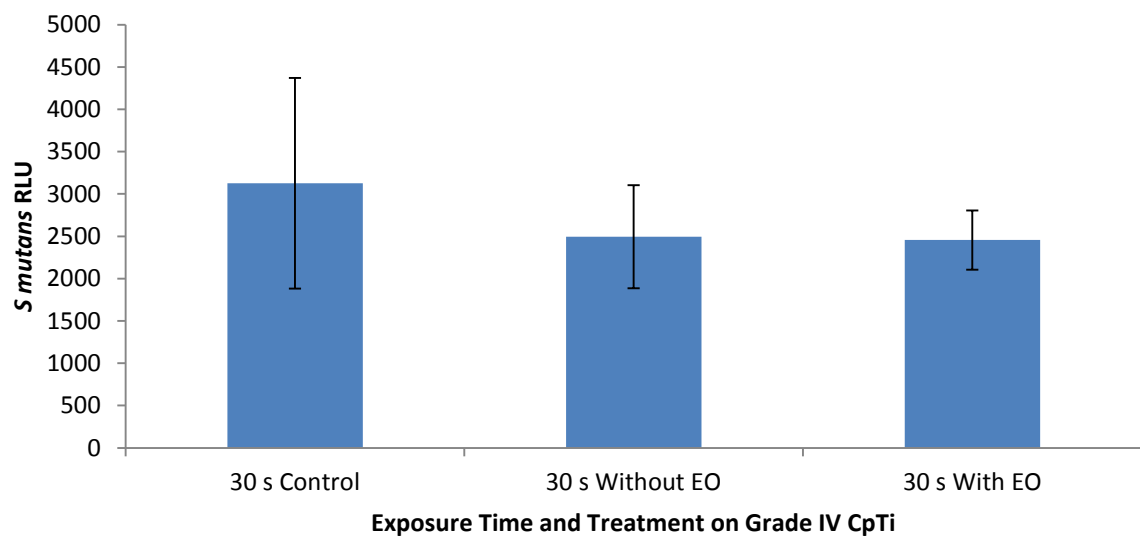
There was no significant differences observed in the bacterial viability between the *S mutans* exposed to the control formulation and the mouth wash formulations (P<0.05) (figure 3.121).

CHAPTER 4: DISCUSSION.

4.1 The effect of Ti dental implant surface topology on bacterial adhesion.

Ti dental implants have been developed to have discreet differences in their surface topology intended for specific biological purposes. The rough surface textures which are found on the majority of the dental implant fixture are designed to encourage the enhanced recruitment of osteoblasts and subsequently mediate osseointegration. Surface roughening process for Ti such as sandblasted, large-grit and acid-etched (SLA) treatments are commonly utilised by most dental implant manufacturers to prepare the surfaces of components which are to be embedded in bone. (Lee et al., 2013). It has been previously reported that SLA treated Ti surfaces (Hyeongil et al., 2008) have beneficial effects on the biocompatibility and the formation of bone around the dental implant surface mediated through promoting osteoblast differentiation and adhesion. SLA treatment of Ti dental surfaces results in a complete change in the surface topology from the 'as machined state' resulting in the formation of micro-pits and sharp peaks which mediate a specific cellular interaction including the promotion of differentiation of mesenchymal stem cells into osteoblasts (Olivares, 2011).

Other regions of the main dental implant fixture and frequently the trans- or supra-gingival dental implant components (e.g. healing abutments) are fabricated with polished or machined collars that are designed to reduce cellular interactions. The reduction in the colonisation of such surfaces with plaque forming bacteria is universally accepted as being important in reducing the propensity for peri-implant inflammation leading to crestal bone loss (Botos et al, 2011). The components with polished surfaces are however important in mediating favourable soft tissue outcomes, initially guiding the epithelial tissues into a form

that represents the tissue architecture observed around teeth. Over a period of 6-12 weeks following implant uncovery there is a formation of a mature peri-implant mucosa which is characterised by the presence of an epithelial cuff around the exposed implant components with some alignment of collagen fibres (Cristina et al., 2012). The formation of the peri-implant mucosa around the dental implant is itself important in creating a seal against potentially pathogenic bacteria in biofilms that are associated with peri-implant disease.

The polished surfaces on the Ti dental implant components are mostly achieved through mechanical processing however the final surface textures can vary considerably because of the different Ti substrates employed for the manufacture of dental implants. The common Ti substrates possess different surface harnesses (Grade V > IV > II) which will determine to some extent the resultant surface topology which can have an effect on bacterial adhesion.

The initial attachment of bacteria on Ti implant surfaces begins at sites where bacteria can be sheltered from shear forces generated during mastication and swallowing. It is at these sites where bacteria initially establish themselves through complex series of processes leading to irreversible attachment Gharechahi et al, (2012). The surface roughness is a major factor in determining the surface area available for bacteria to attach and specific components of topology such as peak to valley height can influence the degree of protection from displasive shear forces. It has been extensively demonstrated that rougher Ti surfaces lead to greater microbial plaque accumulation. Kawai et al., 2000 demonstrated a positive correlation between the surface roughness and increased plaque volume; and Einwag et al., 1990 reported that *S mutans* adhered to the rougher Ti dental implant surfaces more frequently when compared with smoother surfaces. Investigations by Ikeda et al., 2007 and Mei et al., 2011, reported a direct correlation between surface roughness

and bacterial adhesion. Park et al., 2012 added to the understanding of the correlation between surface roughness and bacterial adhesion by qualifying that it is not just the quantifiable surface roughness that influences the adhesion of bacteria but identifying that specific features of the surface topography that are more influential. The surface topography includes features related to the materials and its processing route such as the size and the depths and reproducibility of features that are present.

It is evident that surface roughness and implicitly the surface energy of dental implants can mediate the biological behaviour/interactions of eukaryotic and prokaryotic cells. Surface design is therefore of considerable interest to implant devices manufacturers and clinicians alike (Albrektsson & Wennerberg, 2004). The majority of the data reported in this field has failed to adequately describe the surface roughness and surface topography when investigating early bacterial adhesion and mature biofilm formation. The lack of characterisation makes it difficult to compare findings between studies. In this body of work it was essential to firstly systematically explore how quantifiable surface topology influenced surface energy and subsequent bacterial attachment. This understanding also enabled the identification of 'model' surfaces to be used in studies aimed at modifying or disrupting early bacterial attachment.

A range of surface textures were introduced into common biomedical Ti Grades (II, IV, V) using conventional grinding and polishing techniques with SiC abrasives. Scanning electron microscopy was first employed to visualise the created surfaces and the clear differences between Ti Grades and surface features was attributed to the hardness of the machined substrate (figures 3.1, 3.2 and 3.3). As the SiC abrasive grade increased (towards smaller abrasive particles) the surface 'waviness' which represents reproducible features introduced

by the machining tool (the abrasive grit) became less pronounced. Importantly such features are evident on the machined / polished surfaces of dental implant components which are not polished to the equivalent state of the mirror polish (P4000 SiC polished with colloidial silica) generated in this study. Whilst not homogeneously distributed across the surface 'waviness' features consisting as uniform peaks on troughs could provide a locus for the initial attachment of bacterial cells providing shelter from shear forces (Gharechahi, et al., 2012).

To enable comparison with other studies and also to determine whether any specific features of surface topology could be used as a predictive measure for determining initial bacterial attachment, surface metrology was performed. Surface modification through SiC abrasive polishing was demonstrated to visibly modify the surface features however a large range of metrological parameters were likely to have been affected including the mean surface roughness (Ra), the mean of maximum peak height (Rp), the maximum valley depth (Rv), the mean of the maximum roughness height (Rz), the mean height of the roughness profile elements (Rc), the mean height of the surface profile (Rt), the mean of the root mean squares (Rq), the mean skewness (Rsk) and the mean kurtosis (Rku) of the prepared Ti surface. Exploration of these parameters was important because specific surface features such as the presence of protected niches for early bacterial attachment are often not discriminated when only the mean surface roughness (Ra) is reported (Gadelmawla et al., 2002). Contact angle measurements were undertaken to provide information on surface wettability and indirectly measure surface energy with a view to identifying any correlations with early bacterial attachment. The contact angles were determined with two media distilled water, artificial saliva at both room temperature and body temperatures. There

were no significant differences detected between the Ti substrates with the different surface polishing treatments for Grades II, IV and V at both room and body temperatures. A significant reduction in the contact angles were detected with artificial saliva compared with distilled water which was attributed to the proteinaceous composition of the artificial saliva. The lack of correlation between contact angle and surface metrology parameters suggests that at the scale of the introduced topographies, surface features had little effect on wettability with relevant media. Reduction in the feature size to the nano-scale as demonstrated later with the nano-tubule engineered surfaces can however introduced significant modification to the surface wettability which was not introduced through surface polishing and grinding.

The effect of initial bacterial adhesion and attachment was determined on Grade II, IV and V prepared Ti surfaces to determine whether roughness parameters can influence the predictability of bacterial attachment. A review by Gharechahi et al (2012) described that a rougher surface influences increased bacterial attachment therefore the hypothesis tested was that would be an obvious trend between bacterial attachment and specific surface roughness parameters. Importantly in Gharechahi et al., (2012) did not discriminate the specific metrological features of the surface topology as was reported in this study. The bacterial adhesion assays performed in this study with the monocultures of *S sanguinis, S mutans, F nucleatum* and the polycultures of *S sanguinis, F nucleatum* on Grade II, IV and V prepared Ti surfaces were a limited early adhesion model representative of the first hours of bacterial attachment and surface proliferation only.

The current study failed to identify any strong correlations between specific metrological parameters and mean CFU/mL. Some general trends were however observed which suggest differences between the microbial species that were studied. The adhesion of *E coli* to commercially pure Ti surfaces (principle alloys in dentistry) reduced significantly as the surface finish was increased to its most polished state but this expected finding was not observed with *S sanguinis, S mutans* or *F nucleatum*. An important consideration is what surface the bacterial actually interact with. This study demonstrated that the surface energy is minimally affected by surface finish/ surface roughness. Bacteria were cultured in artificial saliva – a protein rich media which will adsorb to the prepared Ti surfaces. As the contact angles were largely consistent for all Ti Grades and surface finishes it would be expected that the surface adsorption would also be similar. Coating of the entire surface with artificial saliva may to some extent negate subtle effects that the surface topology plays on bacterial adhesion. Given the lack of obvious correlations between surface metrology parameters and microbial adhesion to prepared Grade II, IV and V Ti surfaces, the adhesion of *S sanguinis, F nucleatum, E coli* and *S mutans* was further investigated with increased sample numbers on the roughest P220, smoothest P4000 and the P1200 prepared surface (determined by mean Ra).

On the Grade II surface more obvious trends were observed with significant reductions in the mean CFU/mL of *S sanguinis, E coli, S mutans* on the P1200 and P4000 prepared surfaces compared with the P220 prepared surface, however there were no significant differences observed with the mean CFU/mL with *F nucleatum*. On the Grade IV Ti surface there was a significant increase in the mean CFU/mL of *S sanguinis, E coli* and *S mutans* on the P1200 surface compared with the P220 prepared surface but again there were no

significant differences observed with *F nucleatum* bacteria. On the Grade V Ti surface a more obvious trend was observed with significant reductions in the mean CFU/mL of *E coli, S mutans* and *F nucleatum* on P1200 and P4000 prepared surfaces compared with P220. *S sanguinis* demonstrated a significant increase in mean CFU/mL on P1200 and P4000 surface compared with P220. The correlation between the mean CFU/mL and surface metrology parameters were unsurprisingly stronger when a higher statistical Power was employed however importantly the correlations were still not conclusive. This suggests that the metrological parameters fail to adequately describe the relationship between bacterial adhesion and the Ti surfaces topology and reflects the complexity of early bacterial surface adhesion. The findings are important from a clinical significance perspective as there is huge interest in implant surface decontamination and clinicians are traditionally very careful to avoid introduction of new surface textures to the polished components of the implant. The current study suggests that there is considerably more complexity in the relationship between implant surface colonisation and surface finish however future studies are required to validate these findings with more complex and mature biofilms.

4.2 Bacterial adhesion to engineered Ti surfaces.

As processing and manufacturing technology develops, it is likely that additive layer manufacture of dental implants and the introduction of designed surface topologies will become commercially feasible. It is important to note that the effect of surface roughness and surface topology decreases when the bacterial biofilm matures therefore the studies undertaken were designed to determine the effect of initial bacterial adhesion to the created Ti surfaces. Selective laser melting is a rapid additive manufacturing process that is able to produce complex 3-D structures through computer-aided design minimising the

delay between the design and manufacturing stages (Vandenbroucke et al, 2007 and Qui et al, 2013). The SLM additive process builds samples layer by layer from Ti-6Al-4V powders. The SLM manufacturing process therefore has interests in the field of dentistry for the creation of unique dental implants. The aim of this study was to determine the adhesion of oral bacterial on SLM manufactured surfaces. SLM samples (manufactured from Grade V Ti alloy) designed specifically for this study included a flat SLM sample and "chessboard" morphology on the surface created by altering the direction of scanned spacing on the islands (figure 3.41). The created samples were similar to the samples created by Qui et al., (2013). The surfaces of the SLM prepared surfaces were initially characterised with SEM and compared control samples ground to a rough P220 surface or polished to a smooth P4000 finish. It was observed that the SLM process formed pores and spherical topological features on the Ti surface which is thought to be caused by the incomplete re-melting of some localised surface areas of the previous layer (Qui, et al, 2013). The formation of the pores has implications for initial bacterial colonisation as they could potentially adhere to the pores and be shielded from the shear forces. (figure 3.42, 3.43, 3.44 and 3.45).

Despite these specific surface topologies the contact angles on the SLM flat sample surface and the SLM patterned surfaces were similar to those obtained on the SiC ground Ti surfaces (figure 3.46). The data demonstrated that the Ti samples were highly wettable which would promote protein adsorption such as the constituents of artificial saliva in a conformation that exposes adhesion motifs enhancing bacterial cell adhesion (Gittens et al., 2014). Subsequently the adhesion *S sanguinis, E coli, S mutans* and *F nucleatum* was determined on the SLM flat and the SLM "5 x 5 mm" checker board patterned surface alongside the P200 and P4000 Grade II prepared surfaces (figure 3.47, 3.48, 3.49 and 3.50).

It was found that there was a general pattern in which there was a significant reduction in bacterial adhesion between the P220 rough surface and the SLM patterned and the SLM flat surfaces. The exception to this pattern was observed with the *E coli* bacteria (figure 3.48) where no significant reduction was observed. The data obtained implies that the SLM patterned surface possess a topology to which bacteria are not able to adhere as easily. It was also found that the adhesion of the bacteria on the SLM flat surface was not significantly different compared to the smooth P4000 Ti surface except in the case of *F nucleantum*. The *F nucleatum* is a larger bacterial cell (Kolanbrander et al., 2010) and as a result is able to adhere to smooth surfaces more effectively. Due to the heterogeneity of the SLM samples specific surface roughness measurements were not performed.

To determine the formation of a mature *S sanguinis* biofilm on the SLM "5 x 5 mm" checkerboard patterned and the SLM flat surface. The samples were incubated in the CDC bioreactor to determine bacterial colonisation and bacterial distribution on the SLM surface. It was observed that although some bacteria were able to successfully colonise around voids and raised structures present on the prepared surface the majority of the surfaces were free of bacteria (figure 3.54). The data although at very early stages implies SLM can create surfaces that are not ideal for early bacterial colonisation. Interestingly there was considerable variability in the findings with one SLM flat surface demonstrating extensive biofilm formation. This finding may be related to the maturity of the biofilm which limits the extrapolation of these findings.

Typically it is understood that by reducing the surface roughness of a biomaterial, initial bacterial adhesion is also reduced, however there is now evidence that the introduction of specific topologies on the micron- and nano-scale increases surface roughness and may

affect cellular attachment to "traffic" cells or to confine the ease of proliferation across the surface.

Previous reports have shown that titanium nanostructured with specific topographies can promote the adhesion and differentiation of osteoblasts and other types of eukaryotic cells whilst suppressing or promoting the adhesion of bacteria (Ercan et al., 2012). Experiments with anodised samples with 15 and 100nm diameter nanotubular surfaces, prepared in the same way as in this study showed that more osteoblasts adhered to 15nm diameter nanotubes than 100nm ones (Park et al., 2009, Bauer et al., 2011b, Park et al., 2012, Gongadze et al., 2013). A nanotubule diameter of 15-30nm seems to favour adhesion of mammalian cells of several different kinds including mesenchymal stem cells, osteoblasts and osteoclasts and may reflect optimal 10nm clustering of integrins on a surface with this spacing (Park et al., 2009). Here we have shown that for the oral bacteria tested in this study the opposite is true: there was more bacterial adherence to the 100nm diameter nanotubes than 15nm nanotubes and nanopores. This suggests than the latter could be less vulnerable to infection where there is competition between mammalian cells and bacterial cells in "the race for the surface" (Gristina, 1987). Pucket et al., (2010) similarly showed that certain Ti surfaces with nanometer sized features could promote osteoblast adhesion whilst reducing attachment of *Staphylococcal* and *Pseudomonas* bacteria in comparison with conventional and nanorough Ti over a similar 1 hr attachment period. Peng et al., (2013) showed that *Staphylococcus epidermidis* adhesion was reduced and osteoblast-like cell adhesion enhanced on 80nm nanotubular compared with 30nm arrays. Bacterial adherence appears to be correlated with increased fluorine content of the surface in the case of both Gram negative and Gram positive bacteria (Katsikogianni et al., 2006, Puckett et al., 2010). This is

consistent with the XPS analysis of our surfaces which indicated that the fluoride content increased in the order NT15< NT50<NT100, according to the progressively longer exposure to HF during the anodisation process. However, the larger diameter tube size and higher fluoride content was not correlated with a higher surface activity/hydrophilicity as shown by previous workers: the nanoporous surface with no F was the most hydrophobic, followed by NT15>NT50>NT100. At present the reason for this is unknown and requires further investigation. Surface activity and hydrophobicity are affected by ionic and non-ionic factors including surface roughness (Machado et al., 2012) and in the case of nanotubular surfaces by the presence of air in the tubules and their height (Quere, 2002) and by annealing temperature and ageing (Hamlekhan A et al., 2014).

XPS analysis indicated the presence of small amounts of carbon from the air or electrolytes and trace amounts of silicon (contaminant) on some samples. The percentages of carbon are similar to those reported by Zhu et al., (2004) and Regonini et al., (2010): carbon decreased in the order above but C-O and O=C-O increased NT15 → NT50 → NT100. In our case the contact angle for compact oxide (CO) is around 60 degrees and for 100 nm nanotubes around 70 degrees whilst the difference between these two surfaces in adhesion of bacteria is much larger. It is clear that hydrophobicity/hydrophilicity is not the only factor which determines the adhesion of bacteria. In the case of the nanotubular surfaces, fluoride could be a key factor and exert an effect via protein adsorption; in this case mucin, the protein present in artificial saliva, and this should be tested in a future study. It may be possible to reduce the fluoride content by annealing at 400 °C (Regonini et al., 2010), although its presence may be beneficial to limit biofilm formation. In previous work (Peng et al., 2013) image analysis was used to estimate numbers of attached bacteria and

subsequent live/dead staining suggested that many of the bacteria were dead, even though more may have initially adhered, possibly due to the toxic effect of the fluoride which increases membrane permeability and inhibits glycolysis (Marquis, 1995). In this study bacterial attachment was estimated by counting colony forming units originating from live bacteria recovered from the surfaces but it is now necessary to investigate how long streptococci and other bacteria can survive and whether they are able to divide and form a biofilm on the nanotubular surfaces.

4.3 UV photocatalytic effects on oral biofilms.

The Ti oxide layer found on implant surfaces is a naturally occurring oxide of Ti that exhibits important photocatalytic properties. This study aimed to investigate UV photocatalysis with naturally formed and artificially thickened surface oxide layers. Subsequently the study aimed to investigate the photocatalytic properties on the viability of the oral bacteria of *S sanguinis.*

Previous work by Kwon et al., (2004) investigating the effect of photocatalytic properties on TiO_2 failed to thoroughly characterised the UV light source which makes the reproducibility of experiments difficult and subsequently comparison of findings impossible. In this study, the Omnicure® series 1000 UV light engine was characterised to determine the absolute irradiance spectra. The spectral output found to have an absolute irradiance of 91 mW/cm^2 at 1 % power which was made of five peaks at 313, 335, 365, 407 and 440 nm with the highest peak being observed at 365nm (figure 3.60). The data was in agreement with the information provided by the manufacturer and illustrates the broad spectrum of activity from UVA (320 nm-400 nm), UVB (290 mm-320nm) and the visible light spectrum (380 nm-780 nm). The correlation between the spectral output and the increasing intensity from 1 %

to 25 % was found to have a linear relationship with an R^2 of 0.79. It was found that the absolute irradiance values at 25 % were 923 mW/cm^2.

The photocatalytic activity of UV irradiated TiO_2 was determined through the degradation of methylene blue dye. The photocatalytic assay was developed by initially determining adsorption spectra of methylene blue (figure 3.62) where an adsorption peak of 665 nm was observed with various dye concentrations ranging from 1 ppm to 500 ppm. The absorption peak was in agreement with the study carried out by Balachandran et al., (2013). A concentration of 3.12 µL (5 ppm) of the methylene blue dye was utilised in this study. The lower concentration of methylene blue fits with Beer Lambert law which states that light transmittance is dependent on the concentration of molecules found in a solution at a given light path. In this study the distance between the light source and curvettes containing methylene blue dye were kept constant, to keep the light path constant. At the lower concentrations of methylene blue dye there was a linear relationship with adsorption (figure 3.4) however as the concentration increases above 10 ppm there is a plateau and therefore the Beer Lambert law cannot be applied. It was found during the development of the assay that methylene blue dye degradation was most efficient at the lower concentration of pH of 3, this is in agreement with a study carried out Mohabansi et al., (2011) where a pH of 2 was found increase the efficiency of the photocatalytic assay.

UV photocatalysis of TiO_2 is sensitive to the thickness of the oxide film. In this study the TiO_2 was grown either through anodic or thermal oxidation. SEM imaging identified that the morphology of the CpTi Grade II, IV and the Grade V alloy became rougher after thermal oxidation treatment at 50, 100 and 150 hrs. It would have been valuable to undertake XRD to determine the crystalline form of the TiO_2 present on the surface however previous

literature has stated that the thermal treatment results in the formation of a thick crystalline rutile TiO_2 layer (Kumar et al., 2010). The increased surface roughness observed with the temperatures of 50, 100 and 150 hrs on the Grade II, IV and V Ti surfaces was also in agreement with Kumar et al., (2010) where thermal oxidation at the temperatures of 500, 650 and 800 °C increased the surface roughness as thermal oxidation temperatures increased. The data implies that there is a correlation with increased temperatures at which the Ti surfaces are oxidised results in increased TiO_2 layers allowing the operator to optimise the growth of the oxide layer on Ti surfaces.

Methylene blue degradation assays were developed to determine the photocatalytic activity of the Grade II, Grade IV and Grade V oxidised Ti with the well characterised UV light source. The general trend that was observed with the assays illustrated that control polished Ti surfaces of the Grade II, IV and V demonstrated photocatalytic activity with 923 mW/cm^2 for 120 mins compared to the methylene blue control. The photocatalytic activity was enhanced with the thermal oxidised samples on all the Grades of Ti that were investigated with the 100 hr and 150 hr thermal treated samples displaying the largest photocatalytic activity (figures 3.68, 3.69 and 3.70). The data illustrated as expected that photocatalytic activity increased with the increased TiO_2 layer there is enhanced photocatalytic activity. The enhanced surface roughness also increases the surface area to which the UV light source has an effect on and implies thermal oxidation at higher temperatures will result in further increases of the photocatalytic activity. This is in agreement with previous work by Kwon et al., 2004 who investigated the degradation of methylene blue with thermally oxidised surfaces and found that the maximum photocatalytic decomposition of the methylene blue solution was achieved at 400 °C. For clinical benefit it is important to

understand whether photocatalytic activity is maintained following surface contamination. In Figure 3.72 the results of methylene blue degradation studies on a Grade IV Ti surface contaminated with artificial saliva and TSB are reported. It was found that the contaminated surface did not affect the photocatalytic activity and suggests that this phenomenon could be potentially exploited in the oral cavity of the patient after placement of the implant. However further work would need to be undertaken to determine whether more complex contaminants of the oral cavity would play a part in the decreased photocatalytic activity.

The effect of the photocatalysis of Ti oxide surfaces on bacterial viability was later assessed by studying *S sanguinis* bacteria on Grade IV and Grade V Ti surfaces. It was determined that there was a significant reduction in adhesion to the 50 hr thermally treated surface when compared with the control. However there was no significant reduction in bacterial numbers on a 100 hr and 150 hr thermal treated sample after 60 s of UV irradiation (figure 3.72 and 3.73). It was identified that the time of UV irradiation on the thermal treated samples plays a major role in the biological effects of photocatalysis. This was in agreement with previous work by Kwon et al., (2004) and Gopal et al., (2012) who noted in their studies that the effect only became potent after 5 and 10 mins, respectively.

The effect of UV irradiance on photocatalysis was also studied by modifying the power output of the UV light source and investigating viability of *S sanguinis* on the thermally treated Ti samples. It observed that even without UV irradiation there was a significant decrease in *S sanguinis* adhesion on the 50 hr, 100 hr and 150 hr thermally treated samples when compared with the polished control. This was in contrast to previous literature (Pucket et al., 2010) that attributed the decreased surface roughness polished Ti to

decreased initial bacterial adhesion. However the data of this study (figure 3.74) demonstrated that there was a significant decrease on the 100 hr and 150 hr thermally treated surfaces with UV irradiation at 923 mw/cm^2. There was no significant reduction observed when compared with UV irradiation at 559 mw/cm^2 implying that higher irradiance was required for radical generation. SEM imaging demonstrated that *S sanguinis* cells were adhered evenly on the Ti polished surface however on the thermal treated surfaces the *S sanguinis* cells were found to be bunched up (figures 3.76 a,b,c and d). Such bunching has been proposed to be a protective mechanism of *S sanguinis* bacteria and by agglomerating together as a means of shielding themselves from the oxygen free radicals, inhibiting growth (Nakano et al., 2013).

A faster technique of growing (thickening) the TiO$_2$ passive film on the surface of Ti is through anodisation (anodic oxidation). The use of anodic oxidation can be used to create defined thicknesses of TiO$_2$ coatings and could potentially be utilised as a part of prophylaxis treatment to minimise bacterial adhesion prior to implant placement. Another potential use of this technique would involve the intra-oral treatment of Ti surfaces. In this study, freshly polished P4000(c) SiC grit surfaces (Grades II, IV and V Ti) substrates were anodically oxidised at voltages of 10, 70 and 120 V in a sodium tetraborate electrolyte solution. The anodic oxidation process resulted in the formation of coloured interference films related directly to the thickness of the TiO$_2$ surfaces -as gold (10V), blue (70V) and a mixture of pink and blue (120V) (indicative of some heterogeneity in film thickness). Beyond voltage the colour that arises through the oxidation process is also dependent on the pH of the electrolyte solution, type of electrolyte and temperature (Diamanti and Pedefeeri, 2007; Dimanti et al., 2008; and Moon et al., 2013). The colours arise due to the interference light

reflecting off the anodic oxide layer and the inner layer –the Ti metal /Ti oxide interface (Moon et al., 2013). EDX analysis subsequently demonstrated significant increases in the surface oxygen content as the anodising voltage was increased from 10 V to 70 V and to (figure 3.99). The data confirms that the higher voltage applied to the Ti in the electrolyte solution resulted in the formation of a thicker oxide layer which was in agreement with work by (Gopal et al., 2010). SEM imaging identified a modification to the surface morphology of the prepared Ti samples with the different anodising voltages and it was observed that the roughness increased as the voltage applied increased. It was evident that pre-existing surface features such as linear ridges or defects became more pronounced with anodisation on all Ti Grades (figure 3.79 – 3.87). Contact angle measurements demonstrated that the surfaces remained highly hydrophilic with no significant modification in the angles recorded before and after anodisation.

Photocatalytic assays were also performed for the anodised Ti samples of all Grades. Samples were thoroughly cleaned to remove the sodium tetraborate electrolyte residues which were initially demonstrated to significantly interfere with the assay. It was noticeable from the data with irradiation at 923 mw/cm^2 the photocatalytic activity was significantly higher with the anodised samples when compared with the controls. On all Grades the Ti samples anodised at 70 V and 120 V (thicker TiO$_2$ film) were found to have the greatest photocatalytic effect (figures 3.91, 3.92 and 3.93) and was in agreement with the literature. The effect of UV irradiation pre-treatment on bacterial cell viability on TiO$_2$ surface was subsequently studied using the oral bacteria *S sanguinis*, *E coli* and *S mutans*. Figures 3.94-102 demonstrate a significant impact of photocatalysis on the viability of the *S sanguinis* bacteria with again a positive relationship between increasing passive oxide film thickness

and efficacy. A similar effect was observed with *E coli* and *S mutans* on Ti surfaces of all Grades after 1 min of UV irradiation with the most pronounced effects observed on surface oxidised at 70 and 120V. Interestingly the data also demonstrated that on non irradiated Ti surfaces early surface bacterial adhesion increased on the rougher surfaces created with the highest anodisation voltages of 70 V and 120. Subsequently after UV irradiation at an intensity of 923 mw/cm^2, it was demonstrated that bacterial viability was significantly reduced on the rougher surfaces. As photocatalytic surfaces may have a limited time efficacy it would therefore be essential to identify where the balance increasing surface roughness and increasing photocatalytic activity lay before any clinical implementation. Although the data has illustrated the effectiveness of increasing the photocatalytic activity with thickened passive oxide layers considerable challenges remain to adopt this system for the clinical environment such as identifying any effects on the health of the peri-implant tissues.

4.4 Enhancing the efficacy of Chlorhexadine Gluconate on Ti implant surface biofilms

The current gold standard in the treatment of peri-implant mucositis and peri-implantitis is the CIST protocol (Fronum et al., 2012). Depending on the severity and progression of peri-implant disease the CIST protocol is implemented and then managed through sequential intervention stages. Within the CIST protocol, antimicrobial mouthwashes have a role however to date few are developed specifically for their use against Ti surface biofilms. The introduction of novel antimicrobial formulations with enhanced penetrative properties against the pathogenic biofilms would be of considerable interest to clinicians and patients alike. The formulation could be utilised in the short term as a prophylaxis treatment and in the long term as a treatment in peri-implant disease. Biofilms form an extracellular polymeric substance (EPS) that prevents antimicrobials from penetrating thereby preventing

surface disinfection. It has been recently reported that Eucalyptus Oil (EO) obtained from the plant species known as Eucalyptus Globulus may have an effect on biofilm permeation. EO contains the mono terpene known as 1, 8-cineole which mediates the enhanced permeation and when combined with an active antimicrobial could enhance commercial mouth wash formulations CHG. Studies by Hendry et al., (2008) and Karpanen et al., (2010) have demonstrated the synergistic activity of EO and CHG. Hendry et al., (2008) created a CHG and isopropyl alcohol (IPA) biocide formulation contained in a wipe for applications as a surface disinfectant in the clinical setting. The CHG: IPA formulation was comprised of 2% EO, 2% CHG and 70% IPA. Further work by Karpanen et al., (2010) investigated the effectiveness of the formulation in skin antisepsis and it was found that the EO enhanced the penetration of CHG in the skin layers. Therefore it was hypothesised that the CHG:IPA formulation has potential applications for enhanced penetration of bacterial biofilms on oral surfaces. This study investigated the adaptation and development of the CHG:IPA formulation for use as an oral mouth wash and its effectiveness against oral biofilms associated with peri-implant disease such as *S sanguinis* and *S mutans*. The removal and replacement of IPA from the composition was deemed essential for health purposes.

The initial aim was to investigate the antimicrobial effect of formulations adapted for a mouth wash application against the pathogenic oral bacteria of *S sanguinis* and *S mutans*. To adapt the CHG:IPA formulation created by Hendry et al. (2008), the antimicrobial activity of the constituents were determined on *S sanguinis* and *S mutans*. The antibacterial activity was determined by carrying out an MIC/MBC assay. The concentrations of the constituents were investigated by initially preparing doubling dilutions. It was found that the IPA had a MBC concentration of 17.5%, the CHG had an MBC of 0.3125 % (3125 µg/mL) and the EO did

not have any antimicrobial activity on *S sanguinis* and *S mutans*. The MBC data of EO was particularly significant because it illustrated that this constituent did not play an antimicrobial role against the bacterial cultures of *S sanguinis* and *S mutans.* However, to make the formulation relevant in the clinical setting, the IPA was substituted with an alcohol base that is used in current mouthwash formulations such as ethanol. Ethanol was found to have an MBC of 17.5% -the data is illustrated in Tables 3.5, 3.6, 3.7 and 3.8. The MBC data of ethanol was in agreement with a study carried out by Sissos et al., (1996) to which ethanol at 10% concentration did not have an effect on plaque biofilm. In addition a previous study reported that a blended essential oil mouthwash formulation was more effective with ethanol Marchetti et al., (2011) and hence its inclusion was deemed as suitable replacement for IPA. The data that was obtained provided some antimicrobial information however, the range between concentrations was large for example, and ethanol concentration had a concentration gap of 8.75%. Smaller concentration ranges were then studied on both bacteria of *S mutans* and *S sanguinis.* It was found that during the development of the mouthwash formulation the constituents were not able to mix fully and as a result the emulsifier of Tween-80 was included. Groppo et al., (2002) described Tween as an emulsifying agent that does not interfere with antimicrobial properties of essential oils. Tween-80 was subsequently included in the MIC/MBC study to determine if it had antimicrobial properties against *S sanguinis* and *S mutans*.

The concentration ranges tested in Tables 3.9 and 3.10 were reduced to 6 to 15 % (ethanol), 1 to 5 % (EO), 0.125 to 2 % (Tween) and 0.1 to 0.5 % (CHG). It was observed that on both *S mutans* and *S sanguinis* that these individual concentrations acting in isolation of ethanol, EO and Tween did not illicit antimicrobial effects. The constituent of CHG was found to be

antimicrobial on both *S sanguinis* and *S mutans* however at concentrations >0.2mg/mL. Data obtained from the MIC/MBC assays provided information to focus the development of the formulation. The final formulation consisted of 0.2% CHG, 2% Tween, 2% EO and 10% ethanol. The concentrations included in the formulation were included to reflect commercial mouth wash formulations that contain such as 10 % ethanol and 0.2% CHG. Helms et al., (1995) describes CHG as having a bitter taste and interferes with taste perception therefore further refinement of the mouthwash formulation would need to be carried out so that the patient can have a pleasant taste and the bitterness of the CHG to be masked.

Biofilms of *S sanguinis* and *S mutans* were subsequently grown on Grade IV Ti surfaces and SEM imaging confirmed the formation of a "young" biofilm using outlined bioreactor protocols (figure 3.103a-3.103c). Initially time dependant assays were developed to determine if the original IPA:EO biocide formulation possessed antimicrobial effects on *S sanguinis* biofilms on the Grade IV Ti with surface finishes of discs P220, P1200 and P4000. The biocidal activity was confirmed when significantly reduced *S sanguinis* viability was observed when compared to the control composed of distilled water and CHG (figure 3.104) Importantly substitution of IPA to ethanol did not affect the antimicrobial effect observed on *S sanguins* and *S mutans* (figures 3.105 and 3.106). After demonstrating the effectiveness of the CHG:EO formulation the assay was then optimised to determine the effect of CHG:EO on biofilms which were demonstrated to be similar in appearance to those observed on polished dental implant components e.g. a healing abutment (figure 3.103d). The optimised CHG:EO formulation was further tested to determine its effectiveness in clinically relevant exposure times judged to be between 2 and 30 mins. It was observed that on both *S*

sanguinis and *S mutans* bioflims the CHG:EO mouthwash formulation led to significant decreases in bacterial viability in a short a period of 2 mins when compared with the formulation without EO (figures 3.110-3.113). The results however were unusual that there appeared in a number of instances giving increased numbers of colonies after longer exposure times. This was attributed to possible degradation of the components over longer exposure times and possible recovery of bacterial numbers. Given the efficacy at 2 mins the exposure time was lowered further to 30 s and the number of samples for analysis increased to provide better statistical data. It was observed that there was there was no significant difference of the control exposure (CHG containing) on viability of either *S mutans* or *S sanguinis* however the developed CHG:EO formulation resulted in a significant reduction in viable microbes over this short exposure time.

It has been reported that the EO has now been used in a variety of applications such as in the fight against the hospital acquired superbugs that are resistant to commercial antimicrobials. A study carried out by Sherry et al., (2001) demonstrated that a topical application of the eucalyptus oil can remove the methicillin resistant *Staphylococcus aureus* (MRSA). In another study carried out by Trivedi and Hotchandani (2004) EO (63% 1, 8-cineole) inhibited the growth of resistant bacterial strains of *Klebsiella* spp., *Proteus* app., *Pseudmonas* app., *Escherichia coli,* and *Staphylococcus aureus.* The findings of this study are confirmatory and have strongly illustrated that EO works in combination with CHG to enhance the penetration of the CHG into biofilms resulting in the enhanced bacteria on Ti surfaces.

CHAPTER 5: CONCLUSION.

The overall focus of this thesis was the impact of material factors on peri-implant disease and its management. A series of studies were conducted to identify how implant surface variables influenced early bacterial attachment and immature biofilms formation. Subsequently novel surface engineering approaches were studied to identify whether they could offer a clinical benefit beyond current technologies. Finally the disruption of biofilms formed on Ti implant surfaces was studied exploiting a novel approach to increase the permeability of the surface biofilms to bactericidal agents. The thesis produced data to support the following conclusions.

- The relationship between topology (generated through grinding and polishing methods) and early bacterial attachment is highly complex and could not be attributed to any specific metrological parameter.

- The polished surfaces were analogous to those encountered in dental implant components that span the gingival tissues e.g. the collar of the fixture or healing abutments. Therefore in the presence of relevant physiological media such a artificial saliva the influence of small modification in surface roughness is unlikely to be predictably associated with increased bacterial adhesion. This has implication clinically on the debridement of these surfaces.

- The surface wettability determined with contact angle measurements using water and artificial saliva as the probing media could not be directly correlated with early bacterial adhesion and it is suggested that such measures are unlikely to be strongly predictive of such behaviour.

- In general with the microbes studied there was a tendency towards decreased bacterial adhesion (in an early colonising model) on the most highly polished surfaces.

- Given the huge variability in early bacterial attachment the selection of surface finishes that demonstrated the highest reproducibility in terms of bacterial cell counts was essential for use in future mechanistic studies. The failure to adopt this approach in the reported literature means that it is extremely hard to compare findings between studies.

A further aim of the study was to determine the interactions between bacteria and surfaces that had been specifically engineered with different topologies.

- Selective laser machining (SLM) was identified as a fabrication route that could produce specific surface features in Ti on a small micron scale.

- SLM surfaces were easily generated and preliminary studies suggest that the resultant topologies were resistant to the early adhesion of the bacteria studied and to immature biofilm formation.

- The introduction of nanotubular structures can modify the surface topology resulting in the creation of hydrophobic surfaces.

- Nanotubular features on Ti surfaces significantly influenced bacterial cell interactions depending on the radius of the tubules and the related surface energies.

- Nanotubular structures may offer some potential to prevent biofilms formation on Ti implant surfaces.

A further aim was to determine the effect of photocatalysis on the prevention and disruption of bacterial colonisation.

- In contrast to previous studies in this area the UV light source was fully characterised and photocatalytic degradation assay optimised.

- Ti surface oxide films were demonstrated to be thickened either thermally or through anodic oxidation, however the resultant surface topologies varied considerably between the two approaches.

- Photocatalysis using UV excitation of TiO_2 films was demonstrated to be effective with enhanced activity achieved by increasing the thickness and roughness of the TiO_2 passive oxide layer and by increasing the irradiation power and time.

- Pre-treatment of Ti surfaces with artificially thickened TiO_2 films resulted in a significant reduction in mean bacterial adhesion and the effect was sustained even if the surface had been contaminated previously.

- The photocatalytic assays and viability assays demonstrated that photocatalysis could potentially be employed as a prophylactic or treatment modality for dental implant surfaces.

The final aim was to determine the effect of novel chemo-mechanical methods on the disruption of early bacterial colonisation on Ti surfaces.

- A possible mouthwash formulation with enhanced penetrative properties of EO was developed from an IPA:EO biocide formulation described by Hendry et al., (2008) MIC/MBC assays demonstrated that CHG was the bactericidal component of the

formulation. Tween, EO, ethanol were not bactericidal components of the formulation.

- The exposure of the CHG:EO formation was demonstrated to significantly reduce the exposure time required to kill the oral microbes studied when compared with conventional CHG formulations.

- The effect of EO was attributed to facilitating increased permeation of CHG into the biofilms formed on the surfaces of Ti.

CHAPTER 6: FUTURE WORK.

The current study has provided a detailed account in terms of the correlation of bacterial adhesion on a thoroughly characterised Ti surface roughness topologies. The data could potentially be extrapolated to predict bacterial attachment to the surface roughness topologies of dental implant systems that currently utilised. Although no obvious pattern of *S sanguinis, E coli, S mutans* and *F nucleatum* adhesion to the prepared Ti surfaces was detected, further work could possibly be undertaken by repeating the adhesion experiments with monoculture and polyculture biofilms grown in a biofilm reactor. The reactor will provide a model system for determining the growth of mature biofilms on Ti surface roughness topologies with the presence of shear forces such as those observed during swallowing.

Work presented in the thesis also evaluated the initial adhesion of bacteria to the engineered SLM "5x5mm",SLM "flat" and Ti nanotubule surfaces with 15, 50 and 100 nm diameters. The engineered Ti surfaces could potentially be utilised to create novel surfaces of Ti dental implant surfaces. It was found that adhesion of *S sanguinis, S mutans* and *F nucleatum* was significantly reduced on the SLM "5x5mm" and SLM "flat" compared to the control P220 rough surface. The findings demonstrated that novel dental implant surface topologies could be employed to reduce bacterial adhesion however; future work could investigate the adhesion of osteoblasts to the surface to determine the osseointegration ability. The NT 15, 50 and 150 nm Ti surfaces have previously shown to increase the adhesion of osteoblasts and encourage osseointegration. The findings presented in the study demonstrated that the NT 15 nm surface had the lowest mean CFU/mL compared to the NT

50 and 100 nm surfaces. The NT 15 nm prepared surface implied that it would enhance osseointegration and reduce bacterial adhesion. Further work could be carried out by evaluating the adhesion of bacterial polycultures and established biofilms with the biofilm reactor to determine the effect of bacterial colonisation on the Ti surface.

The work presented in the study also investigated management and treatment strategies of peri-implant disease, the first treatment modality determined the photocatalytic effect on thermally and anodically prepared Ti surfaces, it was demonstrated that rough surface textures were created which could possibly enhance osseointegration. The thermally and anodic prepared Ti surfaces led to increased photocatalytic activity against the initial attachment of bacterial cultures of *S sanguinis, E coli, S mutans* and *F nucleatum*. Further work could be carried to determine the effect of photocatalytic activity on established bacterial biofilms and to determine whether the system would a detrimental effect on mammalian cells.

Finally, the second treatment modality investigated the effect of a chemo disinfection treatment modality in the form of mouthwash formulation with enhanced penetrative properties against bacterial biofilms. It was found the EO, which has been previously demonstrated to enhance penetration of bacterial biofilms caused a significant reduction in the mean CFU/mL of *S sanguinis* and *S mutans* at time points of 30 s, 2, 15 and 30 mins. Further evaluation of the formulation would need to be carried out to evaluate its effect on the soft tissues and the epithelial cells of the oral cavity.

CHAPTER 7 REFERENCES.

Abad, M.J., Ansuategui, M. & Bermejo, P. (2007). Active antifungal substances from natural sources . *ARKiVOC.* 166-145.

Adell, R., Lekholm, U., Rockler, B., & Brånemark, P.I. (1981). A 15-year study of osseointegrated implants in the treatment of the edentulous jaw. *International Journal of Oral Surgery*. 10: 387–416.

Albrektsson, T. & Isidor, F. (1994). Consensus report of Session IV, In: Lang, N. P. & Karring, T. (eds) *Proceedings of the 1st European Workshop on Peridontology*. London: Quintessence Publishing Co. Ltd. 365-369.

Albrektsson, T. & Wennerberg, A. (2004). Oral implant surfaces: part 1—review focusing on topographic and chemical properties of different surfaces and in vivo responses to them. *International Journal of Prosthodontics.* 17: 536–543.

ASTM. (2011). Standard specification for unalloyed Titanium, for surgical implant applications (UNS R50250, UNS R50400, UNS 50550, UNS R50700). *ASTM International.* Designation: F67-06.

ASTM. (2011). Standard test method for analysis of Titanium and Titanium alloys by atomic emission plasma spectrometry. *ASTM International.* Designation: E2371-04.

Ataoglu, H., Alptekin, N.O., & Haliloglu, S. (2004). A three-year follow-up report of a comparative study of ITI Dental implants and Branemark system implants in the treatment of partially edentulous maxilla. *Clinical Implant Dentistry and Related Research*. 6: 130-141.

Barbour, ME., Dominic, J.O.S., & Daryll C.J..(2007). Chlorexhidine adsorption to Anatase and Rutile titanium dioxide. *Colloids and Surfaces*. 307: 116-120.

Balachandran, K., Sivaraj, R., & Venckatesh, R. (2013). Removal of methylene blue dye using prepared nano Titanium Dioxide (TiO_2) Photocatalyst. *Journal of Environmental Nanotechnology*. 2: 11-15.

Bauer, S., Pittof, A., Tsuchiya, H. & Schmuki, P. (2011b). Size-effects in TiO_2 nanotubes: Diameter dependent anatase/rutile stabilization. *Electrochemistry Communications.*13: 538-541.

Batish, D.R., Singh, H.P., Kohli, R.K., & Kaur, S. (2008). Eucalyptus essential oil as a natural pesticide. *Forest Ecology and Managemen*t. 256: 2166-2174.

Becker, W., Becker, B.E., Newman M.G., & Nyman S. (1990). Clinical and microbiological findings that may contribute to dental implant failure. *International Journal of Oral Maxillofacial Implants*. 5: 31–38.

Bekbolet, M. (1996). Inactivation of *Escherichia coli* by photocatalytic oxidation. *Chemosphere.* 32: 959-965.

Bennick, A., Char, G., Goodlin, R., Abrams, S., Tustain, D., & Madapallimattam, G. (1983). The role of human salivary acidic proline-rich proteins in the formation of acquired dental pellicle *in vivo* and their fate after adsorption to the human enamel surface. *Archives of Oral Biology.* 28: 19-27.

Benowitz, N.L. (1996). Pharmacology of nicotine addiction and therapeutics. *Annual Reviews on Pharmacology and Toxicology.* 36: 597-613.

Bloyce, A., Qi, P-Y., Dong., H & Bell, T. (1998). Surface modification of titanium alloys for combined improvements in corrosion and wear resistance. *Surface Coatings Technology.* 107: 125-132.

Boland, D.J., Brophy, J.J., & House, A.P.N. (1991). Eucalyptus leak oils, Use, Chemistry, Distillation and Marketing. Inkata press, Melbourne/Sydney.

Bos, R. (1996). Co-adhesion of Oral microbial pairs under flow in the presence of saliva and lactose. *Journal of Dental Research.* 75: 809-815.

Botos, S., Yousef, H., Zweig, B., Flinton, R., Weiner, S. (2011). The effects of laser microtexturing of the dental implant collar on crestal bone levels and peri-implant health. *The International Journal of Oral & Maxillofacial Implants*. 26: 492-8.

Boyce, JM. & Pitter, D. (2002). Guideline for hand hygiene in health-care settings, recommendations of the healthcare infection control practices advisory committee and the HICPAC/SHEA/APICIDSA hand hygine task force. *CDC Morbidity and mortality weekly report*. 51: 13.

Brånemark, P.I. (1959). Vital microscopy of bone marrow in rabbits. Thesis, University of Lund, Sweden. *Scandinavian Journal of Clinical and Laboratory investigation*. S38:1-82.

Brooker, MIH., Kleining, D.A. (2006). Field guide to Eucalyptus. Vol 1. South-eastern Australia, third edition. Bloomings, Melbourne.

Brunella, M.F., Diamanti, M.V., Pedeferri, M.P., Fonzo, F. Di.,Casari, C.S., & Bassi, Li. (2007). Photocatalytic behaviour of different titanium dioxide layers. *Thin Solid Films*. 515: 6309-6313.

Campoccia, D., Montanaro,L & Arciola, C.R. (2006). The significance of infection related to orthopaedic devices and issues of antibiotic resistance. *Biomaterials.* 27: 2331-2339

Casida, J.E. & Quistad, G.B. (1995). Pyrethrum flowers: Production, Chemistry, toxicology and uses. *Oxford Univ. Press, Oxford*, UK, 356.

Caswell, W.C. and Clark A.E. (eds.) (1991). Dental implant prosthodontics. Philadelphia, London, Lippincott.

Chopra, I. & Roberts, M. (2001). Tetracycline Antibiotics: Mode of action, applications, molecular biology and epidemiology of bacterial resistance. *Microbiology and Molecular Biology, and Epidemiology of Bacterial Resistance*. 65: 232-260.

Chopra, I. (2007). The increasing use of silver-based products as antimicrobial agents: a useful development or a cause of concern. *Journal of Antimicrobial Chemotherapy.* 59: 587-590.

Cimanga, K., Ambu, K., Tona, L., Apres, S., Bruyne, De. T., Hermans, N., Totte, J., Pieters, & Vlietinck, A.J. (2002). Correlation between chemical composition and antibacterial activity of

essential oils of some aromatic medicinal plants growing in the Democratic Republic of Congo. *Journal of Ethanopharmacology*. 79: 213-220.

Cleplik, F., Tabenski,L., Buchalla, W. & Maisch, T. (2014). Antimicrobial photodynamic therapy for inactivation of biofilms formed by oral key pathogens, *Frontiers in Microbiology.* 5: 405.

Costerton, J.W., Geesy, G.G. & Cheng, K-J. (1978). How bacteria stick*. Scientific American.* 238: 85-95.

Costerton , J.W., Stewart, P.S. & Greenberg, E.P. (1999). Bacterial biofilms: a common cause of persistant infections. *Science.* 284**:** 1318-1322.

Cristina C. Villar, Guy Huyni-B.A, Michael P. Mills & David L. (2012). Wound healing around dental implants. *Cochrane Endodontic Topics*. 25: 44- 624

Cranin, AN.(1970). *Oral implantology*. Springfield 11, Charles C Thomas, publisher.

Crubezy. E, Murail. P, Girard. L. & Bernadou JP. (1998). False teeth of the roman world. *Nature.* 391: 29.

Diamanti, M.V. & Pedeferri, M.P. (2007). Effect of anodic oxidation parameters on the titanium oxides formation. *Corrosion Science*. 49: 939-948.

Diamanti, M.V., Del Curto, B. & Pedeferri, M.P. (2008). Interference colors of thin oxide layers on titanium, *Color Research and Application*. 33: 221-228.

Diamanti, M.V., Ormellese M., Marin, E., Lanzutti, A., Mele, A. & Pedeferri, M.P. (2011). Anodic titanium oxide as immobilized photocatalyst in UV or visible light devices. *Journal of Hazardous Materials*. 186: 2103-2109.

Dobson, J. & Wilson, M. (1992). Sensitization of oral bacteria in biofilms to killing by light from a low-power laser. *Archives of Oral Biology*. 37: 883–887.

Dong, H., Bloyce, A., Morton, P.H. & Bell., T. (1997). Surface engineering to improve tribological performance of Ti-6Al-4V. *Surface Engineering*. 13: 402-407.

Donlan, R.M. & Costerton, W.J. (2002). Biofilms: Survival mechanisms of clinically relevant microorganisms. *Clinical Microbiology Reviews.* 15: 167-193.

Duke, J.A. (2004). Dr Duke's Phytochemical and Ethanobotanical databases. Available online at http://www.ars-grin.gov/duke/ [Accessed July 2, 2013].

Einwag, J., Ulrich, A. & Gehring, F. (1990). In-Vitro Plaque Accumulation on Different Filling Materials, Effect of Surface Roughness and Materials Composition on Biofilm Formation.22-25.

Enan, E., Beigler, M. & Kende, A. (1998). Insecticidal action of terpenes and phenols to coackroaches: effect on octopamine receptors. In: *proceedings of the international symposium on plant protection*, Gent, Belgium.

Ercan, B., Taylor, E., Alpaslan, E. & Webster, T. J. (2012) Diameter of titanium nanotubes influences anti-bacterial efficacy. *Nanotechnology.* 29: 295102.

European Environment Agency. (2006). *Pollution from antifouling paint* [online]. Available online at http://www.eea.europa.eu/themes/biodiversity/multimedia/pollution-from-antifouling-paint/view [Accessed: 11 Nov 2010].

FAO. (1995). Eucalyptus oil. Chapter 5. In: Flavour and Fragrances of plant origin. Food and Agriculture Organization of the united nations, Rome, Italy. Avaliable online at http://www.fao.org/docrep/v5330e/V5350e07.html [Accessed on 2 July 2013].

Feloutzis, A., Lang, N.P., Tonetti, M. S. & Burgin, W. (2003). IL-1 gene polymorphism and smoking as risk factors for peri-implant bone loss in a well-maintained population. *Clinical Oral Implants Research*. 14: 10-17.

Ferreira, S., Silva, G., Cortelli, J. Costa, J. & Costa, F. (2006). Prevalence and risk variables for peri-implant disease in Brazilian Subjects. *Journal of Clinical Periodontology.* 33: 929-935.

Fiorelllini, J., Nevins, M. (2000). Dental implant considerations in the diabetic patient. *Periodontology 2000*. 23: 73-77.

Fröjd, V., Chavez, D.P.L, Andersson., M., Wennerberg., A., Davis., JR., Svensater., G. (2011). In situ analysis analysis of multispecies biofilm formation on customised titanium surfaces. *Molecular Oral Microbiology*. 26: 1-12.

Froum, S.J. & Rosen, P. S. (2012). A proposed Classification for Peri-implantitis. *The International Journal of Periodontics & Restorative Dentistry.* 32: 533-540**.**

Fujishima, A., Honda, K., Kikuchi,S. Kagaku, Z. (1969). Photosensitised electrolytic oxidisation on semiconducting n-type TiO_2 electrode, *Kogyo kgaku*. 72: 108-113.

Fujishima A. & Honda K. (1972). Electrochemical photolysis of water at a semi conductor electrode. *Nature.* 238: 37.

Fujishima, A. (2000). Titanium dioxide phtocatalysis. *Journal of Photobiology and Photochemistry.* 1: 1-21.

Fujishima, A. & Kubota, Y. (2013). Broad spectrum microbial activity of photocatalysis by TiO_2. *Catalysis*. 3: 310-323.

Gadelmawla, E. S., Koura, M. M., Maksoud, T. M. A., Elewa, I. M., & Soliman, H. H. (2002). Roughness parameters. *Journal of Materials Processing Technology*, *123*(1), 133–145.

Galindo-Mereno, P., Fauri, M., AvilaOrtiz, G., Fernandez-Barbero, JE., Cabera-leon, A., & Sanchez-Fernandes, E. (2005). Influence of alcohol and tobacco habits on peri-implant bone loss: a prespective study. *Clinical Oral Implants Research*. 16: 579-586.

Gao, X. & Wachs, E. (2013). Titania-Silica as Catalyst: molecular structural Characteristics and Physiocochemical properties. *Catalysis Today*. 51: 233.

Gharechahi, M., Moosaiva, H., & Forghani, M. (2012). Effect of Surface Roughness and material composition on biofilm formation. *Journal of Biomaterials and Nanobiotechnology* 3: 541-546.

Gongadze, E., Kabaso, D., Bauer, S., Park, J., Schmuki, P. & Iglic, A. (2013). Adhesion of Osteoblasts to a Vertically Aligned TiO2 Nanotube Surface. *Mini-Reviews in Medicinal Chemistry.* 13: 194-200.

Gopal, J. Gerorge, R.P., Muraleedharan, P., Khatak, H.S. (2010). Biofouling. *The journal of Bioadhesion and Biofilm research*. **20**: 167-175.

Gristina, A. G. (1987). Biomaterial-centered infection: microbial adhesion versus tissue integration. *Science.* 237**:** 1588-1595.

Groppo, F. C., Ramacciato, J.C., Simoes, RP., Florrio, FM. & Sartoratto, A. (2002). Antimicrobial activity of garlic, tea tree oil, and chlorhexidine against oral microorganisms. *International Dental Journal.* 52: 433-437.

Gruica, B., Wang, H. Y., Lang, N.P., & Buser D. (2004). Impact of IL-1 genotype and smoking status on the prognosis of osseointegrated implants. *Clinical Oral Implants Research*. 15: 393-400.

Haas, R., Haimbock, W., Mailath, G. & Watzek, G. (1996). The relationship of smoking on peri-implant tissue: a retrospective study. *The Journal of Prosthetic Dentistry.* 76: 592-596.

Hamlekhan, A., Butt, A., Patel, S., Royhaman, D., Takodis, C. E. A. (2014). Fabrication of Anti-Aging TiO2 Nanotubes on Biomedical Ti Alloys. *Public Library of Science.* 9**:** 96213.

Hanaor, D., & Sorrell, C. (2010.). Review of the anatase to rutile phase transformation. *Journal of Materials Science*. 46: 855–874.

Hannig, C. & Hannig, M. (2009). The oral cavity-a key system to understand substratum-dependent bioadhesion on solid surfaces on man. *Clinical Oral Investigation.* 13**:** 123-129.

Hannig, C. & Hannig, M. (2010). Nanomaterials in preventative dentistry. *Nature Nanotechnology.* 5: 565-568.

Heasman. P, Esmail. Z & Barclay. C. (2010). Peri-implant diseases. *Restorative Dentistry.* 37: 511-516.

Heitz-Mayfield, L. J. A. (2008). Peri-implant disease: Diagnosis and risk factors. *Journal of Clinical periodontology*. 35: 292-304.

Heitz-mayfield, L. J.A, & Lang, N.P. (2010). Comparative biology of chronic and aggressive periodontitis vs. peri-implantitis. *Periodontology 2000.* 53: 197-181.

Helms, J. A., Della-Fera, M.A., Mott, A.E. & Frank, M.E. (1995). Effects of Chlorexhidine on human taste perception. *Archives of Oral Biology*. 40: 913-920.

Hendry, E, Conway B. & Worthington T. (2012). Antimicrobial efficacy of novel Eucalyptus oil, Chlorexhidine Digluconate and Isopropyl Alcohol Biocide Formulation. *International Journal of Molecular Sciences*. 13: 14016-14025.

Hendry, E. R., Worthington, T., Conway, B.R. & Lambert, P.A. (2009). Antimicrobial efficacy of eucalyptus oil and 1,8-cineole alone in combination with chlorhexidine digluconate against microorganisms grown in planktonic and biofilm cultures. *Journal of Antimicrobial Chemotherapy*. 64: 1219- 1225.

Houas, A., Lachheb, H., Ksibi, M., Elaloui, E. Guillard, C & Herrmann JM. (2001). Photocatalytic degradation pathway of methylene blue in water. *Applied Catalysis B: Environmental.* 31: 145-57.

Hyeongil, K., Seong-Ho, C., Jae-Jun, R., Seung-Yong, K., Ju-Han, P., & In-Seop, L. (2008). The biocompatibility of SLA-treated titanium implants. *Biomedical Materials*: 3, 25011.

Ikeda, M., Matin, K., Nikaido, T. Foxton, R. M. & J. Tagami. (2007). Effect of Surface Characteristics on Adherence of S. mutans Biofilms to Indirect Resin Composites. *Dental Materials Journal.* 915-923.

Ireland, J. C., Klestermann, P., Rice, E.W. & Clark, R.M. (1993). Inactivation of *Escherichia coli* by Titanium Dioxide Photocatalytic Oxidation. *Applied and Environmental Microbiology.* 59*:* 1668-1670.

Implantium dental implant Available from:

http://www.implantium.co.uk/osc2/index.php?cPath=327_1_[Accessed 23/05/2011].

Isman, M.B. (2006). Botanical insecticides, deterrents and repellents in modern agriculture and an increasingly regulated world. *Annual Review of Entology*. 51: 45-66.

Jacoby, & William A. (1999). Bactericidal activity of photocatalytic TiO_2 Reaction: toward and understanding of it killing mechaniams. *Applied Environmental Microbiology*. 65, 4091-4098.

Jansson, H., Hamberg, K., De Bruyn, H. and Brattha, G. (2005). Clinical consequences of IL-1 genotype on early implant failures in patients under periodontal maintenance. *Clinical Implant Dentistiry Related* Research. 1: 51-59.

Jeansonne, M. J. & White, R.R. (1994). A comparison of 2.0 % Chlorexhidine Gluconate and 5.25 % sodium hypochlorite as antimicrobial endodontic irrigants. *American Association of Endodontics.* 6: 276-278.

Jenkins, W.M.M. (1983). The prevention and control of chronic periodontal disease, in: J.J. Murray (Ed.), The Prevention of Dental Disease, *Oxford University Press.* 253–298.

Joo, HC., Lim, YJ., Kim, MJ., Kwon HB. & Han, JH. (2010). Characterization on titanium surfaces and its effect on photocatalytic bactericidal activity. *Applied Surface Science.* 257: 741-6.

Kalorama information. (2005).Implant-Based Dental Reconstruction: The worldwide implant and bone graft market. Available: http://www.kaloramainformation.com/Implant-Based-Dental [Accessed 08/11/2012].

Karpanen, T J., Conway B R., Worthington T., Hilton T C., Elliott T S J & Lambert P. (2010). Enhanced chlorexhidine skin penetration with eucalyptus oil. *Bio Med Central Infectious Diseases.* 10: 278.

Karpanen, T.J., Worthington, T., Hendry, E.R., Conway, B.R., & Lambert, P. (2008). Antimicrobial efficacy of chlorexhidine digluconate alone and in combination with

eucalyptus oil, tea tree oil and thymol against planktonic and biofilm cultures of *Staphylococcus epidermidis*. *Journal of Antimicrobial Chemotherapy.* 62: 1031-1036.

Katsikogianni, M., Spiliopoulou, I., Dowling, D. & Missirlis, Y. J. (2006). Adhesion of slime producing Staphylococcus epidermidis strains to PVC and diamond-like carbon/silver/fluorinated coatings. *Journal of Materials Science: Materials in Dentistry.* 17**:** 679-89.

Kawai, K., Urano, M. & Ebisu, S. (2000). Effect of Surface Roughness of Porcelain on Adhesion of Bacteria and Their Synthesizing Glucans. *Journal of Prosthetic Dentistry*. 83: 664-667.

Kim, TN., Balakrishnan, A., Lee, BC., Kim, WS., Smetana, K., Park, JK. & Panigrahi, BB. (2007). In vitro biocompatibility of equal channel angular processed (ECAP) titanium, *Biomedical Materials*. 3: 117-120.

Klasen, HJ. (2000). Historical review of the use of silver in the treatment of burns. *Burns.* 26: 117-130.

Kolenbrander, P. E. & London, J. (1993). Adhere today, here tomorrow: oral bacterial adherence. *Journal of Bacteriology.* 175: 3247-3252.

Kolenbrander, P E., Palmer, R J., Periasamy, S. & Jakubovics, N.S. (2010). Oral multispecies biofilm development and the key role of cell-cell distance. *Nature Microbiology Review*. 8: 471-480.

Kolenbrander, P.E, Palmer, R. J, Saravanan, P. & Jakubovics, N.S. (2002). Communication among oral bacteria. *Microbiology and Molecular Biology Reviews.* 66: 486-505.

Kotsovilis S., Karousis, IK., Trianti, M., Fourmousis, I. (2008). Therapy of peri-implantitis: a systemis review. *Journal of Clinical periodontology.* 35: 621-629.

Koyanagi, T., Sakamoto, M., Takeuchi, Y., Ohkuma, M. & Izumi Y. (2010). Analysis of microbiotica associated with peri-implantitis using 16S rRNA gene clone library. *Journal of Oral Microbiology*. 2: 5104.

Kumar, Satendra., Narayanan T.S.N Sankara., Raman, S. Ganesh Sundara Raman & Seshadri, S.K. (2010). Thermal oxidation of CpTi- An electrochemical and structural characterization. *Material Characterisation*. 589-597.

Kuyyakanond, T. & Quesnel L.B. (1992). The mechanism of action of chlorhexidine. *Federation of European Microbiological Socieites Micobiology Letters.* 15: 211–215.

Kwon., C.H., Hyumin, S., Kim, J.E. & Yoon., K H. (2004). Degradation of methylene blue via photocatalyis of titanium dioxide. *Materials Chemistry and Physics*. 86: 78-82.

Laine, M.L., Leonhardt, A., Roos-Jansaker, P.A.S., Winkelhoff, A.J.V. & Renvert, S. (2006). IL-1RN gene polymorphism is associated with peri-implantitis. *Clinical oral implants research*. 17, 380-385.

Langeneim J.H. (1994). Higher plant plant Terpenoids: a phytocentric overview of their ecological roles. *Journal of Chemical Ecology.* 20: 1223-1280.

Lee, E-J., Kwon, J-S., Uhm, S-H., Song, D-H., Kim, Y. H., Choi, E. H. & Kim, K-N. (2013). The effects of non-thermal atmospheric pressure plasma jet on cellular activity at SLA-treated titanium surfaces. *Current Applied Physics*. *13*, 36–S41.

Leeuwenhoek A. van. (1684). Microscopical observations about animals in the scruf of the teeth. *Philosophical Transation of the Royal Society B: Biological Sciences*. 14: 568-574.

Lekholm, U. Henry, P., Linden, H.K. Bergstrom, C. & Steenberghe, D.V. (1999). Survivial of the Branemark implant in partially edntullous jaws: A 10-year prospective multicenter study. *International Journal of Maxiofacial Implants*. 1: 639-645.

Liao, J, Zhimin, Z., Anchun, M., Lei, Li. & Jianchao, Z. (2010a). Deposition of silver nanoparticles on titanium surface for antibacterial effect. *International Journal of Nanomedicine.* 5: 261-267.

Liao, J., Anchun, M., Zhu, Z., & Quan. (2010b). Antibacterial titanium plate deposited by silver nanoparticles exhibits cell compatibility, *International Journal of Nanomedicine.* 5: 337-342.

Lindhe J & Meyle J. (2008). Peri-implant diseases: Consensus Report of the Sixth European Workshop on Periodontology. *Journal Clinical Periodontology*. 35: 282–285.

Lindquist, L., Carlsson, G. & Jemt, T. (1997). Association between marginal bone loss around osseointegrated mandibular implants and smoking habits: a 10 year follow-up study. *Journal of Dental Research*. 76: 1667-1674.

Listgarten, M. A., & Lai, C.-H. (1999). Comparative Microbiological Characteristics of Failing Implants and Periodontally Diseased Teeth. *Journal of Periodontology*. *70*: 431–437.

Liu, X., Chu, P K., & Ding, C. (2004). Surface modification of titanium, titanium alloys, and related materials for biomedical applicatons, *Materials Science and Engineering.* 47: 49-121.

Machado, M. C., Targuinio, K. M. & Webster, T. J. (2012). Decreased Staphylococcus aureus biofilm formation on nanomodified endotracheal tubes: a dynamic airway model. *International Journal of Nanomedicine.* 7**:** 3741-3750.

Marsh, P.D. (2004). Dental Plaque as a microbial biofilm. *Caries Research*. 38: 204-21.

Maness, P-C, Smolinski, S., Blake, D M., Huang, Z., Wolfrum, E. J. & Jacoby, WA. (1999). Bactericidal activity of photocatalytic TiO_2 reaction: toward an understanding of its killing mechanism. *Applied Environmental Microbiology.* 65: 4094-4098.

Mangano, C., Rosa, A D., Desiderio, V., D'aquino, R.,Piattelli, A., Francesco, F D., Tirino, V., Mangano, F., & Papaccio, G. (2010). The Osteoblastic differentiation of dental pulp stem cells and bone formation on different titanium surface textures. *Biomaterials*. 31: 3543-3551.

Marchetti, E., Mummolo, S., Di Mattia, J., Casalena, F., Di Martino, S., Mattei, A., and Marzo, G. (2001). Efficacy of essential oil mouthwash with and without alcohol: a 3-day plaque accumulation model. *Trials*. 12: 282.

Marsh, P.D. (2004). Dental Plaque as a microbial biofilm. *Caries Research*. 38: 204-211.

Marquis, R. E. (1995). Antimicrobial Actions of Fluoride for Oral Bacteria. *Canadian Journal of Microbiology.* 41**:** 955-964.

Masadeh M.M, Gharaibeh, S.F., Alzoubi, K.H., Al-Azzam, S.I and Obeidat,W.M. (2013). Antimicrobial activity of common mouthwash solutions on multidrug-resistance bacterial biofilms. *Journal of Clinical Medical Research*. 5: 389-394.

Matsunaga, T., Tomoda, R., Nakajima, T., & Wake, H. (1985) Photoelectrochemical Sterilization of microbial cells by semiconductor powders. *Federation of European Microbiological Socieites Micobiology Letters.* 29: 211-214.

McDermott, N.E., Chuang, S.K., Woo, V., and Dobson, T.B. (2003). Complications of dental implants: identification, frequency, and associated risk factors. *The international journal of oral and maxillofacial implants*. 18: 848-855.

McKinney, Ralph V, Jr. (1991). Endosteal Dental Implants. Mosby Year book, St. Louis.

Meisel, P. & Kocher,T. (2005). Photodynamic therapy for periodontal diseases: state of the art. *Journal of Photochemistry & Photobiology B: Biology.* 79: 159-170.

Michael, J.J. & Robert R.W. (1994). A comparison of 2.0% Chlorexhidine Gluconate and 5.25% sodium hypochlorite as antimicrobial endodontic irrigants. *American Association of Enododontics*. 6: 276-278.

Mohabansi, N.P., Patil, V.B. & Yenkie, N. (2011). A comparative study on photo degradation of methylene blue dye effluent by advanced oxidation process using TiO2/ZnO photo catalyst. *Rasayan Journal of Chemistry.* 4: 814-819.

Mombelli, A. & Niklaus, P.L. (2000). The diagnosis and treatment of peri-implantitis. *Periodontology*. 17: 63-76.

Moon, J., Kemell, M., Park, B., Suominen, A., Makila, E., Punkkeinen, R., Hedman,H-P., Kim, H., Lassilia, L V. & Tuminen, A. (2013). The correlation between the interference colour

and growth procedure of anodic titanium dioxide nanotube arrays. *Coloration Technology*. 130: 1-7.

Newman, H.N. & Wilson, M. (1999). dental plaque revisited oral biofilms in health and disease. *Journal of Periodontology Research.* 7: 438.

Nakano Ryuichi, Hara, Marayuki., Ishiguro, Hitoshi., Yao, Yanyan Ochiai, Tysuoshi., Kazuya., Murakami, Taketoshi, Kajioka, Jitsuo., Sunada, Kayano., Hasimoto Kazuhito. (2013). Broad Spectrum microbiocidal activity of photocatalysis of TiO_2. *Catalysis*. 3: 310-323.

Niels, H., Bjarnsholt, T., Givskov, S O., Ciofu., O. (2010). Antibiotic resistance of bacterial biofilms. *International Journal of Antimicrobial Agents.* 35: 322-332.

Norowski, P.A. & Bumgardner, J.D. (2008). Review: Biomaterial and antibiotic strategies for Peri-implantitis. Journal of biomedical materials research part B. *Applied Biomaterials*. 530-543.

Olivares-Navarrete, R., Hyzy, SL., Park, JH., Dunn, GR., Haithcock, DA., Wasilewski, CE., Boyan, BD. & Schwartz, Z. (2011). Mediation of osteogenic differentiation of human mesenchymal stem cells on titanium surfaces by a Wnt-integrin feedback loop. *Biomaterials.* 32: 6399-6411.

Oss, Van C.J. (1986). Nature of the antigen- antibody interaction. Primary and secondary bonds: optimal conditions for association and dissociation. *Journal of chromatography.* 376: 111-119.

Pabst, M.J., Pabst, K.M., Collier , J.A., Coleman, TC., Lemmons-Prince, ML., Godat. MS., Waring, MB. & Babu, JP. (1995). Inhibition of neutrophil and monocyte defensive functions by nicotine. *Journal of Periodontology.* 66: 1047-1055.

Pankey G. A. & Sabath L.D. (2004). Clinical relevance of bacteriostatic versus bactericidal mechanisms of action in the treatment of gram-positive bacterial infections. *Clinical Infectious Diseases.* 38: 864-870.

Park, J., Bauer, S., Schlegel, K. A., Neukam, F. W., Von Der Mark, K. & Schmuki, P. (2009). TiO2 Nanotube Surfaces: 15 nm - An Optimal Length Scale of Surface Topography for Cell Adhesion and Differentiation. *Small.* 5**:** 666-671.

Park, J., Song, C., Jung, J. Ahnand & S. Ferracane, J. (2012). The Effects of Surface Roughness of Composite Resin on Bio- film Formation of *Streptococcus mutans* in the Presence of Saliva, *Operative Dentistry.*532-539.

Pawar, V.C. & Thaker, V.S. (2006). *In vitro* efficacy of 75 essential oils against *Aspergillus niger*. *Mycoses.* 49: 316-323.

Peng, Z., NI, J., Zheng, K., Shen Y., Wang, X., HE, G., Jin, S. & Tang, T. (2013). Dual effects and mechanism of TiO2 nanotube arrays in reducing bacterial colonization and enhancing C3H10T1/2 cell adhesion. *International Journal of Nanomedicine.* 8**:** 3093-3105.

Persson G.R., Salvi G E, Heitz-Mayfield L J A, Lang N P. (2006). Antimicrobial therapy using a local drug delivery system (Arestin (R)) in the treatment of peri-implantitis. *International Microbiological Outcomes.* 17: 386-393.

Puckett, S. D., Taylor, E., Raimondo, T. & Webster, T. J. (2010). The relationship between the nanostructure of titanium surfaces and bacterial attachment. *Biomaterials.* 31**:** 706-713.

Pye, A.D., Lockhart, D.E.A., Dawson. M.P., Murray, C.A. & Smith. A.J. (2009). A review of dental implants and infection. *Science Direct.* 72: 104-110.

Qiu, C., Adkins, N.J.E., Attallah, M.M. (2013). Microstruture and tensile properties of electively laser-melted of HIPed laser melted Ti-6Al-4V. *Material Science and Engineering .* 578: 230-239.

Quere, D. (2002). Surface chemistry: Fakir droplets. *Nature Materials.* 1**:** 14-15.

Rai, M., Yadev, A., & Gade, A.(2008). Silver nanoparticles as a new generation of antimicrobials. *Biotechnology Advances.* 27*:* 76-83

Regonini., Jaroenworaluck, A., Stevens, R. & Bowen, C. R. (2010). Effect of heat treatment on the properties and structure of TiO_2 nanotubes: phase composition and chemical composition. *Surface and Interface Analysis.* 42**:** 139-144.

Richard., J.W., Spencer, B.A., McCocy, L.F., Carina, E., Washington, J. & Edgar, P. (2002). Acticoat versus silverlon: the truth. *Journal of Burns surgical wound Care.* 11-20.

Rimondini, L., Fare, S., Chiesa. & Pedeferri, M.P. (2003). The effect of composition, wettability and roughness of the substrate on *in vivo* early bacterial colonization of titanium, *Journal of Applied Biomaterials & Biomechanics:* 1, 131-138.

Ring, ME. (1995a). A thousand years of dental implants: a definitive history—Part I. *Compendium of Continuing Education in Dentistry.* 10, 1060-1069.

Ring, ME. (1995b). A thousand years of dental implants: a definitivehistory—Part II. *Compendium of Continuing education in dentistry.* 11: 1134-1142.

Rosen Paul, Clem Donald, Cochran David, Froum Stuart, McAllister Bradley, Renvert Stefan, Wang Hom-Lay. (2013). Peri-implant Mucosistis and Peri-implantitis: A current Understanding of their diagnosis and clinical implications. *Journal of Periodontology.* 84: 436-443.

Roos-Jansaker, A.M., Lindahl, C., Renvert, H. & Renvert S. (2006). Nine- to fourteen-year follow-up of implant treatment. Part II: presence of peri-implant lesions. J*ournal of Clinical Periodontology.* 33: 290-295.

Rupp, F., Haupt, M., Klostermann, H., Kim, HS., Eichler, M., Peetsch, A., Scheideler, L., Doering, C., Oehr, C., Wendel, HP., Sinn. S., Decker, E, von Ohle C, Geis-Gerstorfer J.(2010) Multifunctional nature of UV-irradiated nanocrystalline anatase thin films for biomedical applications. *Acta Biomateriala,* 6: 4566-77.

Rutar, A., Lang, N.P., Buser, D., & Bürgin. W. (2000). Retrospective assessment of clinical and microbiological factors affecting peri-implant tissue conditions. *Clinical oral implants research.* 12: 189-195.

Saito, T., Iwase, T., Morioka, T., Mode of photocatalytic bactericidal action of powdered semiconductor TiO$_2$ on mutans streptococci. (1992). *Journal Photobiology B Biology*. 14, 369-379.

Sans, M., Newman, M.G., Anderson,L., Matoska,W., Otomo-Corgel. J, Saltini. C. (1982). Clinical enhancement of post periodontal surgical therapy by a 0.12% chlorexhidine gluconate mouthrinse. *Journal of Peridontology.* 60, 570-581.

Sawase, T., Wennerberg, A., Baba, K., Tsuboi ,Y., Sennerby, L., Johansson, CB. & Albrektsson, T. (2001). Application of oxygen ion implantation to titanium surfaces: effects on surface characteristics, corrosion resistance, and bone response, *Clinical Implant Dentistry and Related Research.* 3*:* 221-229.

Schwartz, Z and Boyan, B.D. (1994). Underlying mechanisms at the bone-biomaterial interface. *Journal of Cellular Biochemistry.* 56: 340-347.

Sherry, E., Boeck, H. & Warnke, P.H. (2001). Topical application of a new formulation of eucalyptus oil phytochemical clearsmethicillin-resistant *sstaphylococcus aureus* infection. *American Journal of Infection Control.* 29: 346.

Shin, D.H., Shokuhfar, T., Choi, H.C., Lee, S., & Friedrich, C. (2011). Wettability changes of TiO_2 nanotube surfaces. *Nanotechnology*. 5: 31574-315711.

Silla, M.P., Company, J.M.M. Silla, J.M.A. (2008). Use of chlorhexidine vaernishes on preventing and treating periodontal disease. A review of Literature. *Medicine Oral Patologia Oral Cirgia Bucal.* 4: 57-60.

Sissons, C.H., Wong, L. and Cutress, T.W. (1996). Inhibition by ethanol of the growth of biofilm and dispersed microcosm dental plaques. *Archives of Oral Biology.* 1: 27–34.

Snauwaert, K., Duyck, J., Steenberghe, D.V. Quiryran, M., Naert, I. (2000). Time dependent failure rate and marginal bone loss of implant supported prostheses. A 15-year follow- up study. *Clinical Oral Investigation*. 4: 13-20.

Straumann. (2010). Straumann receives Frost and Sullivan medical device technology of the year award for Roxoloid [Online]. Available from: http://www.straumann.com/com-index/com-media-relations/ci_media_releases.htm?news=E1E3F4E9EFEEBDF3E8EFF7A0EFE2EABDB1B1B4B8B6 Accessed [16/06/2011].

Steenberghe, V., Quirynen, M & Naer, L. (1999). Survival and success rates with oral endosseous implants. *Educational Workshop on Peridontology*. 3rd. Berlin, Quintessence Publisher. 242-54.

Suketa, N., Sawase, T., Kitaura, H. Naito, M. Baba, K., Nakayama, K., Wennerberg.A, & Atsuta, M. (2005). An Antibacterial Surface on dental implants, Based on the photocatalytic bactericidal effects, *Clinical Implant Dental Related Research*. 7: 105-111.

Tachikawa, T. and Majima, T. (2010). Single-molecule, single-particle fluorescence imaging of TiO$_2$ based photocatalytic reactions. *Chemical Society Review.* 39: 4802-4819.

Takasaki, A.A., Aoki, A., Mizutani, K., Schwarz, F., Schulean, A., Wang, C-Y., Koshy, G., Romanos, G., Ishikawa, I., and Izumi, Y. (2009). Application of antimicrobial photodynamic therapy in periodontal and peri-implant diseases. *Periodontology*. 109-140.

Teughels, W., Van Assche, N., Sliepen, I., & Quirynen, M. (2006). Effect of material characteristics and/or surface topography on biofilm development. *Clinical Oral Implants Research*. 17: 68–81.

Thomas D.,T. & Laney, W R. (1999). Dental implants: are they for me? [Online] University of Connecticut Health Centre. Centre for Implant and Reconstructive dentistry.

Trivedi, N.A. & Hotchandani, S.C. (2004). A study of the antimicrobial activity of oil of *Eucalyptus*. Indian Journal of Pharmacology. 36: 93-94.

USEPA (United States Environment Protection Agency). (1993). R.E.D. FACTS. Flower and vegetable oils. Avaliable online at http://www.epa.gov/oppsrrd1/REDs/factsheets/4097fact.pdf [Accessed 12th November 2013].

Vandenbroucke, B. & Kruth, JP. (2007). Selective laser melting of biocompatible metals for rapid manufacturing of medical parts, *Rapid Prototyping Journal*. 13, 196-203.

Strydonck, V.DA., Slot, DE., Van der velden U. & Van der Weijden F. (2012). Effect of a chlorexhidine mouthrinse on plaque, gingival inflammation and staining in gingivitis patients: A systematic review. *Journal of Clincal Periodontology. 39:* 1042-55.

Veksler, A.E., Kayrouz, G.A., & Newman, M.G. (1991). Reduction of salivary bacterial by per-procedural rinses with Chlorexhidine 0.12%. *Journal of Periodontology*. 62: 649-651.

Weiss, M. B., & Rostoker, W. (1981). Development of a new endosseous dental implant. Part I: Animal studies. *The Journal of Prosthetic Dentistry*. 46 :646–651.

Williams RC. (1990). Periodontal disease. *New England Journal of Medicine.* 322: 373-382.

Wilson, T. & Nunn, M. (1999). The relationship between the interleukin-1 periodontal genotype and implant loss. Initial data. *Journal of Periodontology*. 70: 724-729.

World Health Organisation.(WHO). (2011). Ultraviolet radiation [Online]. Available from: http://www.fda.gov/RadiationEmittingProducts/RadiationEmittingProductsandProcedures/Tanning/ucm116425.htm Accessed [16/06/2011].

Yoshinari, M, Oda, Y., Kato, T. & Okuda, K. (2001). Influence of surface modifications to titanium on antibacterial activity in vitro, *Biomaterials.* 22: 2043-2048.

Zhu, X. L., Chen, J., Scheideler, L., Reichl, R. & Geis-Gerstofer, J. (2004). Effects of topography and composition of titanium surface oxides on osteoblast responses. *Biomaterials.* 25**:** 4087-4103.

CHAPTER 8: APPENDIX I

8.1 Mechanical debridement with a NiTi brush.

The effectiveness of a NiTi mechanical debridement brush was evaluated on gold coated Grade IV P4000 surfaces. The NiTI brush mechanically debrided the gold coated discs at a 90° angle to the surface of the Grade IV Ti disc

8.1.1 Materials and methods.

The NiTi brush is intended to remove biological materials from the implant surface (Hans Korea, Korea). The NiTi brush was evaluated to determine the efficacy of mechanical debridement. CpTi Grade IV P4000 prepared Ti surfaces were gold sputter coated for 4 min at 50 mA (Emitech K550 X, Kent, UK). The NiTi brush was inserted into a hand piece (KaVO Dental Ltd, Amersham, Buckinghamshire, UK) and placed 90 degrees to the sample surface for 30s as a means of debriding as instructed by a dentist at the University of Birmingham Dental School. In the SEM CpTi Grade IV surfaces were mapped with EDX to determine where the Gold coating had been removed from the Ti surface (n=3).

8.1.2 Results.

Figure 8.1. Histogram illustrating the % gold weight pre and post debridement with the NiTi brush on gold coated Grade IV titanium (mean ± SD, n=8, *=p<0.05).
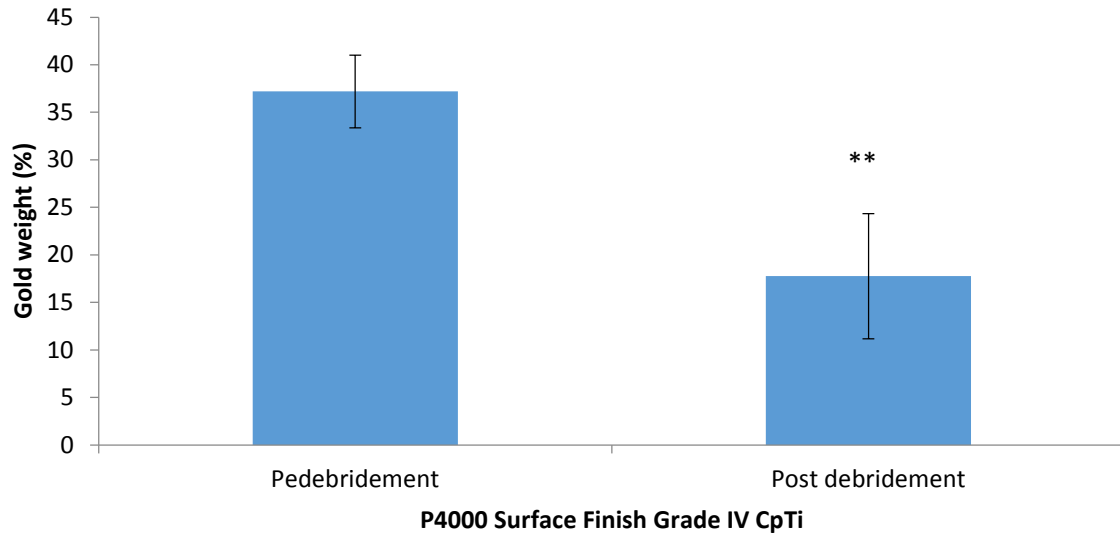
The histogram (figure 8.1) illustrates that gold weight percentage was significantly reduced

from 37.19 % to 17.76 % after mechanical debridement with the NiTi brush (P<0.01).